UNIVERSITÀ DEGLI STUDI DI TRIESTE

UNIVERSITÀ DEGLI STUDI DI UDINE

Dottorato di Ricerca Interateneo in

Ingegneria Civile–Ambientale e Architettura

Curriculum: Ingegneria Civile

Settore Scientifico Disciplinare: Tecnica delle Costruzioni CEAR-07/A

XXXVIII Ciclo

OPEN ISSUES ON TIMBER ENGINEERING: Q-BEHAVIOUR FACTOR OF LIGHT FRAME TIMBER BUILDINGS AND VIBRATION COMFORT ASSESSMENT OF TIMBER JOISTED FLOORS

Dottorando
Alessandro Mazelli

Coordinatore
Prof. Alberto Sdegno

Supervisore di Tesi
Prof. Chiara Bedon

Co-Supervisore di Tesi
Prof. Antonino Morassi

Anno Accademico 2024/2025

A ABSTRACT

The renewed focus on timber structures in recent decades has led to a rapid evolution of the research but, despite the significant progress, codes and regulations still require continuous updating, as many open issues remain to be studied. This dissertation, in fact, analyse two open topics.

The first part of the thesis analyses the seismic behaviour of Light-Frame Timber LFT structures, to obtain a reliable range of the q-behaviour factor for the seismic design. Current codes, in fact, suggest values that are not consistent with the actual response of LFT walls. First, a literature review studied different structural typologies, focusing then on LFT structures and their hysteretic cyclic behaviour. Successively, a laboratory tested full-scale LFT wall was used to calibrate FEM models, and the sheathing-to-framing connection was parameterised, varying its ductility and the shear capacity, in order to define a set of LFT walls. These walls, in fact, were used to assemble six reference buildings, which were subjected to Incremental Dynamic Analysis. Twenty seismic events were considered, and each pair of accelerograms was applied simultaneously in both principal directions of the buildings. The over 7000 non-linear dynamic analysis were then used to calculate the q-behaviour factors.

The second part of the dissertation considered the comfort vibration assessment for timber joisted floors. Since assessment methods are typically expensive and time consuming, this work proposes a valid alternative using smartphone devices. A preliminary review is reported, highlighting typical structural solutions for joisted timber floors, but also human-induced load models and key parameters to define comfort.

Successively, a full-scale timber floor was built and tested. The specimen was equipped with force-balance accelerometers and smartphone. Corrective coefficient for the smartphone outcomes were extracted and a test protocol was proposed. Moreover, starting from a FEM model of the tested floor, a parametric analysis was developed. Varying a set of 12 parameters, 15,000 different floor configurations were obtained. Each configuration was then subjected to probabilistic walking loads, in order to provide useful information to improve the vibration check according to Eurocode. Finally, the smartphone-based assessment was successfully applied to three case studies in L'Aquila.

C | CONTENTS

SUMMARY

Thanks to the increasing attention on sustainability and low environmental impact, wooden structures are becoming widespread even in areas where, traditionally, buildings were made of masonry or reinforced concrete. This renewed focus on wooden structures in recent decades has led to a rapid evolution of research in the field. Despite significant progress, however, codes and regulations still require continuous updating, as many open issues remain to be studied. This dissertation, in fact, analyse two topics that are still open and internationally debated.

The first part of the thesis analyses the seismic behaviour of Light-Frame Timber LFT structures, in order to obtain a reliable range of the structural behaviour factor q for the seismic design. Current codes, in fact, suggest values that are not consistent with the actual ductile response of LFT walls. Such values are based on on-site construction methods typical of North America and rarely used in Europe, where LFT structures are generally prefabricated. To obtain a range of q-factor values for LFT structures, six reference buildings were designed according to Eurocode provisions and analysed using a nonlinear incremental dynamic IDA approach. The first part of the dissertation is divided into eight chapters.

The first chapter provides an overview of timber construction typologies, and considers the main design suggestions of international codes, such as Eurocode, Canadian regulations and U.S. building code.

The second chapter focuses on LFT structures. The in-plane behaviour of LFT shear walls was analysed in detail, highlighting the critical role of connections. Energy dissipation, in fact, is concentrated

in mechanical steel fasteners like nails and screws. Studies on the monotone and hysteretic behaviour of hold-downs, angle brackets and nailed connections are discussed.

Successively, a literature review on approaches for calculating the q-factor was reported in chapter 3, considering both experimental and numerical methods. For the numerical approaches, static and dynamic methods were also compared.

Starting from a laboratory tested full-scale LFT wall, in chapter four two FEM models of a 3x3 m LFT wall were assembled. In particular, the hysteresis parameters of the connections were calibrated to experimental outcomes.

The nailed connection calibrated in chapter four was then parameterized in chapter five by varying the connectors' resistance and their displacement ductility, obtaining three resistance classes and three ductility classes. Moreover, for each ductility class, different sets of LFT walls were built, in order to assemble the case study buildings.

In chapter six, in fact, six example buildings with 2, 3, and 4 floors, irregular and regular in plan and elevation, were designed, verified, and assembled using the previously constructed LFT wall sets.

To evaluate the structural behaviour factor q, an IDA approach was implemented. In chapter seven, each building was analysed by means of nonlinear dynamic analysis with 20 pairs of accelerograms. Given the large amount of analyses and the need to reach the collapse the structure incrementally, a MATLAB code was developed and SAP2000 software's OAPI interface was used.

Finally, the results of over 7,000 nonlinear dynamic analyses were reported in chapter eight. For each building type and each ductility class, the data were processed to obtain ranges for the structural behaviour factor. The results were divided by type and compared with the values suggested by current codes and with examples in the literature based on static analyses. Finally, a value of q was suggested for structures in low and high ductility classes.

The second part of the dissertation, on the other hand, considered the issue of comfort vibration assessment in timber joisted floors. Even if wooden structures are not widely spread on Italian territory or in areas

traditionally linked to other construction materials (i.e. concrete, masonry), timber was usually used in historical floors. Assessment methods are typically expensive, since they are time consuming and involve professional accelerometers.

To propose a valid alternative to standard on-site procedures, the second part of the thesis analysed the implementation of smartphone sensors for the fast assessment of timber floors, in order to evaluate comfort parameters typically used in international standards.

The first chapter reports a literature review on timber floors. A first part highlights the construction technologies for historical timber floors, such as one-way joisted floors or "cassettoni" floors. A second analyses focused on modern timber structures, considering glulam and CLT flooring and composite solutions. Moreover, beam vibration theory is presented, and the parameters influencing the dynamic response of timber floors are examined.

Human Induced Vibrations are discussed in chapter two. The literature review focused on both types of action (i.e. walking, running, jumping) and modelling strategies. Deterministic approaches, in fact, cannot take into account the intra- and inter-subject variabilities. To properly model these variables, a probabilistic approach is needed. Finally, an overview of the most used parameters for comfort assessment is reported.

In the third chapter, current codes are taken into account. The review considered the Italian building code and the Eurocode 5 provisions in terms of vibration check. Moreover, ISO standards, Guidelines and extra-European codes are discussed.

A full-scale timber floor was built and tested in chapter four. In collaboration with the University of L'Aquila, three beams joisted floor specimen was equipped with force-balance accelerometers and smartphone. Walking and jumping sessions allow to compare records and to elaborate corrective coefficient for the smartphone outcomes. A test protocol was then built, based on the tests results.

Starting from a FEM model of the tested floor, a parametric analysis was developed in chapter five. Parameters like span, section, number of beams, stiffness of connections, screed thickness and damping were varied to obtain 15,000 different floor configurations.

Each configuration was subjected to human walking sessions, generated by a probabilistic model. Thanks to the parametric analysis, useful information was obtained to improve the vibration check according to Eurocode.

Finally, in chapter six the smartphone-based assessment is applied to three case studies in L'Aquila. The procedure gave good results, demonstrating that the smartphone can be a valid alternative for the vibration comfort assessment of flexible floors.

PART ONE

–

EVALUATION OF THE Q-BEHAVIOUR FACTOR BASED ON INCREMENTAL DYNAMIC APPROACH FOR LIGHT-FRAME TIMBER BUILDINGS

I-1 INTRODUCTION

The climate change of the last decade seriously impacted the life on the earth, with extreme heat, drought, fires, tornadoes, flood, heavy rains, landslides and other phenomena which also affected structures and infrastructures. One of the main goals of the society should be to "reduce disaster risk and losses in lives, livelihoods and health and in the economic, physical, social, cultural and environmental assets of persons, businesses, communities and countries", as declared by the Sendai Framework [1]. But long-term, large-scale solutions are urgently needed, and a more important use of timber structures could be a mitigation option to avoid emissions and to combat climate change. After, "housing a growing population in homes made out of wood instead of conventional steel and concrete could avoid more than 100 billion tons of emissions of CO_2 until 2100" [2].

Nowadays, wood is rediscovering a new life as a building material, thanks to its sustainability, energy-consumption and unique aesthetic. Timber show great advantages in terms of high strength-to-weight ratio and prefabrication, thus enabling the opportunity to fast assembly of lighter structures. Moreover, it is worth to note the good performance of wooden buildings in seismic prone areas, thanks to the low mass and the possibility of dissipating earthquake energy through the connections. This growing sensibility towards environmental preservation helped the spread of wooden buildings also in areas where other materials, as reinforced concrete or masonry, were traditionally used, as in southern Europe

Even if timber structures were historically used for low-rise buildings (with some exception, e.g. Pagoda temples in China and Japan),

the development of engineered wood product such as Glue-Laminated Timber (Glulam or GLT), Laminated Veneer Lumber (LVL) and Cross-Laminated Timber (CLT) has enabled the possibility of high-rise multi-storey buildings. The new products, in fact, overcame limitations of traditionally sawn timber, such as grater mechanical properties, larger sections and spans and less waste of material [3].

1.1 Timber Structures

Several structural timber typologies have been developed over time. In the following paragraphs, three of the most commonly used are proposed: Light-Frame Timber, Heavy-Frame Timber and Mass Timber Structures (Cross Laminated Timber - CLT).

1.1.1 Light-Frame Timber

Light-Frame Timber technology was used in North America since early 1800. Timber members are thin and closely spaced, assembling walls composed by vertical studs covered by light-weight wooden panels, such Oriented Strand Boards OSB or plywood. Vertical elements carry the gravitational loads (Fig. 1).

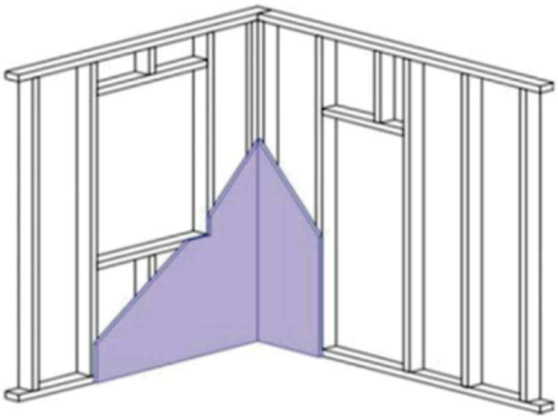

Fig. 1 – Light-Frame timber system.

Thanks to the panel connected by small diameter nails, the wall works as a shear-wall against horizontal actions. Floor are made of joist and nailed panel, which represent the platform for the next level of floors. This building technique, in fact, is known as “platform frame”. On the

other hand, if the vertical elements are continuous at each floor, the assembly method is known as "balloon frame".

In the past 15-20 years, experimental programmes have investigated the hysteretic behaviour of LFT walls and buildings, proving their good performance in case of seismic event thanks to the limited weight and the high ductility and energy dissipation, which is ensure by sheathing-to-framing and wall-to-foundation connections. It is worth noticing that balloon frame and platform frame houses were generally built directly by carpenters, while nowadays the construction is part of a prefabrication process, where the LFT panels arrive at the yard site complete with thermal insulation, water, heating and air conditioning systems, and building finishes (Fig. 2).

Fig. 2 – Example of Light-Frame Timber building from the CASE project of L'Aquila (image from [4]).

However, structural lightness and low massiveness represent also a weak point for areas culturally linked to other construction technologies like masonry and concrete, thus preventing further spread of LFT buildings. Moreover, the system is not suitable for high-rise buildings, where CLT and hybrid solution are more convenient.

1.1.2 Heavy-Frame Timber

Heavy timber frames are present also in cultural and heritages. An example are Chinese temples, were massive columns with diameters of 400-700 mm were used together with mortise-tenon joints. The flexibility ensured by timber and joints, and the dissipation through

friction of the mortise-tenon carpentry, allowed these structures to face earthquake actions.

Recently, advanced knowledge in timber engineering allowed the introduction of multi-span and multi-storey wooden buildings, built with moment resisting frames (Fig. 3). Since timber is an elastic-fragile material, modern seismic regulations (e.g. EC8) allocate the dissipation in joints. Joints, in fact, can dissipate energy through the plastic deformations of metallic connectors. However, joints are also the structural elements that carry vertical loads.

In recent times, with regards to the seismic resistant structural type, the acquired knowledge and technology on timber engineering allow to introduce timber multi-storey multi-span buildings, with moment resisting frames and concentric or eccentric braced structures, widely used in the seismic resistant steel structures (Fig. 4).

Fig. 3 – Example of Heavy-Frame Timber building from the CASE project of L'Aquila (image from [4]).

Moreover, heavy moment resisting frame can be used were shear walls cannot be positioned. It is the case, for example, of Japan houses where narrow sites in urban areas are present. These houses with garages, parking areas, and stores show the impossibility of arranging shear walls, and, thus, moment resisting frames are necessary to face seismic action.

Fig. 4 – Innovation Factory, Hellbronn (Germany), from Waechter Architects.

However, in moment resisting frames, the beam-column connection not only dissipates energy during seismic action, but needs also to carry vertical loads. Thus, it has an important role in bearing the design loads. Therefore, in order to possibly design dissipative timber structures, the dissipation capacity should be provided by ad hoc conceived devices. Several innovative solutions are available in the literature.

Post-Tensioned Timber (PTT) uses timber as the primary material for structures. This system uses unbonded stressed steel cable or bars inside timber beams, together with energy dissipaters (Fig. 5)[5].

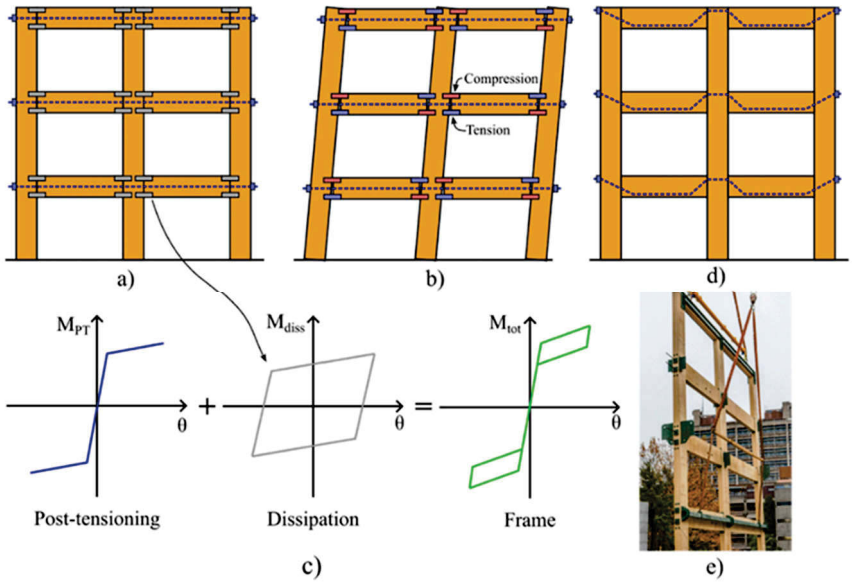

Fig. 5 – Seismic performance of a PTT structure (from [5]).

Rocking between beam and column, tendon stretching, and plastic deformation of the dissipaters allow the system to resist lateral loads and dissipate seismic energy. Moreover, this technology can be used to achieve longer spans, if the structure is located in low-seismicity areas.

Another efficient solution to design heavy frame timber buildings involves steel links. Steel links can provide a high dissipative capacity under lateral load. On the other hand, the vertical loads are carried by standard steel connections, which should be designed according to a Capacity Design approach, in order remain in elastic field.

1.1.3 Cross Laminate Timber

Cross Laminated Timber (CLT) consists of several layers of lumber boards, glued together on the wide faces typically at 90 degrees. CLT panels are generally composed by 3 (minimum) up to seven layers, and even more in some cases.

CLT structures have several advantages, starting from structural robustness, cost and constructional efficiency. Moreover, the possibility of deigning ductile joint between panels and the greater in-plane stiffness of CLT wall with respect to traditional timber buildings, make CLT structure an interesting solution in earthquake prone areas (Fig. 6).

Fig. 6 – Example of CLT building from the CASE project of L'Aquila (image from [4]).

Generally, the vertical panel-to-panel joints and wall-to-base connections (hold-downs and angle brackets) are designed to dissipate energy thanks to plastic deformation (Fig. 7). Floor panel-to-panel and panel-to-wall screwed connection are typically brittle. Moreover, also corner wall-to-wall vertical joint show a brittle behaviour [6]

CLT buildings can adopt a balloon-type or a platform-type assembly method. In balloon-type construction, CLT walls are continuous over two or more levels. In some cases, the panel reaches the whole building height. On the other hand, in platform-type buildings, each floor is the base for the CLT wall of the storey above.

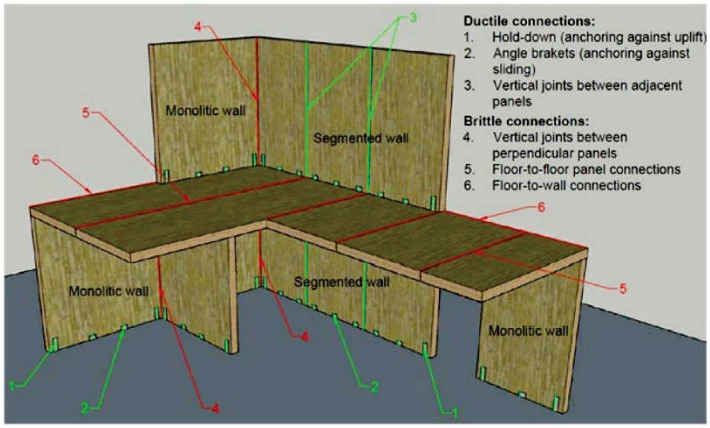

Fig. 7 – Platform frame CLT building, with indication of dissipative and non-dissipative joints (from [6]).

1.1.4 Hybrid Structures

Heavy timber frame, light timber frame and also CLT system can be coupled to other construction materials, such as concrete or steel.

Reinforced concrete cores and shear-walls are used to carry lateral actions like wind or earthquake forces, while timber elements transfer gravity loads to the foundation. Floor and roof diaphragms are also made of glulam (Fig. 8).

Fig. 8 – Gleis21, Vienna (Austria), 2019.

Furthermore, examples of hybrid structures include light frame timber walls with mass timber floors and roofs, steel elements for long-span timber floor systems (Fig. 9).

Fig. 9 - Rhode Island school of design (from woodworks.org).

1.2 Seismic Regulations

Current seismic design practice allows the engineers to use a so called "behaviour factor q" in order to decrease the seismic design action. According to the Eurocode, q is the "factor used for design purposes to reduce the seismic actions in a linear static or modal analysis in order to account for the non-linear response of a structure, associated with the material, the structural system and the design procedures". In fact, the behaviour factor involves not only the dissipative capacity of the components (i.e. connections for timber buildings), but also design and material overstrength. Herein, an overview on European and extra European codes is presented.

1.2.1 Eurocode

According to Eurocode 8 [7], structures in seismic prone regions should be designed according to a "no-collapse requirement". In particular, the buildings must be designed for a reference seismic action, associated with a typical probability of exceedance of 10% in 50 years, which corresponds to a return period of 475 years. Percentage and return period can vary according to the building typology. Moreover, the structure must not lose its structural integrity after the earthquake, ensuring a residual load carrying capacity. In addition, building should satisfy a "damage limitation requirement", thus avoid damage under earthquake of larger probability of exceedance, typically set to 10% in 10 year (return period of 90 years).

In order to satisfy the Ultimate Limit State, structure should be designed both in terms of resistance and energy dissipation capacity. In timber structures, mechanical joints are the elements where severe plastic deformation occurs and where the energy is dissipated. On the other hand, other elements are provided with sufficient strength (i.e. the timber elements, which show brittle failure mechanisms).

The q-behaviour factor proposed by EC8 are reported in Fig. 10. For example, Light-Frame timber buildings are associated to "High capacity to dissipate energy", allowing a maximum q-factor of 5.0. It is

worth noticing that the suggested value is quite high for European LFT buildings.

Table 8.1: Design concept, structural types and upper limit values of the behaviour factors for the three ductility classes.

Design concept and ductility class	q	Examples of structures
Low capacity to dissipate energy - DCL	1.5	Cantilevers; Beams; Arches with two or three pinned joints; Trusses joined with connectors.
Medium capacity to dissipate energy - DCM	2.0	Glued wall panels with glued diaphragms, connected with nails and bolts; Trusses with doweled and bolted joints; Mixed structures consisting of timber framing (resisting the horizontal forces) and non-load bearing infill.
	2.5	Hyperstatic portal frames with doweled and bolted joints (see **8.1.3(3)**P).
High capacity to dissipate energy - DCH	3.0	Nailed wall panels with glued diaphragms, connected with nails and bolts; Trusses with nailed joints.
	4.0	Hyperstatic portal frames with doweled and bolted joints (see **8.1.3(3)**P).
	5.0	Nailed wall panels with nailed diaphragms, connected with nails and bolts.

Fig. 10 – Table 8.1 from EC8 for the q-behaviour factor of timber structures (from [7]).

1.2.2 Italian Building Code

To perform linear static or dynamic analysis, the Italian building code [8] proposes q values for low- and high-ductility class. With respect to Eurocode 8 [7], the Italian code considers two static ductilities of fasteners to define the structural ductility classes. A ductility equal to 4 allow to design in low-class, while a static ductility equal to 6 is the minimum to design in high ductility class. Behaviour factors are reported in Fig. 11.

For light frame timber buildings, ("Pannelli di parete a telaio leggero con diaframmi chiodati, collegati mediante chiodi, viti e bulloni"), the code proposes the same value of the eurocode. On the other hand, a q=3 is suggested for low ductility class CDB. As mentioned previously, it is worth noticing that a value of 5 can be considered quite high, since do not reflect the European typical construction assembly. As mentioned before, light frame timber was built on site, while European LFT segments are typically precast.

Moreover, updated values for CLT ("pannelli di tavole incollate a strati incrociati") are needed, since q=2.5 appears too conservative [9].

Tab. 7.3.II – *Valori massimi del valore di base q_0 del fattore di comportamento allo SLV per diverse tecniche costruttive ed in funzione della tipologia strutturale e della classe di duttilità CD*

	q_0	
Tipologia strutturale	CD"A"	CD"B"
Costruzioni di legno (§ 7.7.3)		
Pannelli di parete a telaio leggero chiodati con diaframmi incollati, collegati mediante chiodi, viti e bulloni Strutture reticolari iperstatiche con giunti chiodati	3,0	2,0
Portali iperstatici con mezzi di unione a gambo cilindrico	4,0	2,5
Pannelli di parete a telaio leggero chiodati con diaframmi chiodati, collegati mediante chiodi, viti e bulloni.	5,0	3,0
Pannelli di tavole incollate a strati incrociati, collegati mediante chiodi, viti, bulloni Strutture reticolari con collegamenti a mezzo di chiodi, viti, bulloni o spinotti Strutture cosiddette miste, con intelaiatura (sismo-resistente) in legno e tamponature non portanti		2,5
Strutture isostatiche in genere, compresi portali isostatici con mezzi di unione a gambo cilindrico, e altre tipologie strutturali		1,5

Fig. 11 – Table 7.3.II of the Italian Building Code reporting the q-behaviour factors for timber structures [8].

1.2.3 Canadian Regulations

In Canada, wooden structures are common. In particular, LFT platform-type structures are widely used. The Canadian National Building Code NBS [10] specify the loads for structural design, CSA086 [11] provides designers with the methodologies for calculating the resistance values of structural wood products to resist gravity and lateral loads, while material resistance is given by material standards.

Since the experience in design and construction practise gained in wooden structures over the years, Canadian regulation allow a simplified procedure for small size buildings. In particular, they can be built without a full structural design. The structure is based only on simple rule given by construction practices that have a proven performance history, reported on Chapter 9 of the code. Generally prescriptive use is allowed if the following conditions are met:

- three-stories or less,
- 600 m^2 or less,
- uses repetitive wood members spaced within 600 mm,
- spans are less than 12.2 meters,
- floor live loads do not exceed 2.4 kPa,

- residential, office, mercantile or medium-to low-hazard industrial occupancy.

If the aforementioned conditions are not satisfied, a complete structural design is needed, considering both chapter 4 and chapter 9 of the National Building Code of Canada (NBCC).

It is worth noticing that provision for CLT structures are not yet present. However, CLT handbooks and guides are available from FPInnovations and Canadian Wood Council [12].

1.2.4 U.S. Regulations

As in Canada, also in the United States wooden structures are widely spread, both for residential and medium/high-rise buildings. Similarities to Canadian regulation are present, and small timber houses do not need specific structural design, which is mandatory for more important buildings. Larger structures, like multi-storey buildings, should be designed according to the International Building Code [13]; in particular, static and seismic design of timber structures are reported in chapter 16 and 23 of the IBC.

1.3 Objectives and scopes

Following earlier studies, this study aims to contribute towards the calibration of a reliable q-factor for light frame buildings. In particular, considering that 3D irregular structures are more vulnerable to earthquakes, the main goals are:

- To define a reference range of structural behaviour factors q for LFT buildings, analysing full 3D models subjected to bi-directional ground motion input;
- To investigate the sensitivity of the q-factor to irregularities, both in plan and in elevation.

Compared to other studies in the literature, this research considers in fact full 3D models for selected reference buildings, which are

subjected to twenty pairs of accelerograms. Each pair is applied simultaneously to these buildings, monitoring the 3D structural behaviour, and deriving useful feedback for the estimation of the q-factor. The results of this research were first published in [14]. In this dissertation, parts of the original article are reproduced with permission from Springer Nature.

1-2 LIGHT-FRAME TIMBER WALLS

Light Frame Wood (LFT) shear walls are made up of a frame, with regularly spaced vertical studs, and timber-based panels (typically Oriented Strength Board OSB, plywood gypsum), which are connected together along the perimeter by small diameter nails. Hold-downs are used at the corners to absorb tension induced by bending moment (compression is transferred by contact of wall-frame elements to the slab), while angle brackets are used for shear forces at the base and the top of the panel.
The following paragraph discuss the in-plane behaviour of the LFT walls. Furthermore, a section is dedicated to the crucial role of the connections. Finally, innovative solution for Light-Frame structures are presented and FEM modelling strategies are discussed.

2.1 In-Plane behaviour

The stiffness of a LFT wall subjected to a lateral force, and therefore its top displacement, can be evaluated by the sum of different contributions, which are shown in Fig. 12. The total stiffness K_w of the wall follows equation (1), where δ_w is the total top displacement of the wall, δ_c is the deformability linked to the base rotation, δ_s is the shear panel deformation, δ_{ns} is the sheathing-to-frame deformation, δ_b is the bending deformation of the wall and δ_{sf} is the horizontal slip due to the shear connectors.

$$K_w = \frac{1}{\delta_w} = \frac{1}{\delta_c + \delta_s + \delta_{ns} + \delta_b + \delta_{sf}} \quad (1)$$

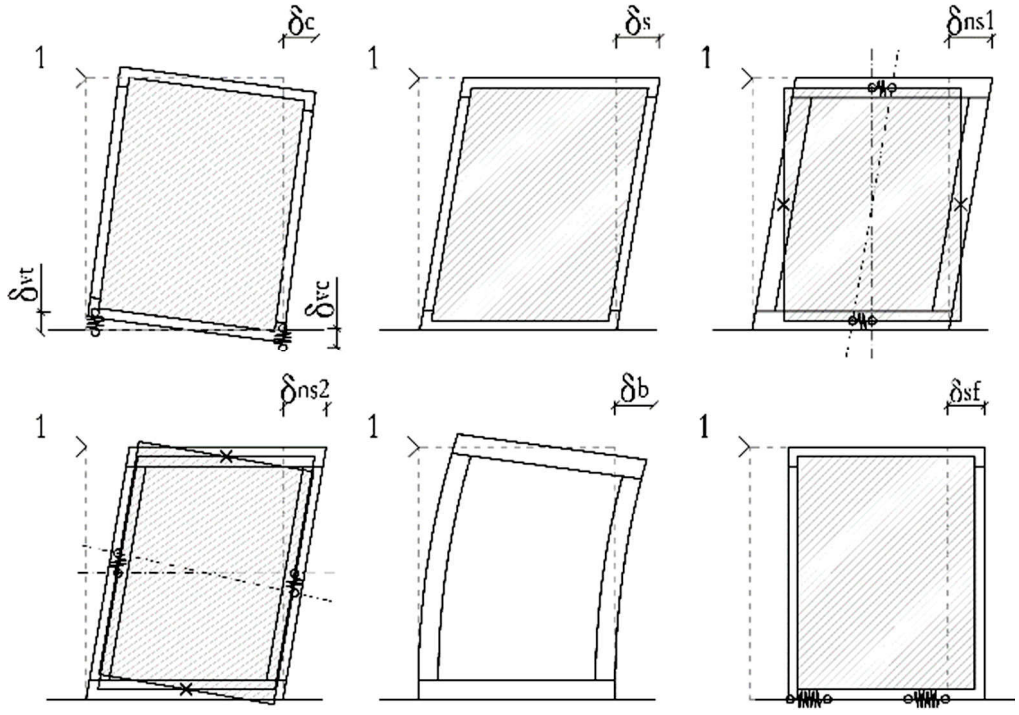

Fig. 12 – Contributions to top displacement of a LFT shear wall.

International codes propose analytical methods to evaluate the stiffness of LFT, starting from the contribution evidenced in Fig. 12.

New Zealand Standard [15] considers the deformability of the LFT wall as a sum of four components. The deflection, in fact, includes the base rotation δ_c, the shear deformation of the wood panel δ_s, the shear deformation of the sheathing-to-frame connection δ_{ps} and the bending deformation δ_b. The total displacement of the wall δ_w is evaluated by means of equation 2.

$$\delta_w = \delta_c + \delta_s + \delta_{ps} + \delta_b \tag{2}$$

The New Zealand standard [15] equation does not consider the rigid body motion of the wall due to the deformation of the angle brackets. The slip is negligible only if the connectors are designed following a Capacity Design approach and therefore are extremely stiff. Otherwise, it is always possible to add the base slip contribution to equation 2.

In Fig. 13 the contribution of the different components of the drift are evaluated according to for ideal LFT panels with an height of 3 m, but with different lengths. The percentage related to the role of nail deformations increases at the growing of the base length.

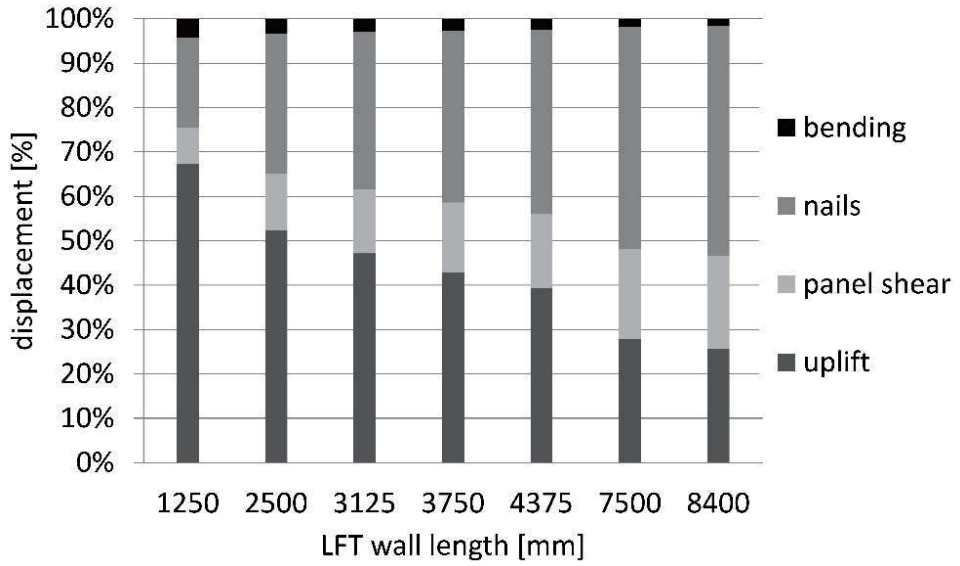

Fig. 13 - Percentage values for the different components of the top displacement of a LFT wall according to [15].

Even for the American International Building Code IBC [13] and for the Canadian Standards Association CSA O86 [11], the top displacement of an LFT wall is the sum of four terms: the inter-storey displacement due to flexural deformation, the shear deformation of the panel, the sliding of the nails and the deformation due to the lifting of the wall. The parameters to compute the stiffness are derived from tables depending on the geometry of the wall, the materials used for the frame and the panels and the diameter of the nails used for the sheathing to frame connection. The formulations are calibrated on analytical and experimental results.

Thus, to represent the LFT behaviour in a FEM model, it is necessary to describe all these contributions, in order to obtain results as close as possible to the actual one.

2.2 Connections

Connection have a fundamental role in the mechanical properties of the LFT walls and in the dissipation capacity. However, timber is a brittle material both subjected to tensile or bending, and, thus, energy dissipation has to be allocated in the mechanical joints. Therefore, dissipation is linked to metal fasteners plasticization and to the embedment of timber at the interface with the fasteners. Typically, the dissipation is allocated in the sheathing-to-framing connection, whereas the hold-downs and the angle brackets remain elastic. Furthermore, the non-dissipative connections and timber elements need to be designed according to the capacity design approach [16][17][18].

In order to transfer the lateral loads to the foundations, the building has to be anchored to the storey below and then to the foundations. Anchoring is normally required at both ends of shear walls to account for uplift forces and at the bottom plate to account for the sliding, see Fig. 14.

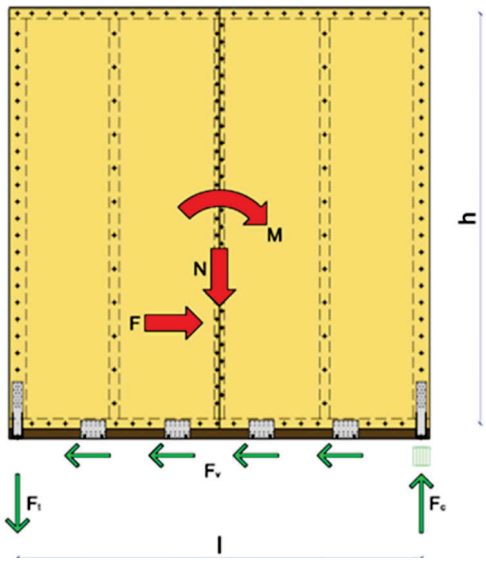

Fig. 14 – Actions on a LFT shear wall. The bending moment M is transferred thanks to hold-down at the end; the shear force F is taken by angle brackets. Axial force is generally transferred by contact (from [19]).

Uplift and sliding forces are anchored independently with specific connectors, hold-downs and angle-brackets respectively.

In the following paragraphs, the typical wall-to-wall, wall-to-foundation and sheathing-to-framing connection are described.

2.2.1 Hold-downs

Hold-downs are the "standard" connection to transfer the bending overturning moment of the shear wall to the foundation. The connection between the hold-down and the timber wall is obtained by screws or nails, which can be designed to be dissipative or not. The first case is typical of CLT buildings. The second one of low- and mid-rise LFT structures, where the energy dissipation is concentrated in the sheathing-to-framing connection. The hold-down is then anchored to the foundation by mean of a bolt.

Fig. 15 shows the failure mode occurring in hold-down connections.

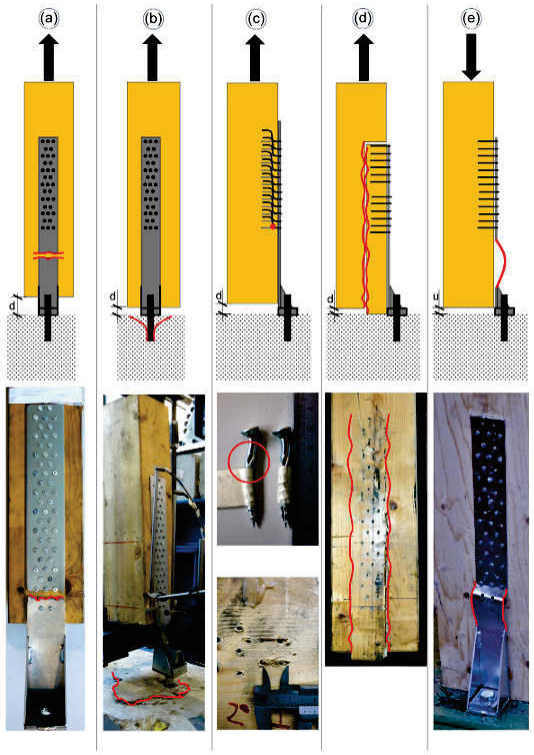

Fig. 15 – Typical failure modes for hold-down connection: (a) steel break-out in tension, (b) anchorage's failure, (c) plastic hinge of screws combined to embedment of timber plug-shear, (e) buckling of steel flange. (from [20])

In particular: (a) steel break-out in tension, (b) anchorage's failure, (c) plastic hinge of screws combined to embedment of timber plug-shear, (e) buckling of steel flange.

Several works in the literature have investigated the non-linear behaviour of hold-downs, using monotonic and/or dynamic approaches.

In [19] a set of 5 hold-downs was subjected to cyclic test.

Fig. 16 show the results of the non-linear cyclic behaviour. The "W" in the label highlight the absence of OSB between the connector and the frame stud. Since the compression is transferred by contact between the steel plate and the foundation, the compression branch is neglected. No instability of steel flange occurred. The label refers to the hold-down model (See [19]).

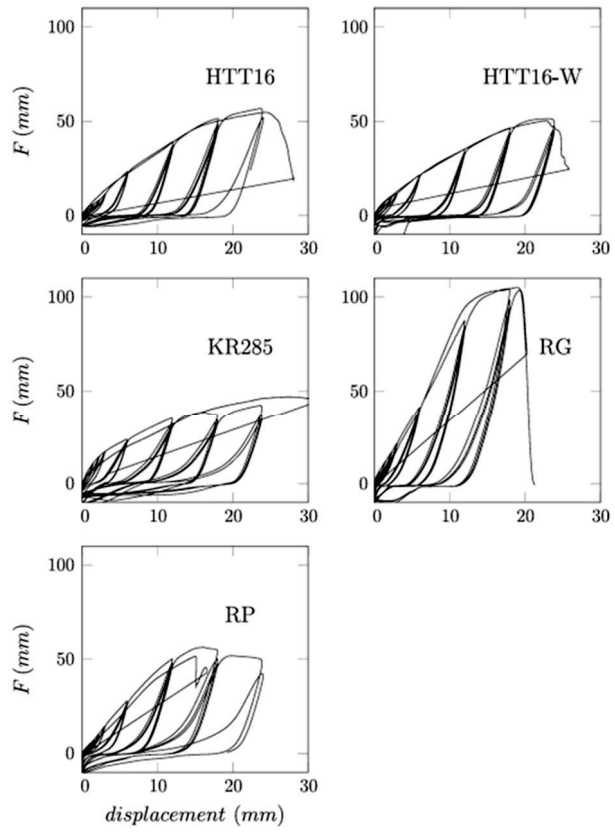

Fig. 16 – Hold-down hysteretic behaviour from [19].

In [21] the hold-downs were cyclically tested considering bidirectional loading (Fig. 17). The investigation showed that additional

force in the other direction has a limited effect on axial capacity of the connector, but the hysteretic affects intensely the behaviour. Furthermore, the shear and tension behaviours are relatively independent.

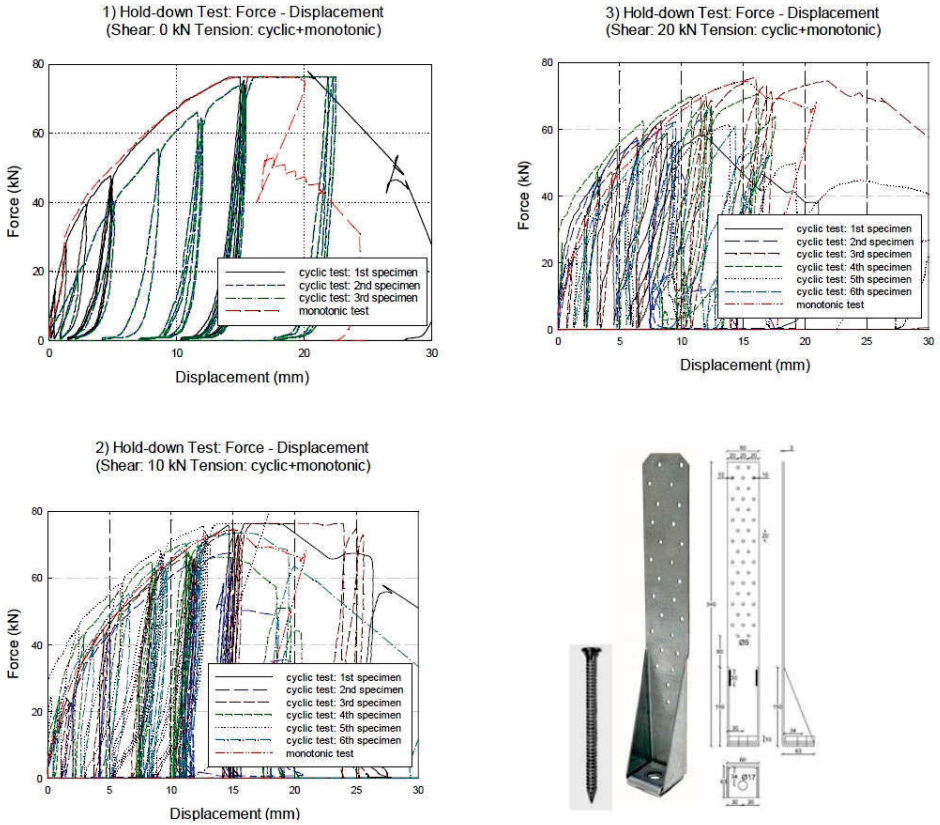

Fig. 17 – Hold-down behaviour in tension varying the acting shear force (from [21].)

New hold-down devices are nowadays designed, in order to improve dissipation capacity especially for CLT buildings. In [22] a novel dissipative hold-down was studied, showing that the connections achieved high ductility with stable energy-dissipating capacity, demonstrating the possibility of providing not only high ductility but also great energy-dissipating capacity.

2.2.2 Angle Brackets

The angle brackets transfer the shear from the wall to the foundation or wall-to-wall between adjacent floors. Their behaviour involve multiple force and bending components (Fig. 18), however the

design phase usually focuses on the shear force, which is the relevant action.

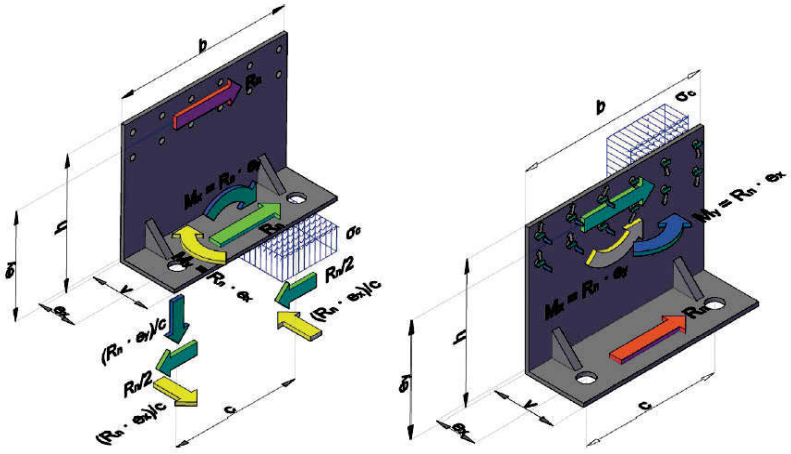

Fig. 18 – Force on angle brackets: anchor bolts (left) and fasteners (right). (From [19])

Several papers in the literature have studied the mechanical behaviour of this type of connection. Typical symmetric non-linear behaviour can be seen in Fig. 19; for label interpretation please see [19].

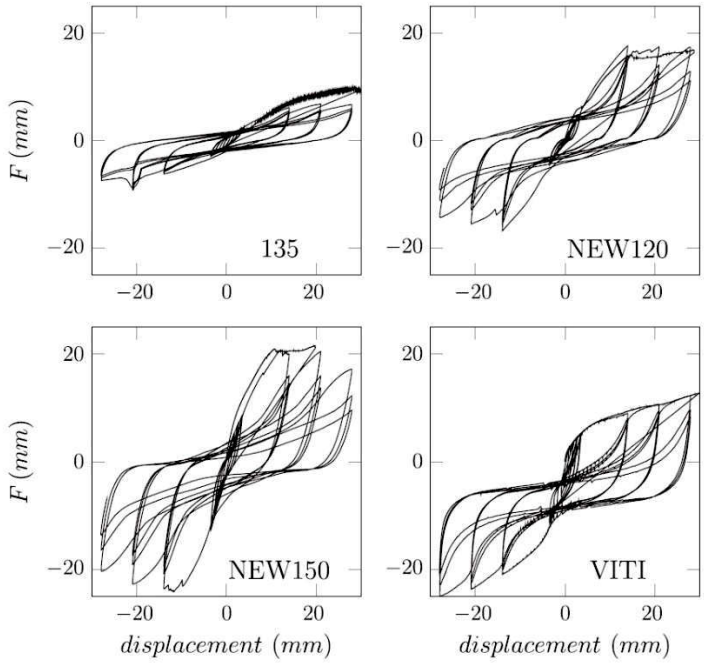

Fig. 19 – Force-displacement cyclic curves for angle brackets (From [19])

Furthermore, in [21] the angle brackets were cyclically tested considering bidirectional loading (Fig. 20). The results highlighted that the shear strength and tensile strength of angle bracket are close and that the shear behaviour and tension behaviour are coupled.

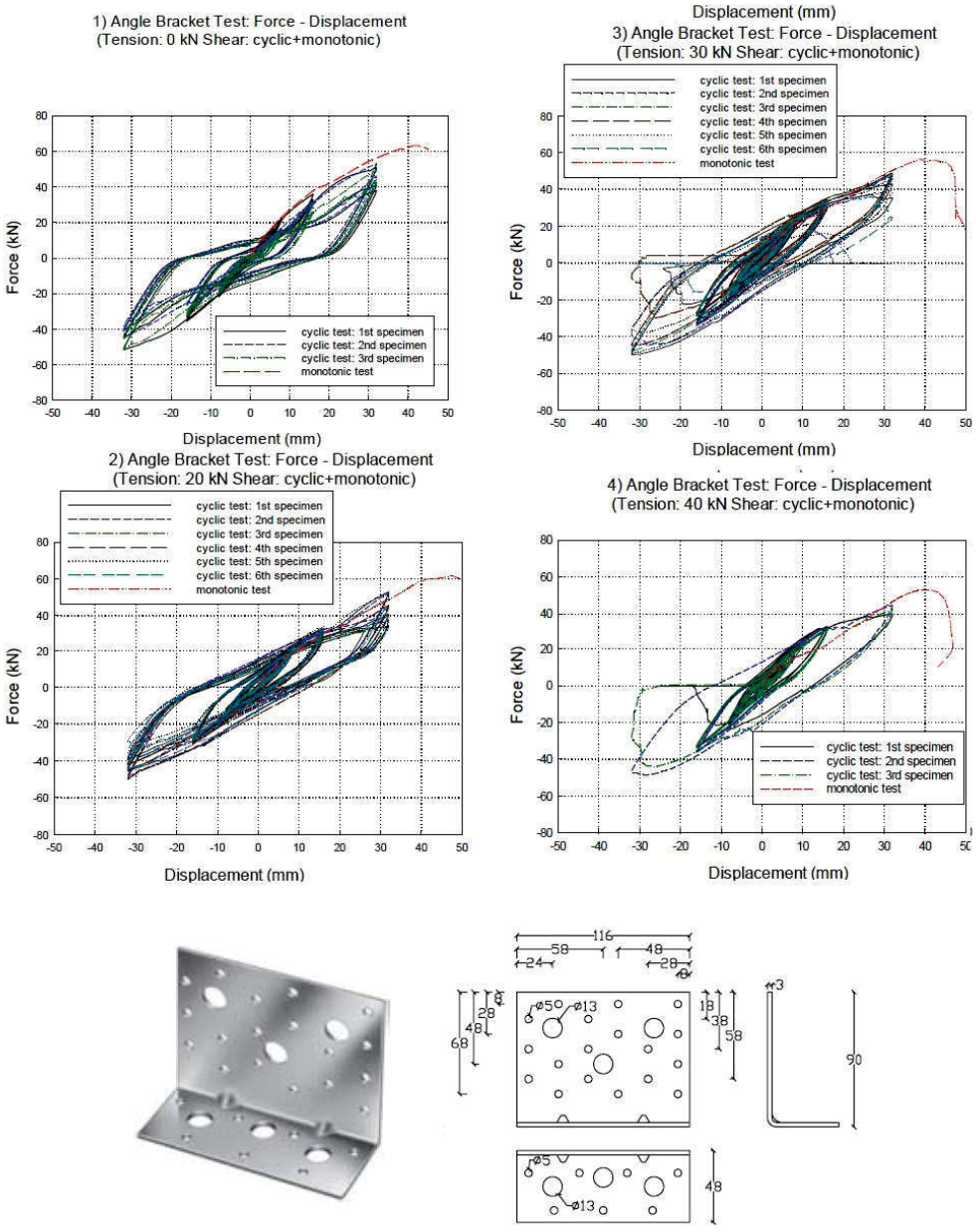

Fig. 20 – Angle brackets tested in shear varying the applied tension force (from [21])

Moreover, also in [23], authors experimentally tested angle brackets subjected to loads acting in different directions. Fig. 21 shows the multi-

directional mechanical behaviour of angle brackets evaluated from monotonic test in tensile. The label of each curve corresponds to the test ID; refer to the paper for further details. The experimental campaign show that the tested connectors are characterized by significant strength and stiffness for different load configurations.

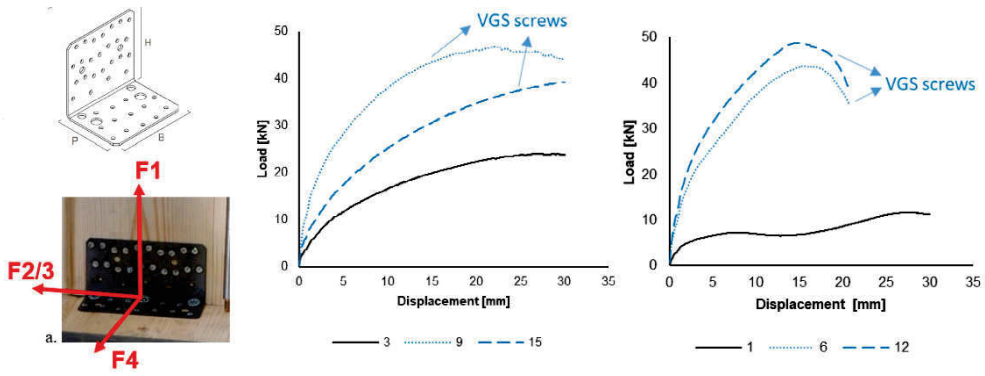

Fig. 21 – Monotonic test on angle brackets (from [23]).

2.2.3 Sheathing-to-framing connection

The global hysteretic behaviour of a LFT wall is mainly governed by the sheathing-to-framing connection. If the other connections (i.e. angle brackets and hold-downs) are calculated according to the Capacity Design, thus deforming linear-elastic, the plastic behaviour of the wall is allocated only in the sheathing-to-framing connection.

A typical nailed connection behavior can be found in [24], see Fig. 22. In the early phase, the force-displacement relationship is linear, and both connector and timber fibers remain elastic. As loading and thus the displacement of the connector increases, the wood fibers crush, causing the possible nail yield. Since a gap is formed in the crushed timber fibers, when the loading is reversed, the connection exhibits low stiffness and strength until the connector again encounters the wood.

Several studies in the literature have tested both experimentally and numerically the behaviour of the sheathing-to-framing connection. Several experimental tests were carried out on typical European LFT shear-walls sheathed with either wooden or gypsum panels by Grossi et al. [25][26] and by Seim et al [27].

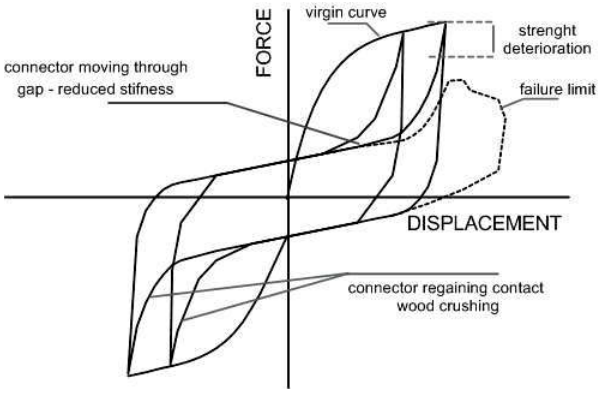

Fig. 22 – Typical cyclic behaviour of a sheathing-to-framing connection (from [24]).

In [28] the authors present the experimental results obtained from tests both on connections between the sheathing panel and a timber stud and on full-scale prefabricated timber frame shear walls. It is worth noticing that the aforementioned tests were performed on European typical connection, that are generally different from in-situ building common in other countries such as U.S.A or Canada.

The cyclic results of smooth nails (a), ring nails (b, c) and staples (d) are reported in Fig. 23.

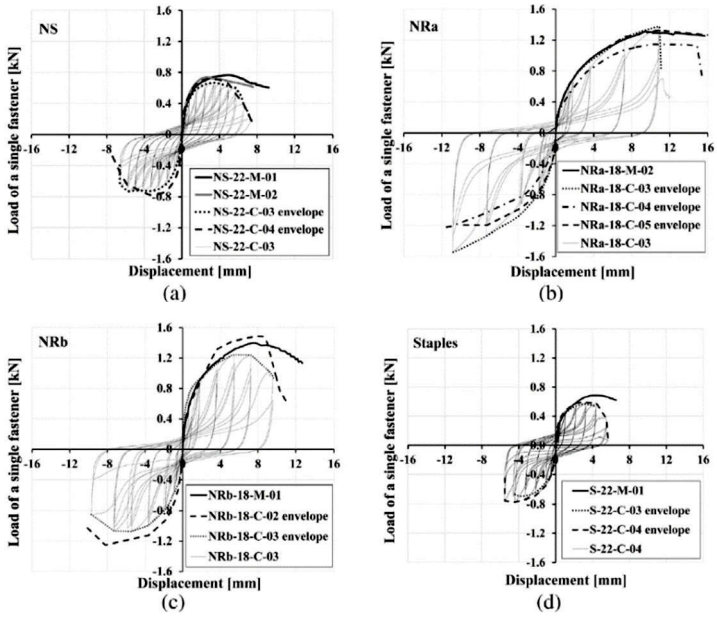

Fig. 23 – Cyclic non-linear behaviour of sheathing-to-framing connection: smooth nails (a), ring nails (b, c) and staples (d). (From [28])

Moreover, in the same study a full-scale LFT wall was cyclically tested, highlighting the crucial role in the dissipation and in the horizontal deformation of the sheathing to framing connection, where 80-90% of the total energy dissipation is concentrated (Fig. 24).

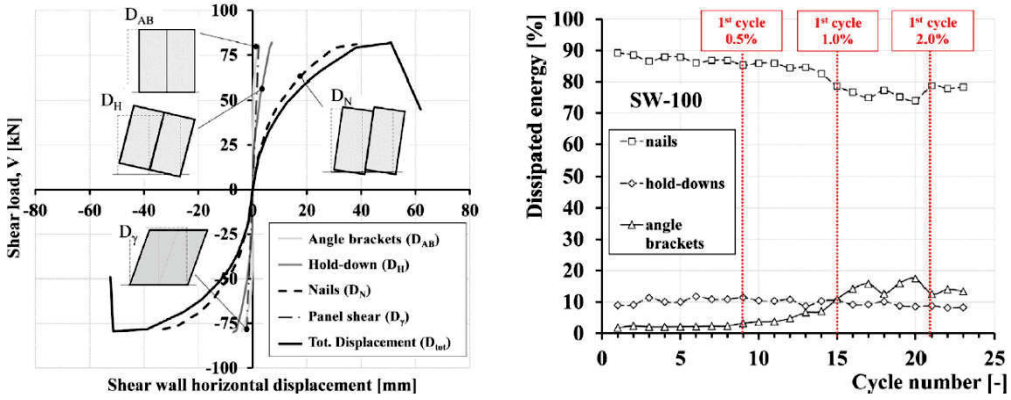

Fig. 24 – Single dissipation components in a LFT shea wall. Backbone curve (left) end dissipated energy (right). Image from [28]

2.3 Novel LFT walls

Alongside the most widespread construction technology for LFT walls, other innovative possibilities have been studied over the years. Next paragraphs show three of the evolution of LFT walls.

2.3.1 Self-centering walls

LFT walls exhibit high ductility and energy dissipation, however relevant residual deformation remains after seismic events. In order to improve the self-centering capacity of the walls, [29] shows the benefits of installing two diagonal steel cable in the LFT frame (Fig. 25). The work shows that pre-tensioning the cable has a great influence on the mechanical behaviour of the system, with an increase of peak load (+77% ÷ +79%), stiffness (+70% ÷ +119%), energy dissipation (+27% ÷ +39%). and self-centering capacity (+73% ÷ 79%) with respect to the no-cable configuration.

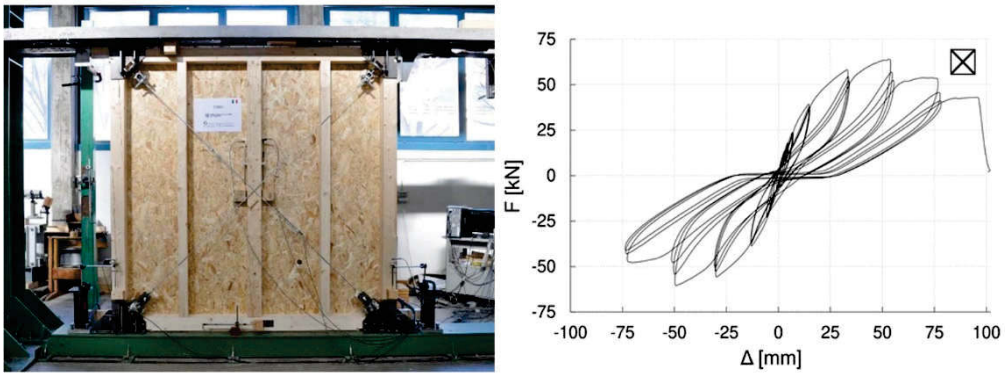

Fig. 25 – On the left, LFT walls with self-centering cable; on the right, non-linear cyclic behaviour of the wall with cables (From [29]).

2.3.2 Hybrid Glulam-OSB walls

In [30] the cyclic lateral behaviour of a new hybrid timber shear wall called Glulam-Frame OSB was studied (Fig. 26). A Glulam frame is connected to the OSB sheathing by means of conventional nails. This technology allows to obtain significant higher strength and stiffness, reaching three times the properties of a CLT wall. Furthermore, the high ductility makes this solution suitable for seismic prone areas. The usage of timber is lower than a CLT wall, but higher with respect to traditional LFT walls.

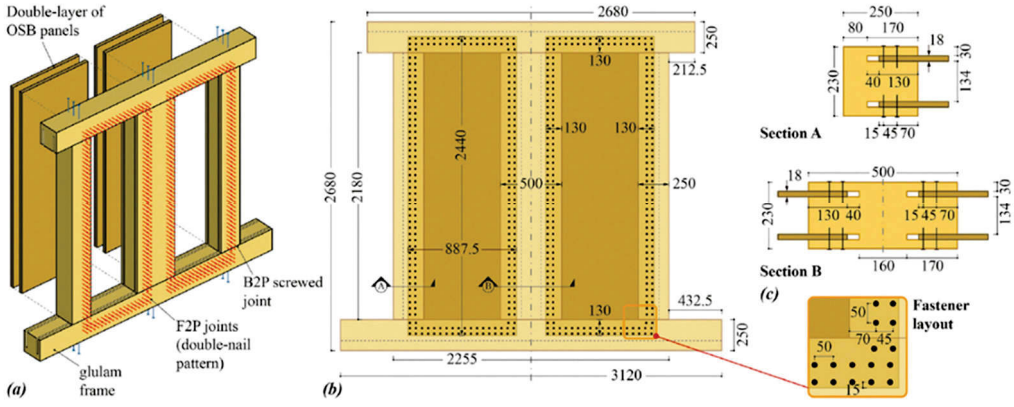

Fig. 26 – Hybrid Glulam-OSB Light-Frame walls from [30].

2.3.3 Hybrid Steel-OSB light frame walls

Even if LFT show high ductility and energy dissipation, often highlight limited in-plane shear resistance. To overcome this problem,

Trutalli et al [31] developed a novel constructive system, composed by steel columns and OSB panel, connected by means of self-drilling screws (Fig. 27). The experimental results show that the system is characterized by high in-plane shear strength and good ductility and dissipative capacity. However, only one specimen was tested, and more test are needed.

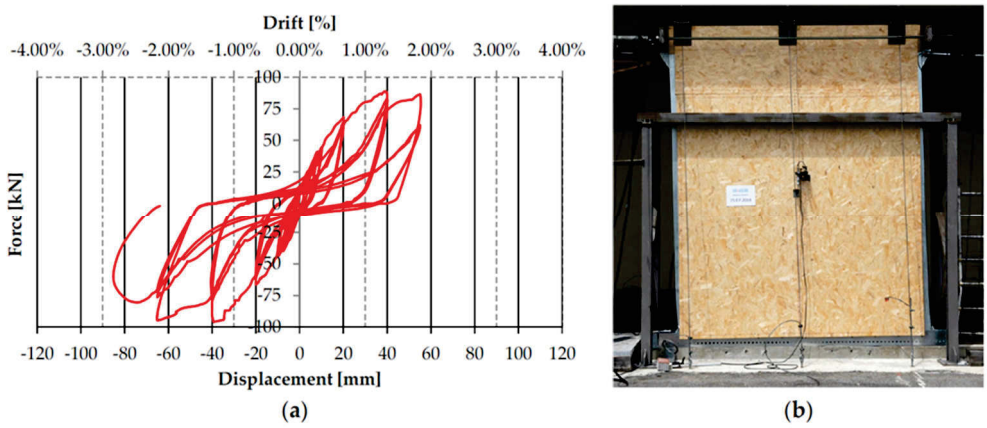

Fig. 27 – Hybrid steel column and OSB panels shear wall proposed by [31]

2.4 FEM modelling approaches

Different approaches to model timber walls are available in the literature, both linear and non-linear. Linear methods are usually used by engineers in the design phases, while non-linear methods are generally applied for research purposes.

When talking about timber shear walls, two typologies are usually considered: CLT for mid- and high- rise buildings and LFT for low- and mid-rise structures. In both linear and non-linear cases, the FEM model of a CLT wall is the assembly of a panel model and panel-connection models. In addition, in the case of a LFT wall, the connection between the sheathing and the frame has to be considered. Since modelling strategies for these two kinds of shear wall are similar, both will be herein discussed.

CLT panels can be described by means of frames or shell elements. In the first case, a hinged frame with a diagonal spring (or truss) is modelled. The diagonal is calibrated to represent the shear and bending deformation of the panel [32][33]. Furthermore, the panel can also be

modelled by a single equivalent frame, as in [34]. In the second case, a 2D shell element is used, either isotropic (defining an equivalent elastic modulus) or orthotropic [9][35][36][37].

LFT walls are typically modelled using beam elements for the framing and a shell element for the sheathing [38][39]. As reported in the following paragraph, the panel can be considered together with the sheathing-to-framing connection, defining an equivalent stiffness.

2.4.1 Component Level approach

In the CL approach, a link (linear or non-linear) is used to model each fastener (i.e. screws, nails) and each anchor (i.e. angle brackets, hold-downs). The CL method was applied by [34][40], where each hold-down and angle-bracket was assigned a linear behaviour.

The approaches to LFT are similar to CLT ones, but the contribute of the sheathing-to-framing connection has to be added. The connection between panels (i.e. OSB, Gypsum) and timber studs can be modelled with a CL approach, defining each nail as in [38][39].

2.4.2 Phenomenological approach

On the other hand, according to a PH approach, the behaviour of all the fasteners and anchors is condensed in a single link, which also englobes the properties of the CLT panel [32][33]. Nevertheless, the analyses in [41] highlight that this approach generally overestimate the uplift forces.

2.4.3 Hybrid approach

It is worth noticing that the modelling solutions do not always belong to one of the two aforementioned classes. Thus, a semi-CL approach can be defined when a single link (or spring) is used to represent a group of fasteners or anchors. Screws connecting the CLT panels were modelled with a single linear spring in [37]. In [42], the authors analysed the shear wall system both with a CL and a semi-CL approach. Finally, a new method was proposed in [43], modelling the

connections between panel and foundation/floors by means of an equivalent shell element.

For the LFT walls, on the other hand, a semi-CL approach can be used, englobing the sheathing-to-framing connection and the shear behaviour of the panel in a single spring [44][45].

1-3 Q-BEHAVIOUR FACTOR

The good performance of timber buildings under earthquake excitations is well known and largely acquired, due to the limited mass and the high ductility ensured by, for instance, mechanical connections between sheathing to framing, wall to wall, wall to foundation. Besides, hysteretic behaviour of LFW structures were investigated by means of tests on shake tables in past years [46][47][48].

It also well known that a reduction of seismic forces is possible due to the beneficial effects of energy dissipation in ductile structures and to inherent over-strength. This theoretical acquisition is considered in seismic design standards and codes, where force reduction factors (e.g. the 'behaviour factor' q in Eurocode 8 [7], or the 'response modification factor' R in US codes) are indicated to quantify the seismic design loads. The entity of these factors was initially based on empirical observations of the behaviour of common structural systems, but uncertainties still regard the value of q [49].

An important contribution for the calibration of the q factor is presented in [50] where the non-linear behaviour of LFT multi-storey shear-wall systems is analysed by means of Non-Linear Static (NLS) analyses. The results show a range of variability of the q factor, strongly dependent on the ductility of the base components. Anyhow the influence of higher modes and ground motion frequency on the distribution of shear and on base shear cannot be caught by Static non-linear analyses [51].

In [52], post-and-beam timber buildings were analysed via pushover analysis to evaluate a reliable q-factor value, which was finally

set to 3.0. The dissipation was allocated only in the sheathing-to-framing connection, that was calibrated on cyclic laboratory tests.

FEMA [53] proposes an archetype creation procedure and a non-linear dynamic analysis approach to evaluate the seismic performance of timber buildings, considering the confidence related to materials, FEM modelling and design requirements. However, presented procedure, as other reported in the literature [54], use simplified planar "pancake" model from [55], which is suitable for regular structures only. More recent works, like [56], use the FEMA procedure on complete 3D buildings, analysing LFT walls with wood screws only in one direction.

Different methods are available in the literature to estimate the q-factor, considering experimental, numerical and hybrid procedures [57].

3.1 Experimental test approaches

Typically, the q-behaviour factor can be obtain from quasi-static cyclic test or shaking table tests.

The first approach evaluates the factor starting from the displacement ductility, defined as the ratio between the ultimate and the yield displacement. However, it is worth noticing that, in timber structures, the yield point is not clearly defined, as the mechanical behavior of the connections involves both timber (brittle) and metal fasteners (ductile) and a not well-defined plastic branch is noticeable (Fig. 28).

According to EN12512 [58], the secant stiffness K is evaluated by means of equation:

$$K = \frac{0.4F'_{max} - 0.1F'_{max}}{s_{0.4} - s_{0.1}} \tag{3}$$

where F'_{max} is the actual maximum value when the corresponding slip is less than 15 mm, otherwise the load corresponding to a 15 mm slip is chosen, and $s_{0.4}$ and $s_{0.1}$ are the slip of the connection corresponding to loads equal to $0.4F'_{max}$ and $0.1F'_{max}$ respectively.

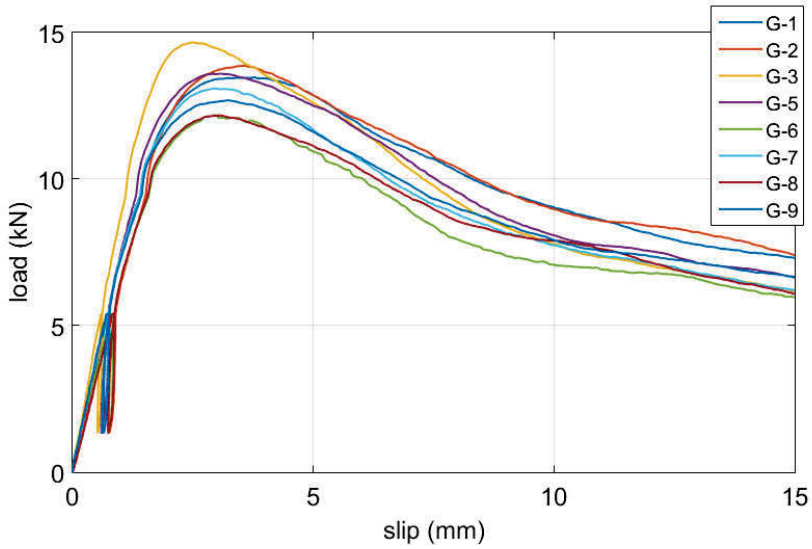

Fig. 28 – Typical behaviour of a timber-to-timber screwed connection, where a not well-defined plastic branch can be noticed. (From [59])

The ductility of the connection μ is defined in equation (3):

$$\mu = \frac{s_u}{s_y} \tag{4}$$

where s_u and s_y are the ultimate slip and the slip at the yield point respectively.

The ultimate slip corresponds to $0.80F'_{max}$. According to [58], when the curve does not have two well-defined linear parts, yield value is determined by the intersection of the following two lines: the first is the line drawn between points $0.4\ F'_{max}$ and $0.1\ F'_{max}$ of the curve, the second is the tangent line with an inclination of ⅙K (Fig. 29).

Shaking table tests, on the other hand, need a wide program set-up and full-scale specimen to be subjected to real earthquake accelerograms [32]. To this aim, several steps are necessary. The full-scale buildings are designed with q=1, i.e. elastic, according to a specified seismic code (e.g. EC8 [7]). The selected PGA represents the yield PGA. Then, the building is subjected to earthquakes, increasing the seismic intensity until the near-collapse condition is achieved. The q-behaviour factor is the ratio between the near-collapse and the design PGA. It is worth noticing that, with this method, the evaluated q-factor has a limited validity, restricted to the selected case study building and to the chosen

earthquake signals. Furthermore, the q-factor is code-dependent, since the building is designed according to a specific chosen standard.

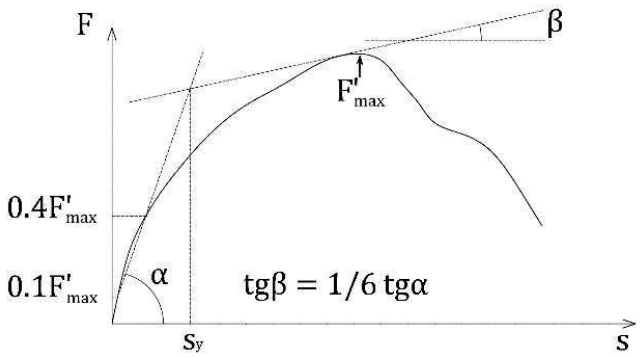

Fig. 29 – Procedure to define the yield displacement s_y according to [58]

3.2 Numerical approaches

Among numerical methods, an action-side or a reaction-side approach can be used to evaluate the q-factor. The action-side proposal of Ceccotti and Sandhaas [60] concerns the evaluation of q by means of the ratio between the near-collapse PGA and the design PGA. The analysed structures must be designed with q=1, and the near collapse PGA can be evaluated through IDA. This method was used to evaluate q for CLT buildings [61][6].

Alternatively, the typical reaction-side method to evaluate q is the ratio between the elastic and the plastic base shear. This approach is independent of the choice of the intensity measure characterizing the earthquake and can be carried out by means of non-linear static or dynamic analyses.

3.2.1 Non-linear static

The evaluation of the behaviour (or force reduction) factor is generally obtained by means of Non-Linear Static analyses via the procedure proposed by [62][63]. The q factor depends on the building displacement ductility and the characteristics period of the ground motion. Another procedure is the one proposed by [64].

In both cases the q-behaviour factor is the product of a ductility factor q_d, accounting for the ductility of the structure, and an

overstrength factor q_R, due to the structural redundancy (Fig. 30). See equation:

$$q = q_\mu \cdot q_D = \frac{F_{el,max}}{F_{EEEP}} \cdot \frac{F_{EEEP}}{F_{el}} \tag{5}$$

where $F_{el,max}$ is the base shear that would be obtained from an elastic analysis; F_{el} is the base shear when the first wall yields; F_{EEEP} is the base shear determined by adopting an EEEP approach [65].

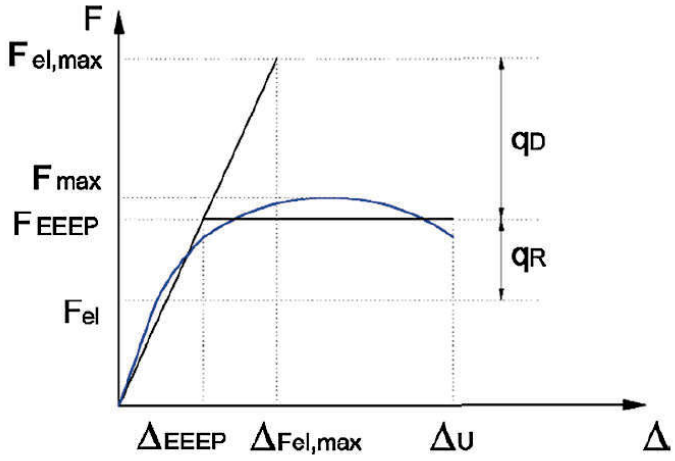

Fig. 30 – Equivalent Energy Elastic Plastic (EEEP) approach to individuate the ductility and overstrength factor (From [50]).

The first method [62][63] is known in literature as *N2 method*. The behavior factor evaluate with this method depends not only on the intrinsic ductility of the structure but also on the periods of the structures and of the ground motion., the one that marks the transition between the constant acceleration and constant velocity parts of the spectrum. [66] have shown that the *N2* method provides good results in evaluating the inelastic spectra for timber buildings while in [67] the *N2* method has been successfully applied to CLT structures. Furthermore, Rossi et al [50] used the N2 method to evaluate reliable range for the q-factor of LFT building.

The second method was proposed by Newmark and Hall [64]. With respect to the N2 method, the procedure requires only the ductility of

the building, and not the ground motion period. An estimation of the q-factor of CLT walls using this method is shown in [57].

In [50], the authors adopted the two methods obtaining some differences, negligible for low sheathing-to-framing ductility and greater for higher ductility.

3.2.2 Non-linear Dynamic

Non-linear dynamic analyses allow to overcome limitation due to static approximation of the dynamic problem, such as the hysteretic behavior (energy dissipation, stiffness and strength degradation) of the components and frequency content of the ground motion.

Three main strategies to execute the non-linear dynamic analyses can be considered: Cloud Analysis, Multi-Stripe Analyses and Incremental Dynamic Analysis. For all these methods, an Intensity Measure and an Engineering Demand Parameter has to be defined. The IM describes the signal, an accelerogram when a seismic analysis is performed. Typical IM are:

- PGA: Peak Ground Acceleration. This is an intuitive parameter. Its use is immediate in seismic assessment as in [68].
- HI: Housner Intensity demonstrated an excellent correlation with inter-storey drift [69][70].
- $S_a(T_1)$: This is the spectral acceleration corresponding to the first mode of the structure. This selection was adopted in the first studies of the IDAs [71][72][73].
- $S_{a,avg}$: This is the geometric mean of the spectral acceleration between $0.2T_1$ and $3T_1$. T_1 is the first mode of the structure. The mean acceleration allows to consider the contributions of the other vibration modes [74].

Cloud Analysis

The Cloud Analysis is based on simple regression in the logarithmic space of structural response versus seismic intensity for a set of registered records. To this aim, the structure is subjected to a set of

unscaled accelerograms, which makes the method more efficient with respect to MSA or IDA (Fig. 31).

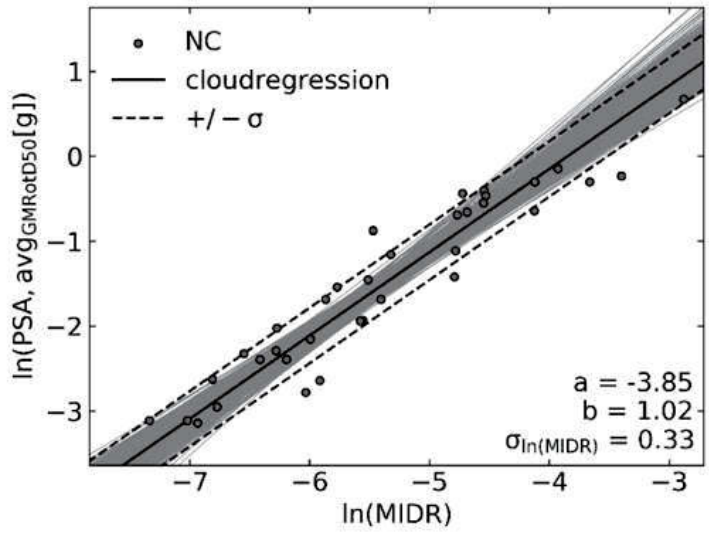

Fig. 31 – Example of Cloud analysis and linear regression from [75].

However, the assumption of a constant conditional standard deviation for probability distribution of the Engineering Demand Parameter (EDP) given the Intensity Measure (IM) is one of the several issues characterising this method: increasing levels of the IM, the conditional dispersion in displacement-based EDP's given IM may increase (see e.g., [71][76]). Furthermore, a strong dependence on the suite of ground motion records can be noted.

Multi-Stripe Analysis

Multiple-stripe analysis (MSA), consists in a group of stripe analyses performed at multiple Intensity Measure levels, where a stripe analysis is represented by a group of structural analyses for a set of ground motion records that are scaled to a common IM. Generally, the set of accelerograms used for each stripe corresponds to the seismic threat at a certain IM. However, there are example in the literature where a single set of accelerograms is scaled to all necessary IM levels. (e.g., [77][78][79]).

Fig. 32 shows a typical output of a MSA analysis, plotting the selected EDP (in this case the interstorey drift ratio) and the chosen IM

(Spectral acceleration). The cases corresponding to collapse (full circles) are distinguished from the non-collapsing ones: for the definition of collapse, see the IDA paragraph.

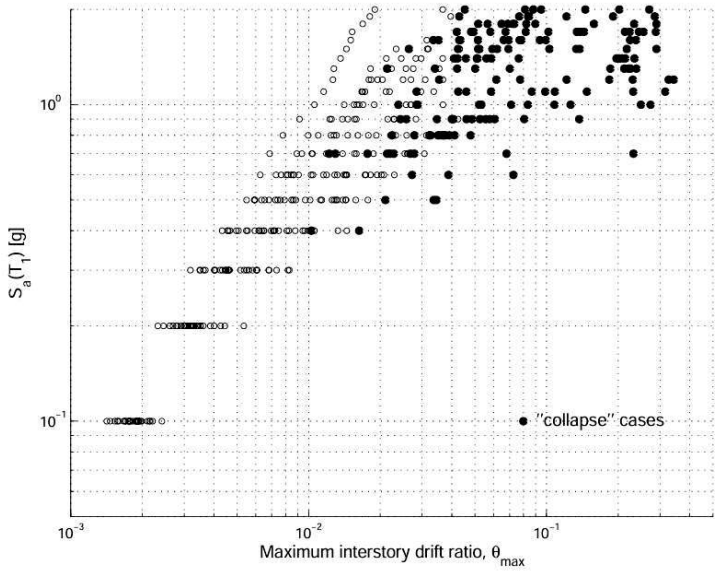

Fig. 32 – Example of MSA from [76].

Incremental Dynamic Analysis

IDA consists of the execution of several nonlinear dynamic analyses under a multiple-scaled set of ground motion records ([71]). Every IDA curve represents the relationship between the Engineering Demand Parameter EDP and the Intensity Measure IM (Fig. 33). With respect to Cloud and Multi-Stripe, IDA requires a large computational effort, since non-linear dynamic analyses have to been performed increasing the scale factor. One issue concerns the scale factor, that can introduce bias if the accelerograms are over-scaled. To this aim a maximum scale factor of 4 should be chosen according to [80].

Particular attention has to be used when defining the collapse condition through IDA. Typically, the collapse condition can be chosen in correspondence of the onset of dynamic instability (i.e. the (almost) horizontal branch of the curve). The label "dynamic instability" is a parallelism to the static instability. The dynamic instability, in fact, stands for "to a little increment of IM corresponds a dramatically large EDP

increase". However, if the curve presents a non-clear horizontal part or it is not monotonic, a reduction of the 80% of the elastic slope can be chosen.

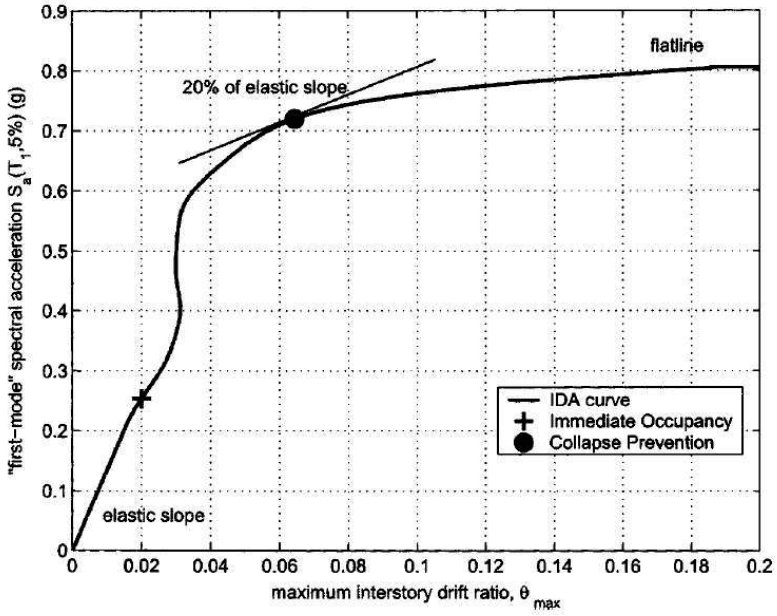

Fig. 33 – Example of IDA curve and definition of collapse point (from [73]).

To evaluate the q behavior factor through non-linear dynamic analyses, two methods can be used: an action side or a reaction side [57]. The action side method evaluates the q-behaviour factor as the ratio between PGA or spectral acceleration:

$$q = \frac{PGA_u}{PGA_y} \tag{6}$$

$$q = \frac{S_a(T_1)_u}{S_a(T_1)_y} \tag{7}$$

Where the subscript u and y stands for ultimate and yield, and T1 is the fundamental vibration period of the structure. The PGA method was used to evaluate q for CLT buildings by [61][6]. An example of the evaluation by means of the spectral acceleration method can be found in [75].

The reaction side approach evaluates the q-behaviour factor as the ratio between forces, i.e. the base shear acting in the ultimate condition and the yield condition. This approach is independent of the choice of the intensity measure characterizing the earthquake and can be carried out by means of non-linear static or dynamic analyses. This solution was used in [81][82][83].

I-4 LFT WALL MODEL CALIBRATION

In the next paragraphs, the experimental test and the FEM model used in the parametric analysis will be introduced, analysed and discussed. The first part describes the full-scale laboratory test on a LFT wall performed in the frame of the ReLUIS consortium [84]. The outcome will be processed to evaluate the backbone curve and the hysteresis properties for the FEM model. Then, the FEM model is presented, and the mechanical properties are calibrated

4.1 Experimental Test

In the frame of the ReLUIS research group of University of Udine, the results of a laboratory test [84] on a full scale LFT wall are here analysed, in order to obtain all the mechanical features describing the non-linear behaviour of the components.

The LFT wall is 2950x2950 mm, thickness 190 mm. Both sides present a 15 mm thick OSB-3 panel and the frame is made of C24 studs (160x160 mm external, 80x160 mm internal). The sheathing-to-framing connection is obtained by means of 2.8 mm nails, spaced 75 mm (150 mm on the internal perimeter). Material properties are listed in Table 1.

Table 1 – Material properties of the timber frame.

(mean values)	C24	OSB3
E_0 [MPa]	11000	4930
E_{90} [MPa]	370	1980
G [MPa]	690	1080
ϱ [kg/m^3]	420	560

Three+three hold-down and six angle brackets were used to anchor the wall to the foundation. See Fig. 34.

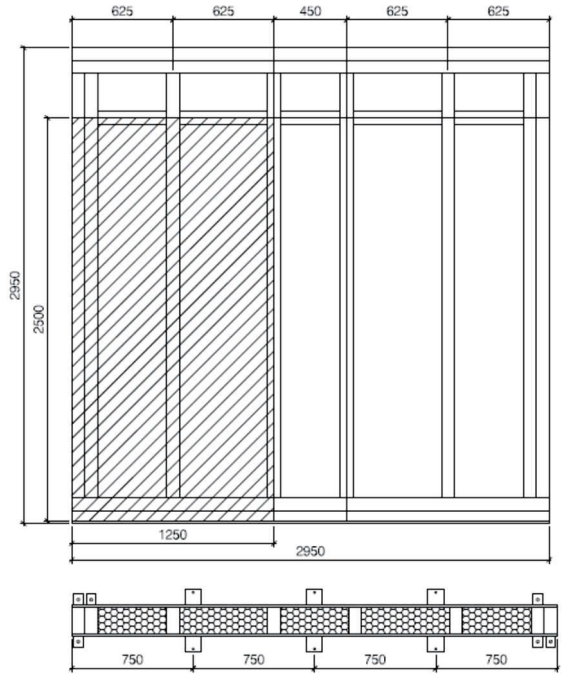

Fig. 34 – LFT full-scale wall specimen.

The cyclic test was performed according to [58], with a displacement-control procedure. The experimental test apparatus (Fig. 35) for the execution of imposed displacement load cycles consists of a hydraulic actuator (to impress the horizontal stress on the top of the wall) and by hydraulic cylinders for the application of the vertical load.

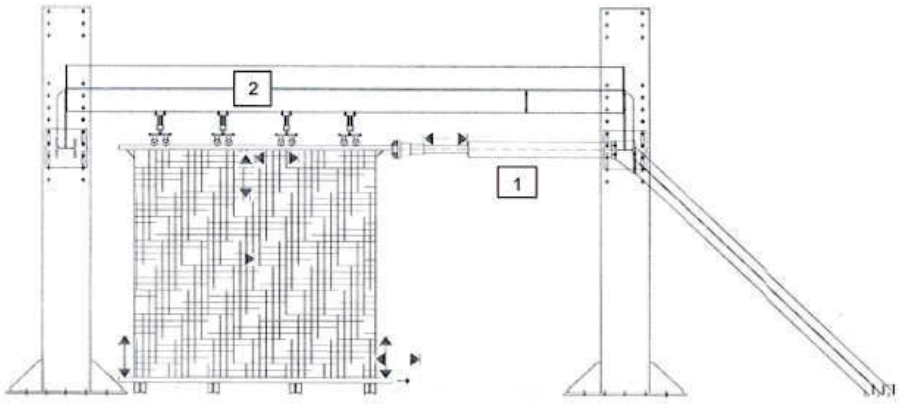

Fig. 35 – Test apparatus for cyclic loading.

The deformations are recorded by means of a series of displacement transducers (LVTD) which measure the in-plane and out-of-plane displacements of the wall, the horizontal displacements at the top and at the base and the vertical displacements at the ends.

The results are herein reported (Fig. 36a: force-displacement cyclic behaviour, Fig. 36b backbone curve). The black lines show the global behaviour of the wall, i.e. the horizontal displacement of the upper stud, varying the total shear at the base. The red curves, on the other hand, represent the horizontal displacement minus the horizontal deformation due to the angle brackets. Furthermore, Table 2 reports the values of the backbone curves of Fig. 36b.

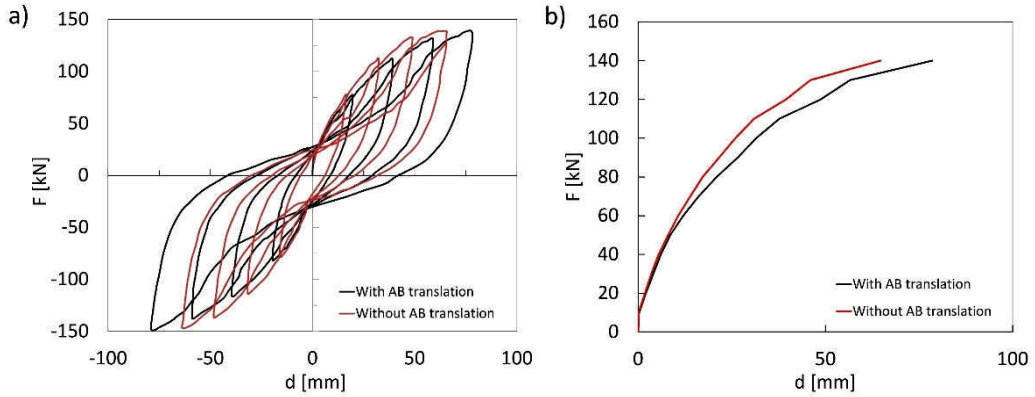

Fig. 36 – Experimental test results; (a) cyclic behaviour, (b) backbone curve. In black, the overall behaviour was reported. In red, the horizontal displacement due to the angle-brackets is subtracted.

Starting from the experimental global curves, the non-linear behaviour of hold-down and angle brackets were obtained. The curve without the uplift due to the hold-downs (and a neglectable contribution of bending) and the horizontal translation of the angle-brackets represents the sheathing-to-framing connection deformation together with the shear deformation of the OSB panels.

The force-displacement curve in Table 2 can be linearized to obtain the capacity curve of a single angle bracket. In a simplified way, the total load shear load can be divided equally between the six angle brackets. Furthermore, since the connection did not reach collapse during the test, a final plastic and failure branch was added, according to literature test on similar devices. This solution will not represent an issue in the

parametric analysis of complete buildings in the next chapters, since both angle brackets and hold-downs will be designed according to Capacity Design and will not reach the collapse condition.

Table 2 – Backbone curves of the experimental tested wall.

Wall - with AB LFTW		AB displacement AB		Wall - without AB LFTW-AB	
d [mm]	F [kN]	d [mm]	F [kN]	d [mm]	F [kN]
0.00	0	0	0	0.00	0
0.26	10	0.15	10	0.11	10
2.07	20	0.26	20	1.81	20
4.07	30	0.55	30	3.52	30
6.05	40	0.58	40	5.47	40
8.56	50	0.54	50	8.02	50
11.98	60	1.3	60	10.68	60
16.18	70	2.31	70	13.87	70
20.98	80	3.76	80	17.22	80
26.56	90	4.93	90	21.63	90
31.57	100	5.58	100	25.99	100
37.65	110	6.73	110	30.92	110
48.73	120	9.23	120	39.50	120
56.66	130	10.64	130	46.02	130
78.54	140	13.84	140	64.70	140

The angle bracket force-displacement curve is reported in Fig. 37.

d [mm]	F [kN]
0.00	0.00
0.54	8.33
5.58	16.67
13.84	23.33
22.00	23.33
30.00	15.00

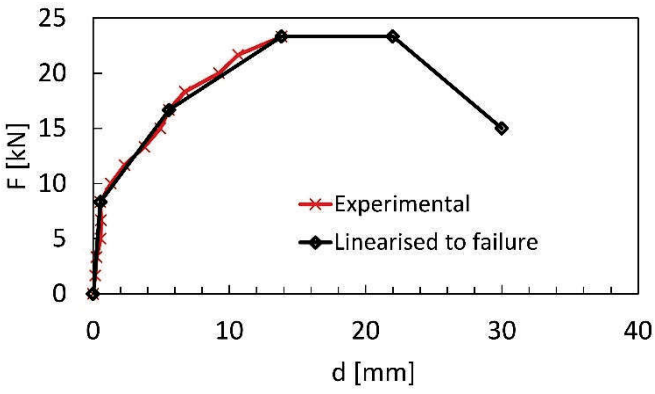

Fig. 37 – Angle bracket non-linear behaviour.

To characterise the hold-down behaviour, the uplift of the wall was analysed. First, the backbone curves were obtained from the transducer measuring the uplift, see Fig. 38. Then the backbone was divided by three

(the number of hold-downs at each side, assuming that all the devices work in the same way) and the backbone was linearized. As in the case of angle brackets, the hold-downs did not reach the failure condition. Thus, to complete the non-linear behaviour of the device a descending branch was added. Since the following IDA analysis will be carried on in a Capacity Design framework, hold-downs are expected to behave elastically, and the validity of the assumption will be verified.

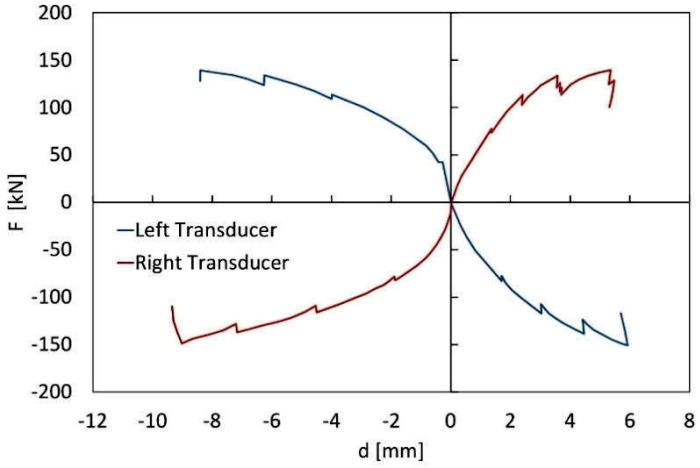

Fig. 38 – Uplift envelope of the tested wall.

The non-linear behaviour of the single hold-down is reported in Fig. 39, together with a table showing the points defining the curve. The compression part is not presented, since it is assumed rigid due to the contact with the foundation.

d [mm]	F [kN]
0.00	0.00
0.61	17.32
2.95	33.52
6.25	44.69
8.40	46.37
12.00	10.00

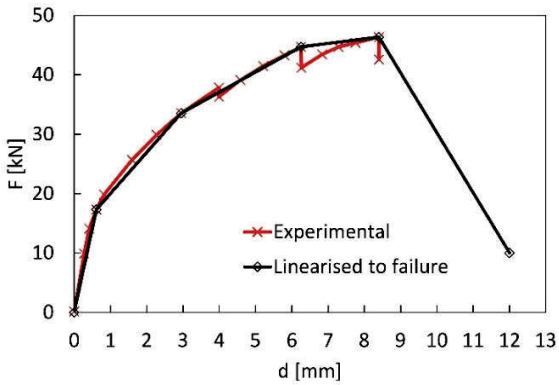

Fig. 39 – Hold-down non-linear behaviour.

4.2 FEM modelling

Two models, a detailed and a simplified FEM one, of the LFT walls were built in SAP2000 [85]. The detailed model was used to create a parameterized set of LFT walls, varying the displacement ductility of the sheathing-to-framing connection, and to derive the parameters to properly define the cyclic characteristics of the simplified model. This last one, in fact, was implemented in the complete 3D reference buildings analysed by IDA approach.

In the next paragraphs, both models will be discussed and calibrated.

4.2.1 Detailed model

To assemble the detailed FE model (Fig. 40), timber studs were modelled as pinned frame element and the OSB panel as shell-thin elements. Non-linear links were used for hold-downs and angle brackets. Each nail of the sheathing-to-framing connection was described by a non-linear link.

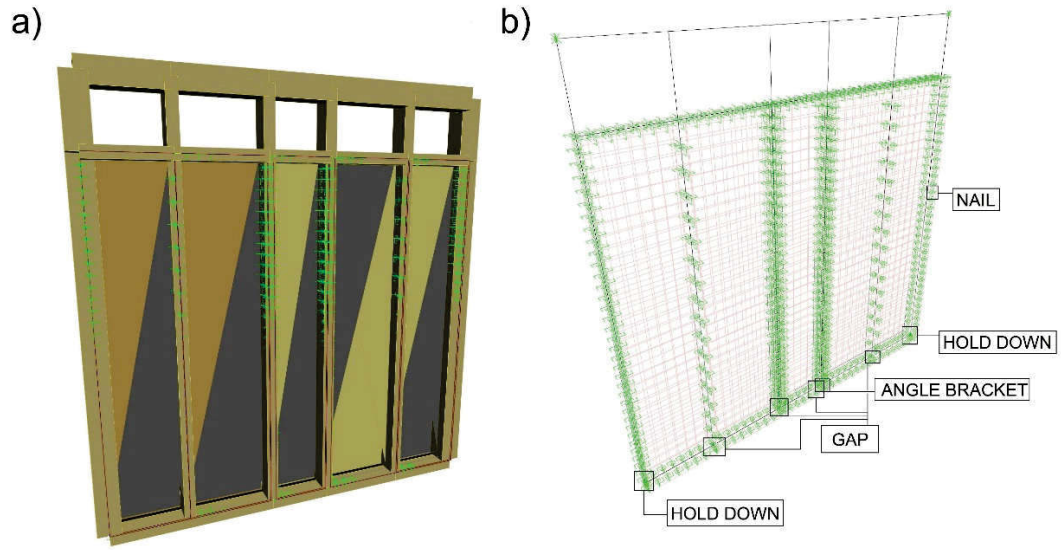

Fig. 40 – Detailed model of the experimental tested LFT wall. (a) FEM model, (b) focus on non-linear link disposition.

It is worth noticing that the independent behaviour of the nail link in x and y directions leads to overestimate the strength of the connection in intermediate directions, and a squared rather than circular force domain is considered [38][85][86].

To overcome this issue, a mean value of the resistance of the nails was used, equal for all fasteners of the model, in order to overlap the numerical and the experimental curves. The C24 and the OSB panels mechanical properties are known and kept constant.

To model the contact between the foundation and the walls, gap elements were added in correspondence of each internal stud; hold downs at both ends already have a high compressive stiffness to simulate the contact, thus no gap elements are further needed.

Since no experimental data were available to define the non-linear behaviour of the single nail of the sheathing-to-framing connection, a proper multilinear curve was defined, starting from data available in the literature. The typical force-displacement curve of a fastener is reported in Fig. 41. The behaviour was taken from [38], for a 2.8 mm nail.

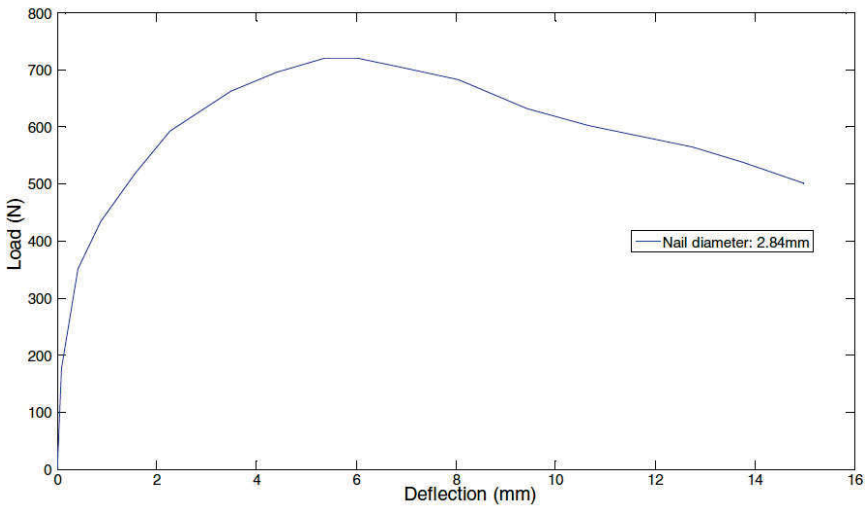

Fig. 41 – Typical force-displacement curve of a single nail connection (From [38])

In order to identify the non-linear behaviour of the nail, the FEM model of the LFT wall was validated through pushover analysis. In Fig. 42, the non-linear pushover outcome is overlap to the experimental curve. Moreover, in Fig. 34 the non-linear behaviour of each component

is reported. In Fig. 43a, the hold-down behaviour is shown. The positive displacement represents the uplift. With respect to Fig. 39, the behaviour was enriched by a compressive branch, to simulate the rigid contact with the foundation. Furthermore, in Fig. 43b the angle-bracket behaviour is reported, symmetric in both directions, according to the outcome of the experimental test (Fig. 37, Table 2). The nail behaviour of Fig. 43c was progressively scaled to fit the experimental global behaviour of the wall. The maximum strength required was increased to 1.40 kN, but no changes were needed to the displacements (Fig. 41).

The results are also comparable to other outcomes about nail testing (Fig. 23). The model is validated, since the optimal overlap between the numerical and experimental curves. The validate non-linear curve of the nails will be used in chapter 5 to create a set of parameterised sheathing-to-framing connections.

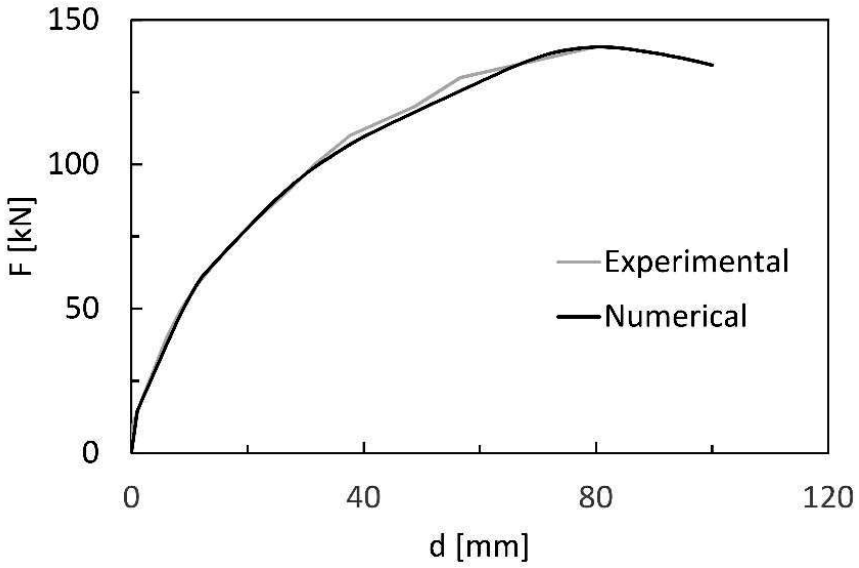

Fig. 42 – Pushover validation of the detailed model.

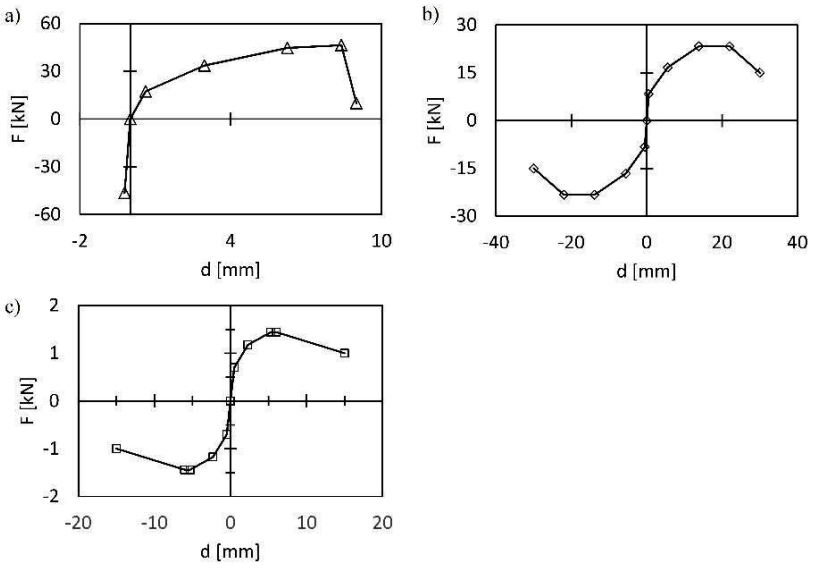

Fig. 43 – (a) hold-down, (b) angle-bracket and (c) single nail non-linear behaviours calibrated on detailed model.

4.2.2 Simplified model

The simplified model was made of two vertical non-linear springs for the hold-downs, one horizontal non-linear spring for the angle brackets and two diagonal non-linear springs for the sheathing-to-framing connection, which considers also the contribution of the shear deformation of the OSB panel. The diagonal spring behaviour, in fact, was obtained removing from the global curve of the wall the contributes of Hold Down and Angle Brackets. Then, a rotation of 45° was applied, to match the inclination of the springs. Timber studs were modelled as pinned frame elements. Finally, gap elements reacting to compression only were inserted to model the contact between the lower stud and the foundation (Fig. 44).

Since the simplified model will be analysed with a non-linear dynamic approach, the full-scale tested wall was used to identify the parameters to describe the cyclic behaviour of the components. For all links a Pivot type hysteresis was chosen, since the FEM models were developed in SAP2000 [85] and the pivot hysteresis gives more possibilities to properly define the cyclic behaviour. The Pivot hysteresis follows Fig. 45, where:

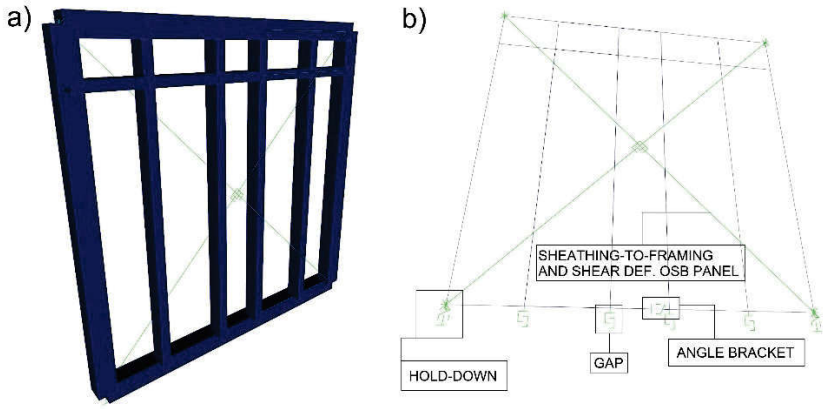

Fig. 44 – Simplified wall model overview (a) and details of non-linear links (b).

- α_1, which locates the pivot point for un loading to zero from positive force. Unloading occurs toward a point on the extension of the positive elastic line, but at a negative force value of α_1 times the positive yield force.
- α_2, which locates the pivot point for unloading to zero from negative force. Unloading occurs toward a point on the extension of the negative elastic line, but at a positive force value of α_2 times the negative yield force.
- β_1, which locates the pivot point for reverse loading from zero toward positive force. Reloading occurs toward a point on the positive elastic line at a force value of β_1 times the positive yield force, where $0.0 < \beta_1 \leq 1.0$. Beyond that point, loading occurs along the secant to the point of maximum previous positive deformation on the backbone curve.
- β_2, which locates the pivot point for reverse loading from zero toward negative force. Reloading occurs toward a point on the negative elastic line at a force value of β_2 times the negative yield force, where $0.0 < \beta_2 \leq 1.0$. Beyond that point, loading occurs along the secant to the point of maximum previous negative deformation on the backbone curve.
- η, which determines the amount of degradation of the elastic slopes after plastic deformation, where $0.0 < \eta \leq 1.0$.

Reproducing the experimental tests, the non-linear cyclic behaviour of the wall was rebuilt. In Table 3, the dissipated energy for each cycle is

reported, highlighting a total difference of -7%, and an overall low variation for high displacement cycles.

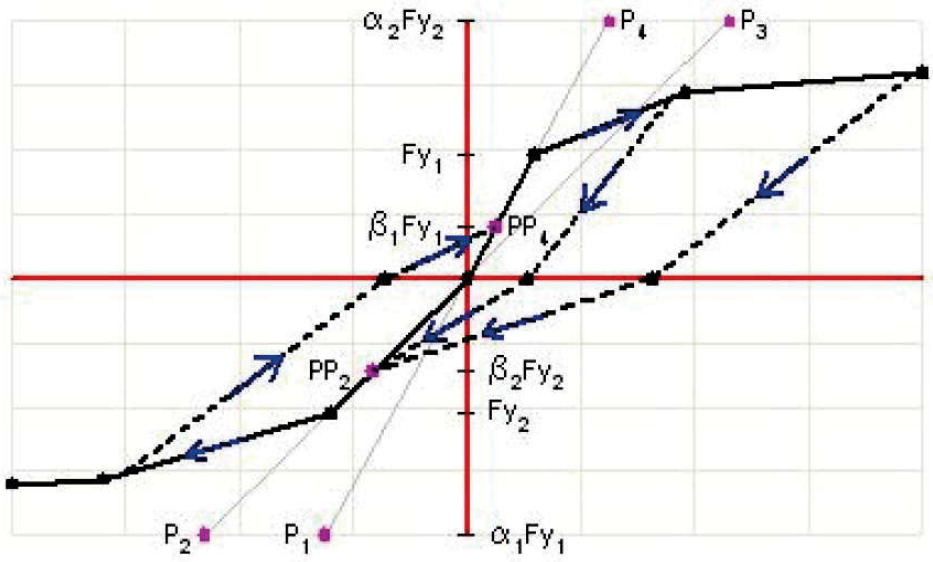

Fig. 45 – Pivot-type hysteresis description (From [85]).

A cycle-by-cycle comparison between experimental and numerical is instead shown in Fig. 46, while the α and β pivot describing the hysteretic behaviour are reported in Table 4.

Table 3 – Dissipated energy: comparison between experimental and FEM model.

Dissipated Energy [kNmm]			
Cycle	Exp	FEM	Diff
1	1719	1063	-38%
2	4844	3735	-23%
3	8146	7751	-5%
4	11275	11558	3%
Total	**25983**	**24106**	**-7.2%**

Table 4 – Parameters describing the Pivot hysteresis, calibrated on experimental test.

Element	α	β
Sheathing-to-Framing	1000	0.45
Angle-Bracket	200	0.05
Hold-down	200	0.30

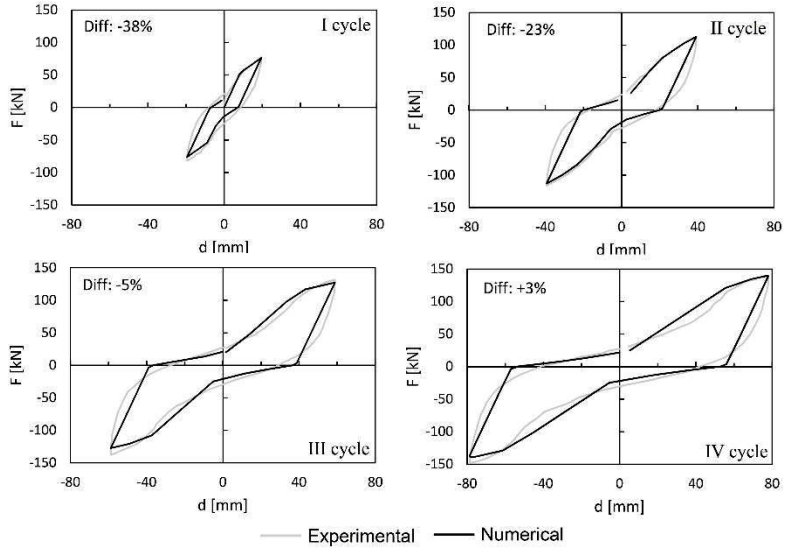

Fig. 46 – cycle by cycle behaviour comparison between experimental test and numerical simulation.

Finally, in Fig. 47 the cyclic behaviour of each component is reported: Hold-down (a), Angle bracket (b) and Sheathing-to-framing connection (c).

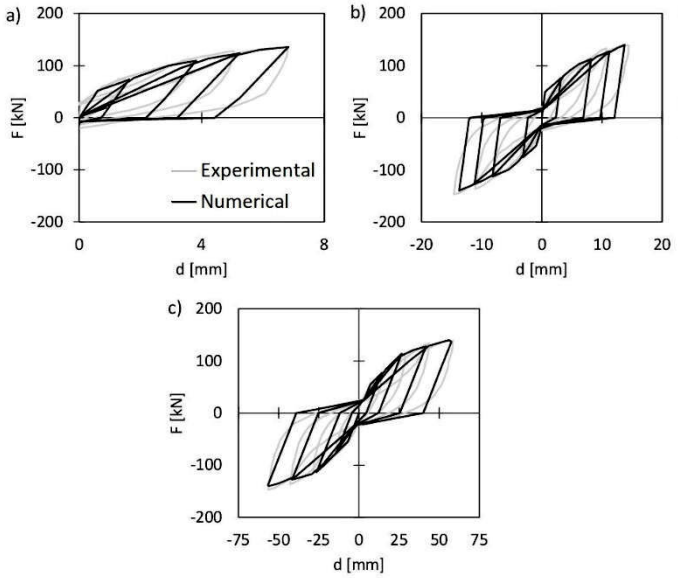

Fig. 47 – Cyclic behaviour of all components. (a) hold-down, (b) angle brackets and (c) sheathing-to-framing connection.

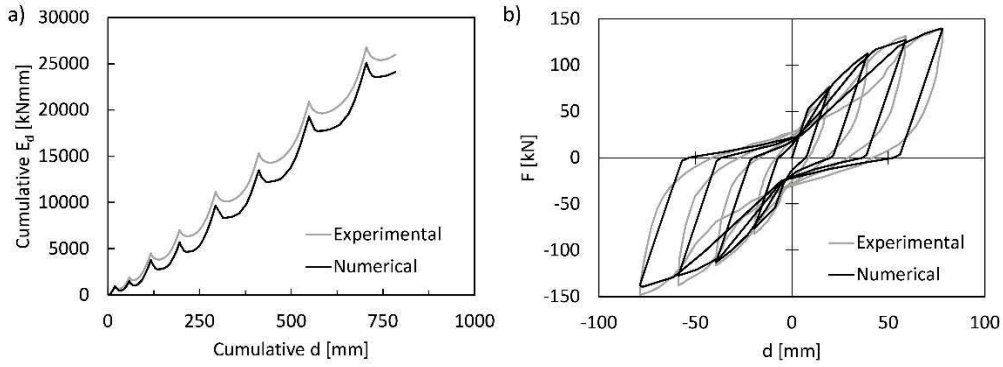

Fig. 48 – Overlap between experimental and numerical cumulated energy (a) and cyclic behaviour (b) of the tested LFT wall.

Furthermore, the complete wall is shown in Fig. 48, highlighting a good fitting of cumulative energy and hysteresis laces and, thus, validating the model.

The so obtained values will be used in the Pivot cyclic behaviour of all the sheathing-to-framing connection of the LFT walls of the reference buildings. Since a capacity design approach will be followed, hold-down and angle-brackets remain elastic, showing a non-hysteretic behaviour. However, to properly define the pivot characteristic of the panel connection, the wall was entirely modelled in this phase.

5 PARAMETRIC ANALYSIS

In this chapter, the parameters varied in the IDA analysis were discussed. First, the sheathing-to-framing connection was parameterised, assigning a defined ductility to the nails. Secondly, a set of LFT walls was created, joining the outcome of the experimental test to the parameterised sheathing-to-framing connection.

5.1 Sheathing-to-framing nailed connection

Starting from the validated nails behaviour of detailed model of Fig. 43c, the displacement ductility μ of the sheathing-to-framing connection was varied, selecting three classes: 4, 6 and 8. In particular, 4 and 6 are the minimum required value to design a Low and High Ductility Class LFT building respectively, according to Eurocode 8 [7] and the Italian Building Code [8]. Furthermore, class 8 was considered to comparison purposes. The ductility was evaluated as the ratio between the ultimate and the yield displacement, according to an Equivalent Energy Elastic Plastic EEEP approach [65]. In particular, the elastic stiffness was evaluated at 40% of the maximum strength. The ultimate displacement is taken in correspondence of 20% force reduction. Furthermore, in order to obtain a wide set of LFT walls, three values for the maximum shear strength of the single nail were selected: 720 N, 1000 N and 1400 N. The first two values, 720 N and 1000 N, are typical of the nails adopted in the constructions and were already used in other literature works [38][50]. The last one is the maximum force of the nails of the experimentally tested wall.

Herein, the procedure used for defining the curves for the nails is reported. The shape of the behaviour is taken according to the experimental evidence. The final shape, instead. was determined iteratively, imposing the desired ductility.

$$F_{max} = 0.72\ kN;\ F_{0.4} = 0.4F_{max} = 0.29\ kN;\ F_{0.8} = 0.8F_{max} = 0.58\ kN$$
$$F_{max} = 1.00\ kN;\ F_{0.4} = 0.4F_{max} = 0.40\ kN;\ F_{0.8} = 0.8F_{max} = 0.80\ kN$$
$$F_{max} = 1.40\ kN;\ F_{0.4} = 0.4F_{max} = 0.56\ kN;\ F_{0.8} = 0.8F_{max} = 1.12\ kN$$

Setting the ductility classes, the following parameters were obtained. Moreover, the ultimate and yield displacement were evaluated matching the dissipated energy of the bilinear EEEP and the multilinear curve. See Table 5.

Table 5 – Parameters of the single nail connections varying the ductility class.

F_{max}=0.72 kN			
Ductility:	4	6	8
d_y [mm]	0.94	0.92	0.91
F_y [kN]	0.66	0.64	0.64
d_u [mm]	3.75	5.52	7.29
k* [kN/mm]	0.70	0.70	0.70
E* [kNmm]	2.15	3.26	4.36

F_{max}=1.00 kN			
Ductility:	4	6	8
d_y [mm]	0.94	0.92	0.91
F_y [kN]	0.91	0.89	0.89
d_u [mm]	3.75	5.52	7.29
k* [kN/mm]	0.97	0.97	0.97
E* [kNmm]	2.99	4.52	6.06

F_{max}=1.40 kN			
Ductility:	4	6	8
d_y [mm]	1.14	1.11	1.10
F_y [kN]	1.25	1.22	1.21
d_u [mm]	4.56	6.67	8.80
k* [kN/mm]	1.10	1.10	1.10
E* [kNmm]	4.99	7.47	9.96

The outcome of the calculation is reported in Fig. 49, where the multilinear nail curve is overlap to the EEEP bilinear for each ductility class μ. It is worth to note that, according to the Johansen model, the failure mode was related to the formation of a single plastic hinge in the nails, as observed in the cyclic laboratory test.

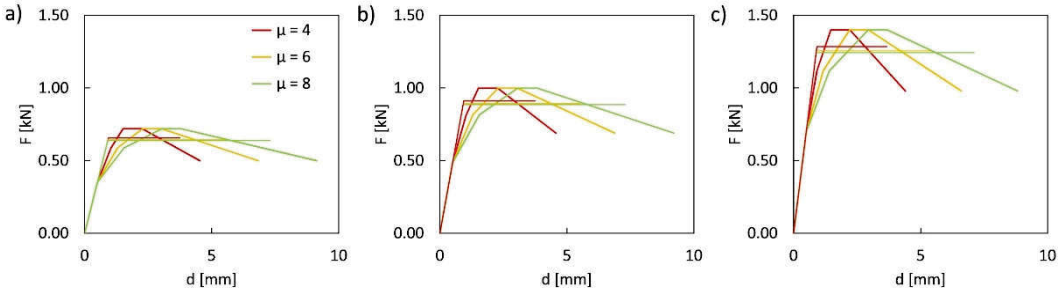

Fig. 49 – Force-displacement non-linear curve for the single nail connection for each ductility class and for capacity equal to (a) 0.72 kN, (b) 1.00 kN and (c) 1.40 kN.

5.2 Set of LFT walls

In order to match the requirements of seismic design phase of the reference buildings, a wide set of LFT walls was created. The connectors spacing was varied, considering 75 and 150 mm, and the OSB panels were placed on one or both sides. Under these assumptions, 36 detailed LFT wall models were build and analysed. Each wall has a label that identifies the nail spacing (75 or 150 mm), the sides covered by OSB panels (1 or 2) and the shear resistance of the sheathing-to-framing connection referred to only one nail (720, 1000, 1400 N).

For each wall, a detailed model was created, according to chapter 4; however, with respect to chapter 4, the wall was fixed at the base, so that only shear deformation caused by sheathing-to-framing connection was recorded. The force-displacement curves of Fig. 49 were assigned to all non-linear springs of the panel connection, and the structure was subjected to pushover analysis. An example of analysis is herein reported, for the 150(1)720 wall. Fig. 50a show the FEM model pushover results related to the sheathing-to-framing connection. Applying the EEEP approach, it is possible to evaluate the yield displacement, which is necessary during the IDA procedure to

individuate the "first yield" condition of the structure. The parameters defining the EEEP of Fig. 50b are reported in Table 6.

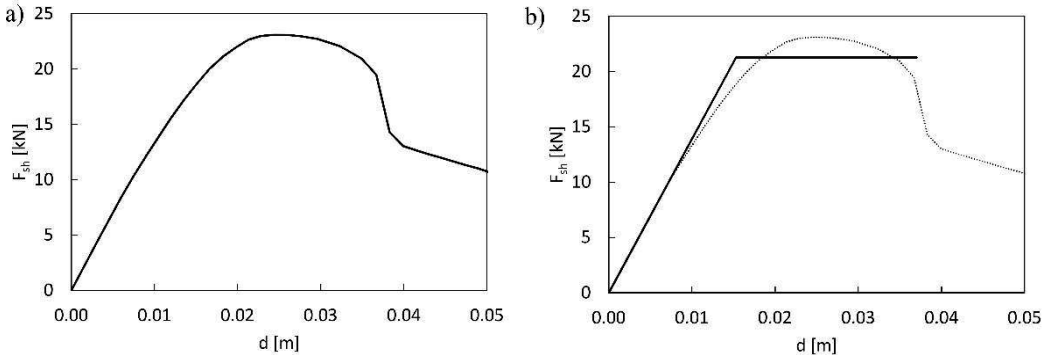

Fig. 50 – Non-linear static analysis of 75(1)720 wall (a) and bilinearization (b) according to EEEP approach [65].

Table 6 - Mechanical properties of the 75(1)720 LFT wall.

75(1)720 – duct 4						Bilinear EEEP	
F_{max}	23.09	kN	E	0.62	kNm	d [m]	F [kN]
$0.80F_{max}$	18.47	kN	k	1390	kN/m	0.0000	0.00
$0.40F_{max}$	9.24	kN	d_y	0.02	m	0.0153	21.26
d_u	0.04	m	F_y	21.26	kN	0.0370	21.26
$d(0.4F_{max})$	0.01	m					

Furthermore, to the FEM curve, a multilinear behaviour was adapted, in order to develope the non-linear behaviour for the simplified model of the wall (the one with two diagonal links representing the shear behaviour of the LFT wall). To this aim, the energy of the two curves was equalled (Fig. 51).

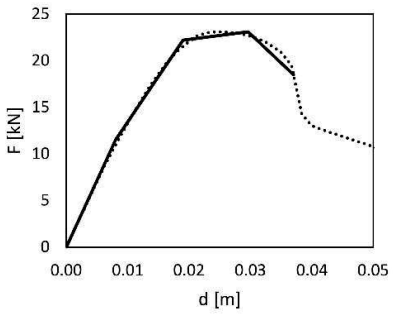

d [m]	F [kN]	E [kNm]	E_{FEM} [kNm]
0.000	0.00		
0.008	11.50		
0.019	22.20		
0.030	23.09		
0.037	18.47	0.471	0.471

Fig. 51 – Adaptation of a multilinear curve to the numerical outcome of the 75(1)720 LFT wall.

Finally, to obtain the non-linear behaviour for the diagonal springs of the simplified model, the curve of Fig. 51 had to be rotated to 45°, according to the following formulations:

$$d_{d,sh} = d_{sh} \cdot \cos \alpha \tag{8}$$

$$F_{d,sh} = \frac{F_{sh}}{2 \cdot \cos \alpha} \tag{9}$$

$$k_{d,sh} = \frac{k_{sh}}{2 \cdot \cos^2 \alpha} = \frac{F_{sh}/d_{sh}}{2 \cdot \cos^2 \alpha} \tag{10}$$

Where α is the inclination of the diagonal, $F_{d,sh}$ and $k_{d,sh}$ are the shear resistance and the stiffness of the diagonal simulating the sheathing-to-framing connection and F_{sh} and k_{sh} are the shear resistance and stiffness of the FEM model. A summary of the complete procedure is reported in Fig. 52.

From all the evaluated configuration, 18 walls revealed suitable for the design procedure of the reference buildings, showing a difference of 15% with respect to the seismic demand, which has been discussed in the next chapter. No configuration showing nail resistance 1400 N were suitable for the reference buildings, since their capacity exceeded the 15% threshold. Moreover, an ID was assigned to each configuration, to make the label presented later in the work more concise.

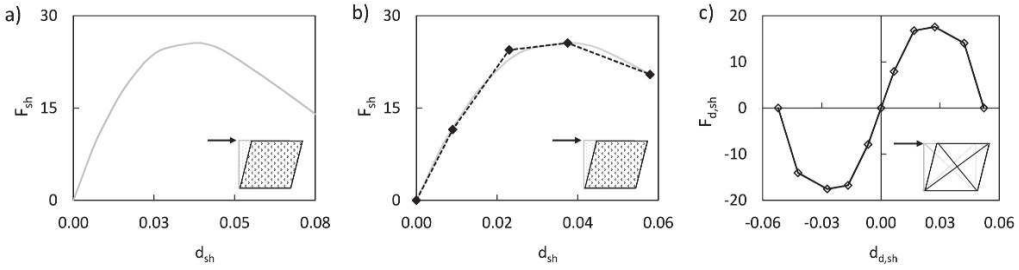

Fig. 52 – Procedure to obtain the non-linear behaviour of the diagonal springs of the LFT simplified model. The pushover curve (a) was transformed into a multilinear curve (b). Then, the rotation to 45° was applied (c).

In conclusion, Table 7 reports the maximum resistance F_{max}, the yield and ultimate displacement d_y and d_u, and the displacement ductility

of the sub-set of walls. It is worth noticing that the ductility class affects the ultimate displacement and, of course, the ductility of the wall. On the other hand, it has a limited influence on maximum shear strength and yield displacement.

Table 7 - Characteristics of the walls selected to assemble the reference buildings. Each wall has a label that identifies the nail spacing (75 or 150 mm), the sides covered by OSB panels (1 or 2) and the shear resistance of the sheathing-to-framing connection referred to only one nail (720 or 1000 N).

μ=4 Wall	**LFT_id**	**F_{max} [kN]**	**d_y [m]**	**d_u [m]**	**Ductility [-]**
150(1)720	1	11.2	0.012	0.036	3.0
150(1)1000	2	18.6	0.014	0.042	3.0
150(2)720	3	26.4	0.010	0.029	3.0
75(1)720	4	23.1	0.015	0.037	2.5
150(2)1000	5	36.5	0.012	0.030	2.5
75(1)1000	6	29.9	0.017	0.039	2.3
μ=6 Wall		**F_{max} [kN]**	**d_y [m]**	**d_u [m]**	**Ductility [-]**
150(1)720	1	12.3	0.013	0.048	3.7
150(1)1000	2	20.6	0.015	0.055	3.7
150(2)720	3	26.7	0.010	0.043	4.0
75(1)720	4	25.6	0.017	0.058	3.4
150(2)1000	5	36.9	0.011	0.043	3.9
75(1)1000	6	32.9	0.019	0.058	3.1
μ=8 Wall		**F_{max} [kN]**	**d_y [m]**	**d_u [m]**	**Ductility [-]**
150(1)720	1	12.7	0.014	0.062	4.4
150(1)1000	2	21.7	0.016	0.072	4.5
150(2)720	3	26.7	0.011	0.056	5.2
75(1)720	4	27.0	0.019	0.077	4.1
150(2)1000	5	37.1	0.012	0.056	4.7
75(1)1000	6	35.5	0.021	0.078	3.7

Furthermore, the aforementioned procedure of Fig. 52 was applied to all the 18 sub-set LFT walls and the curves reported in Fig. 53 were obtained. Finally, hysteretic parameters for the Pivot behaviour calibrated in §4.2.2 by means of the experimental test were assigned.

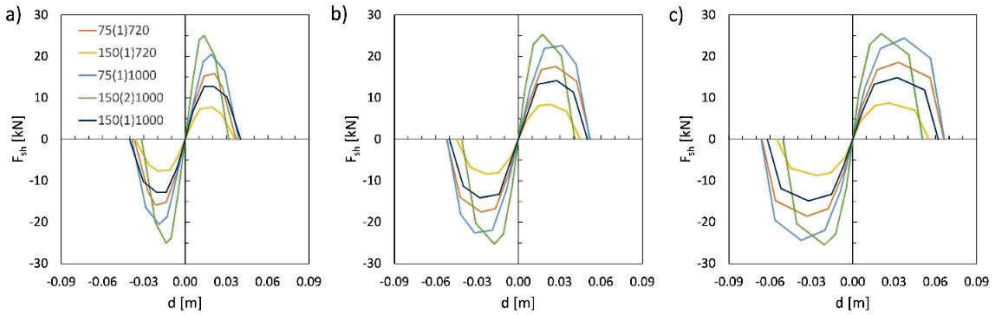

Fig. 53 - Non-linear backbone curves for the diagonal springs of the simplified models for sheathing-to-framing ductility equal to 4 (a), 6 (b) and 8 (c).

I-6 REFERENCE BUILDINGS

Herein, the reference buildings are described. To perform the parametric analysis, a set of six buildings varying the number of storeys and the regularity was assembled. To obtain realistic structures, like the ones of the engineering design practice, existing LFT buildings were taken as a starting point. First, the building geometry is shown and discussed. Then the load analysis is performed, and the design procedure under static loads is described. After an overview of the FEM model, the procedure for the seismic analysis is discussed.

6.1 Description of the Reference Buildings

In order to define a reasonable reference building, a starting point was found in the CASE project of L'Aquila. The typical floorplan and the prospect of the buildings are reported in Fig. 54. The single module is reported in Fig. 55, and were the focus of a Design Guide Line developed in the ReLUIS frame project [87].

Thus, six example buildings (three regular and three not regular, see Fig. 56) were built assembling 2950×2950 mm walls starting from the real structures of Fig. 55, in order to refer directly to the calibration of the components through the experimental tested wall. Each block of the reference buildings can stand alone or be connected to other ones to have more surface area of the apartments. The plan dimensions (10.85 x 6.44 m) of the regular structures were kept constant. On the other hand, the unregular buildings show a ground floor 10.85 x 6.44 m and the typical upper floors 6.00 x 6.44 m.

Fig. 54 – CASE project buildings.

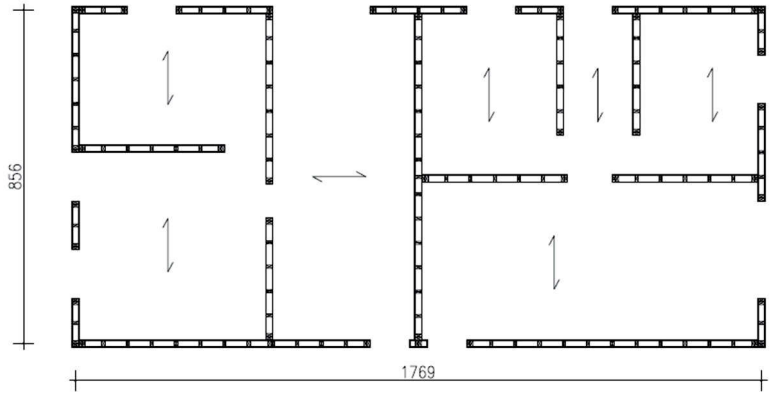

Fig. 55 – Single module typical floorplan.

This choice, together with the different wall arrangements, allow to reach the irregularity both in plan and in elevation. Finally, the number of storeys was varied from 2 to 4 (inter-storey height 3.15 m), in order to analyse low- and mid-rise building behaviour.

The non-regularity was evaluated through the Torsional Irregularity Ratio (TIR) proposed by ASCE [88] which is defined as the ratio of the drift at the building edge to the average drift. The walls layout and plan dimensions were assembled to achieve a TIR $\geq$ 1.2 for all the configurations, that is the suggested condition to consider a building

unregular. The ratio obtained for the three unregular structures are reported in Table 8.

Table 8 – Calculated TIR for irregular reference buildings.

2 storeys	3 storeys	4 storeys
1.20	1.19	1.21

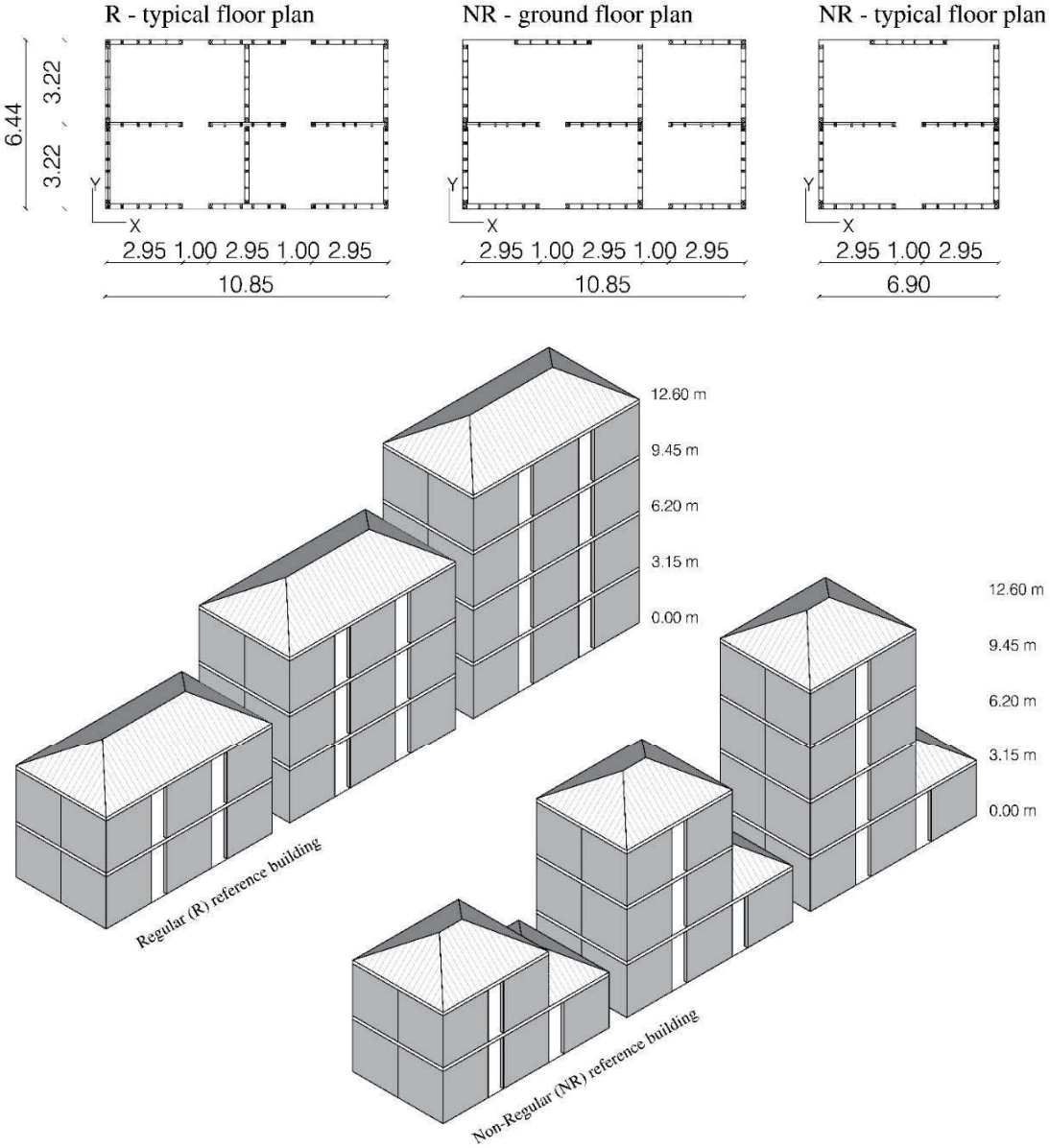

Fig. 56 – Floor plan and elevation of the six reference buildings

6.2 Design and Check procedure

The reference buildings were designed according to Eurocode 5 [89] and Eurocode 8 [7] provisions. Timber joisted floors were selected, with Gl24h beams 80x160 mm, spaced 625 mm. OSB panels were considered over and below (Fig. 57). Furthermore, finishing layers were considered, as in Table 9.

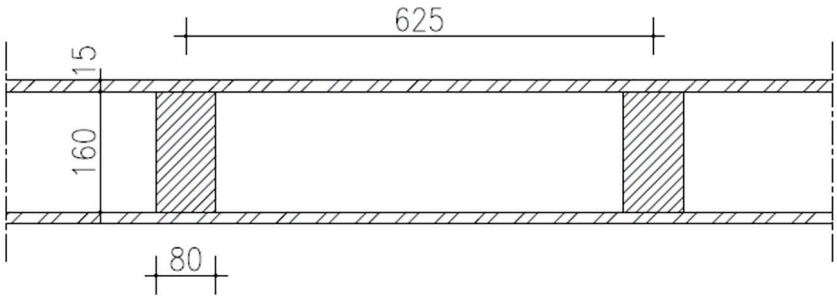

Fig. 57 – Section of the timber floor of reference building, made of glulam beams and OSB panels.

Table 9 – Structural and non-structural loads of typical timber floor.

Layer	th [mm]	ρ [kg/m^3]	kg/m^2
Tiles	15	1600	32
Screed	50	1900	95
Acoustic insulation	30	70	2
Insulation	40	1800	72
Timber structure	-	-	60
Plasterboard panel	15	900	14
Partitions			80
		Tot.	355

The total weight of the typical floor was assumed 3.55 kN/m^2. The upper storey corresponds to the roof. In this case, no partitions and tiles are considered, but the weight of the roof structure, that was taken only as added mass, was considered. The weight of the last storey was 1.00 kN/m^2 (Table 10).

Table 10 – Structural and non-structural loads of top floor (roof).

Layer	th [mm]	ρ [kg/m^3]	Kg/m^2
Insulated sandwich panel	40	-	10
Secondary timber structure	-	-	29
Insulation	100	70	7
Timber Floor			60
		Tot.	106

As for the floors, the calculation of the self-weight of the LFT walls is herein reported. The structure is the same tested in chapter 4 (Fig. 58). The number of hold-downs and angle-bracket of Fig. 58 is just indicative. The amount, such as the nail spacing, will be evaluated during the verification phase.

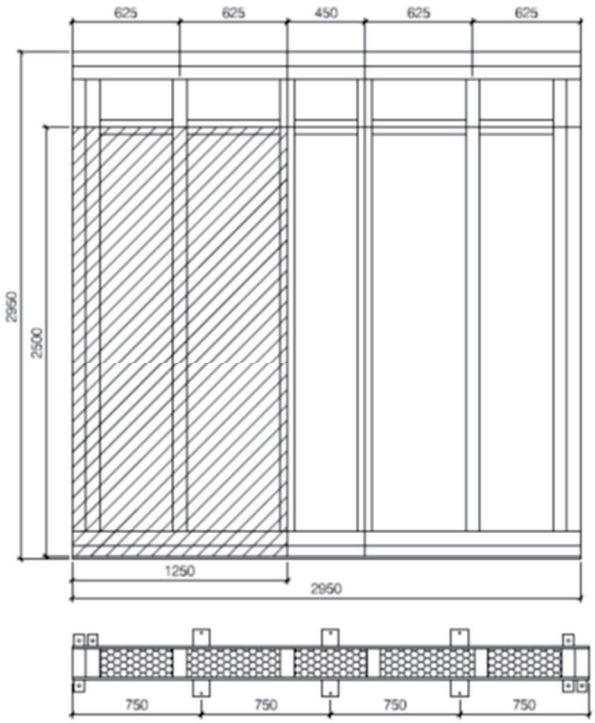

Fig. 58 – Typical LFT wall used in the assembly of reference building. The number of angle-brackets and hold-downs.

External and internal walls have different finishing, so the weight of both walls is below calculated, considering insulation and plasterboard

panels. Thus, a load G = 2.57 kN/m and G = 2.24 kN/m were obtained for external and internal walls respectively. See Table 11 and Table 12.

Table 11 – External LFT walls loads.

Layer	th [mm]	ρ [kg/m^3]	m [kg/m^2]
Plasterboard 2 panel	25	900	24
Steel frame + insulation	50	40	3
Timber frame + OSB	190		42
insulation	160	40	6
External finishing	40	245	12
Total	312		87

Table 12 – Internal LFT walls loads.

Layer	th [mm]	ρ [kg/m^3]	m [kg/m^2]
Plasterboard panel	15	900	14
LFT + OSB	190		42
Insulation	160	40	6
Plasterboard panel	15	900	14
Total	220		76

Finally, a live load of 2.00 kN/m^2 is considered at each intermediate floor, whereas a live load of 0.50 kN/m^2 is selected for the roof, according to [8].

The seismic analysis was performed by modal superposition, in order to simulate the typical engineering practice. To this aim, a Eurocode 8 [7] response-spectrum with PGA=0.35g, soil type A and q=3 was chosen to verify the Life Safety ultimate state. It is worth noticing that the choice of a q-factor to modify the design spectrum affects only the resistance of the shear wall system, since the ductility of sheathing-to-framing connection will be parameterised. The stiffness of the walls was kept constant. In fact, the choice to design with an elastic analysis (q=1) would have led to oversized walls, which would not have reflected current design practice. In addition, [50] showed that the soil type has a negligible influence on the evaluation of the behaviour factor. Below, the parameters describing the response spectrum are show (Table 13).

Table 13 – Life Safety response spectrum

Soil	A-T1	
a_g	0.35	g
S	1	
T_B	0.15	s
T_C	0.40	s
T_D	2.00	s
q	3.00	-

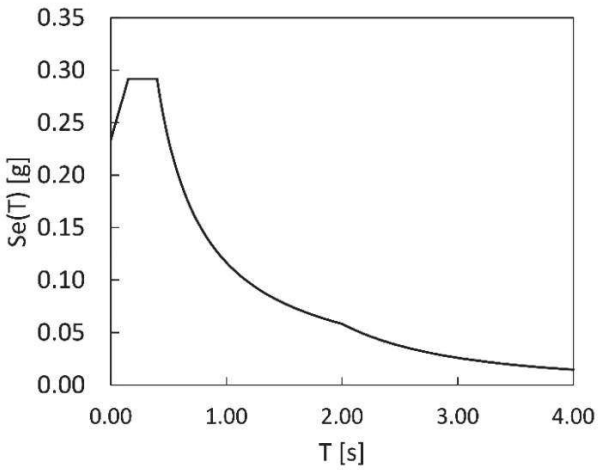

All the actions on the reference buildings were obtained from FEM elastic models. Each wall was considered as an assembly of studs (frame elements) and two diagonal springs (linear elastic links) representing the in-plane stiffness, assumed as the experimental one (K = 4360 N/mm). Furthermore, a constraint was applied to each floor, to describe a rigid floor diaphragm. The stiffness assigned to each diagonal elastic link K_d needs to be evaluate considering the 45° inclination (Fig. 59).

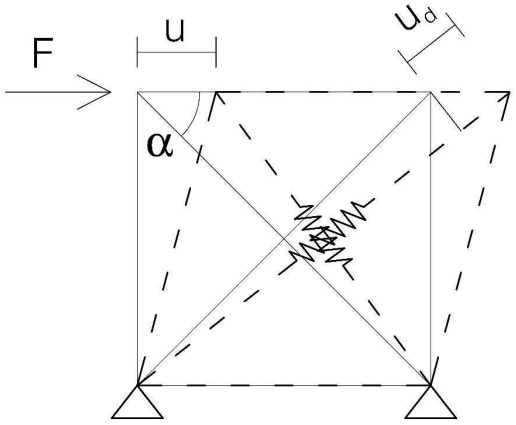

Fig. 59 – Two diagonal spring model of LFT wall.

The stiffness of the wall follows equation:

$$K = F/u \tag{11}$$

Where F is the horizontal applied force and u is the horizontal displacement. Known the alpha angle, the stiffness of the spring K_d can be calculated starting from the elongation u_d:

$$u_d = u \cdot cos\,\alpha \tag{12}$$

$$F_d = \frac{F}{2 \cdot cos\,\alpha} \tag{13}$$

$$K_d = \frac{K}{2 \cdot cos^2\,\alpha} \tag{14}$$

Furthermore, since the FEM model consists in diagonal springs, the shear acting on each wall is not the sum of the shear on the studs. It is necessary, in fact, to post-process the data, reconstructing the shear starting from the axial load on the spring. For a three-storey wall, see Fig. 60.

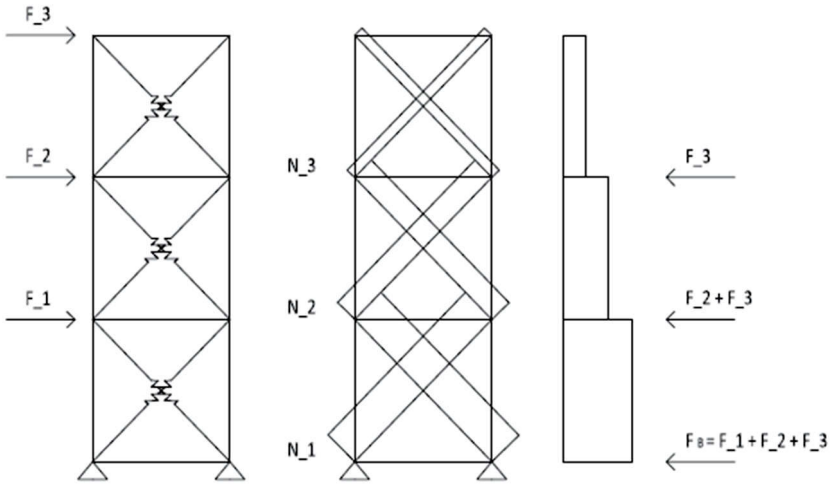

Fig. 60 – Evaluation of the base shear for a three storey LFT wall.

Thus, the shear acting at the base of the shear wall is:

$$F = 2N_1 \cos\alpha \tag{15}$$

Where:
N_1 is the axial force on the spring at base floor

$\alpha = \tan^{-1}(H/L)$ is the inclination angle of the diagonal, with H and L the height and the width of the wall.

The total bending moment at the base of the 3 storeys LFT wall can be obtained from equation:

$$M = F_1 \cdot h_1 + F_2 \cdot h_2 + F_3 \cdot h_3 \tag{16}$$

Where:

F_i is force at the i-th storey of the building;

h_i is the arm of the force;

Tension and compression on the stud at each end of the wall can be obtained as the ratio between the bending moment M and the length of the wall L.

$$T = M/L \tag{17}$$

The procedure can be easily extended to different numbers of storeys. Finally, as an example, the FEM model of the four storeys reference building is reported in Fig. 61. All numerical models were built in the same way.

Fig. 61 – FEM model of the irregular four storey building.

6.3 Static Design

All six reference buildings were designed following Eurocode 5 [89] for static loads, under Ultimate and Serviceability Limit State (ULS and SLS respectively). Floors were checked for bending and shear (ULS), and for deflection (SLS). Furthermore, the vertical studs of the LFT wall were verified under orthogonal compression and instability (ULS). These standard checks aim to obtain a typical LFT building, so the partial coefficient at ULS and SLS were applied.

For ULS verification, the simplified following combination stands, since only one live load was considered:

$$E_{d,ULS} = \gamma_{G1} G_{1k} + \gamma_{G2} G_{2k} + \gamma_Q Q \tag{18}$$

Where E_d is the action on the structure, γ_i are the partial coefficient (1.3, 1.3 and 1.5 respectively), G are the dead loads (structural and non-structural) and Q is the live load, assumed 2.00 kN/m^2. The SLS verification, on the other hand, followed the characteristic and the quasi-permanent combinations:

$$E_{d,SLS,c} = G_{1k} + G_{2k} + Q \tag{19}$$

$$E_{d,SLS,qp} = G_{1k} + G_{2k} + \psi_{21} Q \tag{20}$$

Where ψ_{21} is the combination factor for the live load, equal to 0.3 for residential load.

The strength verifications were conducted assuming the design resistance as:

$$f_d = \frac{k_{mod} f_k}{\gamma_m} \tag{21}$$

Where f_d and f_k are the design and the characteristic tension, k_{mod} is a factor considering the duration of the load, and γ_m is the safety coefficient. The verification herein reported are referred to the worst conditions, i.e. the floor with the longest span and the regular 4 storeys

building internal LFT wall, which is the one with the highest acting normal force. In particular, a k_{mod} equal to 0.8 was selected for ULS verification (mean duration for the live load. The combination with the dead load gave a better load condition). The safety coefficients were taken equal to 1.50 for solid timber studs and equal to 1.45 for glulam beams, according to [8], since higher than those proposed by EC5.

6.3.1 Floor verification

The verified floor has 3.14 m net span and is made of a Gl24h 120x200 mm glulam beam. The composite action between the beam and the OSB panel were here neglected, in order to check in favour of safety. For a geometry overview of the section, see Fig. 57. The acting moment and shear were evaluated for a simply supported beam at both ends. The verification report is shown in Table 14, where the orthogonal compression in the bearing on the wall, the shear and the bending are all verified.

Table 14 – Floor verification.

Data_				kN/m²	kN/m	γ	kN/m			
B	0.12	m	G_{1k}	0.55	0.34	1.30	0.45			
H	0.20	m	G_{2k}	3.00	1.88	1.30	2.44			
i	0.625	m	Q_k	2.00	1.25	1.50	1.88			
J	8E-05	mm⁴								
E	11500	MPa	Sigma_check_		M = 5.80 kNm		V = 7.39 kN			
G	650	Mpa								
L_{net}	3.14	m	Bearing compr. ORTHO		0.77	<	1.48	Mpa	Ok!	
L_{design}	3.34	m								
f_{md}	14.22	Mpa	Shear Verification		0.46	<	1.47	Mpa	Ok!	
F_{c90d}	1.48	Mpa								
f_{vd}	1.47	Mpa	Bending verification		7.25	<	14.22	Mpa	Ok!	

Furthermore, the deflection limit was here checked. The midspan deflection was evaluated for a simply supported beam, considering also the shear contribution (Table 15).

Table 15 – Deflection verification of the typical floor.

Data_				kN/m²	kN/m	w_{inst}	k_{def}	ψ_{2j}	w_{fin}
B	0.12	m	G_{1k}	0.55	0.34	0.64	0.6		1.02
H	0.20	m	G_{2k}	3.00	1.88	3.48	0.6		5.57
i	0.625	m	Q_k	2.00	1.25	2.32	0.6	0.3	2.74
J	8E-05	mm⁴							
E	11500	MPa	Deflection_check:						
G	650	MPa	w_{max}	2.32	9.33	2.74			
L_{net}	3.14	m	w_{lim}	11.13	13.36	16.70			
L_{design}	3.34	m		L/300	L/250	L/200			
				21%	70%	16%			
				Ok!	Ok!	Ok!			

The long-term deformations were evaluated considering a k_{def} equal to 0.6, and decreasing the stiffness modulus of the glulam, in accordance with [89].

6.3.2 LFT wall verification

The typical 2950x2950 mm LFT wall was used for each reference building. In order to verify if the stud section is sufficient (160x80 mm internal studs, 160x160 at both ends), an orthogonal compression check was performed, and the instability was finally verified, both in accordance to Eurocode 5 [89] provisions.

Table 16 – ULS vertical stud verification.

Loads_					Data_		
Typical Floor	Wall G_k	2.24	kN/m		$f_{c,0,d}$	11.59	MPa
	Floor G_k	3.55	kN/m²		$f_{c,90,d}$	1.38	MPa
	Floor Q_k	2.00	kN/m²		b vert. Stud	80	mm
Roof Floor	Floor G_k	2.24	kN/m²		h vert. Stud	160	mm
	Roof G_k	1.00	kN/m²		h hor. Stud	160	mm
	Floor Q_k	0.00	kN/m²		Stud spac.	625	mm
Load on stud - internal wall_					Floor Span	3140	mm
	$1.3 \cdot G_k$	$1.5 \cdot Q_k$	ULS				
Base floor	10.88	5.89	16.76	kN			
I floor	10.88	5.89	16.76	kN			
II floor	10.88	5.89	16.76	kN			
III floor	13.43	0.00	13.43	kN			
		Total:	63.72				

Check_					
Othogonal compression stud					
$k_{c,90}$	1.25	-			
A_{eff}	64933	mm²			
$\sigma_{c,90}$	0.98	<	1.38	MPa	Ok!
Instability check stud					
kcrit	0.72				
$\sigma_{c,0,d}$	4.98	<	11.59	MPa	Ok!

The summary of the most loaded stud is reported in Table 16, corresponding to a 160x80 in an internal LFT wall collocated in the base floor of the 4 storeys building.

Thus, the so designed floors and LTF walls are verified under static loads.

6.4 Seismic design

Since the aim of the research is to evaluate the q-behaviour factor for LFT buildings, the seismic design is approached differently with respect to the static check. The safety factors of material and connections were set to 1.0, in order to not add code-dependent overstrength. In this way, the q-factor is not linked to the standard used to design the structure and can be related to standards later, adding a design overstrength factor.

The Life Safety Limit State actions were taken in accordance to the previous paragraphs, applying equation (15) and (16) to obtain the shear acting on sheathing-to-framing connections and angle brackets, and normal stress on hold-downs.

For regular building, since symmetric conditions applies, LFT walls were design according to four types: internal and external walls, in X and Y direction according to Fig. 62.

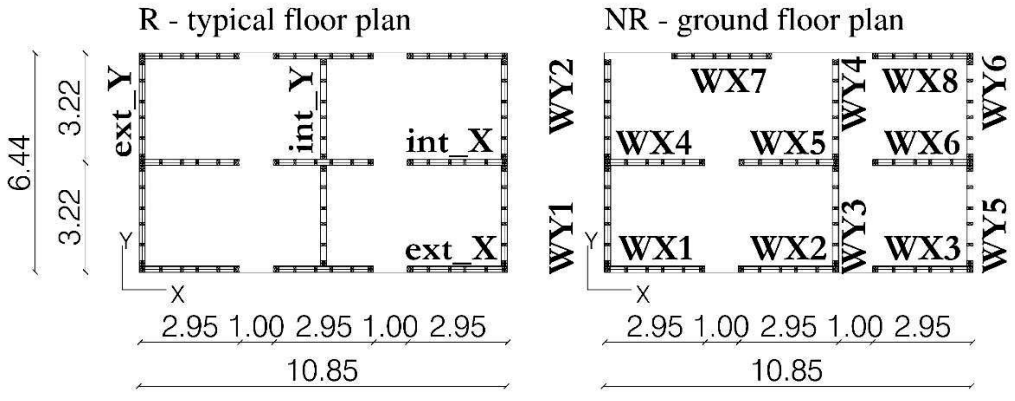

Fig. 62 – Labelling of LFT walls for regular and non-regular buildings.

This assumption was not suitable for non-regular buildings, were the checks were performed wall by wall, considering however a limited set of walls, in order to simulate practice design where it is not convenient to have a huge variability in construction detailing.

In the tables reported herein, the shear verification for each building and for each ductility class was performed. To each wall of Fig. 62, a LFT wall of paragraph 5.3 was attributed. Furthermore, a maximum difference between capacity and demand was set, considering ±15%, in order to not affect the results of the q-behaviour but also to represent a typical design procedure, where the capacity is never perfectly equal to the demand. Since no safety factors were applied, the difference was taken also in the minus direction. As it can be seen, some results exceed these values, but it was considered acceptable. The set of walls created in the previous paragraph, in fact, reproduce typical walls arrangement, setting nail spacing of the design practice. To overcome the problem of exceeding the 15% limit it would be necessary to use wall with particular fasteners disposition, which would be unrealistic (e.g. nails spaced 132 mm…). From Table 17 to Table 22, the label of each wall (according to Table 7), the number of the storey, the shear demand F_{ed} and the ratio between capacity and demand F_{rd}/F_{ed} is reported, for ductility classes of sheathing-to-framing connections equal to 4, 6 and 8.

Known the demand, the minimum number of Angle-Brackets and Hold-Down was evaluated. A Capacity Design approach was used, according to [16]. A γ_{rd}=1.6 was set, and an α value was evaluated for each i-th storey and for each wall according to:

$$\alpha_i = \gamma_{rd} \frac{F_{rd,i}}{F_{ed,i}} \tag{22}$$

Where F_{rd} and F_{ed} are the capacity of the sheathing-to-framing connection and the acting seismic shear force, as defined form Table 17 to Table 22.

Table 17 – Regular building – 2 storeys.

ID	Storey	Fed	μ=4 Frd/Fed	μ=4 LFT_id	μ=6 Frd/Fed	μ=6 LFT_id	μ=8 Frd/Fed	μ=8 LFT_id
int_X	1	21.48	1.01	2	1.07	2	1.01	2
ext_X	1	22.71	0.95	2	1.01	2	0.95	2
int_Y	1	31.02	1.14	6	1.21	5	1.14	6
int_Y	1	34.73	1.02	6	1.08	5	1.02	6
int_X	2	12.43	0.90	1	1.07	1	1.02	1
ext_X	2	12.82	0.87	1	1.04	1	0.99	1
int_Y	2	16.87	1.28	2	1.36	2	1.28	2
int_Y	2	18.81	1.15	2	1.22	2	1.15	2

Table 18 – Regular building – 3 storeys.

ID	Storey	Fed	μ=4 Frd/Fed	μ=4 LFT_id	μ=6 Frd/Fed	μ=6 LFT_id	μ=8 Frd/Fed	μ=8 LFT_id
int_X	1	29.35	1.02	6	1.12	6	1.21	6
ext_X	1	30.98	0.96	6	1.06	6	1.15	6
int_Y	1	35.27	1.03	5	1.05	5	1.01	6
int_Y	1	39.98	0.91	5	0.92	5	0.93	5
int_X	2	24.33	0.95	4	1.05	4	1.11	4
ext_X	2	25.22	0.92	4	1.01	4	1.07	4
int_Y	2	27.89	1.07	6	0.96	3	0.97	4
int_Y	2	31.35	0.95	6	1.05	6	1.13	6
int_X	3	12.82	0.87	1	0.96	1	0.99	1
ext_X	3	12.88	0.87	1	0.95	1	0.99	1
int_Y	3	14.15	1.31	2	0.94	1	0.94	1
int_Y	3	15.83	1.17	2	0.84	1	0.84	1

Table 19 - Regular building – 4 storeys.

			μ=4		μ=6		μ=8	
ID	Storey	Fed	Frd/Fed	LFT_id	Frd/Fed	LFT_id	Frd/Fed	LFT_id
int_X	1	28.31	1.06	6	1.16	6	0.95	4
ext_X	1	29.87	1.00	6	1.10	6	0.90	4
int_Y	1	36.45	1.00	5	0.90	6	0.97	6
int_Y	1	36.45	1.00	5	1.01	5	1.02	5
int_X	2	24.54	1.07	3	1.09	3	1.10	3
ext_X	2	26.78	0.98	3	1.00	3	1.00	3
int_Y	2	29.89	1.00	6	1.10	6	1.19	6
int_Y	2	29.89	1.00	6	1.10	6	1.19	6
int_X	3	19.99	0.93	2	1.03	2	1.08	2
ext_X	3	20.21	0.92	2	1.02	2	1.07	2
int_Y	3	23.09	1.00	4	0.89	2	0.94	2
int_Y	3	26.35	1.00	3	1.01	3	1.02	3
int_X	4	11.03	1.02	1	1.11	1	1.15	1
ext_X	4	10.66	1.05	1	1.15	1	1.19	1
int_Y	4	11.22	1.00	1	1.09	1	1.13	1
int_Y	4	11.22	1.00	1	1.09	1	1.13	1

Table 20 – Non-regular building – 2 storeys.

ID	Storey	Fed	μ=4 Frd/Fed	LFT_id	μ=6 Frd/Fed	LFT_id	μ=8 Frd/Fed	LFT_id
WX1	1	18.54	1.00	2	1.11	2	1.17	2
WX2	1	18.52	1.00	2	1.11	2	1.17	2
WX3	1	19.04	0.98	2	1.08	2	1.14	2
WX4	1	18.42	1.01	2	1.12	2	1.18	2
WX5	1	18.44	1.01	2	1.12	2	1.17	2
WX6	1	18.84	0.99	2	1.09	2	1.15	2
WX7	1	22.56	1.02	4	1.13	4	1.20	4
WX8	1	23.28	0.99	4	1.10	4	1.16	4
WY1	1	36.75	0.99	5	1.00	5	1.01	5
WY2	1	37.00	0.99	5	1.00	5	1.00	5
WY3	1	20.91	1.10	4	0.98	2	1.04	2
WY4	1	21.35	1.08	4	0.96	2	1.01	2
WY5	1	17.41	1.07	2	1.18	2	1.24	2
WY6	1	17.41	1.07	2	1.18	2	1.24	2
WX1	2	13.66	0.82	1	0.90	1	0.93	1
WX2	2	13.32	0.84	1	0.92	1	0.95	1
WX4	2	15.90	1.17	2	1.29	2	0.80	1
WX5	2	15.33	1.21	2	1.34	2	0.83	1
WX7	2	19.97	1.16	4	1.03	2	1.08	2
WY1	2	20.26	1.14	4	1.02	2	1.07	2
WY2	2	20.40	1.13	4	1.01	2	1.06	2
WY3	2	18.21	1.02	2	1.13	2	1.19	2
WY4	2	18.32	1.02	2	1.12	2	1.18	2

Table 21 – Non-regular building – 3 storeys.

ID	Storey	Fed	μ=4 Frd/Fed	LFT id	μ=6 Frd/Fed	LFT id	μ=8 Frd/Fed	LFT id
WX1	1	21.8	1.06	4	0.95	2	0.99	2
WX2	1	21.8	1.06	4	0.95	2	1.00	2
WX3	1	23.1	1.00	4	1.11	4	0.94	2
WX4	1	21.6	1.07	4	0.95	2	1.00	2
WX5	1	21.7	1.07	4	0.95	2	1.00	2
WX6	1	22.8	1.01	4	1.12	4	0.95	2
WX7	1	26.5	1.00	3	0.97	4	1.02	4
WX8	1	28.4	1.05	6	1.16	6	0.95	4
WY1	1	40.5	0.90	5	0.91	5	0.92	5
WY2	1	40.9	0.89	5	0.90	5	0.91	5
WY3	1	22.0	1.05	4	0.93	2	0.98	2
WY4	1	22.7	1.02	4	0.91	2	0.96	2
WY5	1	19.1	0.97	2	1.08	2	1.13	2
WY6	1	19.1	0.97	2	1.08	2	1.13	2
WX1	2	24.5	0.94	4	1.04	4	1.10	4
WX2	2	23.9	0.97	4	1.07	4	1.13	4
WX4	2	28.6	0.92	3	0.93	3	0.94	3
WX5	2	27.7	0.95	3	0.96	3	0.97	3
WX7	2	36.2	1.01	5	1.02	5	1.03	5
WY1	2	32.8	1.11	5	1.12	5	1.13	5
WY2	2	33.0	1.10	5	1.12	5	1.12	5
WY3	2	30.0	1.00	6	1.10	6	1.18	6
WY4	2	30.2	0.99	6	1.09	6	1.17	6
WX1	3	13.0	0.87	1	0.95	1	0.98	1
WX2	3	12.8	0.88	1	0.96	1	1.00	1
WX4	3	15.6	1.19	2	0.78	1	0.81	1
WX5	3	15.2	1.22	2	0.80	1	0.83	1
WX7	3	18.9	0.98	2	1.09	2	1.15	2
WY1	3	17.5	1.07	2	1.18	2	1.24	2
WY2	3	17.5	1.06	2	1.17	2	1.23	2
WY3	3	16.3	1.14	2	1.26	2	1.33	2
WY4	3	16.4	1.13	2	1.26	2	1.32	2

Table 22 – Non-regular buildings – 4 storeys.

ID	Storey	Fed	μ=4 Frd/Fed	LFT_id	μ=6 Frd/Fed	LFT_id	μ=8 Frd/Fed	LFT_id
WX1	1	20.4	1.13	4	1.01	2	1.06	2
WX2	1	20.3	1.14	4	1.01	2	1.07	2
WX3	1	21.8	1.06	4	0.94	2	0.99	2
WX4	1	20.2	1.14	4	1.02	2	1.07	2
WX5	1	20.3	1.14	4	1.02	2	1.07	2
WX6	1	21.4	1.08	4	0.96	2	1.01	2
WX7	1	25.0	1.06	3	1.07	3	1.08	4
WX8	1	27.2	1.10	6	0.98	3	0.99	4
WY1	1	39.2	0.93	5	0.94	5	0.95	5
WY2	1	39.7	0.92	5	0.93	5	0.93	5
WY3	1	20.9	1.10	4	0.98	2	1.04	2
WY4	1	21.7	1.06	4	0.95	2	1.00	2
WY5	1	19.3	0.96	2	1.07	2	1.12	2
WY6	1	19.3	0.96	2	1.07	2	1.12	2
WX1	2	25.0	0.92	4	1.02	4	1.08	4
WX2	2	24.4	0.95	4	1.05	4	1.11	4
WX4	2	29.3	1.02	6	1.12	6	1.21	6
WX5	2	28.4	1.05	6	1.16	6	1.25	6
WX7	2	37.4	0.98	5	0.99	5	0.99	5
WY1	2	34.8	1.05	5	1.06	5	1.07	5
WY2	2	35.1	1.04	5	1.05	5	1.06	5
WY3	2	32.4	0.92	6	1.01	6	1.10	6
WY4	2	32.8	0.91	6	1.00	6	1.08	6
WX1	3	19.4	1.19	4	1.06	2	1.12	2
WX2	3	19.0	1.22	4	1.08	2	1.14	2
WX4	3	23.0	1.00	4	1.11	4	1.17	4
WX5	3	22.4	1.03	4	1.14	4	1.20	4
WX7	3	28.3	1.06	6	1.16	6	1.25	6
WY1	3	26.9	0.98	3	0.99	3	1.00	3
WY2	3	27.1	0.97	3	0.99	3	0.99	3
WY3	3	25.0	0.92	4	1.02	4	1.08	4
WY4	3	25.2	0.91	4	1.01	4	1.07	4
WX1	4	10.7	1.05	1	1.14	1	1.19	1
WX2	4	10.6	1.06	1	1.16	1	1.20	1
WX4	4	13.3	0.84	1	0.92	1	0.96	1
WX5	4	13.0	0.86	1	0.94	1	0.97	1
WX7	4	15.2	1.22	2	0.81	1	0.84	1
WY1	4	15.0	1.24	2	0.82	1	0.85	1
WY2	4	15.1	1.24	2	0.81	1	0.84	1
WY3	4	14.0	0.80	1	0.88	1	0.91	1
WY4	4	14.1	0.80	1	0.87	1	0.90	1

The value of α was taken as the minimum among the values at each floor, but always greater than or equal to 1.6. The total number of angle-brackets N_{AB} and the number of hold-downs N_{HD} for each end were evaluated according to the following equations:

$$N_{AB} = \frac{\alpha \cdot F_{ed,i}}{V_{rd,AB}} \tag{23}$$

$$N_{HD} = \frac{\alpha \cdot N_{ed,i} - N_{grav}}{N_{rd,HD}} \tag{24}$$

Where F_{ed} and N_{ed} are the seismic shear and tension, N_{grav} is the compression due to dead loads and $V_{rd,AB}$ and $N_{rd,HD}$ are the capacity of a single component, taken from the experimental tests (see §4.1). Since the behaviour of both devices was considered elastic during the dynamic analysis, no rounding was performed. However, a maximum of 4 hold-downs for each side was considered acceptable, since a larger number would create difficulties in assembly and problem linked to minimum spacing between connectors.

Results of the evaluation of N_{AB} and N_{HD} are reported from Table 23 to Table 28.

Table 23 – Regular buildings – 2 storeys – Angle brackets and Hold-downs.

ID	Storey	$V_{ed,CD}$	$N_{ed,CD}$	μ=4		μ=6		μ=8	
				N. AB	N HD	N. AB	N HD	N. AB	N HD
int_X	1	34.37	50.62	1.47	1.09	1.57	1.18	1.48	1.10
ext_X	1	36.34	56.86	1.56	1.23	1.57	1.24	1.56	1.23
int_Y	1	54.72	90.47	2.35	1.95	2.58	2.15	2.43	2.03
int_Y	1	55.57	91.62	2.38	1.98	2.58	2.14	2.43	2.02
int_X	2	19.88	18.27	0.85	0.39	0.91	0.43	0.86	0.40
ext_X	2	20.52	20.58	0.88	0.44	0.89	0.45	0.88	0.44
int_Y	2	29.76	32.53	1.28	0.70	1.40	0.77	1.32	0.73
int_Y	2	30.10	32.84	1.29	0.71	1.40	0.77	1.32	0.72

Table 24 – Regular buildings – 3 storeys – Angle brackets and Hold-downs.

ID	Storey	$V_{ed,CD}$	$N_{ed,CD}$	μ=4 N. AB	N HD	μ=6 N. AB	N HD	μ=8 N. AB	N HD
int_X	1	46.97	101.00	2.01	2.18	2.01	2.18	2.01	2.18
ext_X	1	49.57	111.80	2.12	2.41	2.12	2.41	2.12	2.41
int_Y	1	58.32	137.45	2.50	2.96	2.42	2.87	2.42	2.87
int_Y	1	63.97	149.84	2.74	3.23	2.74	3.23	2.74	3.23
int_X	2	38.94	55.53	1.67	1.20	1.67	1.20	1.67	1.20
ext_X	2	40.36	61.55	1.73	1.33	1.73	1.33	1.73	1.33
int_Y	2	46.11	75.67	1.98	1.63	1.91	1.58	1.91	1.58
int_Y	2	50.16	82.11	2.15	1.77	2.15	1.77	2.15	1.77
int_X	3	20.52	18.20	0.88	0.39	0.88	0.39	0.88	0.39
ext_X	3	20.61	20.24	0.88	0.44	0.88	0.44	0.88	0.44
int_Y	3	23.39	25.41	1.00	0.55	0.97	0.53	0.97	0.53
int_Y	3	25.33	27.47	1.09	0.59	1.09	0.59	1.09	0.59

Table 25 – Regular buildings – 4 storeys – Angle brackets and Hold-downs.

ID	Storey	$V_{ed,CD}$	$N_{ed,CD}$	μ=4 N. AB	N HD	μ=6 N. AB	N HD	μ=8 N. AB	N HD
int_X	1	45.29	123.68	1.94	2.67	2.00	2.76	1.94	2.67
ext_X	1	47.79	139.84	2.05	3.02	2.05	3.02	2.05	3.02
int_Y	1	53.25	164.41	2.28	3.55	2.28	3.55	2.28	3.55
int_Y	1	61.48	187.25	2.64	4.04	2.64	4.04	2.64	4.04
int_X	2	39.26	80.22	1.68	1.73	1.73	1.79	1.68	1.73
ext_X	2	42.85	91.63	1.84	1.98	1.84	1.98	1.84	1.98
int_Y	2	46.11	108.08	1.98	2.33	1.98	2.33	1.98	2.33
int_Y	2	52.62	122.21	2.26	2.64	2.26	2.64	2.26	2.64
int_X	3	31.98	42.97	1.37	0.93	1.41	0.96	1.37	0.93
ext_X	3	32.33	47.81	1.39	1.03	1.39	1.03	1.39	1.03
int_Y	3	35.06	57.87	1.50	1.25	1.50	1.25	1.50	1.25
int_Y	3	39.46	64.91	1.69	1.40	1.69	1.40	1.69	1.40
int_X	4	17.65	14.38	0.76	0.31	0.78	0.32	0.76	0.31
ext_X	4	17.06	15.96	0.73	0.34	0.73	0.34	0.73	0.34
int_Y	4	18.46	19.88	0.79	0.43	0.79	0.43	0.79	0.43
int_Y	4	20.61	22.18	0.88	0.48	0.88	0.48	0.88	0.48

Table 26 – Non-Regular buildings – 2 storeys – Angle brackets and Hold-downs.

ID	Storey	$V_{ed,CD}$	$N_{ed,CD}$	μ=4 N. AB	μ=4 N HD	μ=6 N. AB	μ=6 N HD	μ=8 N. AB	μ=8 N HD
WX1	1	29.95	51.83	1.28	1.12	1.42	1.25	1.27	1.11
WX2	1	29.92	48.40	1.28	1.04	1.42	1.17	1.27	1.03
WX3	1	30.76	31.32	1.32	0.68	1.46	0.75	1.31	0.67
WX4	1	29.76	52.16	1.28	1.12	1.41	1.26	1.26	1.11
WX5	1	29.80	45.83	1.28	0.99	1.41	1.12	1.26	0.98
WX6	1	30.44	29.70	1.30	0.64	1.44	0.72	1.29	0.63
WX7	1	36.45	59.84	1.56	1.29	1.73	1.46	1.55	1.27
WX8	1	37.61	38.63	1.61	0.83	1.78	0.93	1.60	0.82
WY1	1	59.38	98.96	2.55	2.13	2.82	2.36	2.52	2.11
WY2	1	59.78	99.05	2.56	2.14	2.84	2.37	2.54	2.11
WY3	1	33.78	68.02	1.45	1.47	1.60	1.62	1.43	1.45
WY4	1	34.50	68.27	1.48	1.47	1.64	1.63	1.46	1.46
WY5	1	28.13	29.80	1.21	0.64	1.33	0.71	1.19	0.64
WY6	1	28.13	29.79	1.21	0.64	1.33	0.71	1.19	0.64
WX1	2	22.07	22.34	0.95	0.48	1.05	0.54	0.94	0.48
WX2	2	21.52	21.75	0.92	0.47	1.02	0.52	0.91	0.46
WX4	2	25.69	24.71	1.10	0.53	1.22	0.60	1.09	0.53
WX5	2	24.76	23.86	1.06	0.51	1.17	0.58	1.05	0.51
WX7	2	32.27	29.21	1.38	0.63	1.53	0.71	1.37	0.62
WY1	2	32.74	35.89	1.40	0.77	1.55	0.86	1.39	0.77
WY2	2	32.96	35.90	1.41	0.77	1.56	0.86	1.40	0.77
WY3	2	29.42	32.26	1.26	0.70	1.40	0.77	1.25	0.69
WY4	2	29.60	32.16	1.27	0.69	1.40	0.77	1.26	0.69

Table 27 – Non-Regular buildings – 3 storeys – Angle brackets and Hold-downs.

ID	Storey	$V_{ed,CD}$	$N_{ed,CD}$	μ=4 N. AB	μ=4 N HD	μ=6 N. AB	μ=6 N HD	μ=8 N. AB	μ=8 N HD
WX1	1	34.84	95.00	1.49	2.05	1.49	2.05	1.49	2.05
WX2	1	34.81	90.72	1.49	1.96	1.49	1.96	1.49	1.96
WX3	1	36.93	37.92	1.58	0.82	1.58	0.82	1.58	0.82
WX4	1	34.57	100.36	1.48	2.16	1.48	2.16	1.48	2.16
WX5	1	34.68	92.94	1.49	2.00	1.49	2.00	1.49	2.00
WX6	1	36.51	36.19	1.56	0.78	1.56	0.78	1.56	0.78
WX7	1	42.35	119.25	1.82	2.57	1.82	2.57	1.82	2.57
WX8	1	45.45	47.02	1.95	1.01	1.95	1.01	1.95	1.01
WY1	1	64.80	157.20	2.78	3.39	2.78	3.39	2.78	3.39
WY2	1	65.39	156.56	2.80	3.38	2.80	3.38	2.80	3.38
WY3	1	35.24	118.65	1.51	2.56	1.51	2.56	1.51	2.56
WY4	1	36.26	118.30	1.55	2.55	1.55	2.55	1.55	2.55
WY5	1	30.52	32.38	1.31	0.70	1.31	0.70	1.31	0.70
WY6	1	30.52	32.38	1.31	0.70	1.31	0.70	1.31	0.70
WX1	2	39.18	60.51	1.68	1.30	1.68	1.30	1.68	1.30
WX2	2	38.17	59.03	1.64	1.27	1.64	1.27	1.64	1.27
WX4	2	45.76	68.13	1.96	1.47	1.96	1.47	1.96	1.47
WX5	2	44.32	66.12	1.90	1.43	1.90	1.43	1.90	1.43
WX7	2	57.90	82.37	2.48	1.78	2.48	1.78	2.48	1.78
WY1	2	52.50	88.31	2.25	1.90	2.25	1.90	2.25	1.90
WY2	2	52.87	87.52	2.27	1.89	2.27	1.89	2.27	1.89
WY3	2	47.97	81.33	2.06	1.75	2.06	1.75	2.06	1.75
WY4	2	48.34	80.42	2.07	1.73	2.07	1.73	2.07	1.73
WX1	3	20.74	20.42	0.89	0.44	0.89	0.44	0.89	0.44
WX2	3	20.41	20.08	0.87	0.43	0.87	0.43	0.87	0.43
WX4	3	25.02	23.21	1.07	0.50	1.07	0.50	1.07	0.50
WX5	3	24.37	22.60	1.04	0.49	1.04	0.49	1.04	0.49
WX7	3	30.25	26.87	1.30	0.58	1.30	0.58	1.30	0.58
WY1	3	27.93	30.61	1.20	0.66	1.20	0.66	1.20	0.66
WY2	3	28.06	30.30	1.20	0.65	1.20	0.65	1.20	0.65
WY3	3	26.07	28.58	1.12	0.62	1.12	0.62	1.12	0.62
WY4	3	26.23	28.25	1.12	0.61	1.12	0.61	1.12	0.61

Table 28 – Non-Regular buildings – 4 storeys – Angle brackets and Hold-downs.

ID	Storey	$V_{ed,CD}$	$N_{ed,CD}$	μ=4 N. AB	μ=4 N HD	μ=6 N. AB	μ=6 N HD	μ=8 N. AB	μ=8 N HD
WX1	1	32.58	119.27	1.40	2.57	1.40	2.57	1.40	2.57
WX2	1	32.50	114.39	1.39	2.47	1.39	2.47	1.39	2.47
WX3	1	34.91	35.77	1.50	0.77	1.50	0.77	1.50	0.77
WX4	1	32.30	127.67	1.38	2.75	1.38	2.75	1.38	2.75
WX5	1	32.42	127.58	1.39	2.75	1.39	2.75	1.39	2.75
WX6	1	34.24	33.76	1.47	0.73	1.47	0.73	1.47	0.73
WX7	1	39.96	153.48	1.71	3.31	1.71	3.31	1.71	3.31
WX8	1	43.56	44.99	1.87	0.97	1.87	0.97	1.87	0.97
WY1	1	62.79	201.49	2.69	4.35	2.69	4.35	2.69	4.35
WY2	1	63.58	199.93	2.73	4.31	2.73	4.31	2.73	4.31
WY3	1	33.44	161.03	1.43	3.47	1.43	3.47	1.43	3.47
WY4	1	34.72	159.86	1.49	3.45	1.49	3.45	1.49	3.45
WY5	1	30.90	32.79	1.32	0.71	1.32	0.71	1.32	0.71
WY6	1	30.90	32.79	1.32	0.71	1.32	0.71	1.32	0.71
WX1	2	40.07	87.33	1.72	1.88	1.72	1.88	1.72	1.88
WX2	2	39.07	85.29	1.67	1.84	1.67	1.84	1.67	1.84
WX4	2	46.85	98.08	2.01	2.12	2.01	2.12	2.01	2.12
WX5	2	45.43	103.19	1.95	2.23	1.95	2.23	1.95	2.23
WX7	2	59.80	119.19	2.56	2.57	2.56	2.57	2.56	2.57
WY1	2	55.60	134.74	2.38	2.91	2.38	2.91	2.38	2.91
WY2	2	56.19	132.90	2.41	2.87	2.41	2.87	2.41	2.87
WY3	2	51.84	125.63	2.22	2.71	2.22	2.71	2.22	2.71
WY4	2	52.43	123.69	2.25	2.67	2.25	2.67	2.25	2.67
WX1	3	31.00	46.52	1.33	1.00	1.33	1.00	1.33	1.00
WX2	3	30.38	45.59	1.30	0.98	1.30	0.98	1.30	0.98
WX4	3	36.86	52.38	1.58	1.13	1.58	1.13	1.58	1.13
WX5	3	35.92	58.43	1.54	1.26	1.54	1.26	1.54	1.26
WX7	3	45.28	61.64	1.94	1.33	1.94	1.33	1.94	1.33
WY1	3	42.98	73.58	1.84	1.59	1.84	1.59	1.84	1.59
WY2	3	43.31	72.12	1.86	1.56	1.86	1.56	1.86	1.56
WY3	3	39.99	68.58	1.71	1.48	1.71	1.48	1.71	1.48
WY4	3	40.38	67.11	1.73	1.45	1.73	1.45	1.73	1.45
WX1	4	17.15	16.08	0.74	0.35	0.74	0.35	0.74	0.35
WX2	4	16.93	15.84	0.73	0.34	0.73	0.34	0.73	0.34
WX4	4	21.24	18.37	0.91	0.40	0.91	0.40	0.91	0.40
WX5	4	20.87	23.06	0.89	0.50	0.89	0.50	0.89	0.50
WX7	4	24.30	20.21	1.04	0.44	1.04	0.44	1.04	0.44
WY1	4	23.97	26.26	1.03	0.57	1.03	0.57	1.03	0.57
WY2	4	24.08	25.75	1.03	0.56	1.03	0.56	1.03	0.56
WY3	4	22.40	24.53	0.96	0.53	0.96	0.53	0.96	0.53
WY4	4	22.53	24.02	0.97	0.52	0.97	0.52	0.97	0.52

Both anchoring devices were modelled as non-linear elastic links, according to the laboratory outcome. Since they work in parallel, the global stiffness of the group of connectors was evaluated as N_{AB} or N_{HD} springs in parallel.

6.5 Final remarks

It is worth noticing that all the energy dissipation in this study is allocated in the sheathing-to-framing connection. Other source of ductility, such as hold-down and angle-brackets plasticisation are neglected, since a Capacity Design approach was applied. Under this assumption, rocking behaviour of tall walls was not considered. Thus, the q-behaviour factor of this research must be taken as a lower limit: the values, especially for higher ductility classes, could be increased to consider also other dissipation sources.

I-7 IDA APPROACH

In this chapter, the complete IDA procedure to compute the q-behaviour factor was described. In the first paragraph the Incremental Dynamic Analysis is discussed, and the Intensity Measures and the Engineering Demand Parameter were set. Furthermore, the complete set of ground motions was reported. In the second paragraph, the complete procedure to compute the q-behaviour factor was report, highlighting the yield point evaluation method for each reference building and ductility class.

7.1 IDA Analysis

IDA consists of the execution of several nonlinear dynamic analyses under a multiple-scaled set of ground motion records [71]. Every IDA curve represents the relationship between the Engineering Demand Parameter EDP and the Intensity Measure IM.

In this research, the typical reaction-side method to evaluate q was used, evaluating the ratio between the elastic and the plastic base shear. This approach is IM independent, and overcome the issue of a suitable measure for the structures, which is still a debated topic.

In order to perform the IDA analysis, two IMs were selected among those presents in chapter 3.

The Peak Ground Acceleration represent an intuitive and simple parameter to describe the seismic input. Evaluated as the maximum recorded horizontal acceleration, the PGA is structure-independent and is an intrinsic parameter of the accelerogram. Given this consideration, a non-optimal correlation between the buildings and the PGA is

expected; however, the PGA allows to compare the IDA curves for all the reference buildings at once.

To avoid the aforementioned issue on the PGA, the average spectral acceleration $S_{a,avg}$ was also used, defined as the geometric mean of spectral acceleration values between two selected periods. In this case, 0.2·T and 3·T where selected according to [74], where T is the period of the first vibration mode of the structure. Table 29 shows the fundamental periods for each reference structure; the mean T_{1m} of the two translation modes in X and Y (T_{1x} and T_{1y}) was taken to compute the $S_{a,avg}$. Good results were obtained in the literature using $S_{a,avg}$ as IM [75][90]. The presence of the fundamental vibration frequency of the building, in fact, link the intensity measure to the structural response itself, giving a more reliable indicator. As discussed previously in the work, the q-factor evaluation method is IM-independent. Nevertheless, the IDA curves are always rescalable to other IMs [71].

Table 29 – First mode periods (T_{1x} and T_{1y}) and mean period T_{1m} of the reference buildings.

Regularity	**N. Storeys**	**T_{1x}** [s]	**T_{1y}** [s]	**T_{1m}** [s]
R	2	0.37	0.31	0.34
R	3	0.56	0.46	0.51
R	4	0.77	0.64	0.70
NR	2	0.34	0.33	0.34
NR	3	0.53	0.45	0.49
NR	4	0.73	0.63	0.68

Furthermore, an Engineering Demand Parameter was defined. In the literature, several EDP are available. Typically, interstorey drift or mean interstorey drifts are used when considering the global behaviour of a building. Furthermore, a component level definition can be done, analysing the chord rotation of vertical members, or the state of connections. In this research, the Roof Drift Ratio was selected as EDP, defined as the ratio between the maximum roof displacement and the building height. This choice allows also a parallelism with pushover analysis, where the center of mass of the upper floor is generally chosen as control point. Furthermore, the RDR is suitable for the collapse

detection, since considering the building entirely collapsed when only one wall reaches the ultimate conditions is too conservative.

To further proceed, the collapse point of the structure needs to be defined. According to Chapter 3, the collapse point was identified in correspondence of the onset of dynamic instability, set as 80% reduction of the elastic stiffness.

An algorithm to perform the complete IDA analysis was developed in MATLAB [91], using the OAPI of SAP2000 [85]. For each IDA, several non-linear dynamic analyses were executed, one for each level of PGA.

The FEM model of the reference buildings were built using the simplified wall models of Chapter 4 (Fig. 63).

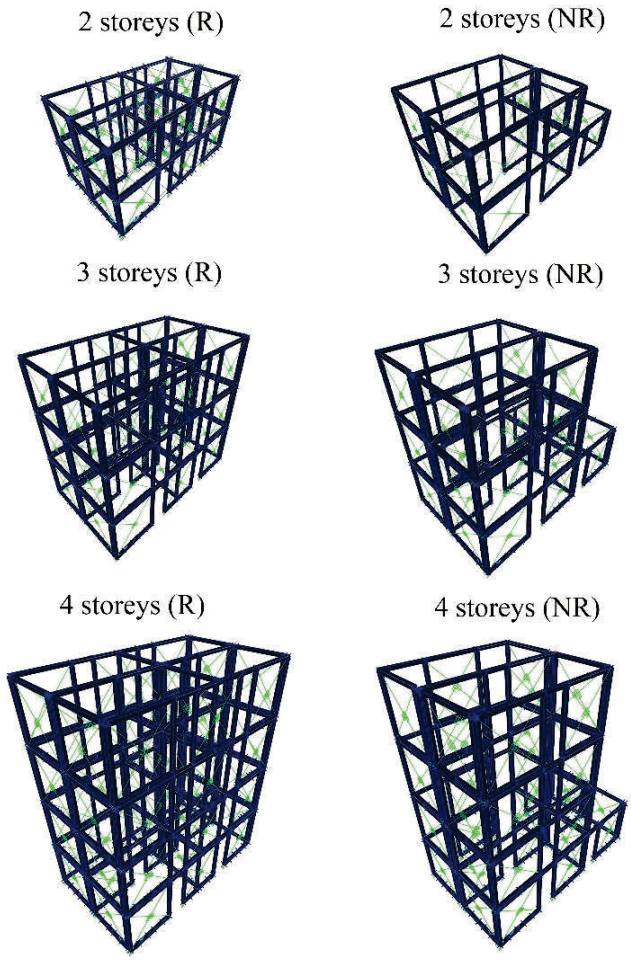

Fig. 63 – FEM models of the reference buildings for the IDA procedure.

The diagonals spring were assigned with the non-linear behaviours calculated in §4.2.2, according to the seismic demand. Hold-downs and angle brackets were considered non-linear elastic, and their behaviour was checked during the dynamic analysis, to ensure the elastic behaviour assumption was valid. The experimental force-displacement curves of Chapter 4 were used, inserting anchors in parallel to achieve the number needed from Capacity Design. A constraint reproducing the rigid diaphragm condition was set at each level, and a Rayleigh damping at 2% was considered.

Since the collapse was seek, a constant pass was used, increasing the IM till dynamic instability, 0.10g each step. When the flat line is detected (as a >80% reduction of the elastic stiffness, which was evaluated as the drift in the first step over the PGA), a bisection method was used, in order to define the collapse point with a precision of 0.0125g. In Fig. 64 an example of IDA is reported, taken from the results of this research. A zoom-in was done, to highlight the bisection procedure. Since step VIII individuated the collapse, the step was halved to 0.05g for step IX. Proceeding in this way, step XI was reached, finding the collapse point at 0.7125 m/s^2 The IDA curves were then re-scaled to $S_{a,avg}$. The complete procedure is summed in Fig. 65.

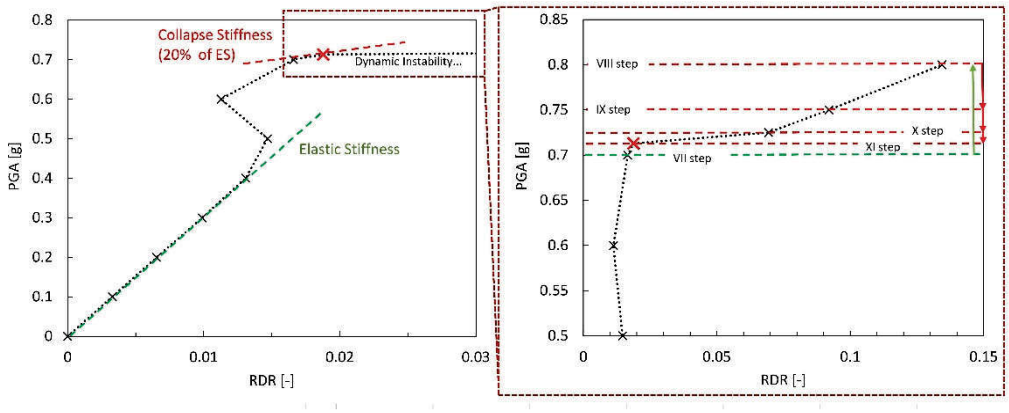

Fig. 64 – IDA procedure to detect the collapse point. On the right, the bisection process.

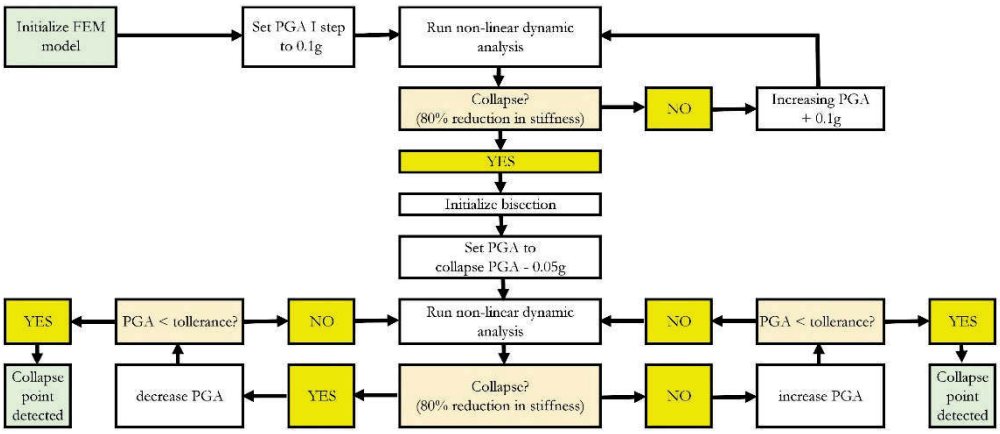

Fig. 65 – Complete IDA algorithm.

Ten to twenty records are sufficient for a reliable IDA analyses [71][92]. Thus, twenty records were selected by means of Rexel software [93] (Table 30). 360 IDAs were carried out, 60 for each ductility class, for a total of more than 7000 single non-linear dynamic analyses. Since the evaluation of the q-factor was performed for European buildings, a preference to earthquake coming from Italy and the Europe was considered. Nonetheless, a minor part of signals from Turkey and Asia were considered, to have a wider set of accelerograms. Moreover, no spectrum-compatibility was considered, since no specific location in Europe was selected. Indeed, to perform IDA analysis, different signals are necessary, to cover a wide set of possible earthquakes. To this aim, near field and strong motion signals were taken into account ($R<35$ km and $M_w>5$, see Table 30).

The pairs of accelerograms were applied together in X and Y direction. The RDR was evaluated step-by-step during the non-linear dynamic analysis, as a vectoral sum of the two components.

On the other hand, the maximum value of IM in X and Y was selected. As reported in [94], the use of the arithmetic mean, the geometric mean, the maximum value or the SRSS combination leads to comparable results, thus not affecting the analyses. Moreover, the choice does not affect the evaluation of the q-factor, since the base shear are evaluated independently of the choice of the IM.

Table 30 – List of record used in the IDA procedure.

ID	Earthquake name	Waveform ID	Database	Data	M_w	R (km)	PGA_X (m/s^2)	PGA_Y (m/s^2)
1	Friuli Earthq 1st shock	IT0014	ITACA	06/05/1976	6.4	22	3.39	3.09
2	L'Aquila Mainshock	IT0792	ITACA	06/04/2009	6.3	5	5.35	6.44
3	Campano Lucano	291	ESM	23/11/1980	6.9	16	1.53	1.73
4	Friuli (Aftershock)	146	ESM	15/09/1976	6.0	14	3.40	3.30
5	Kalamata	414	ESM	13/09/1986	5.9	11	2.35	2.67
6	Erzican	535	ESM	13/03/1992	6.6	13	3.81	5.03
7	Umbria Marche	594	ESM	26/09/1997	6.0	11	5.14	4.54
8	Montenegro	196	ESM	15/04/1979	6.9	25	4.45	3.00
9	South Iceland	4673	ESM	17/06/2000	6.5	15	2.04	4.68
10	Bam (Iran)	230	ISMN	26/12/2003	6.5	6	7.85	6.28
11	Bingol	7142	ESM	01/05/2003	6.3	14	5.05	2.92
12	Tabas	182	ESM	16/09/1978	7.3	12	3.32	3.78
13	SE of Tirana	3802	ESM	09/01/1988	5.9	7	1.11	4.04
14	Friuli Earthq 2nd shock	80	ITACA	11/09/1976	5.6	15	3.22	2.93
15	Friuli Earthq 3rd shock	89	ITACA	15/09/1976	5.9	17	2.58	2.11
16	Irpinia earthquake	181	ITACA	23/11/1980	6.9	33	2.21	3.10
17	East sicily	335	ITACA	13/12/1990	5.6	31	2.46	2.04
18	App. Umbro-marchigiano	442	ITACA	06/10/1997	5.4	11	5.21	3.13
19	Central_italy (Amatrice)	EMSC-20160824 _0000006	ITACA	24/08/2016	6.0	9	8.50	3.68
20	Central_italy (Amatrice)	EMSC-20161030 _0000029	ITACA	30/10/2016	6.5	26	5.22	3.94

7.2 Evaluation of the q-behaviour factor

In this work, the approach proposed by Mwafy and Elnashai [81] was implemented and adapted to LFT buildings, evaluating q as base shears ratios. Moreover, with the IDA approach there is no need to find a link between the displacement ductility of the structure and the q factor. This step is necessary only with a non-linear static method.

Following §3.2.2, the behaviour factor q was obtained as the product of a ductility factor q_μ and an overstrength factor q_D in equation:

$$q = q_\mu \cdot q_D \tag{25}$$

The ductility factor q_μ is strictly connected to the actual non-linear behaviour of the structure. It was evaluated by means of equation:

$$q_\mu = \frac{V_{b(Dyn,e)}}{V_{b(Dyn,c)}} \tag{26}$$

where $V_{b(Dyn,c)}$ is the base shear which corresponds to collapse of the building and $V_{b(Dyn,e)}$ is the base shear obtained by an elastic analysis of the structure under the same records.

The q_D factor accounts for the over-strength due to the structural redundancy and post-elastic hardening. It is evaluated by equation:

$$q_D = \frac{V_{b(Dyn,c)}}{V_{b(St,y)}} \tag{27}$$

$V_{b(St,y)}$ is the base shear corresponding to the first yield in the structure and it is evaluated by means of a static non-linear analysis. In the IDA, the point of the first yielding cannot be distinguished easily. Increasing the seismic intensity, there could be more IM levels with only one wall that had reached yield. Therefore, the base shear which corresponds to the first yield, derived from nonlinear static analysis, was used as base shear of yielding point. It means that the end of the linear zone can be considered the same in both IDA and pushover analyses [81]. This solution was used in other literature works to evaluate the q-factor [82][83]. The yield point of the walls was evaluated in Chapter 5 by EEEP approach.

In particular, four pushover analysis were done for each ductility class, for each reference building and for each direction. The value of base shear corresponding to the first yield in a wall was recorded, based on the yield displacements evaluated in Chapter 5. To evaluate the q-factor, the mean value among the four shear forces from pushover for each direction was used.

It is worth noting that the q-factor of equation (6) is "intrinsic" and, thus, code independent. It takes into account the energy dissipation (q_μ) and all over-resistances due to post-elastic hardening behaviour and

structural redundancy (q_D). In fact, the design overstrength factor for the seismic design of example building was set to 1.

In order to perform comparisons with current codes like the Italian Building Code [8] and the Eurocode [7], a further step is necessary. To this aim, the intrinsic q-factor can be multiplied by 1.5 to obtain the q_{code} value, as presented by other authors [50], see the following formulation:

$$q_{code} = 1.5 \cdot q = 1.5 \cdot q_{\mu} \cdot q_D \tag{28}$$

I-8 RESULTS ON PARAMETRIC IDA

The results of the whole IDA procedure are herein presented. Since the processing phase was applied to 360 single IDA curves, involving over 7000 non-linear analyses, a complete example of post-processing was discussed in detail, considering one reference building and one IDA study. The procedure was then extended to all the cases

Furthermore, the results of the entire procedure were reported and discussed in a compact form, focusing on regular and irregular buildings. Finally, a comparison was done, and the q-behaviour factors were evaluated.

8.1 Post-processing phase

In this paragraph, the post-processing procedure to evaluate the q-behaviour factor is proposed, focusing on a single case. The procedure was then applied to all the reference buildings and ductility classes.

Let the two storeys, ductility class 4, regular case be the illustrative example of the post-processing procedure. Fig. 66 below describes the FEM model of the structure, in accordance with the previous chapters.

Pairs of accelerograms were applied simultaneously in both X and Y directions, according to the principal axis defined in Fig. 62. The q-behaviour factor of the building under a selected pair of ground motion was evaluated accordingly to its direction of collapse. When a hybrid X-Y collapse was detected, the smaller between the two q-factor was considered.

Roof Drift Ratio (RDR) was recorded at each step of the incremental analysis, composing the displacement in both direction and then dividing it by the height of the building (6.2 m). The curves were then reported in Fig. 67.

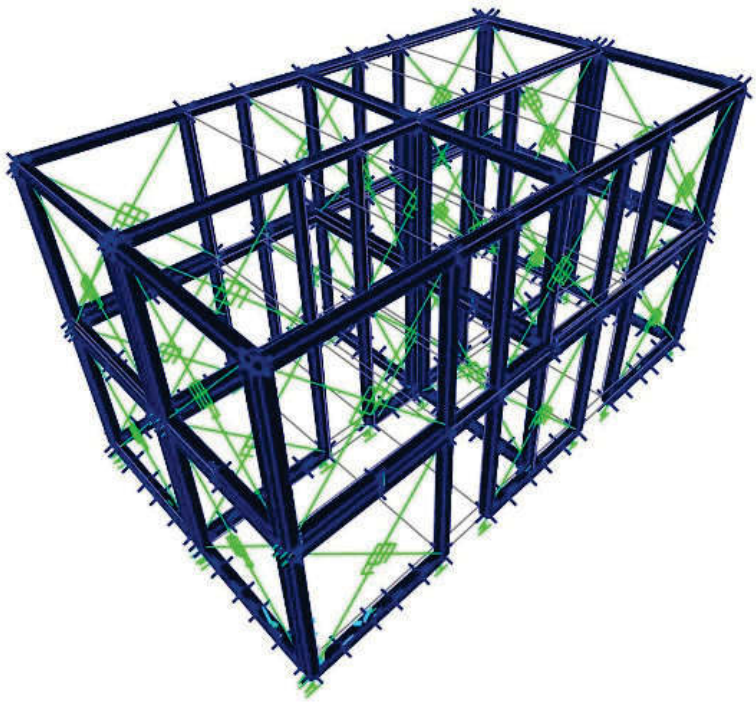

Fig. 66 – FEM model of the 2 storeys regular building

PGA shows different outlier curves, reaching high intensity value (1.138-1.725g, maximum scale factor of the signal 3.266 < 4.000, value set as upper limit). This outcome was expected, since PGA is not linked to the structural behaviour, i.e. does not consider the vibration modes or other properties of the building (see Chapter 3.2.2). Furthermore, signals with high PGA at collapse showed a response spectrum with low spectral acceleration in correspondence of the fundamental frequency of the structure.

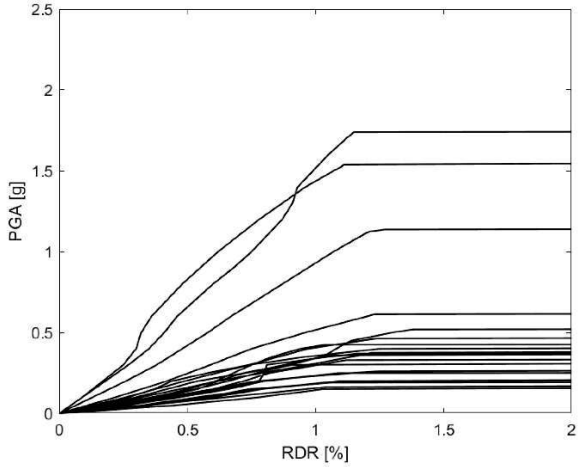

Fig. 67 – IDA study for the 2 storeys regular building (ductility = 4, PGA).

Thus, a heavier scaling was necessary to obtain the dynamic instability. This can be seen in Fig. 68, where the spectra of Signal 18 (Umbro-Marchigiano) was reported, the one leading to a PGA of 1.725g and a Scale Factor of 3.266; the dashed line shows the mean period of the first translational modes in X and Y (0.34 s).

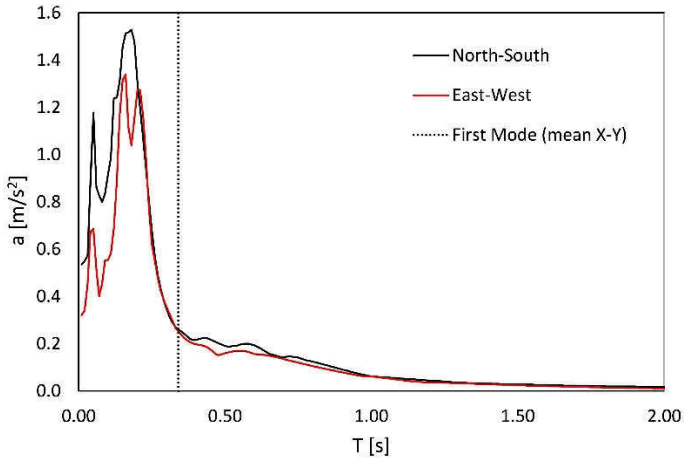

Fig. 68 – Umbro-Marchigiano earthquake response spectrum. A dashed black line highlights the mean first period of the two-story regular building.

Furthermore, the IDA curves of Fig. 67 were re-scaled to $S_{a,avg}$, see Fig. 69. Changing from PGA to spectral acceleration has a high impact on the dispersion of the dynamic instability branches. Outliers are not

visible, since this IM is more linked to the vibrational behaviour of the analysed structures.

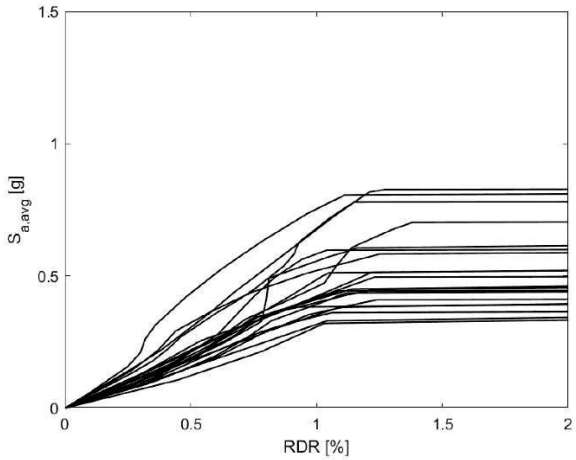

Fig. 69 – IDA study for the 2 storeys regular building (ductility = 4, $S_{a,avg}$).

In correspondence of each collapse point detected, the base shear $V_{b(Dyn,c)}$ was recorded. Then, according to the procedure of Chapter 7.2, the structure was subjected to an elastic analysis under the same pair of accelerogram of the IDA, but scaled to the Collapse amplitude in order to evaluated the shear $V_{b(Dyn,e)}$.

Moreover, it was necessary to calculate the shear corresponding to the first yield in a wall. Thus, pushover analyses were performed, under the hypothesis of coincidence of the elastic branch between IDA curves and non-linear static curves, as discussed in Chapter 7.2. The FEM model was subjected to two group of forces in X and Y direction. Since symmetry conditions apply, only one sign was considered, and analysis were performed in positive direction. A modal and a constant acceleration distribution were applied, according to [7] [8] (Fig. 70).

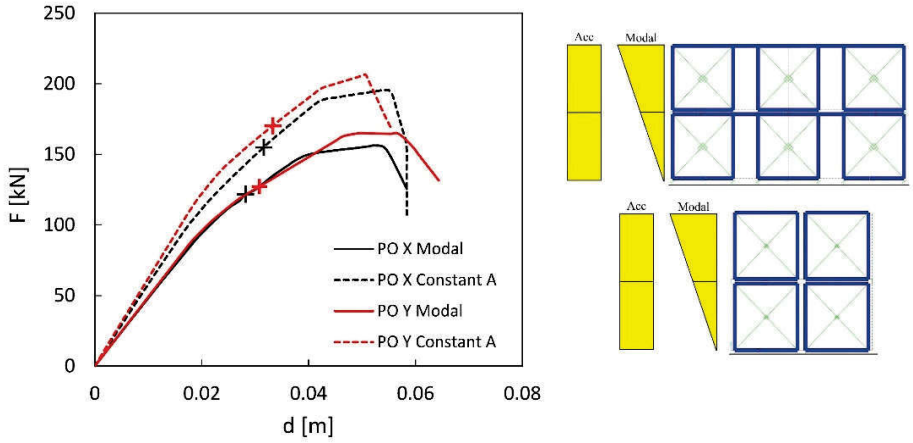

Fig. 70 – Pushover curves for the 2 storeys regular buildings and for the two load distributions.

In Table 31, the base shear value corresponding to the yield state are reported. The yield state was defined in correspondence of the first wall reaching the yield displacement according to Table 7. The mean value between the two distribution $V_{b(St,y)}$ was then used to compute the overstrength factor for both directions.

For non-regular building, the mean value among all 4 pushovers was calculated (considering both negative and positive directions, since no symmetry conditions apply).

Table 31 – Base shear corresponding to yield of the first wall from pushover analysis for the 2 storeys regular buildings.

Direction	Distribution	F_y [kN]
X	Gr1	121.71
X	Gr2	154.91
X - mean	-	138.31
Y	Gr1	127.16
Y	Gr2	170.20
Y - mean	-	148.68

Finally, since all terms to apply equation (28) and compute the q-behaviour factor are known, Table 32 was developed.

Table 32 – Evaluation of the q_{code} factor for the 2 storeys regular buildings.

IDA	$V_{b(Dyn,c)}$ [kN]	CollDir	$V_{b(Dyn,e)}$ [kN]	$V_{b(St,y)}$ [kN]	q_μ	q_d	q	DOF	q_{code}
1	171.6	Y	320.6	127.2	**1.9**	1.3	2.5	1.5	**3.8**
2	196.1	Y	390.7	127.2	**2.0**	1.5	3.1	1.5	**4.6**
3	158.5	X	177.5	121.7	**1.1**	1.3	1.5	1.5	**2.2**
4	132.0	Y	150.5	127.2	**1.1**	1.0	1.2	1.5	**1.8**
5	175.6	Y	297.0	127.2	**1.7**	1.4	2.3	1.5	**3.5**
6	150.4	Y	273.1	127.2	**1.8**	1.2	2.1	1.5	**3.2**
7	188.9	X	261.7	121.7	**1.4**	1.6	2.1	1.5	**3.2**
8	191.7	Y	331.7	127.2	**1.7**	1.5	2.6	1.5	**3.9**
9	202.3	Y	456.8	127.2	**2.3**	1.6	3.6	1.5	**5.4**
10	192.1	X	331.5	121.7	**1.7**	1.6	2.7	1.5	**4.1**
11	192.0	X	250.1	121.7	**1.3**	1.6	2.1	1.5	**3.1**
12	155.4	Y	378.9	127.2	**2.4**	1.2	3.0	1.5	**4.5**
13	132.3	Y	538.5	127.2	**4.1**	1.0	4.2	1.5	**6.4**
14	186.5	X	299.5	121.7	**1.6**	1.5	2.5	1.5	**3.7**
15	199.3	Y	337.6	127.2	**1.7**	1.6	2.7	1.5	**4.0**
16	190.0	X	196.7	121.7	**1.0**	1.6	1.6	1.5	**2.4**
17	177.4	Y	177.9	127.2	**1.0**	1.4	1.4	1.5	**2.1**
18	194.5	X	325.6	121.7	**1.7**	1.6	2.7	1.5	**4.0**
19	189.1	X	260.9	121.7	**1.4**	1.6	2.1	1.5	**3.2**
20	177.3	X	252.8	121.7	**1.4**	1.5	2.1	1.5	**3.1**
mean	177.7	%X	300.5	124.7	**1.7**	1.43	2.40	1.50	**3.6**
sigma	21.3	45%	95.1	2.78	**0.67**	0.18	0.74	0.00	**1.10**
CoV	0.120	%Y	0.316	0.022	**0.392**	0.128	0.306	0.000	**0.306**
min	132.0	55%	150.5	121.7	**1.0**	1.0	1.2	1.5	**1.8**
max	202.3		538.5	127.2	**4.1**	1.6	4.2	1.5	**6.4**

For each IDA curve, from 1 to 20, the collapse $V_{b(Dyn,c)}$, elastic $V_{b(Dyn,e)}$ and first yield $V_{b(St,y)}$ base shear are shown, together with the collapse direction "CollDir", indicating if the structure collapsed in X or Y direction. The ductility factor q_μ and the overstrength factor q_d were calculated according to formulation (26) and (27). Their product represents the intrinsic q-factor. To obtain the "code depending" factor q_{code}, a Design Overstrength Factor DOF equal to 1.5 was used, according to the procedure discussed in Chapter 7.2.

The collapse directions are split equally between X and Y (45% vs 55%). However, a CoV of 0.306 and a standard deviation of 1.10 were detected, signal of relative high dispersion. A mean value of 3.6 was finally found for the q_{code} factor.

The aforementioned procedure was applied to all the reference buildings and ductility classes. In the following paragraphs, the results were reported. The complete tables, such as Table 32, were reported in the Appendix A, to make all the data available.

8.2 Regular Buildings

Fig. 71 shows the IDA curves for regular buildings in grey. Moreover, median curve and 16°/84° percentiles curves are reported in red. Each box represents a structure with a given ductility of the sheathing-to-framing connection (4, 6, 8) and a given number of floors (2, 3, 4). The Roof Drift Ratio (RDR) is shown on the abscissa, obtained as the ratio between the maximum horizontal displacement reached by the center of gravity of the last floor and the overall height of the building. The PGA is shown on the ordinate. As discussed in the previous chapters, the collapse point of the building is assumed to correspond to the onset of dynamic instability, identified by the horizontal branch of the curve (a small increase in PGA corresponds to a high maximum displacement). The structure is considered collapsed when there is a decrease in the stiffness of the building of 80%, quantified as the variation in slope of the tangent to the curve with respect to the initial elastic stiffness. Based on the results in Fig. 71, for a fixed ductility class, the RDR shows a decreasing trend as the number of floors increases. On the other hand, the RDR increases for higher ductility classes. Finally, a higher ductility class corresponds to a higher average collapse PGA. As already specified in chapter 7.2, the choice of the PGA as an intensity measure does not affect the calculation of the behaviour factor. However, from the graphs, it emerges that the PGA is not a suitable IM to describe the examined structures, since, depending on the accelerogram considered, outlier can be seen, as highlighted in the previous paragraph. Examining the signals, in fact, it is visible that, in correspondence with the fundamental periods of the reference structures, the spectral acceleration is very low. The PGA, however, is convenient in this case to be able to have all the buildings at the same scale and to be able to analyse the behaviours in their entirety.

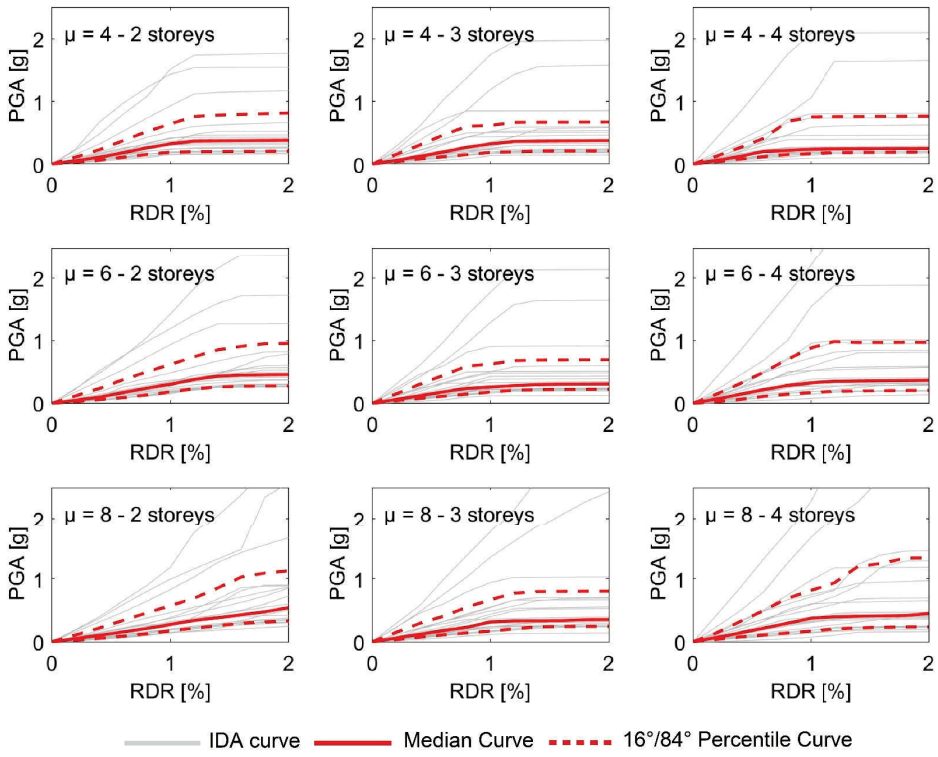

Fig. 71 – IDA study for regular buildings, varying ductility and number of storeys. PGA selected as IM. Median and 16°/84° percentile shown in red.

The IDA curves of Fig. 71 were then rescaled, in order to pass from PGA to $S_{a,avg}$. Based on the results in Fig. 72, fixed the ductility class, the RDR decreases as the number of floors increases and, as generally expected, the RDR increases for higher ductility classes. Furthermore, a lower $S_{a,avg}$ at collapse has been detected for higher number of storeys. It is worth to note that this evidence has not to be considered as a signal that taller buildings are less resistant. The reason is found in the selected IM, which is an average spectral acceleration and is generally lower for higher periods. Therefore, considering the values in Table 29, the $S_{a,avg}$ for larger T are smaller. Moreover, the results of the IDA are less scattered with respect to PGA IDA curves, meaning that the $S_{a,avg}$ is more suitable to represent the LFT reference buildings.

Equations (26), (27) and (28) were used to calculate the behaviour factors q_{code} for regular buildings. The values are reported in Table 33.

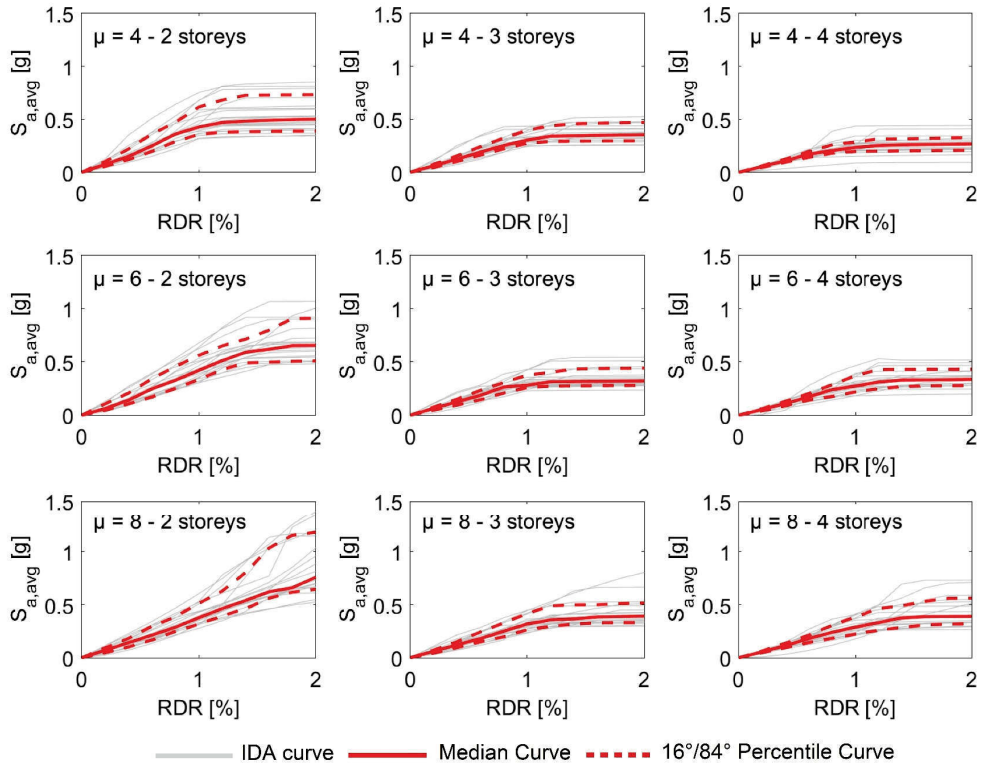

Fig. 72 – IDA study for regular buildings, varying ductility and number of storeys. $S_{a,avg}$ selected as IM. Median and 16°/84° percentile shown in red.

As expected, the ductility factor q_μ increases with the ductility class of the sheathing-to-framing connection, but also with the number of storeys. The data show similar CoV values. The overstrength factor q_d is greater with increasing ductility, and the dispersion found is lower. For a ductility class equal to 4, a value of global behaviour factor q_{code} equal to 2.9 was obtained, which confirms the value q=3 suggested by the Italian Building Code [8] for Low Ductility Class timber structures.

Table 33 – q-factors for regular buildings, varying the ductility and the number of storeys. The "Total" part of the table reports the values considering all the three buildings.

		q_μ			q_d			q			q_{code}		
		4	6	8	4	6	8	4	6	8	4	6	8
Total	mean	**1.6**	**1.9**	**2.1**	**1.2**	**1.3**	**1.5**	**1.9**	**2.4**	**3.1**	**2.9**	**3.6**	**4.7**
	median	1.4	1.8	2.0	1.2	1.3	1.4	1.8	2.3	2.8	2.7	3.4	4.2
	sigma	0.49	0.63	0.66	0.20	0.17	0.27	0.66	0.87	1.14	1.00	1.31	1.71
	CoV	0.32	0.33	0.31	0.17	0.13	0.19	0.35	0.36	0.37	0.35	0.36	0.37
	min	1.0	1.1	1.2	1.0	1.0	1.0	1.0	1.1	1.4	1.5	1.7	2.1
	max	4.1	3.9	4.3	1.6	1.5	2.1	4.2	5.2	6.3	6.4	7.7	9.5

		q_μ			q_d			q			q_{code}		
		4	6	8	4	6	8	4	6	8	4	6	8
2 storeys	mean	**1.7**	**2.3**	**2.5**	**1.4**	**1.3**	**1.6**	**2.4**	**3.0**	**4.0**	**3.6**	**4.5**	**6.0**
	median	1.7	2.1	2.3	1.5	1.3	1.4	2.4	2.9	3.8	3.6	4.3	5.8
	sigma	0.66	0.72	0.82	0.18	0.10	0.34	0.73	0.87	1.30	1.08	1.31	1.94
	CoV	0.39	0.31	0.33	0.12	0.08	0.21	0.30	0.29	0.33	0.30	0.29	0.33
	min	1.0	1.2	1.5	1.0	1.1	1.3	1.2	1.6	2.3	1.8	2.4	3.4
	max	4.1	3.9	4.3	1.6	1.4	2.1	4.2	5.2	6.3	6.4	7.7	9.5
		q_μ			q_d			q			q_{code}		
		4	6	8	4	6	8	4	6	8	4	6	8
3 storeys	mean	**1.4**	**1.6**	**1.8**	**1.1**	**1.1**	**1.3**	**1.6**	**1.8**	**2.4**	**2.4**	**2.8**	**3.7**
	median	1.3	1.5	1.7	1.1	1.1	1.4	1.6	1.7	2.3	2.4	2.5	3.5
	sigma	0.34	0.53	0.42	0.13	0.15	0.19	0.42	0.57	0.69	0.64	0.86	1.03
	CoV	0.25	0.32	0.23	0.11	0.13	0.14	0.26	0.31	0.28	0.27	0.31	0.28
	min	1.0	1.1	1.2	1.0	1.0	1.0	1.0	1.1	1.4	1.5	1.7	2.1
	max	2.3	3.1	2.7	1.4	1.5	1.7	2.5	3.4	4.2	3.6	5.2	6.4
		q_μ			q_d			q			q_{code}		
		4	6	8	4	6	8	4	6	8	4	6	8
4 storeys	mean	**1.6**	**1.8**	**2.1**	**1.1**	**1.3**	**1.4**	**1.8**	**2.4**	**3.0**	**2.7**	**3.6**	**4.5**
	median	1.5	1.7	2.2	1.1	1.4	1.4	1.7	2.3	2.9	2.5	3.4	4.3
	sigma	0.36	0.45	0.52	0.15	0.18	0.14	0.51	0.76	0.80	0.81	1.14	1.20
	CoV	0.23	0.25	0.24	0.13	0.14	0.10	0.29	0.32	0.27	0.30	0.32	0.27
	min	1.1	1.2	1.4	1.0	1.0	1.1	1.1	1.4	1.7	1.7	2.1	2.6
	max	2.7	3.0	3.5	1.5	1.5	1.6	3.5	4.3	4.8	5.3	6.5	7.2

8.3 Non-Regular Buildings

Similarly to the case of regular buildings, the IDA curves for all cases (number of floors and ductility classes, Fig. 73, Fig. 74) and the table with the calculation of the behavior factors obtained with the application of formulas 3, 4, 5 and 6 (Table 34) are reported below.

The behaviours highlighted previously also occur in the non-regular case. As the ductility increases, the collapse PGA increases but, as the number of floors of the building increases, the maximum RDR achievable by the structure decreases.

As expected, also in this case the ductility factor q_μ increases as the ductility class of the panel-frame connection increases. The data show similar CoV values.

The overstrength factor q_d increases as the ductility increases. Furthermore, the dispersion found is lower than the ductility factor.

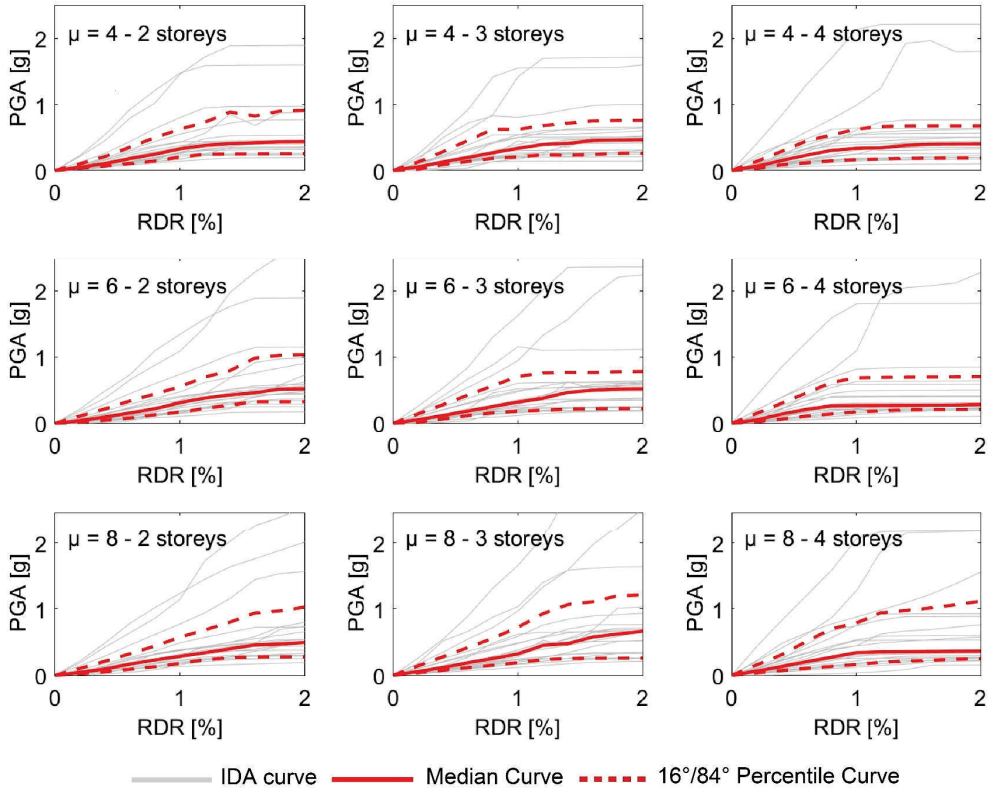

Fig. 73 – IDA study for non-regular buildings, varying ductility and number of storeys. PGA selected as IM. Median and 16°/84° percentile shown in red.

Moreover, the rescaled IDAs show that the $S_{a,avg}$ is suitable also for non-regular buildings.

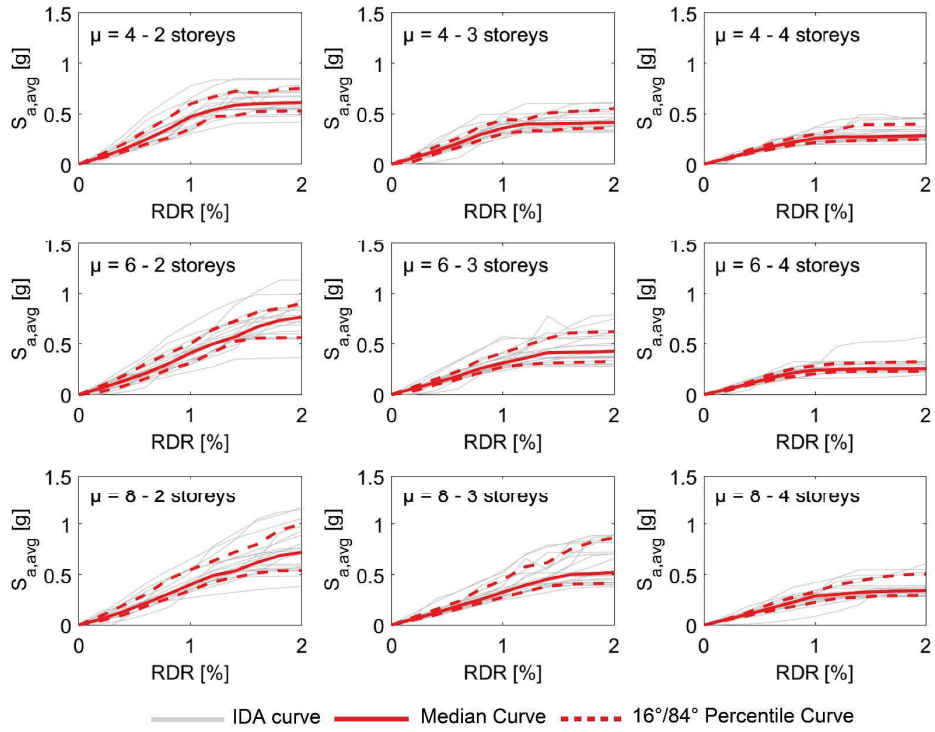

Fig. 74 – IDA study for non-regular buildings, varying ductility and number of storeys. $S_{a,avg}$ selected as IM. Median and 16°/84° percentile shown in red.

Finally, calculations were performed, to evaluate the behaviour factors. For a ductility class equal to 4 and 6, the values 3.4 and 3.7 were obtained. The first confirms the value q=3 foreseen by [8] for wooden structures of Low Ductility Class, while the second, once again, draws attention to the need to revise downwards the value of 5 suggested by [7][8] for structures in High Ductility Class.

Table 34 – q-factors for non-regular buildings, varying the ductility and the number of storeys. The "Total" part of the table reports the values considering all the three buildings.

		q_μ			q_d			q			q_{code}		
		4	6	8	4	6	8	4	6	8	4	6	8
Total	mean	**1.7**	**1.9**	**2.2**	**1.3**	**1.3**	**1.5**	**2.3**	**2.5**	**3.2**	**3.4**	**3.7**	**4.7**
	median	1.6	1.7	1.9	1.3	1.3	1.5	2.2	2.3	2.7	3.3	3.4	4.1
	sigma	0.57	0.58	0.80	0.17	0.17	0.13	0.69	0.79	1.27	1.02	1.18	1.90
	CoV	0.33	0.31	0.37	0.13	0.13	0.10	0.30	0.32	0.40	0.30	0.32	0.40
	min	1.0	1.0	1.0	1.0	1.0	1.1	1.1	1.1	1.4	1.8	1.7	2.1
	max	3.8	3.8	4.5	1.6	1.6	1.7	4.7	4.3	7.3	7.0	6.5	10.9

		q_μ			q_d			q			q_{code}		
		4	6	8	4	6	8	4	6	8	4	6	8
2 storeys	mean	**1.9**	**2.2**	**2.1**	**1.3**	**1.3**	**1.5**	**2.4**	**2.8**	**3.0**	**3.7**	**4.2**	**4.5**
	median	1.8	2.1	2.0	1.3	1.3	1.5	2.3	2.7	2.7	3.4	4.1	4.1
	sigma	0.62	0.69	0.75	0.11	0.11	0.13	0.68	0.82	1.08	1.02	1.23	1.61
	CoV	0.32	0.32	0.36	0.08	0.09	0.09	0.28	0.29	0.36	0.28	0.29	0.36
	min	1.1	1.0	1.0	1.0	1.0	1.1	1.3	1.3	1.5	1.9	1.9	2.3
	max	3.8	3.8	4.5	1.4	1.5	1.7	3.9	4.3	6.8	5.9	6.5	10.1
		q_μ			q_d			q			q_{code}		
		4	6	8	4	6	8	4	6	8	4	6	8
3 storeys	mean	**1.8**	**1.8**	**2.4**	**1.4**	**1.3**	**1.4**	**2.4**	**2.3**	**3.5**	**3.7**	**3.4**	**5.2**
	median	1.7	1.6	2.2	1.3	1.3	1.4	2.2	2.1	3.0	3.5	3.1	4.5
	sigma	0.65	0.61	0.93	0.17	0.16	0.09	0.80	0.84	1.42	1.17	1.25	2.13
	CoV	0.37	0.35	0.38	0.12	0.12	0.07	0.33	0.37	0.41	0.32	0.37	0.41
	min	1.0	1.0	1.2	1.0	1.1	1.2	1.5	1.1	1.4	2.3	1.7	2.1
	max	3.6	3.5	4.2	1.6	1.6	1.5	4.7	4.2	6.3	7.0	6.3	9.4
		q_μ			q_d			q			q_{code}		
		4	6	8	4	6	8	4	6	8	4	6	8
4 storeys	mean	**1.6**	**1.7**	**2.0**	**1.3**	**1.3**	**1.6**	**2.0**	**2.3**	**3.0**	**2.9**	**3.5**	**4.5**
	median	1.6	1.7	1.8	1.3	1.3	1.5	2.1	2.1	2.6	2.8	3.1	4.0
	sigma	0.34	0.33	0.65	0.21	0.22	0.16	0.50	0.62	1.26	0.62	0.93	1.88
	CoV	0.21	0.19	0.32	0.17	0.17	0.11	0.25	0.27	0.42	0.21	0.27	0.42
	min	1.0	1.3	1.4	1.0	1.0	1.2	1.1	1.7	1.9	1.8	2.5	2.8
	max	2.4	2.5	4.2	1.6	1.6	1.7	2.9	3.7	7.3	4.3	5.6	10.9

8.4 Results comparison and global q-behaviour factor

The curves corresponding to regular and non-regular buildings have been reported together in Fig. 75 for $S_{a,avg}$. On the other hand, Fig. 76 shows the regular cases in black and the non-regular cases in red, to allow comparison. Analysing the curves, a negligible influence of the regularity can be noted, since similar RDR and $S_{a,avg}$ were reached.

Formulations (26), (27) and (28) were finally applied to the entire data sample obtained from the numerical analyses. Thus, each behaviour factor q for each ductility class was based on 120 collapse point.

The values of q_μ obtained for the three ductility classes in the two cases are comparable and, in the ductility 4 and 8 cases, higher for the non-regular buildings. The CoVs do not vary significantly. Similarly, no marked difference was found in terms of over-resistance factors q_d: the values are similar, but the CoV of the non-regular case is slightly lower.

The findings on the individual factors are then reflected in the global q, where it is interesting to note how, next to almost equal values for ductility 6 (3.6 vs 3.7) and 8 (4.7 vs 4.7), the behavior factor for the regular ductility 4 case is significantly lower (2.9 vs 3.4). Analysing the results, it emerges that the cause of a lower q for the regular case is partly attributable to the 3-storey building, whose designing phase, although carried out according to capacity design criteria and following the current regulations, provides lower results. (20 for each of the 6 buildings). See Table 35.

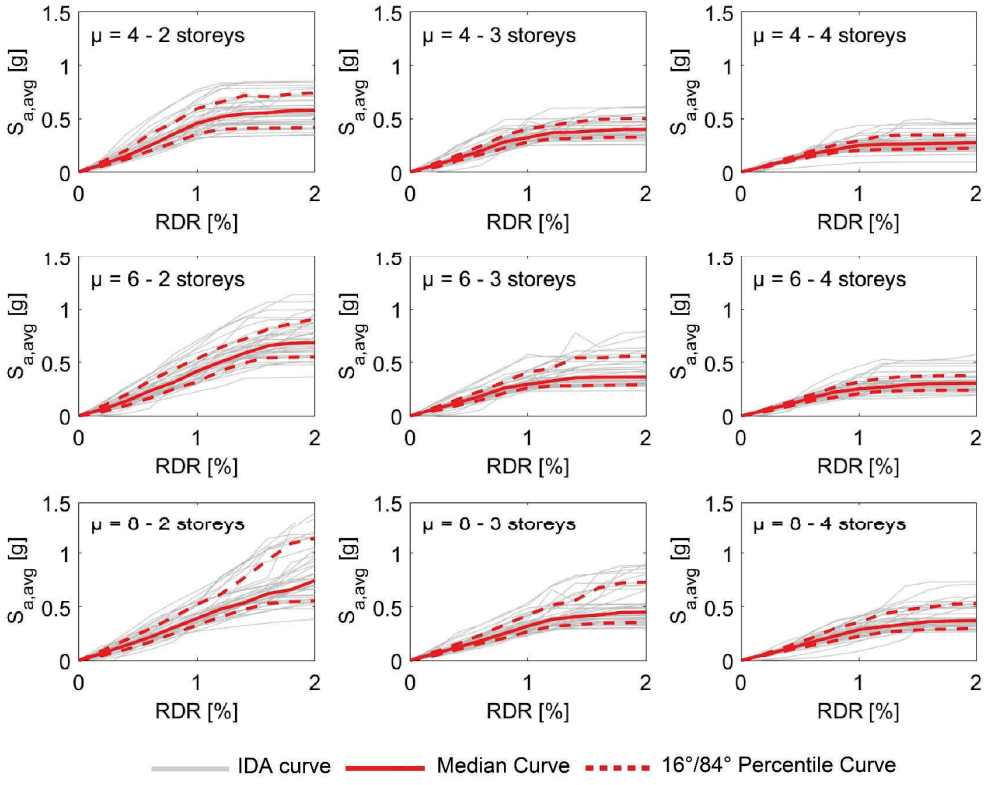

Fig. 75 – IDA study for regular and non-regular buildings, varying ductility and number of storeys. $S_{a,avg}$ selected as IM. Median and 16°/84° percentile shown in red.

In Table 36 the final values of the q_{code} factors are summarized. For ductility class 4, corresponding to the Italian low ductility class, an average final value of 3.2 was obtained, which allows to confirm the value 3.0 proposed by the standard. The value is also higher than the 2.5 suggested by [95]. For ductility class 6, the minimum necessary for connections to allow High Ductility Class design, an average q_{code} equal to 3.7 was evaluated, far from the suggested value of 5.0.

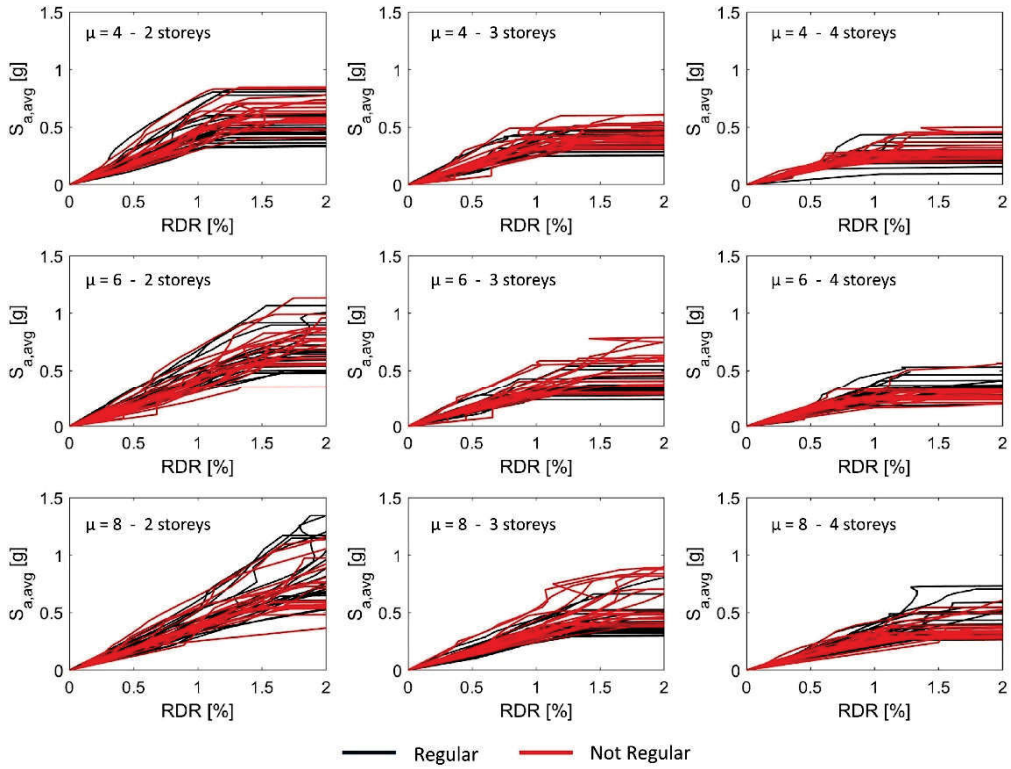

Fig. 76 – IDA study for regular (black) and non-regular (red) buildings, varying ductility and number of storeys. $S_{a,avg}$ selected as IM.

Table 35 - q-factors for regular and non-regular buildings, varying the ductility and the number of storeys. The "Total" part reports the values considering all buildings.

		q_μ			q_d			q			q_{code}		
		4	6	8	4	6	8	4	6	8	4	6	8
Total	mean	**1.6**	**1.9**	**2.2**	**1.3**	**1.3**	**1.5**	**2.1**	**2.4**	**3.1**	**3.2**	**3.7**	**4.7**
	median	1.5	1.8	1.9	1.3	1.3	1.4	2.1	2.3	2.8	3.1	3.4	4.1
	sigma	0.54	0.61	0.73	0.20	0.17	0.21	0.70	0.83	1.20	1.04	1.24	1.80
	CoV	0.33	0.32	0.34	0.15	0.13	0.15	0.33	0.34	0.38	0.33	0.34	0.39
	min	1.0	1.0	1.0	1.0	1.0	1.0	1.0	1.1	1.4	1.5	1.7	2.1
	max	4.1	3.9	4.5	1.6	1.6	2.1	4.7	5.2	7.3	7.0	7.7	10.9
		q_μ			q_d			q			q_{code}		
		4	6	8	4	6	8	4	6	8	4	6	8
2 storeys	mean	**1.8**	**2.2**	**2.3**	**1.4**	**1.3**	**1.6**	**2.4**	**2.9**	**3.5**	**3.6**	**4.4**	**5.2**
	median	1.5	1.7	1.9	1.3	1.3	1.4	1.9	2.2	2.8	2.9	3.3	4.1
	sigma	0.65	0.70	0.81	0.16	0.10	0.27	0.71	0.83	1.29	1.06	1.25	1.93
	CoV	0.36	0.32	0.36	0.12	0.08	0.18	0.29	0.29	0.37	0.30	0.29	0.37
	min	1.0	1.0	1.0	1.0	1.0	1.1	1.2	1.3	1.5	1.8	1.9	2.3
	max	4.1	3.9	4.5	1.6	1.5	2.1	4.2	5.2	6.8	6.4	7.7	10.1

		q_μ			q_d			q			q_{code}		
		4	6	8	4	6	8	4	6	8	4	6	8
3 storeys	mean	**1.6**	**1.7**	**2.1**	**1.3**	**1.2**	**1.4**	**2.0**	**2.1**	**3.0**	**3.0**	**3.1**	**4.4**
	median	1.5	1.7	1.9	1.3	1.3	1.4	1.8	2.1	2.7	2.8	3.2	4.1
	sigma	0.55	0.56	0.77	0.20	0.17	0.16	0.76	0.74	1.22	1.14	1.11	1.83
	CoV	0.35	0.33	0.37	0.16	0.14	0.11	0.38	0.36	0.41	0.38	0.36	0.41
	min	1.0	1.0	1.2	1.0	1.0	1.0	1.0	1.1	1.4	1.5	1.7	2.1
	max	3.6	3.5	4.2	1.6	1.6	1.7	4.7	4.2	6.3	7.0	6.3	9.4
		q_μ			q_d			q			q_{code}		
		4	6	8	4	6	8	4	6	8	4	6	8
4 storeys	mean	**1.6**	**1.8**	**2.1**	**1.2**	**1.3**	**1.4**	**1.9**	**2.4**	**3.0**	**2.8**	**3.5**	**4.5**
	median	1.5	1.6	1.9	1.2	1.3	1.4	1.8	2.1	2.7	2.7	3.1	4.0
	sigma	0.35	0.39	0.58	0.20	0.20	0.16	0.51	0.69	1.04	0.72	1.03	1.56
	CoV	0.22	0.22	0.28	0.16	0.15	0.11	0.27	0.29	0.35	0.26	0.29	0.35
	min	1.0	1.2	1.4	1.0	1.0	1.1	1.1	1.4	1.7	1.7	2.1	2.6
	max	2.7	3.0	4.2	1.6	1.6	1.7	3.5	4.3	7.3	5.3	6.5	10.9

The value of 3.7 is close to the outcome that was found by [50] and CNR DT 206/2018 [95], that propose to consider q=4.0 in the calculation of light frame structures. However, the use of non-linear dynamic analyses (and therefore considering the dissipative hysteretic behaviour of the sheathing-to-framing connection and the influence of the ground motion) suggests a further slight reduction in the q factor and the need to expand the sample of buildings to be analysed and the aspect ratio of the walls. The dispersion values of the results, in fact, remain quite high even with 120 points used for the calculation and only six study buildings.

Table 36 – Value of the q-factors suggested for LFT buildings

	q_{code}		
	4	6	8
mean	**3.2**	**3.7**	**4.7**
median	3.1	3.4	4.1
sigma	1.04	1.24	1.80
CoV	0.330	0.339	0.382

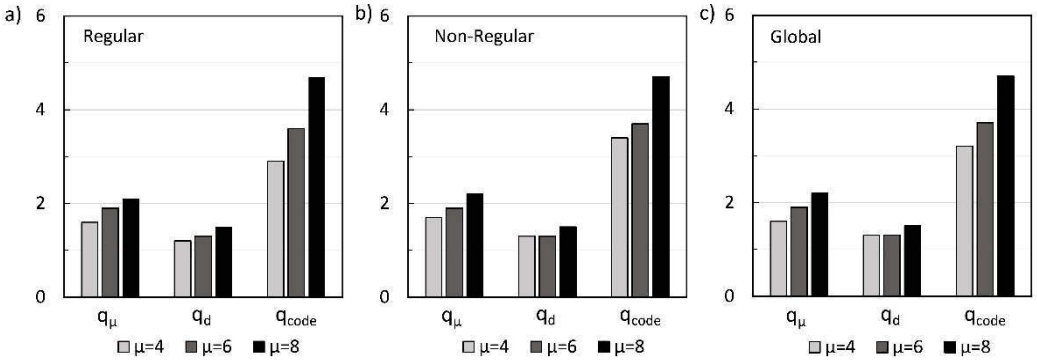

Fig. 77 – Graphical comparison between q_μ, q_d and q_{code} for regular (a) and non-regular (b) structures. The global values are reported in (c).

A conclusive remark is finally proposed, analysing the collapse directions detected during the IDA procedure. For each number of storeys and for each ductility class, the percentage of collapse in X and Y direction are reported. X and Y are referred to the axis defined in Fig. 8. Collapse directions are generally well distributed between the two axes; however, a high dispersion can be observed, especially for the three-story building. This is due to the difference between the capacity and the effective demand detected during the design phase of §3.1.

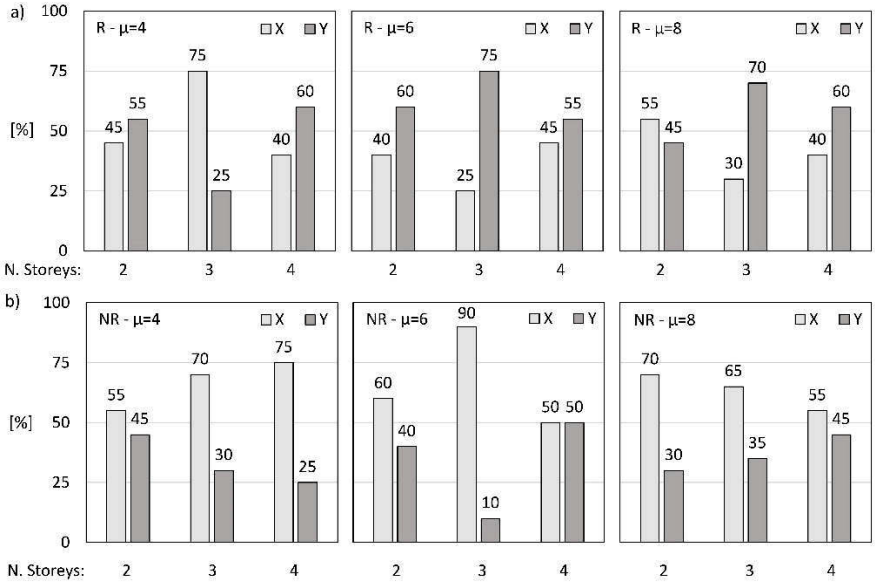

Fig. 78 – Collapse direction for regular (a) and non-regular (b) buildings.

Focusing on the non-regular three-story building with ductility class 6, the collapse occurred in the X direction in 90% of cases. This specific building shows an average capacity-to-demand ratio of all walls equal to 1.00 in the X direction and 1.08 in the Y direction, thus highlighting a difference of the 8%. Therefore, the X direction was found to be the weakest, justifying the large difference between the collapse directions. Similar findings were observed for the other reference buildings. However, this outcome is related to the choice of analysing structures designed according to current practice procedures, since a unitary capacity-to-demand ratio is generally unattainable. Furthermore, this aspect highlights the need to keep the ratio as close as possible to 1, in order to avoid weak directions in the building.

I-C | CONCLUSIONS

Thanks to the low environmental impact and to the good seismic performance, timber building are spreading also in countries were other building material are usually used. Heavy-frame timber, Cross-Laminated-Timber and Light-Frame-Timber building are solutions which can substitute reinforced concrete and steel not only for low- and mid-rise structures, but also for high-rise ones.

When talking of low- and mid-rise structures, LFT is a valuable option, since allows to save material with respect to other solution as CLT, but also because the low mass and the energy dissipation allocated in the steel connections makes this technology suitable for seismic prone areas.

Typical engineering design of LFT structures refers to the q-behaviour factor (or to the R force reduction factor in the USA for example). However, uncertainties still regard the evaluation of a reliable value for LFT buildings. Recent contributions to the calibration of the q-factor refer to non-linear static analyses, thus neglecting the influence of higher modes, the ground motion characteristics and the cyclic behaviour of the walls.

To overcome the aforementioned limitations, in this PhD study, an Incremental Dynamic Analysis approach was applied.

The results of an experimental test on a full-scale 3x3 m LFT wall were used to calibrate a detailed and a simplified Finite Element model. The detailed one was used to create a parameterized set of walls for three sheathing-to-framing connection ductility classes (4, 6 and 8). The value of 4 and 6 were chosen because they represent the minimum

requirements to design in low and high ductility classes according to current regulations in Europe. The simplified model, based on the detailed one, was applied in the assembling of six reference buildings, which were assembled using 3x3 m wall modules, in order to directly refer to the geometrical properties of the laboratory test.

In fact, six example buildings were designed, according to Eurocodes provisions and Capacity Design. Three structures were developed to be regular in plan and in elevation. Symmetry conditions were applied, when assembling 3x3 m LFT walls. Furthermore, another set of three buildings was developed, ensuring a lack of regularity, that was obtained imposing a Torsional Irregularity Ratio equal to 1.2. Since a Capacity Design approach was used, only the sheathing-to-framing nailed connection dissipated energy.

The six example structures of 2, 3 and 4 storeys were then analysed by means of IDA approach to evaluate the ductility and the overstrength factor.

The behaviour of irregular structures does not differ significantly, in terms of q factor, from that of regular structures. This suggests that the coefficient currently suggested to reduce the behaviour factor in the case of irregularity for light-frame structures should be reconsidered and calibrated.

Moreover, the results obtained confirm the behaviour factor of 3.0 for the Low Ductility Class according to the Italian regulations. In fact, the mean values 2.9 and 3.4 were obtained for the regular and irregular cases, with an average global q_{code}=3.2. However, the q factor for the high ductility class is lower than that provided by Eurocode 8. The mean values 3.6 (regular) and 3.7 (non-regular), and therefore the final q_{code} equal to 3.7, are not comparable with the suggested value of 5.0. Moreover, the obtained q_{code} is lower than the value of 4.0 proposed by the CNR DT 206/2018. It is worth to note that, in this research the dissipation linked to hold-down and angle-brackets was neglected. Considering all source for energy dissipation and the rocking behaviour of tallest walls can led to higher q values. However, this study provides a reliable range which can be considered as a lower bound for the definition of an appropriate behaviour factor.

In conclusion, an upgrade of the q-factor coefficients is recommended for light-frame buildings. Therefore, this study suggested a q_{code} value of 3.0 for the low ductility class (connection ductility equal to 4) and a value of 3.7 for the high ductility class (connection ductility equal to 6).

I-R REFERENCES

[1] "Sendai Framework on Disaster Risk Reduction (2015-2030)," https://unece.org/sendai-framework.

[2] A. Mishra *et al.*, "Land use change and carbon emissions of a transformation to timber cities," *Nat Commun*, vol. 13, no. 1, p. 4889, Aug. 2022, doi: 10.1038/s41467-022-32244-w.

[3] A. Buchanan, . "Timber Design Guide," *New Zealand Timber Industry Federation, Wellington, New Zealand, Third ed.*, 2007.

[4] R. Turino, Ed., *L'Aquila, The CASE Project*. Maggioli Editore, 2010.

[5] P. Horne, A. Abu, and A. Palermo, "Moment response of post-tensioned timber beam-column connections in fire – Experimental behaviour of a simple connection," *Fire Saf J*, vol. 141, p. 104008, Dec. 2023, doi: 10.1016/j.firesaf.2023.104008.

[6] A. Aloisio, R. Alaggio, and M. Fragiacomo, "Fragility functions and behavior factors estimation of multi-story cross-laminated timber structures characterized by an energy-dependent hysteretic model," *Earthquake Spectra*, vol. 37, no. 1, pp. 134–159, Feb. 2021, doi: 10.1177/8755293020936696.

[7] EN 1998-1:2013, "Eurocode 8: design of structures for earthquake resistance part 1: general rules, seismic actions and rules for buildings, Brussels, Belgium," 2013.

[8] C.S.LL.PP. Ministry Decree 17/01/2018, "Italian National Building Code NTC 2018," Italy, 2018.

[9] C. Demirci, C. Málaga-Chuquitaype, and L. Macorini, "Seismic drift demands in multi-storey cross-laminated timber buildings," *Earthq Eng Struct Dyn*, vol. 47, no. 4, pp. 1014–1031, Apr. 2018, doi: 10.1002/eqe.3003.

[10] NBCC 2020, "National Building Code of Canada, Institute for Research in Construction, National Research Council of Canada, Ottawa, Ontario," 2020.

[11] Canadian Standards Association, "CSA O86," 2014.

[12] E. Karacabeyli and S. Gagnon, *Canadian CLT Handbook*. FPInnovations, 2019.

[13] IBC, "International Building code," 2021.

[14] A. Mazelli, C. Bedon, and A. Morassi, "Sheathing-to-framing connection ductility role in the q-behaviour factor of Light Frame Timber buildings," *Bulletin of Earthquake Engineering*, Oct. 2025, doi: 10.1007/s10518-025-02308-5.

[15] NZS 3603, "New Zealand Timber Structures Standards," 1993.

[16] D. Casagrande, T. Sartori, and R. Tomasi, "Capacity design approach for multi-storey timber-frame buildings," 2014. [Online]. Available: https://api.semanticscholar.org/CorpusID:114971748

[17] L. Pozza, R. Scotta, D. Trutalli, A. Polastri, and I. Smith, "Experimentally based q-factor estimation of cross-laminated timber walls," *Proceedings of the Institution of Civil Engineers - Structures and Buildings*, vol. 169, no. 7, pp. 492–507, Jul. 2016, doi: 10.1680/jstbu.15.00009.

[18] I. Gavric, M. Fragiacomo, and A. Ceccotti, "Cyclic behaviour of typical metal connectors for cross-laminated (CLT) structures," *Mater Struct*, vol. 48, no. 6, pp. 1841–1857, Jun. 2015, doi: 10.1617/s11527-014-0278-7.

[19] R. Tomasi and T. Sartori, "Mechanical behaviour of connections between wood framed shear walls and foundations under monotonic and cyclic load," *Constr Build Mater*, vol. 44, pp. 682–690, Jul. 2013, doi: 10.1016/j.conbuildmat.2013.02.055.

[20] A. Marchisella and G. Muciaccia, "A new hold-down device for seismic applications in CLT buildings: Design, testing, analytical and numerical assessment," *Eng Struct*, vol. 318, p. 118689, Nov. 2024, doi: 10.1016/j.engstruct.2024.118689.

[21] J. Liu and F. Lam, "Experimental Test of Cross Laminated Timber Connections Under Bi-Directional Loading," in *World Conference on Timber Engineering*, 2016.

[22] J. Chen, H. Xiong, T. Furuta, Y. Lu, and N. Abbas, "Experimental and analytical studies on mechanical performance of innovative energy-dissipating hold-down for CLT structures," *Constr Build Mater*, vol. 317, p. 125966, Jan. 2022, doi: 10.1016/j.conbuildmat.2021.125966.

[23] R. Fanti *et al.*, "Experimental characterization of the multi-directional behaviour of angle brackets and hold-downs," in *World Conference on Timber Engineering (WCTE 2023)*, As, Norway: World Conference on Timber Engineering (WCTE 2023), 2023, pp. 1305–1311. doi: 10.52202/069179-0178.

[24] J. P. Judd and F. S. Fonseca, "Analytical Model for Sheathing-to-Framing Connections in Wood Shear Walls and Diaphragms," *Journal of Structural Engineering*, vol. 131, no. 2, pp. 345–352, Feb. 2005, doi: 10.1061/(ASCE)0733-9445(2005)131:2(345).

[25] P. Grossi, T. Sartori, and R. Tomasi, "Tests on timber frame walls under in-plane forces: part 1," *Proceedings of the Institution of Civil Engineers - Structures and Buildings*, vol. 168, no. 11, pp. 826–839, Nov. 2015, doi: 10.1680/stbu.13.00107.

[26] P. Grossi, T. Sartori, and R. Tomasi, "Tests on timber frame walls under in-plane forces: part 2," *Proceedings of the Institution of Civil Engineers - Structures and Buildings*, vol. 168, no. 11, pp. 840–852, Nov. 2015, doi: 10.1680/stbu.13.00108.

[27] W. Seim, M. Kramar, T. Pazlar, and T. Vogt, "OSB and GFB As Sheathing Materials for Timber-Framed Shear Walls: Comparative Study of Seismic Resistance," *Journal of Structural Engineering*, vol. 142, no. 4, Apr. 2016, doi: 10.1061/(ASCE)ST.1943-541X.0001293.

[28] F. Germano, G. Metelli, and E. Giuriani, "Experimental results on the role of sheathing-to-frame and base connections of a European timber framed shear wall," *Constr Build Mater*, vol. 80, pp. 315–328, Apr. 2015, doi: 10.1016/j.conbuildmat.2015.01.076.

[29] P. Rigo, A. Polastri, A. Mazelli, C. Bedon, and D. Casagrande, "Experimental and numerical analysis on Light-Frame Timber shear-walls coupled with self-centering steel cables," *Constr Build Mater*, vol. 504, Dec. 2025, doi: 10.1016/j.conbuildmat.2025.144393.

[30] T. Carrero *et al.*, "New enhanced hybrid glulam-framed OSB wall for tall timber buildings," *Structures*, vol. 70, p. 107770, Dec. 2024, doi: 10.1016/j.istruc.2024.107770.

[31] D. Trutalli, L. Marchi, R. Scotta, L. Pozza, and L. De Stefani, "Seismic Response of a Platform-Frame System with Steel Columns," *Buildings*, vol. 7, no. 2, p. 33, Apr. 2017, doi: 10.3390/buildings7020033.

[32] A. Ceccotti, "New technologies for construction of medium-rise buildings in seismic regions: the XLAM case," *Structural engineering international: Journal of the international Association for Bridge and structural engineering, IABSE*, pp. 156–165, 2008.

[33] L. Pozza, R. Scotta, D. Trutalli, and A. Polastri, "Behaviour factor for innovative massive timber shear walls," *Bulletin of Earthquake Engineering*, vol. 13, no. 11, pp. 3449–3469, Nov. 2015, doi: 10.1007/s10518-015-9765-7.

[34] M. Mestar, G. Doudak, M. Caola, and D. Casagrande, "Equivalent-frame model for elastic behaviour of cross-laminated timber walls with openings," *Proceedings of the Institution of Civil Engineers - Structures and Buildings*, vol. 173, no. 5, pp. 363–378, May 2020, doi: 10.1680/jstbu.19.00057.

[35] I. Sustersic, M. Fragiacomo, and B. Dujic, "Seismic Analysis of Cross-Laminated Multistory Timber Buildings Using Code-Prescribed Methods: Influence of Panel Size, Connection Ductility, and Schematization," *Journal of Structural Engineering*, vol. 142, no. 4, Apr. 2016, doi: 10.1061/(ASCE)ST.1943-541X.0001344.

[36] X. Zhao, B. Zhang, T. Kilpatrick, and I. Sanderson, "Numerical Analysis on Global Serviceability Behaviours of Tall CLT Buildings to the Eurocodes and UK National Annexes," *Buildings*, vol. 11, no. 3, p. 124, Mar. 2021, doi: 10.3390/buildings11030124.

[37] A. Polastri, M. Izzi, L. Pozza, C. Loss, and I. Smith, "Seismic analysis of multi-storey timber buildings braced with a CLT core and perimeter shear-walls," *Bulletin of Earthquake Engineering*, vol. 17, no. 2, pp. 1009–1028, Feb. 2019, doi: 10.1007/s10518-018-0467-9.

[38] M. M. Bagheri and G. Doudak, "Structural characteristics of light-frame wood shear walls with various construction detailing," *Eng Struct*, vol. 205, p. 110093, Feb. 2020, doi: 10.1016/j.engstruct.2019.110093.

[39] M. M. Bagheri and G. Doudak, "Experimental and numerical study on the deflection of multi-storey light-frame timber shear walls," *Eng Struct*, vol. 233, p. 111951, Apr. 2021, doi: 10.1016/j.engstruct.2021.111951.

[40] E. Ussher, C.-U. D. Gurholt, J. N. Mikalsen, A. Aloisio, and R. Tomasi, "Effect of construction features on the dynamic performance of mid-rise CLT platform-type buildings," *Wood Mater Sci Eng*, vol. 17, no. 4, pp. 261–273, Jul. 2022, doi: 10.1080/17480272.2022.2078223.

[41] L. Pozza, M. Savoia, L. Franco, A. Saetta, and D. Talledo, "Effect of different modelling approaches on the prediction of the seismic response of multi-storey CLT buildings," *International Journal of Computational Methods and Experimental Measurements*, vol. 5, no. 6, pp. 953–965, Nov. 2017, doi: 10.2495/CMEM-V5-N6-953-965.

[42] I. P. Christovasilis, L. Riparbelli, G. Rinaldin, and G. Tamagnone, "Methods for practice-oriented linear analysis in seismic design of Cross Laminated Timber buildings," *Soil Dynamics and Earthquake Engineering*, vol. 128, p. 105869, Jan. 2020, doi: 10.1016/j.soildyn.2019.105869.

[43] V. Rinaldi, D. Casagrande, C. Cimini, M. Follesa, and M. Fragiacomo, "An upgrade of existing practice-oriented FE design models for the seismic analysis of CLT buildings," *Soil Dynamics and Earthquake Engineering*, vol. 149, p. 106802, Oct. 2021, doi: 10.1016/j.soildyn.2021.106802.

[44] D. Casagrande, S. Rossi, T. Sartori, and R. Tomasi, "Analytical and numerical analysis of timber framed shear," in *World Conference on Timber Engineering, Auckland, New Zealand*, 2012.

[45] A. Gubana and A. Mazelli, "EVALUATION OF THE BEHAVIOUR FACTOR BY INCREMENTAL DYNAMIC ANALYSES FOR THE SEISMIC DESIGN OF LIGHT-FRAME TIMBER BUILDINGS," in *13th World Conference on Timber Engineering, WCTE 2023*, 2023. doi: 10.52202/069179-0325.

[46] A. Filiatrault, I. P. Christovasilis, A. Wanitkorkul, and J. W. van de Lindt, "Experimental Seismic Response of a Full-Scale Light-Frame Wood Building," *Journal of Structural Engineering*, vol. 136, no. 3, pp. 246–254, Mar. 2010, doi: 10.1061/(ASCE)ST.1943-541X.0000112.

[47] J. W. van de Lindt, S. Pei, S. E. Pryor, H. Shimizu, and H. Isoda, "Experimental Seismic Response of a Full-Scale Six-Story Light-Frame Wood Building," *Journal of Structural Engineering*, vol. 136, no. 10, pp. 1262–1272, Oct. 2010, doi: 10.1061/(ASCE)ST.1943-541X.0000222.

[48] R. Tomasi, D. Casagrande, P. Grossi, and T. Sartori, "Shaking table tests on a three-storey timber building," *Proceedings of the Institution of Civil Engineers - Structures and Buildings*, vol. 168, no. 11, pp. 853–867, Nov. 2015, doi: 10.1680/jstbu.14.00026.

[49] B. Faggiano *et al.*, "The Italian instructions for the design, execution and control of timber constructions (CNR-DT 206 R1/2018)," *Eng Struct*, vol. 253, p. 113753, Feb. 2022, doi: 10.1016/j.engstruct.2021.113753.

[50] S. Rossi, I. Giongo, D. Casagrande, R. Tomasi, and M. Piazza, "Evaluation of the displacement ductility for the seismic design of light-frame wood buildings," *Bulletin of Earthquake Engineering*, vol. 17, no. 9, pp. 5313–5338, Sep. 2019, doi: 10.1007/s10518-019-00659-4.

[51] C. Demirci, C. Málaga-Chuquitaype, and L. Macorini, "Seismic shear and acceleration demands in multi-storey cross-laminated timber buildings," *Eng Struct*, vol. 198, p. 109467, Nov. 2019, doi: 10.1016/j.engstruct.2019.109467.

[52] N. Gattesco and I. Boem, "Seismic performances and behavior factor of post-and-beam timber buildings braced with nailed shear walls," *Eng Struct*, vol. 100, pp. 674–685, Oct. 2015, doi: 10.1016/j.engstruct.2015.06.057.

[53] A. T. Council, *Quantification of building seismic performance factors*. US Department of Homeland Security, FEMA, 2009.

[54] I. P. Christovasilis, A. Filiatrault, M. C. Constantinou, and A. Wanitkorkul, "Incremental dynamic analysis of woodframe

buildings," *Earthq Eng Struct Dyn*, vol. 38, no. 4, pp. 477–496, Apr. 2009, doi: 10.1002/eqe.864.

[55] H. Isoda, B. Folz, and A. Filiatrault, "Seismic Modeling of Index Woodframe Buildings, CUREE Report No. W-12," Richmond, California, 2001.

[56] Z. Chen and C. Ni, "Seismic force-modification factors for mid-rise wood-frame buildings with shearwalls using wood screws," *Bulletin of Earthquake Engineering*, vol. 19, no. 3, pp. 1337–1364, Feb. 2021, doi: 10.1007/s10518-020-01031-7.

[57] A. Ceccotti, M. Massari, and L. Pozza, "Procedures for seismic characterization of traditional and modern wooden building types," *International Journal for Quality Research*, vol. 10, pp. 47–70, Apr. 2016, doi: 10.18421/IJQR10.01-02.

[58] EN 12512:2006, "Timber structures. Test methods. Cyclic testing of joints made with mechanical fasteners," 2006.

[59] A. Gubana, M. Melotto, L. De Cillia, and A. Mazelli, "Experimental investigation on long-term behavior of timber-to-timber shear connections made by inclined self-tapping screws," in *13th World Conference on Timber Engineering, WCTE 2023*, 2023. doi: 10.52202/069179-0080.

[60] A. Ceccotti and C. Sandhaas, "A proposal for a standard procedure to establish the seismic behaviour factor q of timber buildings," 2010. [Online]. Available: https://api.semanticscholar.org/CorpusID:114921681

[61] L. Pozza and D. Trutalli, "An analytical formulation of q-factor for mid-rise CLT buildings based on parametric numerical analyses," *Bulletin of Earthquake Engineering*, vol. 15, no. 5, pp. 2015–2033, May 2017, doi: 10.1007/s10518-016-0047-9.

[62] P. Fajfar, "Capacity spectrum method based on inelastic demand spectra," *Earthq Eng Struct Dyn*, vol. 28, no. 9, pp. 979–993, Sep. 1999, doi: 10.1002/(SICI)1096-9845(199909)28:9<979::AID-EQE850>3.0.CO;2-1.

[63] P. Fajfar, "A Nonlinear Analysis Method for Performance-Based Seismic Design," *Earthquake Spectra*, vol. 16, no. 3, pp. 573–592, Aug. 2000, doi: 10.1193/1.1586128.

[64] N. M. Newmark and W. J. Hall, "Earthquake spectra and design," 1982. [Online]. Available: https://api.semanticscholar.org/CorpusID:118174293

[65] American Society Standard Method (ASTM) E2126–11, "Standard test methods for cyclic (Reversed) load test for shear resistance of vertical elements of the lateral force resisting systems for buildingsStandard test methods for cyclic (Reversed) load test for shear resistance of vertical elements of the lateral force resisting systems for buildings," 2018.

[66] G. Rinaldin, M. Fragiacomo, and C. Amadio, "On the accuracy of the N2 inelastic spectrum for timber structures," *Soil Dynamics and Earthquake Engineering*, vol. 100, pp. 49–58, Sep. 2017, doi: 10.1016/j.soildyn.2017.05.026.

[67] J. Hummel, W. Seim, and S. Schwendner, "N2 method—Adaption to CLT structures," in *2018 world conference on timber engineering, WCTE 2018*, Seoul, South Korean, 2018.

[68] S. Karapetrou, M. Manakou, D. Bindi, B. Petrovic, and K. Pitilakis, ""Time-building specific' seismic vulnerability assessment of a hospital RC building using field monitoring data," *Eng Struct*, vol. 112, pp. 114–132, Apr. 2016, doi: 10.1016/j.engstruct.2016.01.009.

[69] A. Masi, M. Vona, and A. Digrisolo, "Derivation of Fragility Curves of some structural typologies representative of existing reinforced concrete buildings by non-linear dynamic analysis," in *XVII ANIDIS Symposium*, Bologna (in italian), 2009.

[70] A. Masi, M. Vona, and M. Mucciarelli, "Selection of Natural and Synthetic Accelerograms for Seismic Vulnerability Studies on Reinforced Concrete Frames," *Journal of Structural Engineering*, vol. 137, no. 3, pp. 367–378, Mar. 2011, doi: 10.1061/(ASCE)ST.1943-541X.0000209.

[71] D. Vamvatsikos and C. A. Cornell, "Incremental dynamic analysis," *Earthq Eng Struct Dyn*, vol. 31, no. 3, pp. 491–514, Mar. 2002, doi: 10.1002/eqe.141.

[72] D. Vamvatsikos, "Seismic performance, capacity and reliability of structures as seen through incremental dynamic analysis," Doctoral thesis, Stanford University, Stanford, U.S.A., 2002.

[73] D. Vamvatsikos and C. A. Cornell, "Applied Incremental Dynamic Analysis," *Earthquake Spectra*, vol. 20, no. 2, pp. 523–553, May 2004, doi: 10.1193/1.1737737.

[74] L. Eads, E. Miranda, and D. G. Lignos, "Average spectral acceleration as an intensity measure for collapse risk assessment," *Earthq Eng Struct Dyn*, vol. 44, no. 12, pp. 2057–2073, Sep. 2015, doi: 10.1002/eqe.2575.

[75] M. Fasan, R. Del Bello, G. Smiroldo, and C. Bedon, "Fragility assessment and q-behaviour factor of concentrically braced steel frames under seismic sequences based on Cloud Analysis," *Structures*, vol. 72, p. 108211, Feb. 2025, doi: 10.1016/j.istruc.2025.108211.

[76] F. Jalayer and C. A. Cornell, "Alternative non-linear demand estimation methods for probability-based seismic assessments," *Earthq Eng Struct Dyn*, vol. 38, no. 8, pp. 951–972, Jul. 2009, doi: 10.1002/eqe.876.

[77] N. Shome and C. Cornell, "Probabilistic Seismic Demand Analysis of Nonlinear Structures," PHD Thesis, RMS Program, Stanford University, 1999.

[78] J. W. Baker and C. Allin Cornell, "Spectral shape, epsilon and record selection," *Earthq Eng Struct Dyn*, vol. 35, no. 9, pp. 1077–1095, Jul. 2006, doi: 10.1002/eqe.571.

[79] J. W. Baker, "Probabilistic structural response assessment using vector-valued intensity measures," *Earthq Eng Struct Dyn*, vol. 36, no. 13, pp. 1861–1883, Oct. 2007, doi: 10.1002/eqe.700.

[80] F. Mollaioli and A. Lucchini, "Methods for selection and scaling of natural accelerograms for the non-linear dynamic analysis of structures," in *In: Proceedings of the ANIDIS conference, 2011, Bari, Italy (in italian)*,

[81] A. M. Mwafy and A. S. Elnashai, "Calibration of force reduction factors of RC buildings," *Journal of Earthquake Engineering*, vol. 6, no. 2, pp. 239–273, Apr. 2002, doi: 10.1080/13632460209350416.

[82] N. Fanaie and S. Ezzatshoar, "Studying the seismic behavior of gate braced frames by incremental dynamic analysis (IDA)," *J Constr Steel Res*, vol. 99, pp. 111–120, Aug. 2014, doi: 10.1016/j.jcsr.2014.04.008.

[83] P. Oggu, K. Gopikrishna, and A. Nagariya, "Seismic behavior and response reduction factors for concrete moment-resisting frames," *Bulletin of Earthquake Engineering*, vol. 19, no. 13, pp. 5643–5663, Oct. 2021, doi: 10.1007/s10518-021-01184-z.

[84] A. Gubana and G. Tomasi, "Results analysis of an experimental shear test on a light frame timber wall. Technical Report UNIUD 01 (in italian)," 2013.

[85] CSI, *Computer and Structures inc., SAP User Manual*. 2017.

[86] M. Melotto, "Wood-based in-Plane Strengthening Solutions for the Seismic Retrofit of Traditional Timber Floors in Masonry Buildings," Doctoral thesis, University of Brescia, Brescia, Italy, Brescia, 2017.

[87] A. Gubana, G. Tomasi, A. Mazelli, and C. Genero, "Guide Lines for calculation and seismic design of platform light frame timber residential buildings. Technical Report UNIUD (in italian)," 2021.

[88] American Society of Civil Engineers, *Minimum Design Loads and Associated Criteria for Buildings and Other Structures*. Reston, VA, 2017. doi: 10.1061/9780784414248.

[89] EN 1995-1-1:2005, "Eurocode 5: design of timber structures - Part 1-1: General-common rules and rules for buildings, Brussel, Belgium," 2005.

[90] A. Gubana and A. Mazelli, "Fragility curves for different intensity measures for a gravity load-designed RC hospital building: A case study," *Structures*, vol. 56, 2023, doi: 10.1016/j.istruc.2023.104925.

[91] M. T. M. Inc. Natick, "MATLAB version: 9.13.0 (R2022b)."

[92] National Research Council, "CNR-DT 212/2013 Instructions for the Reliability Assessment of Seismic Safety of Existing Buildings," Rome, 2013.

[93] I. Iervolino, C. Galasso, and E. Cosenza, "REXEL: computer aided record selection for code-based seismic structural analysis," *Bulletin of Earthquake Engineering*, vol. 8, no. 2, pp. 339–362, Apr. 2010, doi: 10.1007/s10518-009-9146-1.

[94] K. Kostinakis, A. Athanatopoulou, and K. Morfidis, "Correlation between ground motion intensity measures and seismic damage of 3D R/C buildings," *Eng Struct*, vol. 82, pp. 151–167, Jan. 2015, doi: 10.1016/j.engstruct.2014.10.035.

[95] National Research Council, "CNR-DT 206/2018 Istruzioni per la Progettazione, l'Esecuzione ed il Controllo delle Strutture di Legno," 2018.

I-A APPENDIX A

In this Appendix, all the tables related to the outcome of the IDA study are reported, divided for number of storeys, ductility and regularity. For each IDA curve, from 1 to 20, the collapse $V_{b(Dyn,c)}$, elastic $V_{b(Dyn,e)}$ and first yield $V_{b(St,y)}$ base shear are shown, together with the collapse direction "CollDir", indicating if the structure collapsed in X or Y direction. The ductility factor q_{μ} and the overstrength factor q_d were calculated according to formulation (26) and (27). Their product represents the intrinsic q-factor. To obtain the "code depending" facto q_{code}, the Design Overstrength Factor DOF was used, according to the procedure discussed in Chapter 7.2.

A.1 Regular buildings

A.1.1 Two storeys building

Ductility 4:

IDA	$V_{b(Dyn,c)}$ [kN]	CollDir	$V_{b(Dyn,e)}$ [kN]	$V_{b(St,y)}$ [kN]	q_μ	q_d	q	DOF	q_{code}
1	171.6	Y	320.6	127.2	1.9	1.3	2.5	1.5	3.8
2	196.1	Y	390.7	127.2	2.0	1.5	3.1	1.5	4.6
3	158.5	X	177.5	121.7	1.1	1.3	1.5	1.5	2.2
4	132.0	Y	150.5	127.2	1.1	1.0	1.2	1.5	1.8
5	175.6	Y	297.0	127.2	1.7	1.4	2.3	1.5	3.5
6	150.4	Y	273.1	127.2	1.8	1.2	2.1	1.5	3.2
7	188.9	X	261.7	121.7	1.4	1.6	2.1	1.5	3.2
8	191.7	Y	331.7	127.2	1.7	1.5	2.6	1.5	3.9
9	202.3	Y	456.8	127.2	2.3	1.6	3.6	1.5	5.4
10	192.1	X	331.5	121.7	1.7	1.6	2.7	1.5	4.1
11	192.0	X	250.1	121.7	1.3	1.6	2.1	1.5	3.1
12	155.4	Y	378.9	127.2	2.4	1.2	3.0	1.5	4.5
13	132.3	Y	538.5	127.2	4.1	1.0	4.2	1.5	6.4
14	186.5	X	299.5	121.7	1.6	1.5	2.5	1.5	3.7
15	199.3	Y	337.6	127.2	1.7	1.6	2.7	1.5	4.0
16	190.0	X	196.7	121.7	1.0	1.6	1.6	1.5	2.4
17	177.4	Y	177.9	127.2	1.0	1.4	1.4	1.5	2.1
18	194.5	X	325.6	121.7	1.7	1.6	2.7	1.5	4.0
19	189.1	X	260.9	121.7	1.4	1.6	2.1	1.5	3.2
20	177.3	X	252.8	121.7	1.4	1.5	2.1	1.5	3.1
mean	177.65	%X	300.48	124.71	1.7	1.43	2.40	1.50	3.61
sigma	21.26	45%	95.09	2.78	0.67	0.18	0.74		1.10
CoV	0.120	%Y	0.316	0.022	0.392	0.128	0.306		0.306
min	132.0	55%	150.5	121.7	1.0	1.0	1.2	1.5	1.8
max	202.3		538.5	127.2	4.1	1.6	4.2	1.5	6.4

Ductility 6:

IDA	$V_{b(Dyn,c)}$ [kN]	CollDir	$V_{b(Dyn,e)}$ [kN]	$V_{b(St,y)}$ [kN]	q_μ	q_d	q	DOF	q_{code}
1	183.0	Y	449.1	141.5	2.5	1.3	3.2	1.5	4.8
2	198.5	Y	464.8	141.5	2.3	1.4	3.3	1.5	4.9
3	169.7	X	437.0	122.9	2.6	1.4	3.6	1.5	5.3
4	189.4	Y	225.1	141.5	1.2	1.3	1.6	1.5	2.4
5	174.9	X	354.0	122.9	2.0	1.4	2.9	1.5	4.3
6	182.3	Y	377.8	141.5	2.1	1.3	2.7	1.5	4.0
7	172.7	X	276.1	122.9	1.6	1.4	2.2	1.5	3.4
8	174.1	Y	400.0	141.5	2.3	1.2	2.8	1.5	4.2
9	188.0	Y	514.8	141.5	2.7	1.3	3.6	1.5	5.5
10	175.0	X	304.1	122.9	1.7	1.4	2.5	1.5	3.7
11	173.5	X	358.6	122.9	2.1	1.4	2.9	1.5	4.4
12	196.2	Y	363.3	141.5	1.9	1.4	2.6	1.5	3.9
13	157.0	Y	603.8	141.5	3.8	1.1	4.3	1.5	6.4
14	157.9	X	530.0	122.9	3.4	1.3	4.3	1.5	6.5
15	199.7	Y	384.0	141.5	1.9	1.4	2.7	1.5	4.1
16	201.0	Y	364.1	141.5	1.8	1.4	2.6	1.5	3.9
17	171.3	Y	235.7	141.5	1.4	1.2	1.7	1.5	2.5
18	167.8	Y	418.8	141.5	2.5	1.2	3.0	1.5	4.4
19	166.3	X	348.4	122.9	2.1	1.4	2.8	1.5	4.3
20	164.3	X	634.5	122.9	3.9	1.3	5.2	1.5	7.7
mean	178.12	%X	402.21	134.06	2.3	1.33	3.02	1.50	4.52
sigma	13.56	40%	109.27	9.33	0.72	0.09	0.86		1.29
CoV	0.076	%Y	0.272	0.070	0.317	0.068	0.285		0.285
min	157.0	60%	225.1	122.9	1.2	1.1	1.6	1.5	2.4
max	201.0		634.5	141.5	3.9	1.4	5.2	1.5	7.7

Ductility 8:

IDA	$V_{b(Dyn,c)}$ [kN]	CollDir	$V_{b(Dyn,e)}$ [kN]	$V_{b(St,y)}$ [kN]	q_μ	q_d	q	DOF	q_{code}
1	196.25	Y	602.55	95.02	3.1	2.1	6.3	1.5	9.5
2	143.97	Y	357.12	95.02	2.5	1.5	3.8	1.5	5.6
3	170.98	X	358.29	129.72	2.1	1.3	2.8	1.5	4.1
4	193.98	Y	296.07	95.02	1.5	2.0	3.1	1.5	4.7
5	199.42	Y	486.88	95.02	2.4	2.1	5.1	1.5	7.7
6	164.50	X	309.21	129.72	1.9	1.3	2.4	1.5	3.6
7	182.41	X	316.28	129.72	1.7	1.4	2.4	1.5	3.7
8	178.01	X	651.78	129.72	3.7	1.4	5.0	1.5	7.5
9	187.24	Y	373.60	95.02	2.0	2.0	3.9	1.5	5.9
10	183.58	X	345.98	129.72	1.9	1.4	2.7	1.5	4.0
11	182.20	X	367.13	129.72	2.0	1.4	2.8	1.5	4.2
12	197.05	Y	514.72	95.02	2.6	2.1	5.4	1.5	8.1
13	182.74	X	516.89	129.72	2.8	1.4	4.0	1.5	6.0
14	163.86	X	710.87	129.72	4.3	1.3	5.5	1.5	8.2
15	201.23	Y	315.71	95.02	1.6	2.1	3.3	1.5	5.0
16	195.07	Y	394.77	95.02	2.0	2.1	4.2	1.5	6.2
17	180.06	Y	520.81	95.02	2.9	1.9	5.5	1.5	8.2
18	175.30	X	295.04	129.72	1.7	1.4	2.3	1.5	3.4
19	176.06	X	439.48	129.72	2.5	1.4	3.4	1.5	5.1
20	176.40	X	735.96	129.72	4.2	1.4	5.7	1.5	8.5
mean	181.51	%X	445.46	114.11	2.5	1.64	3.98	1.50	5.97
sigma	14.10	55%	140.60	17.72	0.82	0.34	1.29		1.93
CoV	0.078	%Y	0.316	0.155	0.333	0.210	0.323		0.323
min	144.0	45%	295.0	95.0	1.5	1.3	2.3	1.5	3.4
max	201.2		736.0	129.7	4.3	2.1	6.3	1.5	9.5

A.1.2 Three storeys building

Ductility 4:

IDA	$V_{b(Dyn,c)}$ [kN]	CollDir	$V_{b(Dyn,e)}$ [kN]	$V_{b(St,y)}$ [kN]	q_μ	q_d	q	DOF	q_{code}
1	189.2	X	244.7	193.65	1.3	1.0	1.3	1.5	1.9
2	190.2	Y	331.7	169.41	1.7	1.1	2.0	1.5	2.9
3	164.0	Y	369.0	169.41	2.3	1.0	2.2	1.5	3.3
4	199.6	Y	263.7	169.41	1.3	1.2	1.6	1.5	2.3
5	240.6	X	350.7	193.65	1.5	1.2	1.8	1.5	2.7
6	192.0	X	276.7	193.65	1.4	1.0	1.4	1.5	2.1
7	241.4	X	363.6	193.65	1.5	1.2	1.9	1.5	2.8
8	248.7	X	339.6	193.65	1.4	1.3	1.8	1.5	2.6
9	204.6	Y	319.7	169.41	1.6	1.2	1.9	1.5	2.8
10	249.7	X	361.3	193.65	1.4	1.3	1.9	1.5	2.8
11	171.2	X	174.2	170.32	1.0	1.0	1.0	1.5	1.5
12	213.8	X	233.1	193.65	1.1	1.1	1.2	1.5	1.8
13	243.6	X	398.1	193.65	1.6	1.3	2.1	1.5	3.1
14	204.7	X	200.2	193.65	1.0	1.1	1.0	1.5	1.6
15	193.1	X	397.3	193.65	2.1	1.0	2.1	1.5	3.1
16	204.7	Y	269.4	169.41	1.3	1.2	1.6	1.5	2.4
17	173.6	X	175.4	170.32	1.0	1.0	1.0	1.5	1.5
18	238.7	X	302.1	193.65	1.3	1.2	1.6	1.5	2.3
19	204.1	X	216.0	193.65	1.1	1.1	1.1	1.5	1.7
20	217.9	X	222.3	193.65	1.0	1.1	1.1	1.5	1.7
mean	209.27	%X	290.44	185.26	1.4	1.13	1.57	1.50	2.35
sigma	26.78	75%	72.58	11.74	0.34	0.11	0.39		0.58
CoV	0.128	%Y	0.250	0.063	0.247	0.100	0.248		0.248
min	164.0	25%	174.2	169.4	1.0	1.0	1.0	1.5	1.5
max	249.7		398.1	193.7	2.3	1.3	2.2	1.5	3.3

Ductility 6:

IDA	$V_{b(Dyn,c)}$ [kN]	CollDir	$V_{b(Dyn,e)}$ [kN]	$V_{b(St,y)}$ [kN]	q_μ	q_d	q	DOF	q_{code}
1	147.2	Y	259.4	135.96	1.8	1.1	1.9	1.5	2.9
2	151.0	Y	221.0	135.96	1.5	1.1	1.6	1.5	2.4
3	192.6	X	436.9	200.04	2.3	1.0	2.2	1.5	3.3
4	171.7	Y	255.5	135.96	1.5	1.3	1.9	1.5	2.8
5	171.0	Y	228.2	135.96	1.3	1.3	1.7	1.5	2.5
6	154.9	Y	282.8	135.96	1.8	1.1	2.1	1.5	3.1
7	164.3	Y	221.1	135.96	1.3	1.2	1.6	1.5	2.4
8	130.3	Y	237.2	135.96	1.8	1.0	1.7	1.5	2.6
9	137.1	Y	228.9	135.96	1.7	1.0	1.7	1.5	2.5
10	275.4	X	392.5	200.04	1.4	1.4	2.0	1.5	2.9
11	142.8	Y	166.7	135.96	1.2	1.1	1.2	1.5	1.8
12	134.2	Y	159.9	135.96	1.2	1.0	1.2	1.5	1.8
13	150.2	Y	467.5	135.96	3.1	1.1	3.4	1.5	5.2
14	208.3	X	228.8	200.04	1.1	1.0	1.1	1.5	1.7
15	145.3	Y	399.4	135.96	2.7	1.1	2.9	1.5	4.4
16	205.4	Y	327.5	135.96	1.6	1.5	2.4	1.5	3.6
17	152.7	Y	229.7	135.96	1.5	1.1	1.7	1.5	2.5
18	261.4	X	329.2	200.04	1.3	1.3	1.6	1.5	2.5
19	215.1	X	247.6	200.04	1.2	1.1	1.2	1.5	1.9
20	138.0	Y	216.8	135.96	1.6	1.0	1.6	1.5	2.4
mean	172.44	%X	276.82	151.98	1.6	1.13	1.84	1.50	2.77
sigma	41.51	25%	86.98	28.47	0.53	0.15	0.57		0.86
CoV	0.241	%Y	0.314	0.187	0.322	0.129	0.310		0.310
min	130.3	75%	159.9	136.0	1.1	1.0	1.1	1.5	1.7
max	275.4		467.5	200.0	3.1	1.5	3.4	1.5	5.2

Ductility 8:

IDA	$V_{b(Dyn,c)}$ [kN]	CollDir	$V_{b(Dyn,e)}$ [kN]	$V_{b(St,y)}$ [kN]	q_μ	q_d	q	DOF	q_{code}
1	167.79	Y	289.38	116.99	1.7	1.4	2.5	1.5	3.7
2	151.01	Y	242.02	116.99	1.6	1.3	2.1	1.5	3.1
3	182.95	X	495.20	169.53	2.7	1.1	2.9	1.5	4.4
4	162.53	Y	287.66	116.99	1.8	1.4	2.5	1.5	3.7
5	177.72	Y	284.12	116.99	1.6	1.5	2.4	1.5	3.6
6	149.16	Y	333.33	116.99	2.2	1.3	2.8	1.5	4.3
7	177.06	Y	260.71	116.99	1.5	1.5	2.2	1.5	3.3
8	135.57	Y	247.74	116.99	1.8	1.2	2.1	1.5	3.2
9	133.64	Y	255.79	116.99	1.9	1.1	2.2	1.5	3.3
10	273.32	X	448.50	193.06	1.6	1.4	2.3	1.5	3.5
11	174.16	X	281.43	169.53	1.6	1.0	1.7	1.5	2.5
12	156.74	Y	213.90	116.99	1.4	1.3	1.8	1.5	2.7
13	190.76	Y	497.09	116.99	2.6	1.6	4.2	1.5	6.4
14	224.26	X	271.73	193.06	1.2	1.2	1.4	1.5	2.1
15	171.94	Y	395.59	116.99	2.3	1.5	3.4	1.5	5.1
16	199.73	Y	398.46	116.99	2.0	1.7	3.4	1.5	5.1
17	166.75	Y	270.37	116.99	1.6	1.4	2.3	1.5	3.5
18	281.61	X	427.96	193.06	1.5	1.5	2.2	1.5	3.3
19	219.40	X	284.46	193.06	1.3	1.1	1.5	1.5	2.2
20	136.15	Y	318.86	116.99	2.3	1.2	2.7	1.5	4.1
mean	181.61	%X	325.21	137.46	1.8	1.34	2.44	1.50	3.65
sigma	41.12	30%	86.68	32.68	0.42	0.19	0.69		1.03
CoV	0.226	%Y	0.267	0.238	0.233	0.142	0.282		0.282
min	133.6	70%	213.9	117.0	1.2	1.0	1.4	1.5	2.1
max	281.6		497.1	193.1	2.7	1.7	4.2	1.5	6.4

A.1.3 Four storeys building

Ductility 4:

IDA	$V_{b(Dyn,c)}$ [kN]	CollDir	$V_{b(Dyn,e)}$ [kN]	$V_{b(St,y)}$ [kN]	q_μ	q_d	q	DOF	q_{code}
1	132.9	Y	201.7	136.00	1.5	1.0	1.5	1.5	2.2
2	119.4	Y	158.3	136.00	1.3	1.0	1.3	1.5	2.0
3	214.4	X	404.8	191.59	1.9	1.1	2.1	1.5	3.2
4	129.9	Y	177.8	136.00	1.4	1.0	1.3	1.5	2.0
5	177.6	Y	249.9	136.00	1.4	1.3	1.8	1.5	2.8
6	146.1	Y	183.8	136.00	1.3	1.1	1.4	1.5	2.0
7	245.9	X	299.2	191.59	1.2	1.3	1.6	1.5	2.3
8	123.6	Y	179.2	136.00	1.4	1.0	1.4	1.5	2.2
9	154.6	Y	209.0	136.00	1.4	1.1	1.5	1.5	2.3
10	249.6	X	440.0	191.59	1.8	1.3	2.3	1.5	3.4
11	247.9	X	671.9	191.59	2.7	1.3	3.5	1.5	5.3
12	136.9	Y	199.9	136.00	1.5	1.0	1.5	1.5	2.2
13	213.8	X	319.7	191.59	1.5	1.1	1.7	1.5	2.5
14	188.4	X	213.1	191.59	1.1	1.0	1.1	1.5	1.7
15	154.5	Y	246.4	136.00	1.6	1.1	1.8	1.5	2.7
16	201.5	Y	258.9	136.00	1.3	1.5	1.9	1.5	2.9
17	156.5	Y	329.0	136.00	2.1	1.2	2.4	1.5	3.6
18	224.1	X	316.9	191.59	1.4	1.2	1.7	1.5	2.5
19	187.0	X	323.8	191.59	1.7	1.0	1.7	1.5	2.5
20	131.8	Y	259.6	136.00	2.0	1.0	1.9	1.5	2.9
mean	176.81	%X	282.14	158.24	1.6	1.12	1.77	1.50	2.66
sigma	44.27	40%	119.63	27.94	0.37	0.15	0.53		0.79
CoV	0.250	%Y	0.424	0.177	0.237	0.132	0.298		0.298
min	119.4	60%	158.3	136.0	1.1	1.0	1.1	1.5	1.7
max	249.6		671.9	191.6	2.7	1.5	3.5	1.5	5.3

Ductility 6:

IDA	$V_{b(Dyn,c)}$ [kN]	CollDir	$V_{b(Dyn,e)}$ [kN]	$V_{b(St,y)}$ [kN]	q_μ	q_d	q	DOF	q_{code}
1	151.05	Y	279.21	131.45	1.8	1.1	2.1	1.5	3.2
2	136.73	Y	184.95	131.45	1.4	1.0	1.4	1.5	2.1
3	263.64	X	543.74	189.19	2.1	1.4	2.9	1.5	4.3
4	128.25	Y	217.59	131.45	1.7	1.0	1.7	1.5	2.5
5	273.91	X	417.43	189.19	1.5	1.4	2.2	1.5	3.3
6	146.23	Y	223.11	131.45	1.5	1.1	1.7	1.5	2.5
7	273.28	X	327.17	189.19	1.2	1.4	1.7	1.5	2.6
8	129.34	Y	244.54	131.45	1.9	1.0	1.9	1.5	2.8
9	184.14	Y	382.9	131.45	2.1	1.4	2.9	1.5	4.4
10	275.68	X	633.92	189.19	2.3	1.5	3.4	1.5	5.0
11	273.9632	X	822.21	189.19	3.0	1.4	4.3	1.5	6.5
12	195.6012	Y	303.23	131.45	1.6	1.5	2.3	1.5	3.5
13	184.0437	Y	309.49	131.45	1.7	1.4	2.4	1.5	3.5
14	208.6663	X	271.41	189.19	1.3	1.1	1.4	1.5	2.2
15	190.6469	Y	280.95	131.45	1.5	1.5	2.1	1.5	3.2
16	198.5457	Y	281.97	131.45	1.4	1.5	2.1	1.5	3.2
17	177.8119	Y	443.83	131.45	2.5	1.4	3.4	1.5	5.1
18	264.93	X	458.77	189.19	1.7	1.4	2.4	1.5	3.6
19	222.8312	X	445.15	189.19	2.0	1.2	2.4	1.5	3.5
20	207.6519	X	322.48	189.19	1.6	1.1	1.7	1.5	2.6
mean	204.35	%X	369.70	157.43	1.8	1.29	2.32	1.50	3.48
sigma	51.87	45%	156.67	29.47	0.44	0.19	0.74		1.11
CoV	0.254	%Y	0.424	0.187	0.249	0.144	0.320		0.320
min	128.3	55%	185.0	131.5	1.2	1.0	1.4	1.5	2.1
max	275.7		822.2	189.2	3.0	1.5	4.3	1.5	6.5

Ductility 8:

IDA	$V_{b(Dyn,c)}$ [kN]	CollDir	$V_{b(Dyn,e)}$ [kN]	$V_{b(St,y)}$ [kN]	q_μ	q_d	q	DOF	q_{code}
1	144.10	Y	341.25	127.71	2.4	1.1	2.7	1.5	4.0
2	153.39	Y	221.38	127.71	1.4	1.2	1.7	1.5	2.6
3	229.04	X	586.45	161.27	2.6	1.4	3.6	1.5	5.5
4	171.18	Y	324.23	127.71	1.9	1.3	2.5	1.5	3.8
5	229.60	X	483.83	161.27	2.1	1.4	3.0	1.5	4.5
6	148.46	Y	251.71	127.71	1.7	1.2	2.0	1.5	3.0
7	225.94	X	326.65	161.27	1.4	1.4	2.0	1.5	3.0
8	149.88	Y	293.44	127.71	2.0	1.2	2.3	1.5	3.4
9	196.83	Y	439.4	127.71	2.2	1.5	3.4	1.5	5.2
10	220.99	X	486.05	161.27	2.2	1.4	3.0	1.5	4.5
11	222.7933	X	770.4747	161.27	3.5	1.4	4.8	1.5	7.2
12	197.69	Y	350.6064	127.71	1.8	1.5	2.7	1.5	4.1
13	198.8432	Y	468.3672	127.71	2.4	1.6	3.7	1.5	5.5
14	216.6163	X	408.9928	161.27	1.9	1.3	2.5	1.5	3.8
15	199.9533	Y	481.4176	127.71	2.4	1.6	3.8	1.5	5.7
16	200.8674	Y	279.6148	127.71	1.4	1.6	2.2	1.5	3.3
17	192.5733	Y	527.0583	127.71	2.7	1.5	4.1	1.5	6.2
18	222.1389	X	620.4212	161.27	2.8	1.4	3.8	1.5	5.8
19	200.2127	Y	352.8002	127.71	1.8	1.6	2.8	1.5	4.1
20	211.5045	X	372.0537	161.27	1.8	1.3	2.3	1.5	3.5
mean	196.63	%X	419.31	141.13	2.1	1.39	2.95	1.50	4.43
sigma	28.46	40%	136.96	16.87	0.52	0.15	0.82		1.22
CoV	0.145	%Y	0.327	0.120	0.247	0.104	0.276		0.276
min	144.1	60%	221.4	127.7	1.4	1.1	1.7	1.5	2.6
max	229.6		770.5	161.3	3.5	1.6	4.8	1.5	7.2

A.2 Non-Regular buildings

A.2.1 Two storeys building

Ductility 4:

IDA	$V_{b(Dyn,c)}$ [kN]	CollDir	$V_{b(Dyn,e)}$ [kN]	$V_{b(St,y)}$ [kN]	q_μ	q_d	q	DOF	q_{code}
1	131.7	X	195.2	109.1	1.5	1.2	1.8	1.5	2.7
2	103.3	X	233.5	101.1	2.3	1.0	2.3	1.5	3.5
3	127.2	Y	134.3	103.6	1.1	1.2	1.3	1.5	1.9
4	144.1	Y	180.3	103.6	1.3	1.4	1.7	1.5	2.6
5	148.4	X	202.1	109.1	1.4	1.4	1.9	1.5	2.8
6	144.0	Y	340.9	103.6	2.4	1.4	3.3	1.5	4.9
7	148.6	X	211.1	109.1	1.4	1.4	1.9	1.5	2.9
8	149.1	X	239.6	109.1	1.6	1.4	2.2	1.5	3.3
9	136.1	Y	327.0	103.6	2.4	1.3	3.2	1.5	4.7
10	149.0	X	291.7	109.1	2.0	1.4	2.7	1.5	4.0
11	149.1	X	207.7	109.1	1.4	1.4	1.9	1.5	2.9
12	138.5	Y	190.9	103.6	1.4	1.3	1.8	1.5	2.8
13	98.8	Y	373.3	95.0	3.8	1.0	3.9	1.5	5.9
14	148.8	X	339.7	109.1	2.3	1.4	3.1	1.5	4.7
15	122.7	Y	213.2	103.6	1.7	1.2	2.1	1.5	3.1
16	144.0	Y	232.2	103.6	1.6	1.4	2.2	1.5	3.4
17	136.0	Y	263.8	103.6	1.9	1.3	2.5	1.5	3.8
18	143.6	X	311.4	109.1	2.2	1.3	2.9	1.5	4.3
19	148.7	X	279.4	109.1	1.9	1.4	2.6	1.5	3.8
20	143.5	X	391.8	109.1	2.7	1.3	3.6	1.5	5.4
mean	137.76	%X	257.95	105.81	1.9	1.30	2.44	1.50	3.67
sigma	14.74	55%	70.80	3.90	0.63	0.11	0.70		1.04
CoV	0.107	%Y	0.274	0.037	0.332	0.084	0.285		0.285
min	98.8	45%	134.3	95.0	1.1	1.0	1.3	1.5	1.9
max	149.1		391.8	109.1	3.8	1.4	3.9	1.5	5.9

Ductility 6:

IDA	$V_{b(Dyn,c)}$ [kN]	CollDir	$V_{b(Dyn,e)}$ [kN]	$V_{b(St,y)}$ [kN]	q_μ	q_d	q	DOF	q_{code}
1	135.6	X	285.3	119.6	2.1	1.1	2.4	1.5	3.6
2	138.8	Y	327.5	99.3	2.4	1.4	3.3	1.5	4.9
3	152.8	X	190.0	119.6	1.2	1.3	1.6	1.5	2.4
4	149.9	X	152.9	119.6	1.0	1.3	1.3	1.5	1.9
5	143.6	Y	286.9	99.3	2.0	1.4	2.9	1.5	4.3
6	158.6	X	273.5	119.6	1.7	1.3	2.3	1.5	3.4
7	161.3	X	223.3	119.6	1.4	1.3	1.9	1.5	2.8
8	144.7	Y	374.8	99.3	2.6	1.5	3.8	1.5	5.7
9	133.5	Y	309.3	99.3	2.3	1.3	3.1	1.5	4.7
10	162.2	X	312.0	119.6	1.9	1.4	2.6	1.5	3.9
11	158.0	X	268.9	119.6	1.7	1.3	2.2	1.5	3.4
12	141.3	Y	303.5	99.3	2.1	1.4	3.1	1.5	4.6
13	129.0	Y	388.5	99.3	3.0	1.3	3.9	1.5	5.9
14	159.8	X	517.8	119.6	3.2	1.3	4.3	1.5	6.5
15	114.9	Y	242.6	99.3	2.1	1.2	2.4	1.5	3.7
16	162.5	X	242.9	119.6	1.5	1.4	2.0	1.5	3.0
17	115.5	X	438.5	119.6	3.8	1.0	3.7	1.5	5.5
18	129.2	Y	338.8	99.3	2.6	1.3	3.4	1.5	5.1
19	163.3	X	301.6	119.6	1.8	1.4	2.5	1.5	3.8
20	159.9	X	382.1	119.6	2.4	1.3	3.2	1.5	4.8
mean	145.72	%X	308.03	111.44	2.2	1.31	2.80	1.50	4.19
sigma	15.60	60%	84.68	10.20	0.68	0.11	0.81		1.21
CoV	0.107	%Y	0.275	0.092	0.317	0.088	0.290		0.290
min	114.9	40%	152.9	99.3	1.0	1.0	1.3	1.5	1.9
max	163.3		517.8	119.6	3.8	1.5	4.3	1.5	6.5

Ductility 8:

IDA	$V_{b(Dyn,c)}$ [kN]	CollDir	$V_{b(Dyn,e)}$ [kN]	$V_{b(St,y)}$ [kN]	q_μ	q_d	q	DOF	q_{code}
1	145.2	Y	660.5	97.8	4.5	1.5	6.8	1.5	10.1
2	128.8	X	264.4	102.3	2.1	1.3	2.6	1.5	3.9
3	153.9	X	248.9	102.3	1.6	1.5	2.4	1.5	3.6
4	154.6	X	157.3	102.3	1.0	1.5	1.5	1.5	2.3
5	149.7	Y	265.5	97.8	1.8	1.5	2.7	1.5	4.1
6	148.5	X	239.5	102.3	1.6	1.5	2.3	1.5	3.5
7	164.1	X	232.5	102.3	1.4	1.6	2.3	1.5	3.4
8	135.3	X	285.5	102.3	2.1	1.3	2.8	1.5	4.2
9	143.4	Y	311.5	97.8	2.2	1.5	3.2	1.5	4.8
10	172.2	X	306.2	102.3	1.8	1.7	3.0	1.5	4.5
11	155.5	X	262.1	102.3	1.7	1.5	2.6	1.5	3.8
12	144.4	Y	336.8	97.8	2.3	1.5	3.4	1.5	5.2
13	138.6	Y	421.9	97.8	3.0	1.4	4.3	1.5	6.5
14	153.2	X	285.4	102.3	1.9	1.5	2.8	1.5	4.2
15	138.0	Y	382.2	97.8	2.8	1.4	3.9	1.5	5.9
16	151.2	X	203.1	102.3	1.3	1.5	2.0	1.5	3.0
17	132.7	X	278.3	102.3	2.1	1.3	2.7	1.5	4.1
18	169.4	X	362.5	102.3	2.1	1.7	3.5	1.5	5.3
19	152.4	X	213.8	102.3	1.4	1.5	2.1	1.5	3.1
20	112.1	X	277.9	102.3	2.5	1.1	2.7	1.5	4.1
mean	147.15	%X	299.79	100.98	2.1	1.46	2.98	1.50	4.47
sigma	14.07	70%	105.19	2.12	0.76	0.14	1.10		1.65
CoV	0.096	%Y	0.351	0.021	0.371	0.093	0.370		0.370
min	112.1	30%	157.3	97.8	1.0	1.1	1.5	1.5	2.3
max	172.2		660.5	102.3	4.5	1.7	6.8	1.5	10.1

A.2.2 Three storeys building

Ductility 4:

IDA	$V_{b(Dyn,c)}$ [kN]	CollDir	$V_{b(Dyn,e)}$ [kN]	$V_{b(St,y)}$ [kN]	q_μ	q_d	q	DOF	q_{code}
1	154.8	X	268.5	109.11	1.7	1.4	2.5	1.5	3.7
2	110.2	X	187.3	109.11	1.7	1.0	1.7	1.5	2.6
3	143.6	X	330.8	109.11	2.3	1.3	3.0	1.5	4.5
4	143.8	Y	235.5	106.52	1.6	1.3	2.2	1.5	3.3
5	139.5	X	213.1	109.11	1.5	1.3	2.0	1.5	2.9
6	160.7	X	231.9	109.11	1.4	1.5	2.1	1.5	3.2
7	179.8	X	279.6	109.11	1.6	1.6	2.6	1.5	3.8
8	128.5	Y	252.9	106.52	2.0	1.2	2.4	1.5	3.6
9	140.4	Y	243.7	106.52	1.7	1.3	2.3	1.5	3.4
10	178.0	X	244.7	109.11	1.4	1.6	2.2	1.5	3.4
11	171.2	X	193.7	109.11	1.1	1.6	1.8	1.5	2.7
12	134.9	Y	422.4	106.52	3.1	1.3	4.0	1.5	5.9
13	179.2	X	365.3	109.11	2.0	1.6	3.3	1.5	5.0
14	144.2	X	264.1	109.11	1.8	1.3	2.4	1.5	3.6
15	137.7	Y	495.8	106.52	3.6	1.3	4.7	1.5	7.0
16	143.3	Y	263.9	106.52	1.8	1.3	2.5	1.5	3.7
17	163.7	X	167.8	109.11	1.0	1.5	1.5	1.5	2.3
18	173.7	X	186.3	109.11	1.1	1.6	1.7	1.5	2.6
19	173.2	X	231.3	109.11	1.3	1.6	2.1	1.5	3.2
20	176.3	X	196.9	109.11	1.1	1.6	1.8	1.5	2.7
mean	153.84	%X	263.78	108.33	1.8	1.42	2.44	1.50	3.66
sigma	19.97	70%	82.98	1.21	0.65	0.18	0.78		1.18
CoV	0.130	%Y	0.315	0.011	0.371	0.124	0.322		0.322
min	110.2	30%	167.8	106.5	1.0	1.0	1.5	1.5	2.3
max	179.8		495.8	109.1	3.6	1.6	4.7	1.5	7.0

Ductility 6:

IDA	$V_{b(Dyn,c)}$ [kN]	CollDir	$V_{b(Dyn,e)}$ [kN]	$V_{b(St,y)}$ [kN]	q_μ	q_d	q	DOF	q_{code}
1	159.7	X	211.8	120.61	1.3	1.3	1.8	1.5	2.6
2	143.5	X	239.0	120.61	1.7	1.2	2.0	1.5	3.0
3	127.6	X	252.0	120.61	2.0	1.1	2.1	1.5	3.1
4	130.4	X	308.0	120.61	2.4	1.1	2.6	1.5	3.8
5	138.5	Y	280.4	90.56	2.0	1.5	3.1	1.5	4.6
6	139.5	X	197.6	120.61	1.4	1.2	1.6	1.5	2.5
7	177.2	X	263.1	120.61	1.5	1.5	2.2	1.5	3.3
8	149.9	X	226.5	120.61	1.5	1.2	1.9	1.5	2.8
9	144.9	X	505.6	120.61	3.5	1.2	4.2	1.5	6.3
10	179.0	X	285.7	120.61	1.6	1.5	2.4	1.5	3.6
11	134.0	X	168.1	120.61	1.3	1.1	1.4	1.5	2.1
12	170.9	X	328.8	120.61	1.9	1.4	2.7	1.5	4.1
13	178.1	X	449.5	120.61	2.5	1.5	3.7	1.5	5.6
14	156.3	X	159.3	120.61	1.0	1.3	1.3	1.5	2.0
15	154.2	X	369.2	120.61	2.4	1.3	3.1	1.5	4.6
16	142.0	Y	291.8	90.56	2.1	1.6	3.2	1.5	4.8
17	135.6	X	137.1	120.61	1.0	1.1	1.1	1.5	1.7
18	176.7	X	246.6	120.61	1.4	1.5	2.0	1.5	3.1
19	149.0	X	177.7	120.61	1.2	1.2	1.5	1.5	2.2
20	146.6	X	202.5	120.61	1.4	1.2	1.7	1.5	2.5
mean	151.68	%X	265.03	117.61	1.8	1.30	2.28	1.50	3.41
sigma	16.77	90%	94.19	9.25	0.61	0.16	0.84		1.25
CoV	0.111	%Y	0.355	0.079	0.347	0.124	0.367		0.367
min	127.6	10%	137.1	90.6	1.0	1.1	1.1	1.5	1.7
max	179.0		505.6	120.6	3.5	1.6	4.2	1.5	6.3

Ductility 8:

IDA	$V_{b(Dyn,c)}$ [kN]	CollDir	$V_{b(Dyn,e)}$ [kN]	$V_{b(St,y)}$ [kN]	q_μ	q_d	q	DOF	q_{code}
1	158.0	X	307.6	112.5	1.9	1.4	2.7	1.5	4.1
2	143.5	Y	479.9	99.8	3.3	1.4	4.8	1.5	7.2
3	152.6	X	364.1	112.5	2.4	1.4	3.2	1.5	4.9
4	148.1	Y	624.0	99.8	4.2	1.5	6.3	1.5	9.4
5	172.5	X	310.1	112.5	1.8	1.5	2.8	1.5	4.1
6	149.5	X	267.4	112.5	1.8	1.3	2.4	1.5	3.6
7	168.7	X	268.2	112.5	1.6	1.5	2.4	1.5	3.6
8	173.2	X	483.9	112.5	2.8	1.5	4.3	1.5	6.5
9	146.7	Y	576.1	99.8	3.9	1.5	5.8	1.5	8.7
10	171.7	X	292.3	112.5	1.7	1.5	2.6	1.5	3.9
11	139.1	X	242.2	112.5	1.7	1.2	2.2	1.5	3.2
12	143.7	Y	429.4	99.8	3.0	1.4	4.3	1.5	6.5
13	150.9	Y	568.6	99.8	3.8	1.5	5.7	1.5	8.5
14	169.2	X	282.3	112.5	1.7	1.5	2.5	1.5	3.8
15	139.7	Y	470.6	99.8	3.4	1.4	4.7	1.5	7.1
16	140.8	Y	336.4	99.8	2.4	1.4	3.4	1.5	5.1
17	135.6	X	159.5	112.5	1.2	1.2	1.4	1.5	2.1
18	170.9	X	464.0	112.5	2.7	1.5	4.1	1.5	6.2
19	158.2	X	211.6	112.5	1.3	1.4	1.9	1.5	2.8
20	155.9	X	246.7	112.5	1.6	1.4	2.2	1.5	3.3
mean	154.43	%X	369.24	108.09	2.4	1.43	3.48	1.50	5.22
sigma	12.70	65%	133.40	6.21	0.93	0.09	1.42		2.13
CoV	0.082	%Y	0.361	0.057	0.384	0.066	0.409		0.409
min	135.6	35%	159.5	99.8	1.2	1.2	1.4	1.5	2.1
max	173.2		624.0	112.5	4.2	1.5	6.3	1.5	9.4

A.2.3 Four storeys building

Ductility 4:

IDA	$V_{b(Dyn,c)}$ [kN]	CollDir	$V_{b(Dyn,e)}$ [kN]	$V_{b(St,y)}$ [kN]	q_μ	q_d	q	DOF	q_{code}
1	143.7	Y	240.8	103.18	1.7	1.4	2.3	1.5	3.5
2	120.5	X	175.8	110.51	1.5	1.0	1.5	1.5	2.2
3	115.9	X	192.6	110.51	1.7	1.0	1.7	1.5	2.6
4	114.7	X	207.3	110.51	1.8	1.0	1.9	1.5	2.8
5	172.3	X	172.8	110.51	1.0	1.6	1.6	1.5	2.3
6	153.8	X	189.0	110.51	1.2	1.4	1.7	1.5	2.6
7	172.3	X	173.9	110.51	1.0	1.6	1.6	1.5	2.4
8	171.8	X	316.6	110.51	1.8	1.0	1.8	1.5	2.8
9	107.8	X	126.4	105.16	1.2	1.0	1.2	1.5	1.8
10	174.0	X	240.0	110.51	1.4	1.6	2.2	1.5	3.3
11	136.0	X	319.9	110.51	2.4	1.2	2.9	1.5	4.3
12	133.1	Y	249.7	103.18	1.9	1.3	2.4	1.5	3.6
13	143.4	Y	248.1	103.18	1.7	1.4	2.4	1.5	3.6
14	141.9	X	171.2	110.51	1.2	1.3	1.5	1.5	2.3
15	132.8	Y	241.6	103.18	1.8	1.3	2.3	1.5	3.5
16	136.5	Y	217.7	103.18	1.6	1.3	2.1	1.5	3.2
17	117.8	X	177.5	110.51	1.5	1.1	1.6	1.5	2.4
18	174.2	X	241.7	110.51	1.4	1.6	2.2	1.5	3.3
19	115.4	X	211.3	110.51	1.8	1.0	1.9	1.5	2.9
20	107.4	X	168.9	110.51	1.6	1.0	1.5	1.5	2.3
mean	139.27	%X	214.13	108.41	1.6	1.25	1.92	1.50	2.88
sigma	23.57	75%	49.14	3.32	0.34	0.22	0.42		0.63
CoV	0.169	%Y	0.229	0.031	0.216	0.173	0.220		0.220
min	107.4	25%	126.4	103.2	1.0	1.0	1.2	1.5	1.8
max	174.2		319.9	110.5	2.4	1.6	2.9	1.5	4.3

Ductility 6:

IDA	$V_{b(Dyn,c)}$ [kN]	CollDir	$V_{b(Dyn,e)}$ [kN]	$V_{b(St,y)}$ [kN]	q_μ	q_d	q	DOF	q_{code}
1	111.9	X	201.9	101.1	1.8	1.1	2.0	1.5	3.0
2	83.9	Y	146.1	86.9	1.7	1.0	1.7	1.5	2.5
3	125.2	X	291.9	101.1	2.3	1.2	2.9	1.5	4.3
4	105.5	X	181.4	101.1	1.7	1.0	1.8	1.5	2.7
5	115.4	Y	154.2	88.7	1.3	1.3	1.7	1.5	2.6
6	105.5	Y	160.3	88.7	1.5	1.2	1.8	1.5	2.7
7	161.3	X	221.5	101.1	1.4	1.6	2.2	1.5	3.3
8	111.3	X	180.2	101.1	1.6	1.1	1.8	1.5	2.7
9	130.1	Y	188.6	88.7	1.4	1.5	2.1	1.5	3.2
10	162.7	X	274.9	101.1	1.7	1.6	2.7	1.5	4.1
11	150.7	X	377.9	101.1	2.5	1.5	3.7	1.5	5.6
12	110.2	Y	188.0	88.7	1.7	1.2	2.1	1.5	3.2
13	136.1	Y	291.3	88.7	2.1	1.5	3.3	1.5	4.9
14	133.6	X	185.5	101.1	1.4	1.3	1.8	1.5	2.8
15	145.2	Y	297.1	88.7	2.0	1.6	3.3	1.5	5.0
16	133.4	Y	245.8	88.7	1.8	1.5	2.8	1.5	4.2
17	118.1	Y	180.1	88.7	1.5	1.3	2.0	1.5	3.0
18	153.4	X	200.4	101.1	1.3	1.5	2.0	1.5	3.0
19	101.2	X	183.4	101.1	1.8	1.0	1.8	1.5	2.7
20	111.5	Y	228.6	88.7	2.1	1.3	2.6	1.5	3.9
mean	125.30	%X	218.95	94.83	1.7	1.32	2.31	1.50	3.47
sigma	21.55	50%	59.88	6.47	0.33	0.21	0.62		0.92
CoV	0.172	%Y	0.273	0.068	0.191	0.161	0.267		0.267
min	83.9	50%	146.1	86.9	1.3	1.0	1.7	1.5	2.5
max	162.7		377.9	101.1	2.5	1.6	3.7	1.5	5.6

Ductility 8:

IDA	$V_{b(Dyn,c)}$ [kN]	CollDir	$V_{b(Dyn,e)}$ [kN]	$V_{b(St,y)}$ [kN]	q_μ	q_d	q	DOF	q_{code}
1	116.5	Y	262.4	87.5	2.3	1.3	3.0	1.5	4.5
2	105.6	Y	179.5	87.5	1.7	1.2	2.1	1.5	3.1
3	146.4	X	263.6	104.7	1.8	1.4	2.5	1.5	3.8
4	151.7	Y	635.4	87.5	4.2	1.7	7.3	1.5	10.9
5	129.8	Y	227.1	87.5	1.7	1.5	2.6	1.5	3.9
6	118.1	Y	176.2	87.5	1.5	1.4	2.0	1.5	3.0
7	170.5	X	249.9	104.7	1.5	1.6	2.4	1.5	3.6
8	117.6	Y	235.6	87.5	2.0	1.3	2.7	1.5	4.0
9	151.1	Y	292.0	87.5	1.9	1.7	3.3	1.5	5.0
10	166.6	X	350.0	104.7	2.1	1.6	3.3	1.5	5.0
11	169.2	X	542.4	104.7	3.2	1.6	5.2	1.5	7.8
12	130.4	Y	223.1	87.5	1.7	1.5	2.6	1.5	3.8
13	143.3	Y	277.3	87.5	1.9	1.6	3.2	1.5	4.8
14	141.1	X	205.0	104.7	1.5	1.3	2.0	1.5	2.9
15	159.1	X	370.0	104.7	2.3	1.5	3.5	1.5	5.3
16	160.2	X	296.9	104.7	1.9	1.5	2.8	1.5	4.3
17	137.2	X	195.9	104.7	1.4	1.3	1.9	1.5	2.8
18	155.5	X	262.3	104.7	1.7	1.5	2.5	1.5	3.8
19	122.3	X	220.5	104.7	1.8	1.2	2.1	1.5	3.2
20	143.5	X	239.0	104.7	1.7	1.4	2.3	1.5	3.4
mean	141.79	%X	285.20	96.95	2.0	1.46	2.96	1.50	4.44
sigma	19.19	55%	116.22	8.81	0.65	0.16	1.26		1.90
CoV	0.135	%Y	0.407	0.091	0.329	0.110	0.427		0.427
min	105.6	45%	176.2	87.5	1.4	1.2	1.9	1.5	2.8
max	170.5		635.4	104.7	4.2	1.7	7.3	1.5	10.9

PART TWO

–

THE VIBRATION COMFORT ASSESSMENT OF TIMBER JOISTED FLOORS VIA SMARTPHONE IN-SITU TESTS

II-1 INTRODUCTION

Walking, running, jumping… everyday human activities can represent the most severe excitation source for flexible floor. Ongoing study among researchers, in fact, aim to evaluate the dynamic behaviour of these structures under the effects of human activity, because these actions are usually considered static loads in structural design [1][2].

To date, there are several studies in the literature that experimentally and numerically analyse the problem of vibrations in timber and composite floors [3][4][5][6][7]. Experimental analyses, in practice, are typically carried out with the support of commercial devices and professional instruments. Although the cost, size/weight and accuracy of these instruments have been significantly improved over time, smartphones can represent a valid alternative, thanks to their built-in high-performance sensors (e.g. accelerometers, GPS, …). Some applications and examples of smartphone-based investigations are already present in the literature for the Structural Health Monitoring SHM of bridges or seismic analysis.

In [8], a vision-based method using smartphone camera is developed and experimentally tested on a bridge model, recording acceleration, displacement and angle, and, then, its feasibility and practicality is validated through cable model test. Results showed good agreement between smartphone and reference sensors. However, tests on full-scale bridge is needed to verify the actual possibility of implementing smartphone use on SHM. Moreover, higher modes cannot be detected by the smartphone.

In [9], the authors assembled GPS receivers, accelerometers, and smartphones, integrating a smart sensor for the SHM of a full-scale bridge with vibrational problems, demonstrating the ability of such smart sensor to detect an abnormal condition of the structure in the vertical direction.

Furthermore, smartphones were used in [10] to evaluate seismic parameters. The main goal was to have a large quantity of data to respond in case of emergency during earthquakes, in order to define shake map based on low-quality spread records. Test were performed on shake-table, demonstrating a slightly overestimation of the Arias Intensity and the suitability of the method for moderate and strong events.

Smartphone sensors were also used to evaluate the dynamic performance of long-span concrete floors in [11], showing good performance for fast preliminary in-situ test but highlighting problems like unstable sampling of smartphone sensors.

Moreover, in [12], smartphone sensors were used to analyse the dynamic performance of a joisted timber floor with OSB top panelling. The authors found that smartphone devices are useful to simplifying the collection and interpretation of vibrational data. However, caution is advised, since limitation to only light-impact loads was found. In addition, data was analysed by means of a software application that automatically gave in output parameters and frequency, thus without transparency on the algorithms used.

In this work, the reliability of smartphones for the comfort assessment of timber floors through experimental investigations is studied, and their possible use for simple but robust and fast in-situ tests is addressed. To this aim, a full-scale timber floor was assembled and dynamically tested under human induced vibration. The main goal was to estimate corrective coefficient to be applied, in order to minimize the difference between smartphone and professional accelerometers records. Furthermore, a test protocol for in-situ tests is proposed, based on the minimum number of walks obtained by the laboratory tests. The protocol was then applied to three case studies.

1.1 Overview on timber floors

In order to understand the dynamic response of timber floor, a first step may focus on construction typologies. Historical and modern floors have different characteristics, both in terms of material and structural conception. Herein, an overview of wooden floor is presented, focusing on used building techniques.

1.1.1 Historical Timber Floors

One-way joists floors

In one-way joists floors, a single series of parallel timber beams is arranged in the direction of the smallest plan dimension, with spans typically of 3-4 meters [13](Fig. 1). The assembly of this kind of floors do not require large wooden elements, generally only the joists, or connections to join different beams. However, it is worth noticing that this type of floor transfers loads only to two of the four walls of the room.

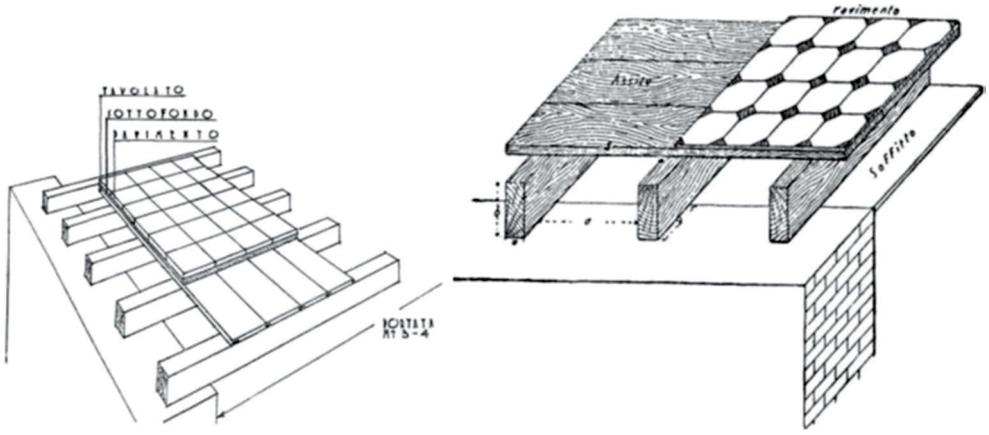

Fig. 1 - One-way historical timber joisted floor (left photo from [14], right photo from [15])

Main beams and secondary joists

This typology of floors is made of two rows of beams (Fig. 2). Main beams are typically oriented to cover the minimum span, spaced 2-4 m.

Secondary joists are placed orthogonally to the main beams. This solution can distribute the load to all the walls, but high concentration of stress at the supports of the main beam occurs.

The presence of main beams divides the floor into multiple spans, and the joists could usually be single or double span long.

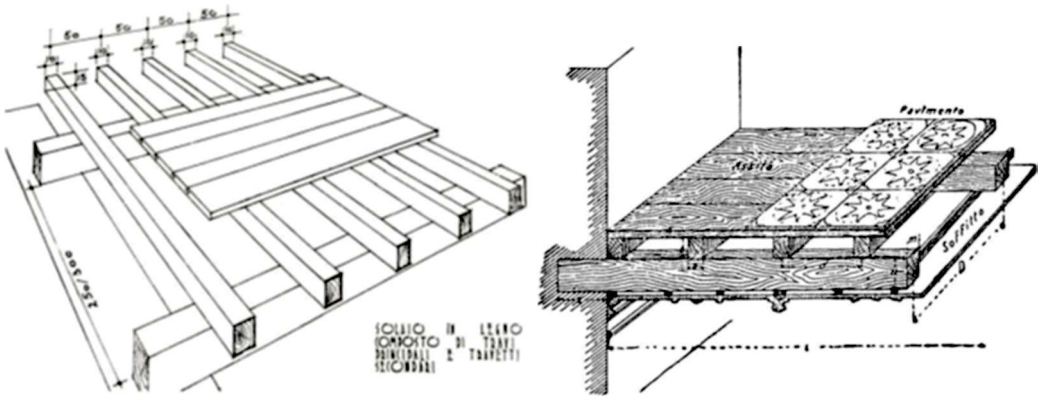

Fig. 2 – Main beams/secondary joist historical timber floors (left photo from [15], right photo from [14])

The necessity of overlapping secondary and principal beam could lead to very thick floors. However, several assembly techniques were developed, to overcome this issue (Fig. 3).

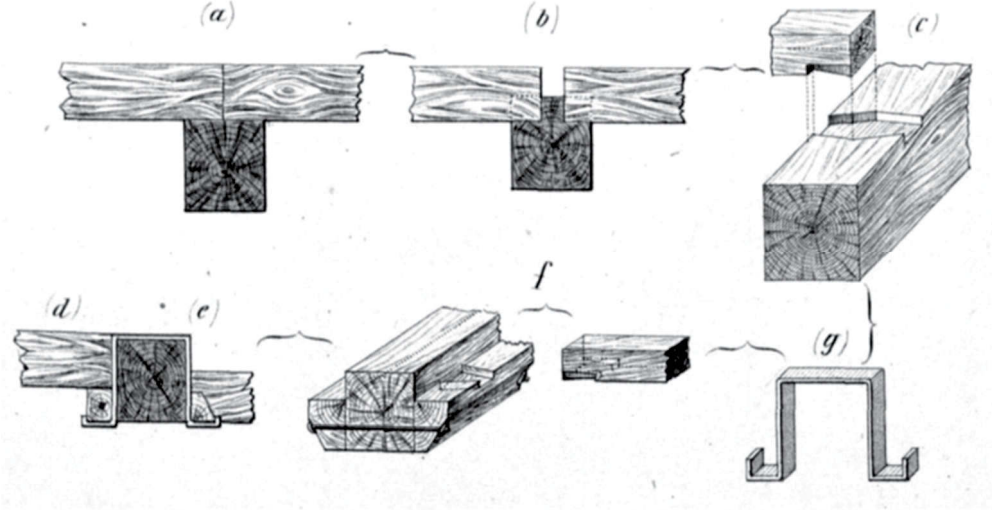

Fig. 3 – Overlapping methods for secondary joists (photo from [16]).

"Cassettoni" floors

In "cassettoni" floors, the secondary beams are inserted into the thickness of the primary joists system (Fig. 4). Both elements have the same section geometry. Moreover, the spacing between principal and secondary joists is the same, leading to a square-shaped division. However, sometimes the secondary beam system is made with boxed planks only, to visually simulate the main beam system. Furthermore, if adequately connected the secondary joists could lead to a bidirectional floor behaviour, increasing the overall resistance of the floor.

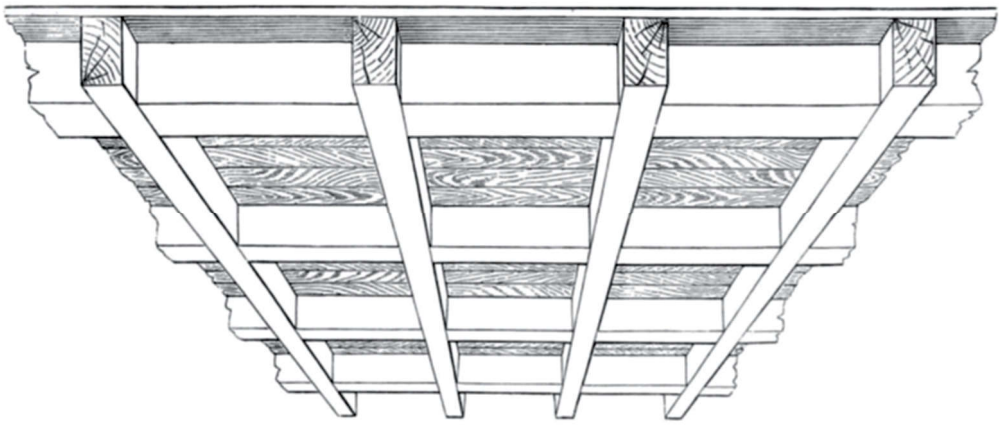

Fig. 4 – "Cassettoni" historical floor (photo from [17]).

Remarks on top plank layer

Wooden planks are a commonly used solution for the upper layer of timber floors. Boards has several advantages like lightness and strength, and they can easily be connected to the beam. Typically, small nails were used to connect plank and beam, or also wooden pins. The planks are continue on multiple supports; 50 to 70 cm spans are usually present between joists. Moreover, planks can show different width, influencing the disposition of joints (aligned in the case of different width, not aligned if the width is constant, see Fig. 5).

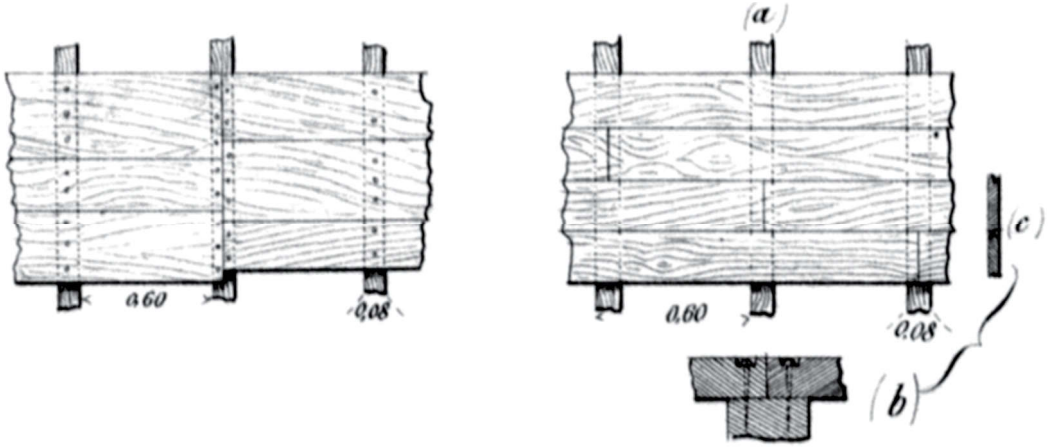

Fig. 5 – Plank alignment to joists (photo from [16]).

1.1.2 Modern timber floors

Joisted floors

Nowadays, timber is still widely used structural material for light-frame floors, obtained as parallel joists members with a mechanically semi-rigidly connected subfloor (e.g. wooden planks, OSB)(Fig. 6). However, a high variety of joists is present on the market, enlarging the possibilities beyond the typical solid/glulam timber rectangular beam. Available joists include sawn lumber, engineered wood products (EWPs), wood I-joists and open-web joists with wood flanges. Since their slenderness, the serviceability typically governs the design phase.

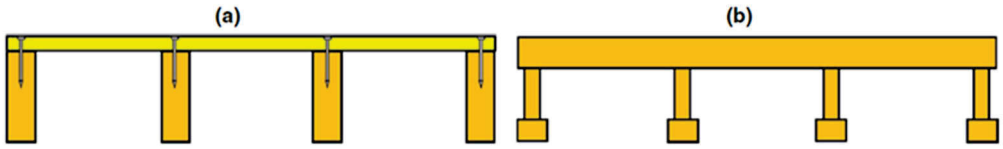

Fig. 6 – Modern joisted floors. (a) beams and topping nailed/screwed to the beams. (b) I-joists floor (image adapted from [18]).

Monolithic Slab floors

Monolithic slab floors are typically made of Cross Laminated Timber CLT or Glued Laminated Timber GLT.

CLT consists of layers (typically three, five or seven) of solid sawn lumber or structural composite lumber (SCL), oriented orthogonally one another and glued to form structural panels. CLT floors do not usually have joists, and are monolithic slab floors obtained of CLT panels jointed together (Fig. 7). Since the joint stiffness is relatively low if compared to the bending stiffness of the panel, the floor exhibits a one-way behaviour, governed by the stiffness of the panel in its major strength direction. Moreover, a CLT floors is heavier if compared to joisted floor with same span and performance, thus showing a lower natural frequency and damping. In addition, panels can be produced to long length, and multi-span continuous floor systems with long CLT panels are common [19].

Fig. 7 – CLT flooring (from [20]).

Moreover, also glue-laminated timber GLT can be used for flooring (Fig. 8). It is created by combining solid sawn lumber members layered parallel on their wide faces, with adhesive between layers. Typically, GLT panel are 60/120 cm wide and up to 1800 cm long [19].

Fig. 8 – GLT flooring (from [20]).

Composite timber-concrete floors

A timber-concrete composite (TCC) floor consists of a bottom timber layer and a top concrete layer, joined together by shear connectors (Fig. 9). In this way, compression forces from bending are carried by the concrete, while tension is resisted by timber. This construction technique can also be used to strengthen and stiffen existing timber floors or new constructions, especially in multi-storey buildings.

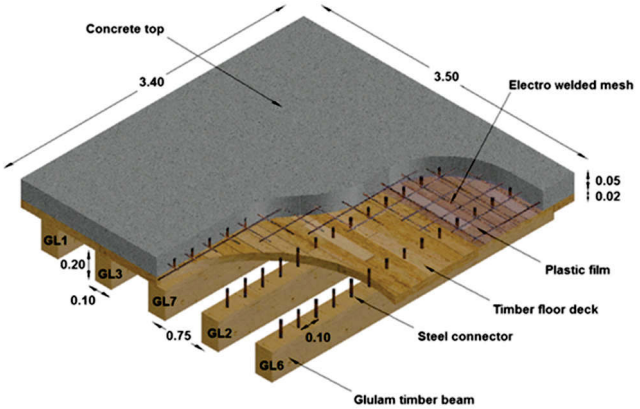

Fig. 9 – Composite timber-concrete floor system (from [21]).

The top concrete layer is usually a reinforced concrete slab. The timber part can be solid wood lumber, glulam, structural composite lumber (SCL), cross-laminated timber (CLT) or made of other engineered wood products [22]. The connection between the two layers can be obtained by means of discrete fasteners (e.g., nails, screws, or notches) or shear connectors transferring the load to a larger surface (e.g., embedded plates, glue). Moreover, a combination of different shear connectors is also possible.

1.2 Introduction to vibration

Vibration in structures (buildings, floors, bridges, etc.) can be caused by different external sources, from road traffic to human activities like walking, running or jumping. Typically, the vibration source reflects on components that can stimulate human senses such as hearing or seeing. The vibration of objects on shelves can be heard and seen, the vibration of the floor can be both heard and felt. These feelings, together with experience, expectation and attitude to the source lead to different stress levels for the occupants, that can also bring to fear linked to the building stability [23]. See Fig. 10.

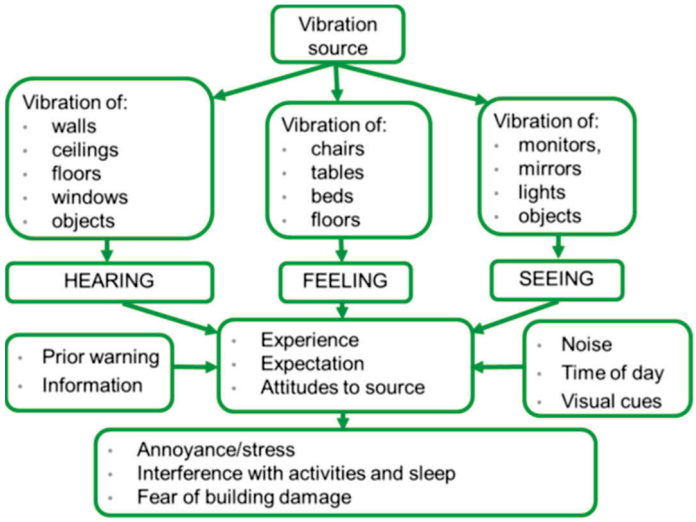

Fig. 10 – Vibration effect on humans (from [23])

Vibration sources can be continuous, impulsive or intermittent. Continuous vibrations can be associated to machinery, steady road traffic or construction activities, and can have a constant or a variable magnitude during time.

Impulsive vibration is a rapid increase in acceleration to a peak vale, followed by a series of vibration cycles with a damped decay. Typically, the duration is less than two seconds. Examples of impulsive excitation are the drop of heavy loads or blasts.

On the other hand, intermittent vibrations can be defined as interrupted periods of continuous or impulsive vibrations. Furthermore, continuous vibrations with high-variability intensity can also be considered intermittent. Jack hammers, trains, but also human activities like walking and running are typical intermittent sources [24].

When talking about timber residential or office floor, the source of vibration is generally the walking of people. However, predicting the human response to the vibration induced by walking is complicated since objective and subjective aspects are involved. Furthermore, inter- or intra-subject variability has to be taken into account, since the perception of comfort varies both among different people (inter-) and inside the same person (intra-), because different sensibilities can be developed [25].

Objective parameters of the vibration are frequency, duration and magnitude. Moreover, the direction of motion can be included.

All these parameters contribute to the vibration assessment of a structure, thus including comfort, performance and health aspects linked to human comments.

To assess the vibration performance of a structure (i.e. a timber floor, in this case) laboratory or in-situ test can be performed.

Laboratory test are useful for the systematic study of each variable involved, since the simulation of controlled real vibration environments can be performed.

In [7] the authors tested a 9 m span joisted floor, in order to elaborate prediction model under human induced vibrations. Three load models for walking loads were applied to a FEM validated model, confirming the great influence of the selected load representation.

Furthermore, a probabilistic approach to vibration design is proposed, to overcome limitation of current design practice.

In [26] a 6 m x 6 m lightweight timber floor was built in laboratory, and tested under human induced vibration. Tests and checks showed that simplified methods are too rigid, giving large inconsistencies between calculated and measured comfort levels.

Experimental tests are also performed on composite hybrid floor structures. In [27] a CLT and a hybrid CLT/Steel long span floors were tested in laboratory, in order to validate a FEM model, successively used to investigate the suitability of hybrid CLT floors for long span configuration. Random walking model was used to simulate the human induced loads on the floor system, highlighting the great influence of damping rather than bending stiffness on the vibration performance.

Moreover, in [28] the vibrational performance of a composite timber-lightweight concrete floors was investigated. Three composite beams were built in laboratory and tested to identify their frequencies and to evaluate an analytical formulation to estimate the first three vibration periods.

On the other hand, field studies are useful for comparing evaluation methods and to assess the absolute acceptability and limits linked to comfort perception.

In [29], CLT and light timber frame floors belonging to five storeys multifamily apartments buildings were numerically, analytically and in-situ tested. From the study, the limitation of analytical methods emerges, since their validity is limited to certain types of floors, which were tested to calibrate the equations. Numerical approaches are reliable, since dynamic properties and human induced loads are considered, but the in-situ testing provides the most appropriate assessment of the floor performance. It is worth noticing, however, that the tests are time consuming and have costs. Moreover, they can be performed only after the building phase finished, thus only to assess the performance and not to design.

Moreover, vibration test can also be carried out on entire buildings, to assess their performance or to evaluate their dynamic properties.

In [30], a 18 storeys mass timber-concrete building was monitored, to assess its dynamic properties by means of in-situ tests. A FEM model

was also developed, and the results compared. Given the number of storeys, a not-negligible influence of the soil interaction and the gravity load-resisting system was found. Moreover, the stiffness proportional damping overestimated the higher modes, causing discrepancies between model and real building.

On the other hand, [31] investigated the influence of the Crest Factor (i.e. the ratio between the maximum and the average acceleration), on the perception of traffic vibration. A five-storey reinforced frame building was monitored for 24 hours, since occupants complained the vibration induced by the traffic on the road located at 1.5 m from the structure.

1.3 Dynamic response of timber floors

The dynamic response of a timber floor, but more generally of every kind of floor, is governed by the dynamic characteristics of the floor itself and by the acting loads. The dynamic characteristics are the vibration frequencies, the modal mass and the damping. On the other hand, human induced loads like walking, running or jumping are the "acting loads" on the floor systems. For the analyses of human induced loads, please see the next chapter.

Herein, the dynamic properties of floor are discussed. First, a quick recall on the dynamic theory of continuous beams is reported (Fig. 11). From the continuous systems dynamic theory, the motion equation of the bent beam is:

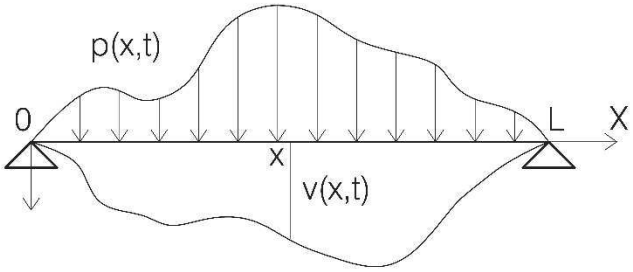

Fig. 11 – Simply supported beam subjected to load p and displacement v.

$$(EJv_{xx})_{xx} + \rho v_{tt} = p \tag{1}$$

Where:

- v(x,t) is the unknown displacement, depending on space (x) and time (t).
- EJ(x) is the flexural stiffness, depending on the position x on the beam.
- ϱ(x) is the mass density per unit length
- p(x,t) is the applied vertical load, depending both on space and time.

Subscript xx e tt are the second derivative with respect to space and time respectively. To study free motion, let impose p(x,t)=0. Moreover, a separate variable solution can be considered, writing the unknown function as the product of two function depending on space and time.

$$v(x,t) = \varphi(x) \cdot Y(t) \tag{2}$$

Substituting (2) in (1), equation 3 can be obtained, valid for every t>0 and x ∈ (0,L), where L is the length of the beam:

$$\frac{[EJ(x) \cdot \varphi(x)_{xx}]_{xx}}{\rho(x)\varphi(x)} = -\frac{Y(t)_{tt}}{Y(t)} \tag{3}$$

Since x and t are independent variables, it is necessary to fulfil both the following equations:

$$\begin{cases} \dfrac{[EJ(x) \cdot \varphi(x)_{xx}]_{xx}}{\rho(x)\varphi(x)} = \omega^2 \quad x \in (0,L) \\ -\dfrac{Y(t)_{tt}}{Y(t)} = \omega^2 \quad t > 0 \end{cases} \tag{4}$$

If EJ and ϱ are assumed constant along x, equation 4 can be rewritten as:

$$\begin{cases} \varphi(x)_{xxxx} - \lambda^4 \varphi(x) = 0,\ \lambda^4 = \omega^2 \dfrac{\rho}{EJ} \\ Y(t)_{tt} + \omega^2 Y(t) = 0 \end{cases} \tag{5}$$

Let the solution assume the form $\varphi(x) = A_1 \sin(\lambda x) + A_2 \cos(\lambda x) + A_3 sh(\lambda x) + A_4 ch(\lambda x)$. Let impose the boundary conditions of a simply supported beam:

$$\begin{cases} v(0,t) = 0 \\ v(L,t) = 0 \\ v_{xx}(0,t) = 0 \\ v_{xx}(L,t) = 0 \end{cases} \tag{6}$$

Then, equation 7 can be obtained:

$$\varphi(x) = A_1 sin(\lambda x) \tag{7}$$

Searching for non-zero solutions, $\lambda L = n\pi$ can be found, which may be rewritten as:

$$\lambda = \frac{n\pi}{L} \quad with\ n \geq 1 \tag{8}$$

Finally, using both equation 7 and 8, the formula for the radian frequency ω_n:

$$\omega_n = \left(\frac{n\pi}{L}\right)^2 \sqrt{\frac{EJ}{\rho}} \tag{9}$$

Since n is an integer multiplier, the deformed shape and the frequency for each mode can be evaluated, together with modal nodes (Table 1 and Fig. 12).

Table 1 – Vibration modes shape and nodes for a uniform simply supported beam.

n = 1	nodes
$\sin\left(\frac{\pi}{l}x\right) = 0$	$x = 0$ $x = L$
n = 2	
$\sin\left(\frac{2\pi}{l}x\right) = 0$	$x = 0$ $x = \frac{L}{2}$ $x = L$
n = 3	
$\sin\left(\frac{3\pi}{l}x\right) = 0$	$x = 0$ $x = \frac{L}{3}$ $x = \frac{2L}{3}$ $x = L$

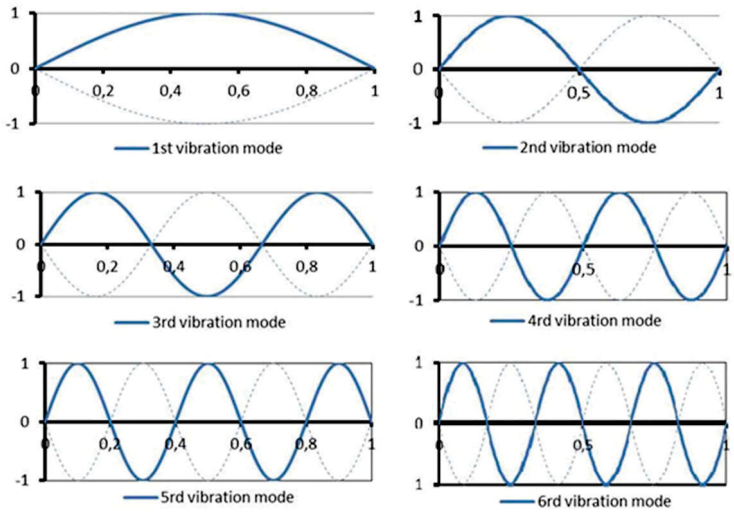

Fig. 12 – First six vibration modes for a simply supported beam.

In the following paragraph the parameters affecting the dynamic response of the floor have been discussed. In particular, frequency, mass and damping are analysed, since they represent the most critical values to be estimated during the structural and the comfort assessment of timber floors.

1.3.1 Frequency

Known the radian frequency ω_n, the frequency of the nth mode can be obtained dividing by 2π:

$$f_n = \frac{n^2\pi}{2l^2}\sqrt{\frac{EJ}{\rho}} \tag{10}$$

Moreover, Equation 10 can be rewritten, introducing a parameter k_n, depending on the boundary conditions.

$$f_n = \frac{k_n}{2\pi}\sqrt{\frac{EJ}{\rho l^4}} \tag{11}$$

Where k_n is a constant representing the support condition for the nth mode of vibration. Table 2 reports values for different boundary conditions [32]:

Table 2 – Coefficient k_n for different boundary conditions.

Support conditions	k_n for mode n		
	n=1	n=2	n=3
Pinned/pinned	π^2	$4\pi^2$	$9\pi^2$
Clamped both ends	22.4	61.7	121
Clamped/free (cantilever)	3.52	22.0	61.7

Moreover, the first fundamental frequency can also be linked to the midspan deflection of the beam. Let consider a simply supported beam, with span L and flexural stiffness EJ. The midspan deflection caused by the dead load q = mg is:

$$w = \frac{5mgl^4}{384EJ} \tag{12}$$

Substituting equation 12 into equation 10 for n=1, the fundamental frequency can be expressed as:

$$f_1 = \frac{18}{\sqrt{w}} \ (w \ in \ mm) \tag{13}$$

Equation 13 can be used to estimate the fundamental frequency of floors.

Modes are typically arranged according to their energy content. The first mode (n = 1) requires the lowest energy content to be excited.

Walking frequency are generally set between 1 Hz and 2.5 Hz and, when the natural frequency of a mode and the step frequency are identical, resonance phenomena can lead to very large response amplitudes. Nonetheless, resonance can also occur for higher modes, i.e., where a multiple of the step frequency coincides with the floor frequency.

In addition to regular walking, excitation from single impacts, such as heel drop, can occur, leading to transient vibrations.

Generally, regular walk is relevant for natural frequency lower than 8 Hz, while impulsive loads like heel drop are relevant for higher frequency. The threshold frequency is defined "cut-off" frequency, and divides the response of the floor into two types: Resonant or Transient (Fig. 13).

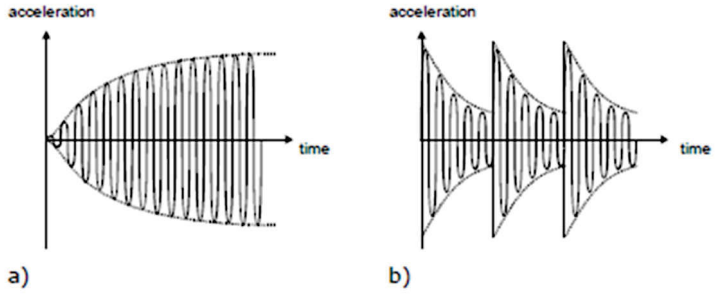

Fig. 13 – Resonant (a) and Transient (b) response of a floor.

Most of the current codes use the cut-off frequency for the vibration check of floors under human walk. Basing only on the first four harmonics composing the footstep, i.e. where the most energy is allocated [33][34], the standards and guidelines consider "resonant response" the amplification occurring when the vibration floor modes coincide with the first four harmonics of the step. Thus, the vibration induced by a single step does not decay before the next one (Fig. 13a). On the other hand, a "transient response" occurs, and the vibration from each step decays before the next footstep arrives (Fig. 13b). This hypothesis was used by [35][32][36], but, even if the cut-off frequency is a common concept among guidelines, the value of this frequency is not unique (Table 3).

Table 3 – Definition of low-/high-frequency timber floor according to standard and guidelines.

Standard/Guideline	Low-frequency	High-Frequency
ISO 10137 [37]	8 Hz < f < 10 Hz	f > 10 Hz
SCI-P354 [32]	f < 10 Hz	f > 10 Hz
CCIP-016 [36]	f < 10.5 Hz	f > 10.5 Hz
EC5 [38]	f < 8 Hz	f > 8 Hz
AISC DG11 [35]	f < 9 Hz	f > 9 Hz
Ohlsson [39]	f < 8 Hz	f > 8 Hz

Examples of cut-off frequencies are proposed by various authors and standards, e.g. CCIP-016 [36] considers a cut-off frequency of 10.5

Hz. SCI P354 [32] proposes a cut-off frequency depending on the floor type, (8 Hz for residential floor, 10 Hz for commercial floors).

Moreover, further research has shown that a resonant amplification can be caused also by energy of harmonics above the fourth, thus highlighting a possible underestimation of the floor response with fundamental frequency up to 15 Hz using the current guidelines [40][41].

Another study from [42] has shown that the classification and the response prediction of floor with frequency borderline to the cut-off frequency is mostly inaccurate.

Furthermore, floors tested on-site had high-frequency modes excited by impulses, even if they were classified as low-frequency according to the cut-off. A solution was proposed, using a response spectrum approach for floor between 1 and 20 Hz [43]. Other possible solutions to the cut-off problem were proposed by [44] (increasing the cut off to 14 Hz) or [42] (using a probabilistic force model combining the approaches for low and high frequency floors). Finally, a single footfall trace model could be used, like the Chen probabilistic model [45] described in Section 2.2.1 of the thesis.

1.3.2 Modal mass

The modal mass of a system is a measure of how much mass is involved in each mode shape, and hence how much kinetic energy there is in the system. Moreover, the modal mass of each mode gives a direct indication on the contribution of the mode on the overall response of the system to an equal modal force. A large modal mass suggests that a lot of energy is required to excite the mode and, thus, it has a slight significance in the response.

The mass, in fact, has a direct influence on the vibration response of the floor. More in detail, the ratio between the body mass of the pedestrian and the mass of the floor influences the amplitude of the vibration [46].

1.3.3 Damping

The damping dissipates energy during the motion of the structure, allowing them to convert kinetic energy into heat and thereby reduce

amplitudes of forced or free dynamic motions. Damping, in fact, causes the vibration of a structure to reduce and stop. The amount of damping required to return the system to its equilibrium position without oscillation in the minimum time is called "critical damping". Generally, two major sources of dissipation can be considered, expressed as a percentage of the critical damping. A "structural damping", caused by internal friction (between elements, connections and supports). A "non-structural damping" component, on the other hand, is caused by finishing and furniture. The addition of dead weight (e.g. installation of non-structural elements) can have a substantial effect on this damping component [47][24]. Moreover, also human occupation sets a damping component, but it is usually ignored, since a high density of occupants is necessary to guarantee the damping effect. However, this component is sometimes considered in CLT handbooks, since human bodies possess significant ability to absorb kinetic energy from vibrating systems. Furthermore, [48] analysed a long-span glulam floor, highlighting the decisive role of the "non-structural" damping in the comfort verification of floors.

However, the damping associated to a structure is difficult to quantify, since all the hidden present sources and the high dispersion of values reported in the literature for historical and modern floors[49][50]. For light frame floor, values of damping varies from 1% proposed by EC5 [38] and [51] to 2.5%. Table 4 summarize the damping ratio suggested by current standard and guidelines.

Damping ratios can be estimate by experimental tests. Nonetheless, laboratory and onsite test programmes are influenced by the test protocol and the postprocessing algorithms used to elaborate the data and the modal parameters. In situ test, in fact, has shown significantly higher values of damping with respect to laboratory test, reaching values up to 6% for timber [52][53][54]. Such differences make it difficult to assess the reliability of older reports and studies, where people walking or dropping the heel on the floors were used to assess the modal parameters. Thus, damping ratio in publication tend to be lower bound values for particular types of structures [55].

Table 4 – Damping ratios for timber floors suggested by different standard and guidelines.

Standard/Guideline	Damping ratios
Eurocode 5 [38]	1%
UK NA Eurocode 5 [56]	2%
ISO 10137 [37]	1% to 5.5%
HIVOSS [46]	1%
Hamm et al. [57]	1%

1.4 Final remarks on the dynamic response

Frequency, modal mass and damping ratio are the primary parameter influencing the dynamic response of a floor. Nonetheless, boundary conditions, connections and non-structural elements can largely complicate the definition of these values.

The "simply supported condition" is typically conservative, since an ideal restraint is hardly found in real buildings. The modelled hinge, in fact, often has a rotational stiffness that helps to stiffen the system and, therefore, to improve the response to vibrations. In [58], a literature review of connection between horizontal diaphragm and walls is presented. Even if the mentioned paper focuses on the seismic design, it provides an overview of typical used systems and laboratory tests, highlighting a lack of information about the mechanical behaviour of these supports both in the literature and in the codes. For modern mass floors (CLT), a proposal for evaluating the stiffness of the panel to wall connection can be found in [59][60]. End-fixity parameters were found, to represent the partial rotational stiffness of the connection, showing differences between the rigidity to be assign for the calculation of deflection and frequency.

Moreover, the presence of a layer of wooden boards can influence the dynamic response of the floor, considering the thickness of the planks and the stiffness of the connection between the element. In the report [61], a parametric analysis was performed varying the section of the wooden boards and the number of joists. From the results, increasing

floorboards thickness and decreasing the joist span can help to satisfy the requirement of vibration comfort.

When talking about floors with principal and secondary beams, also the connection between these two elements can influence the global stiffness of the floor. In [62], experimental test on secondary joists were performed, in order to estimate the flexural rigidity of the connection. The authors found only a weak influence of the connection on the first frequency on the floor.

11-2 HUMAN INDUCED VIBRATIONS

The dynamic response of a floors depends both on the geometrical/mechanical characteristics of the floor and the human induced excitation. A typical distinction for human induced loading can be performed, considering two categories: walking and aerobic loading.

Walking in different patterns and frequencies is a comfort issue, that leads to serviceability criteria to be satisfied. On the other hand, aerobic and rhythmic involves groups or crowd practicing physical activity such as jumping, requiring both a serviceability and a strength verification, especially if resonance occurs [63].

The human induced loading pattern depends on a large number of parameters, leading to a quite complex load definition. The load transmitted by a single step depends on biomechanics information [54,55] on the pedestrian, and can be considered a temporal-spatial phenomenon, characterised by [64][65][66].

Temporal parameters: step frequency, speed, pace time, stance time, swing time, single and double support and similar.

Spatial parameters: step length, step width, foot angle, attack angle, end-of-step, angle and trunk orientation.

Furthermore, pedestrian characteristics are also necessary, in order to investigate and reproduce the walking pattern, such as height, weight or height of the centre of mass.

It is worth noticing that none of the aforementioned parameters has been recognised as "critical", since there is no single parameter which can provide, alone, a complete characterisation of the walking process [33].

One of the main issues regarding the investigation is the laboratory itself. Imposing a "metronome" step or walking on narrow supports leads to "artificial" outcomes, not aligned to the natural walking patterns of pedestrian. Furthermore, people around the world is different, and so are the steps, showing different spatial parameters [67][68].

Differences between real walking and mathematical model are mostly due to intra- and inter-subject variabilities and human-structure interactions [69].

Intra- and inter-subject variabilities take into account the differences that occur in the walking pattern for the same pedestrian (intra-) and among different people (inter-). Intra-subject variability considers variations that happens for the same person during the walk, such as changes in the frequency, in the step length or load. On the other hand, inter-subject variability takes into account variation in speed and frequencies between different individuals, and can be caused by age, gender, location, etc. [25][40][70][71]. Nonetheless, parameter such as frequency, walker weight, force level and so on are crucial to define a proper walk model, but only suggestions are present in the literature to select those parameters [72].

The last aspect, human-structure interaction, is mainly important in structures like bridges or long-span floors, limited effect can be noted on standard span floors [73][74].

2.1 Types of actions

In the following paragraph, an overview on the types of actions involving the pedestrian are described. Walking and running are taken into account, defined not only by frequency (Fig. 14) but also by the shape of the force transmitted to the support. Furthermore, jumping was also herein discussed.

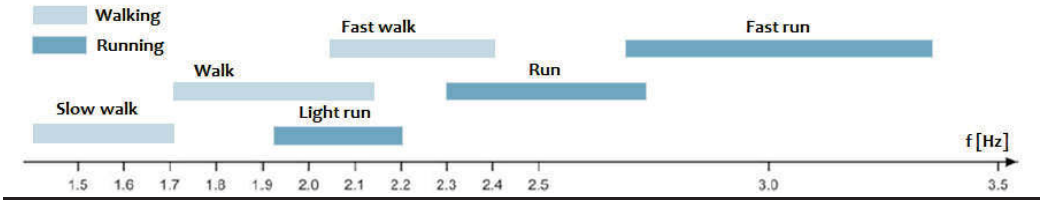

Fig. 14 – Step frequency ranges for walking and running. Adapted from [75].

2.1.1 Walking

Walking is characterised by the continuous contact between the foot and the floor. Typically, a step frequency between 1.0-2.5 Hz can be considered. However, the limit of the range corresponds to a very slow and a very fast walk, generally not representing an actual pedestrian behaviour.

In normal walking, the vertical component of the single step has a saddle (or butterfly) shape (Fig. 15). The first peak corresponds to the impact of the heel on the support, while the second one to the thrust of the sole of the foot. This shape tends to reduce to a semi-sinusoid when running, losing the saddle form. Moreover, the superposition of each steps has to be considered, and there is an overlap time where the two steps contribution sum.

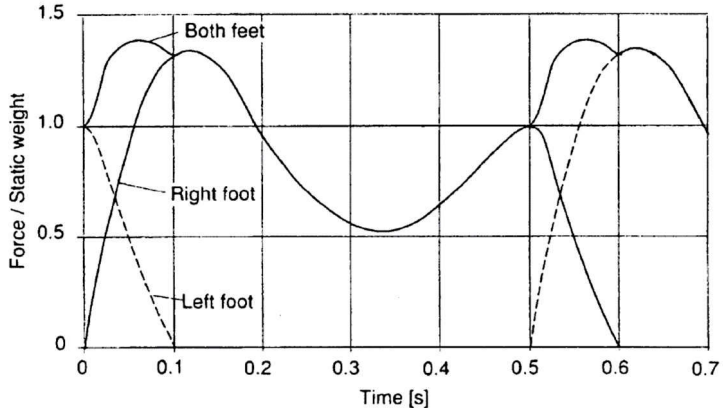

Fig. 15 – Force resulting from walking at 2 Hz (from [76])

The horizontal and longitudinal component of the pedestrian load are less intense and cannot be neglected in bridge structures, where walking can be rapidly disturbed, leading to keeping close to handrails or to a feeling of insecurity. However, typical residential and office floor are restrained, and no problems occur due to the non-vertical components.

2.1.2 Running

With respect to the walking, running is characterised by discontinuous contact with the ground. The components of the two steps do not overlap, see Fig. 16.

Typically, running has step frequencies between 1.9 Hz and 3.5 Hz. However, running barely occurs on residential or office floors, and is more important for vibration checks in footbridges.

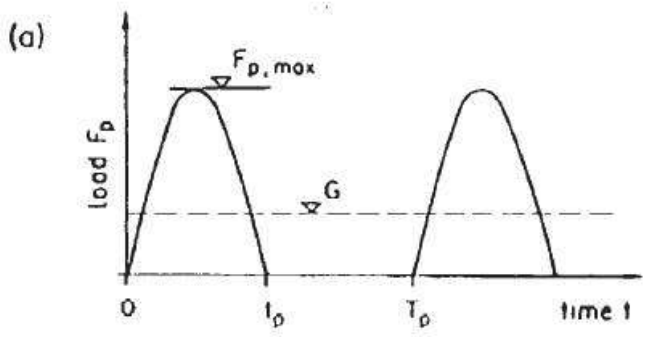

Fig. 16 – Typical running load vs time (from [77]).

2.1.3 Jumping

Jumping can be considered an impulsive action. Jumps are similar to the running-induced loads but have higher amplitudes. Jumping is not a normal type of activity on floors, but for gymnastic halls it should be taken into account. In Fig. 17 an example of recorded jumps is presented [78].

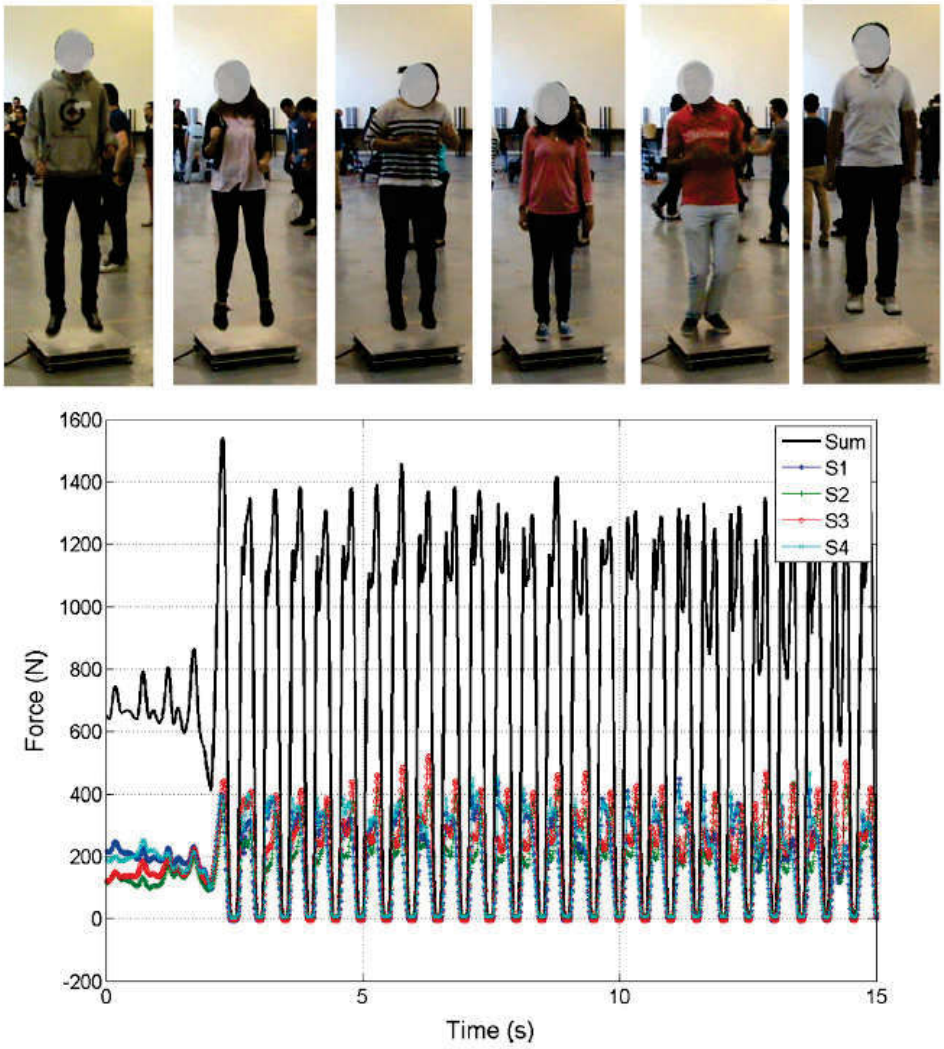

Fig. 17 – Jumping test and recorded data from [78].

Several models are available in the literature to reproduce the load induced by a jump. In Fig. 18, Fig. 19 and Fig. 20, three model are proposed according to [32][78][79].

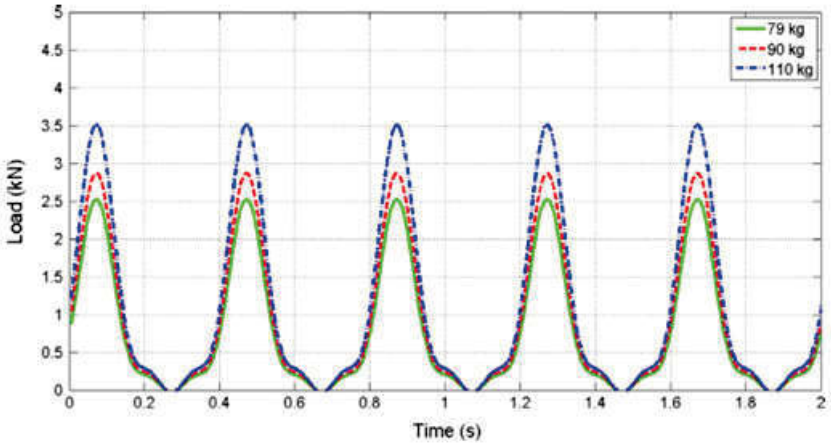

Fig. 18 – Dynamic forces of three pedestrian at 2.5 Hz according to SCI P354 [32].

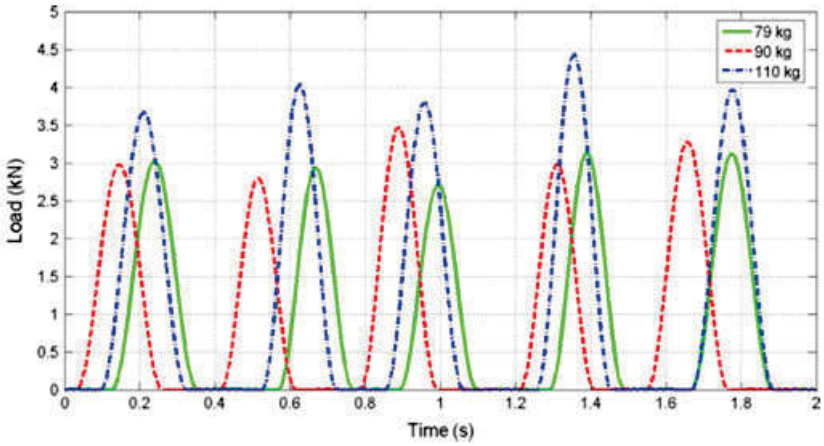

Fig. 19 – Dynamic forces of three pedestrian at 2.5 Hz according to [79].

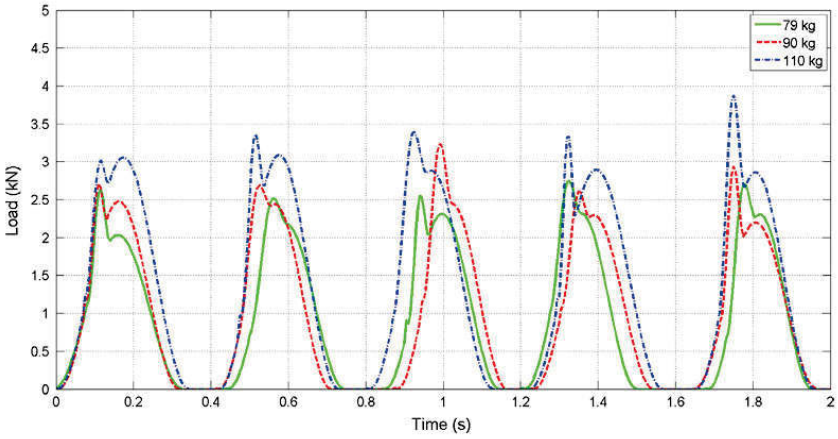

Fig. 20 – Dynamic forces of three pedestrian at 2.5 Hz according to [78].

Residential floor typically does not have problems with crowds or group of people. For example, to consider aerobics and similar activities, [32] suggests how to take into account more people jumping or doing physical activity. However, this isn't the case for residential/office floors. And even in the case of gym floors, typically it is not the floor where the activity is performed that has serviceability issues, but the adjacent rooms, which can be affected by the induced vibrations.

2.2 Pedestrian Load Modelling

Starting from the knowledge of the different types of pedestrian loads, such as walking and running, an approach to model the forces is necessary, in order to carry out Finite Element simulations. In the next paragraphs, focus was made on walking load modelling, since it is the one which will be used in the analysis of the joisted timber floors.

Two approaches can be followed for the FE modelling of the walk: deterministic or probabilistic.

2.2.1 Deterministic approaches

The deterministic approach assumes that all the characteristics of the walk are fixed. Thus, frequency, step length, shape, overlap and dynamic amplification are set in a deterministic way. Different types of modelling deterministic forces are available in the literature: Fourie series, moving load or step-by-step forces.

Any periodic function F(t) with period T can be represented by a Fourier series as given by equation 14. In 1972, [33] were the first proposing the Fourier series to develop a walking force model, implemented then by other authors [80][76][41][63].

In the Bachmann model [76], the walk is represented by a force varying in time F(t), seen as a constant part and a Fourier sum of sine terms:

$$F(t) = G_0 + G_1 \sin 2\pi f_m t + \sum_{i=2}^{n} G_i \sin(2\pi i f_m t - \varphi_i) \qquad (14)$$

Where:

- G_0: pedestrian weight;
- G_i: i-th harmonic amplitude;
- f_m: walking frequency;
- φ_i: phase angle of the i-th harmonic with respect to the first;
- n: number of considered harmonic.

According to [76][77], three harmonics are enough to describe the walking sequence, see Fig. 21. G_0 can be assumed 700 N, whereas $G_1=0.4G_0$ and $G_2=G_3=0.1G_0$. Phase angle for harmonic 2 and 3 can be taken equal to $\pi/2$.

However, other studies investigated different number of harmonics to evaluate deterministic values of dynamic load factors, such as [41][34][76]. It is worth noticing that all the variabilities in the walking process are lost in a Fourier deterministic simplification [81].

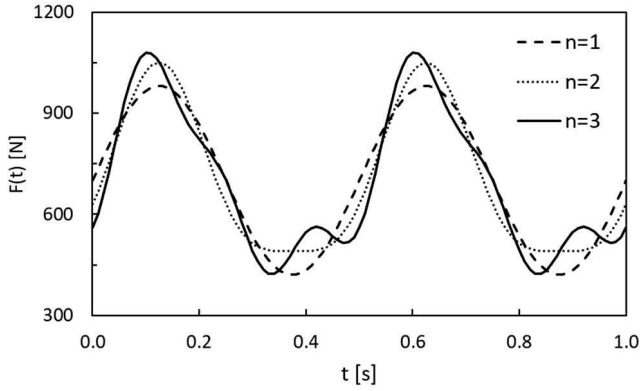

Fig. 21 – Bachmann model of walking load varying the number of considered harmonics.

Furthermore, the vertical force transferred from the pedestrian can be obtained as a sum of single steps over time. For this reason, the model of the single step is necessary. In [75], several studies were conducted, in order to determine the coefficient of the 8-th order polynomial form:

$$\frac{F(t)}{G} = \sum_{i=1}^{8} K_i t^i \tag{15}$$

Where the coefficients K_i are the stiffness related to each order of the formula, depending on the walking frequency. See Table 5.

Table 5 – Coefficient K_i dependent of walking frequency [75].

	f ≤ 1.75 Hz	1.75 Hz ≤ f ≤ 2.00 Hz	f ≥ 2.00 Hz
K_1	-8f+38	24f-18	75f-120
K_2	376f-844	0-404f+521	-1720f+3153
K_3	-2804f+6025	4224f-6274	17055f-31939
K_4	6308f-16573	-29144f+45468	-94265f+175710
K_5	1732f+13619	109976f-175808	298940f-553736
K_6	-24648f+16045	-217424f+353403	-529390f+977335
K_7	31836f-33614	212776f-350259	481665f-888037
K_8	12948f+15532	-81572f+135624	-174265f+321008

Applying formulation 15 for frequency equal to 1.5, 2.0 and 2.5 Hz, graph in Fig. 22 were obtained:

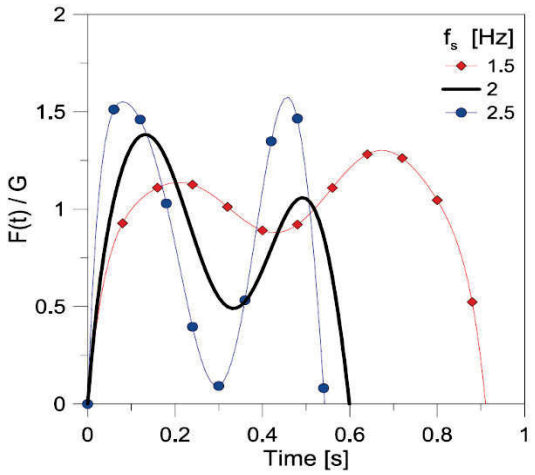

Fig. 22 – Force normalized to g for a single step varying the frequency.

In the study, the authors obtained also calibrated formulations to define the step duration t_s, the velocity v_s, the length of the step L_s and

the overlap time t_0 (Fig. 23), all depending only on the step frequency f_s (Equation)

$$t_s = -0{,}515 \cdot f_s^3 + 3{,}2242 \cdot f_s^2 - 6{,}9773 \cdot f_s + 5{,}8531 \quad (16)$$

$$v_s = 1{,}67 \cdot f_s^2 - 4{,}83 \cdot f_s + 4{,}5 \quad (17)$$

$$L_s = \frac{v_s}{f_s} \quad (18)$$

$$t_0 = t_s - \frac{1}{f_s} \quad (19)$$

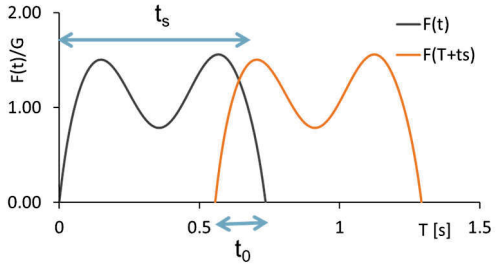

Fig. 23 – Parameters defining the sequence of steps (t_s – step duration; t_t – step overlap).

Finally, all the steps can be summed, in order to obtain the total force which will be applied as a moving load vector varying in time.

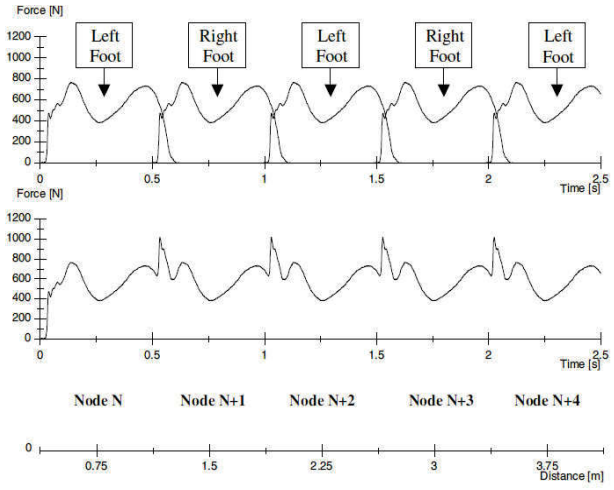

Fig. 24 – Moving load function of a person walking at 2.0 Hz (from [75]).

However, once the force curve for each step is known, the load can be put in the FE model directly in the location were the foot hit the floor, considering a point load (Fig. 25). Then, a dynamic analysis is performed, activating the steps accordingly to the walking sequence and taking into account the step transversal spacing (typically 20 cm) and the overlap t_0.

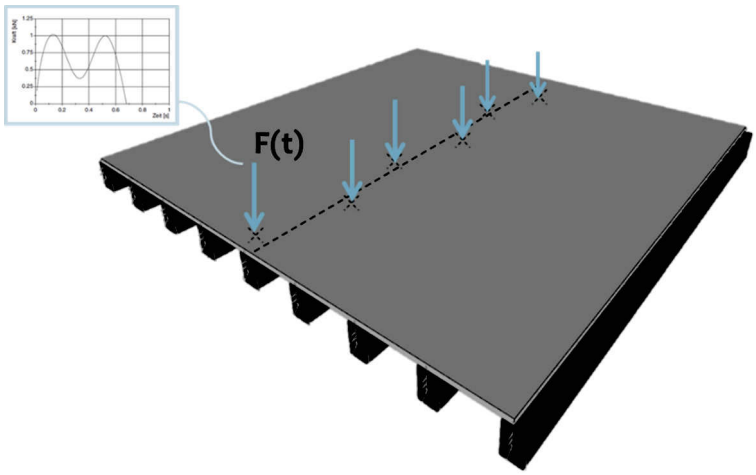

Fig. 25 – Positioning of steps forces on a FE model of a floor.

Nonetheless, the single pedestrian rather than a group of people could be not realistic or not representative of the actual use of the floor [25]. However, the issue regard especially office floors, where many walking paths are excited, rather than residential structures [82].

2.2.1 Probabilistic approaches

Deterministic approaches described in the previous paragraph are not able to consider the randomness given by intra- and inter-subject variabilities. Thus, in order to achieve more realistic predictions, authors studied both light-weight floor with a frequency borderline to the cut-off one [42][83] and random models [84][45], in order to eliminate the necessity to distinguish floor responses based on the fundamental frequency [43][42].

Herein, two probabilistic model are presented, according to Zivanovic et al. [42] and Chen et al. [45].

Zivanovic Model

The model proposed by [42] is a single pedestrian force function developed in time, as an extension of the research of [85] and [84]. This probability-based model takes into account both inter- and intrasubject variability and all frequency content of the walking force up to the fifth harmonic. Even if the walking force model was developed and validated on footbridges, it can be used also for floors with high slenderness, like light-weight timber ones [70].

The advanced version of the model includes the statistical distributions for the Dynamic Load Factors (DLFs) for harmonics and subharmonics, and for frequency content for the full spectrum from $0.25f_p$ to $5.25f_p$, with f_p the pace frequency. Harmonics and Subharmonics follow equation 20 and 21:

$$F_i(t) = W \cdot DLF_i \sum_{\bar{f}_j=i-0.25}^{i+0.25} \overline{DLF_i}\left(\bar{f}_j\right) cos(2\pi \bar{f}_j f_s t + \vartheta(\bar{f}_j)) \tag{20}$$

$$F_i^s(t) = W \cdot DLF_i^s \sum_{\bar{f}_j^s=i-0.75}^{i+0.25} \overline{DLF_i^s}\left(\bar{f}_j^s\right) \cos(2\pi \bar{f}_j^s f_s t + \vartheta(\bar{f}_j^s)) \tag{21}$$

Where, i is the (sub)harmonic considered, $\bar{f}_j$ f_s is a frequency line within the energy range of the harmonic analysed, while $\vartheta(\bar{f}_j)$ is the phase. DLF_i is the DLF for the harmonic analysed, and $\overline{DLF_i}\left(\bar{f}_j\right)$ is the normalised amplitude for the same harmonic for each line. The superscript s refers to subharmonics. Finally, W is the mean value of the pedestrian weight, which can be taken as 750 N. The total force F(t) can be obtained as the sum of the two components, considering all the five (sub)harmonics:

$$F(t) = \sum_{i=1}^{5} F_i(t) + \sum_{i=1}^{5} F_i^S(t) \tag{22}$$

The DLFs have to be estimated for the first five harmonics and subharmonics, covering a frequency range 0.25-5.25f_p. Table 6 reports the mean and standard deviation values to evaluate DLF_i. On the other hand, formulation 23 and 24, together with Table 7 and Table 8, give the information to evaluate $\overline{DLF_i}(\bar{f}_j)$. Values a, b and c were obtained as least square fitting all spectra. For further details, see [42]

Table 6 – Parameter for the Normal Distribution of Dynamic Load Factors according to [42].

Harmonic number	Mean	Standard deviation
2	0.07	0.030
3	0.05	0.020
4	0.05	0.020
5	0.03	0.015

$$\overline{DLF_i}(\bar{f}_j) = a_{i,1} e^{-\left(\frac{\bar{f}_j - b_{i,1}}{c_{i,1}}\right)^2} + a_{i,2} e^{-\left(\frac{\bar{f}_j - b_{i,2}}{c_{i,2}}\right)^2} + a_{i,3} e^{-\left(\frac{\bar{f}_j - b_{i,3}}{c_{i,3}}\right)^2} \tag{23}$$

Table 7 – Fitting parameters for five harmonics (from [42]).

i	1	2	3	4	5
$a_{i,1}$	0.785200	0.513000	0.390800	0.325500	0.280600
$b_{i,1}$	0.999900	2.000000	3.000000	4.000000	4.999000
$c_{i,1}$	0.008314	0.011050	0.009560	0.008797	0.007939
$a_{i,2}$	0.020600	0.133000	0.156700	0.164700	0.158400
$b_{i,2}$	1.034000	1.957000	3.000000	4.001000	5.004000
$c_{i,2}$	0.252400	0.263200	0.055250	0.066410	0.078250
$a_{i,3}$	0.107400	−0.049840	0.068660	0.068880	0.072890
$b_{i,3}$	1.001000	1.882000	2.957000	3.991000	4.987000
$c_{i,3}$	0.036530	0.058070	0.560700	0.375000	0.450100

$$\overline{DLF_i^S}(\bar{f}_j) = a_{i,1}^S e^{-\left(\frac{\bar{f}_j^S - b_{i,1}^S}{c_{i,1}^S}\right)^2} + a_{i,2}^S e^{-\left(\frac{\bar{f}_j^S - b_{i,2}^S}{c_{i,2}^S}\right)^2} \tag{24}$$

Table 8 – Fitting parameters for five sub-harmonics (from [42]).

i	1	2	3	4	5
$a^s_{i,1}$	0.340600	0.302400	0.262700	0.234400	0.264500
$b^s_{i,1}$	0.498800	1.500000	2.500000	3.501000	4.499000
$c^s_{i,1}$	0.008337	0.008735	0.009748	0.009898	0.010190
$a^s_{i,2}$	0.280300	0.134500	0.245600	0.235500	0.238900
$b^s_{i,2}$	1.133000	1.532000	0.231200	−1.576000	1.153000
$c^s_{i,2}$	0.638800	0.723300	2.932000	7.050000	4.561000

Using this model, it is possibility to generate a large number of pedestrians, thus obtaining a consistent variety of responses based on the statistical distributions of DLF and phase angle.

This method was used by [7], considering a basic and an advanced application of the probabilistic walk. In the basic model, the mean DLF values for the harmonics and subharmonics were considered, thus not taking into account the energy leakage. On the other hand, in the advanced model the statistical distributions for the DLFs and frequency content for the full spectrum from 0.25fp to 5.25fp were included. An example of the walking load function for the two models is shown in Fig. 26. (M = 78 kg subject and walking frequency 2.1 Hz.

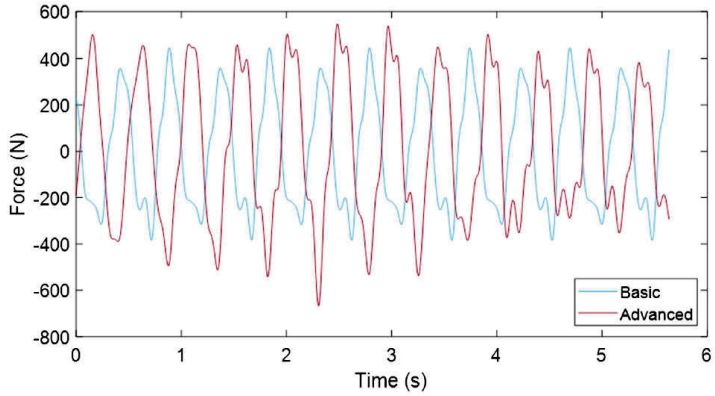

Fig. 26 – Example of applying Zivanovic model with mean values of DLF (basic) and distribution fitting (advanced) from [7].

Chen Model

In the model proposed by Chen et al. [45], the inter-subject and intra-subject variability were taken into account considering a ξ and a ζ

coefficient respectively. The time depending load force F(t), the duration of the step T and the DLF for the first term of F(t) follow equations 25, 26 and 27:

$$F(t) = G\left(a_0 + \sum_{k=1}^{n} a_k \, sin(\frac{2\pi k}{T}t + \varphi_k)\right) \tag{25}$$

$$T = 0.195f_p^2 - 1.118f_p + 2.056 \tag{26}$$

$$a_0 = 0.031f_p + 0.75 \tag{27}$$

The mean dynamic load factor a_k and the mean phase angle φ_k depend on the step frequency f_p, which is not constant during the walk, but changes according to:

$$f_p = \zeta_{fp} f_{p,mean} \tag{28}$$

Where ζ_{fp} is the intra-subject variability of the step frequency that, according to [45], can be taken form a normal distribution N(1.0,0.0325).

To evaluate the mean values of $a_{k,mean}$ and $\varphi_{k,mean}$, the following Table 9 can be used, varying f_p:

Table 9 – Mean value of DLF and phase angle from order 1 to 8 according to [45].

Order	DLF	Phase angle (rad)
1	$0.2080f_p^2$-$0.9373f_p$+1.1998	$0.1730f_p^2$-$0.4087f_p$-0.2936
2	$0.1714f_p$+0.0025	$0.296f_p$-0.5275
3	$0.0129f_p$+0.1216	$0.0815f_p$-0.6305
4	$0.0188f_p$+0.0235	$0.0955f_p$-0.5477
5	0.0364	-0.3563
6	0.0214	-0.4004
7	0.0146	-0.3863
8	0.0114	-0.0851

The outcomes of Table 9 are mean values. In order to obtain the actual values to evaluate F(t), T, a_k and φ_k, inter- and intra-subject variabilities have to be considered. Both follow normal distribution N(1, σ), where 1 is the mean and σ represents the standard deviation. The σ values were obtained by [45] fitting 4814 single footfall traces and 73 volunteers with frequencies ranging between 1.4 and 2.6 Hz, both free and with metronome-imposed time. The standard deviation of the inter-subject variability depends on the frequency of the step f_p (Table 10):

Table 10 – DLF and phase angle standard deviation for the evaluation of the inter-subject variability ξ_{ak} and $\xi_{\varphi k}$ [45].

Order	DLF a	Phase Angle φ (rad)
1	0.31 f_p - 0.232	0.1730 f_p^2 - 0.4087 f_p - 0.2936
2	0.031f_p + 0.053	0.0296 f_p - 0.5275
3	-0.054 f_p + 0.264	0.037 f_p + 0.054
4	-0.0112 f_p + 0.474	0.002 f_p + 0.244
5	0.116 f_p + 0.116	-0.060 f_p + 0.436
6	0.244 f_p - 0.015	-0.021 f_p + 0.428
7	0.352 f_p - 0.224	0-0.214 f_p + 0.880
8	0.362 f_p - 0.252	-1.323 f_p + 5.735

On the other hand, the intra-subject variability was found frequency independent (Table 11):

Table 11 - DLF and phase angle standard deviation for the evaluation of the intra-subject ζ_{ak} and $\zeta_{\varphi k}$ [45].

Order	DLF a	Phase angle φ
1	0.123	0.102
2	0.059	0.058
3	0.101	0.074
4	0.158	0.145
5	0.202	0.209
6	0.296	0.186
7	0.363	0.219
8	0.378	0.201

Starting from the mean values of the dynamic load factor *a* and the phase angle φ, the coefficient to apply formulation 25 can be estimate:

$$a_k = \xi_{ak}\zeta_{ak}a_{k,mean} \quad (29)$$

$$\varphi_k = \xi_{\varphi k}\zeta_{\varphi k}\varphi_{k,mean} \quad (30)$$

In Fig. 27, a randomly generated walk is reported, considering a 1.5 Hz mean step frequency and weight 620 N. It can be noted that each footfall has different shape and duration. Furthermore, the peak loads and the overlap time also changes for each step of the walk.

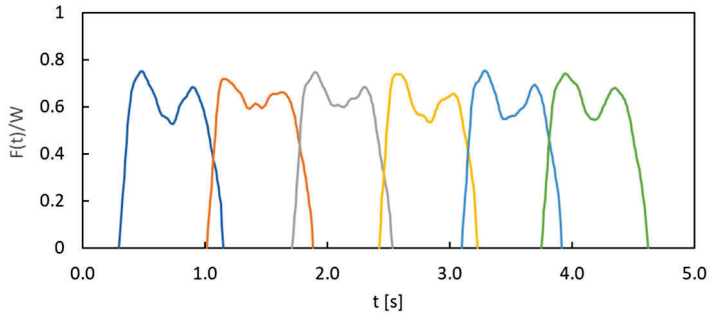

Fig. 27 – Walking sequence of a 620 N weight person at 1.5 Hz according to Chen.

This method was chosen for the parametric analysis of floor to represent the random walk of the pedestrian. A complete flow-chart was developed in section 5.2.3.

2.3 Parameters for comfort assessment

Defining minimum comfort requirements necessarily involves our bodies. Some frequencies resonate with those of our internal organs (Fig. 28), typically between 4 and 8 Hz [86]. All the engineering used to establish minimum standards must be tied to human perception and the probability that vibrations will generate negative judgments from users.

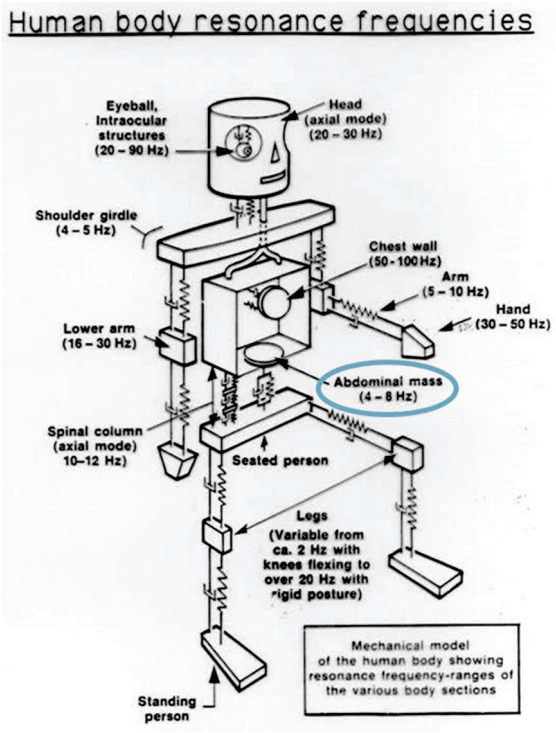

Fig. 28 – Human body resonance frequencies (adapted from [86]).

Herein, the most used parameters to control the vibrations of floors are reported and discussed. More in detail:

- Frequency and deflection;
- Maximum acceleration and velocity;
- Root-Mean-Square RMS and Root-Mean-Quad RMQ evaluation;
- Vibration Dose Value VDV;
- Crest Factor CF;

2.3.1 Frequency and deflection

Deflection control is generally the first requirement to comfort check, since represents the need for a sufficiently out-of-plane rigid floor. Timber floors are flexible, thus a correct stiffness can be advantageous against strong vibration. To avoid the issue, the first natural frequency of the floor should be above a threshold f_{lim}, which represents the limit between the resonant and transient response. The

typical step has a dominant frequency between 1.5 and 2.5 Hz. However, to account for the contribution of higher harmonics, f_{lim} is typically set to four times the walking frequency (6-10 Hz depending on the standard being considered, 8 Hz according to Eurocode 5 [38]).

In Chapter 1.3, the link between frequency f and deflection w was calculated:

$$f_1 = \frac{17.8}{\sqrt{w}} \tag{31}$$

Thus, imposing a limit frequency of 8 Hz, a maximum deflection can be evaluated:

$$w_{max} = \left(\frac{17.8}{f_1}\right)^2 = \left(\frac{17.8}{8}\right)^2 = 5\ mm \tag{32}$$

The estimated maximum deflection corresponds to self-weight and structural loads only. Starting from these assumptions, in Table 12 two timber floors were checked, considering spans of 4 and 5 m, and imposing the deflection of 5 mm. The ratio between the live and the dead load was varied, in order to investigate the maximum variable load that can be carried by the structure checking both deflection and vibration verifications.

If we take a 4 m floor with G=2.00 kN/m^2, the maximum live load to verify is equal to the dead load itself (Q/G=1), thus 2.00 kN/m^2. A higher live load means a higher final deflection and, thus, the verification is not satisfied.

Although frequency and deflection are still an important criterion, widely used in code and standard (see Chapter 3), there is not sufficient correlation between natural frequency of the floor and subjective perception of comfort.

Table 12 – Maximum live load carried by a floor to satisfy both vibration and deflection check, imposing maximum deflection limit.

L [m]	f_{lim} [Hz]	w_{max} [mm]	Q/G 0.50	0.67	1.00	1.50	2.00	4.00	
			$L/w_{Q,inst}$						LIMIT
4.0	8	5.0	1616	1212	808	539	404	202	300
5.0	8	5.0	2020	1515	1010	673	505	252	300
			L/w_{fin}						LIMIT
4.0	8	7.9	369	339	291	240	204	128	250
5.0	8	7.9	461	423	363	300	255	160	250

In [57], the authors gathered info on the subjective evaluation of comfort, varying the type of floor on which the volunteers walked. The results are reported in Fig. 29, considering a scale from 1 (good) to 4 (bad).

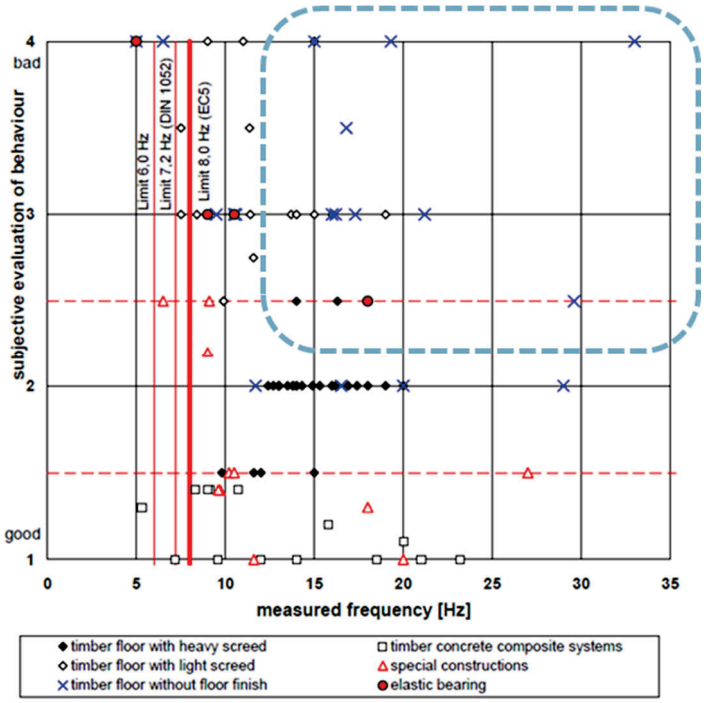

Fig. 29 – Correlation between measured floor frequency and subject evaluation, adapted from [57].

Even if the fundamental measured frequency of the floor was higher (or much higher) than the limit value of 8 Hz, the comfort linked to timber floor without and with finishing is graded 3 and 4, leading to bad perception. Heavier structures as heavy screed timber floors or timber-concrete composites have better behaviour.

2.3.2 Acceleration and velocity

Comfort verifications can be performed in terms of both acceleration and velocity.

Peak acceleration values are possible indicators for predicting the level of comfort associated with a given level, but they are rarely used. (e.g., ISO 2631-2 [87]). Another example is the SETRA Guidelines [77], which define ranges of permissible peak accelerations depending on the minimum, medium, or maximum comfort desired. However, the SETRA guidelines refer to pedestrian bridges (Fig. 30).

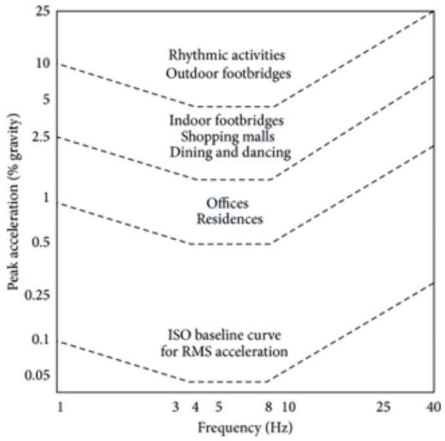

Acceleration ranges	0	0.5	1	2.5
Range 1	Max			
Range 2		Mean		
Range 3			Min	
Range 4				

Table 2.1: Acceleration ranges (in m/s²) for vertical vibrations

Acceleration ranges	0	0.1	0.15	0.3	0.8
Range 1	Max				
Range 2			Mean		
Range 3				Min	
Range 4					

Table 2.2: Acceleration ranges (in m/s²) for horizontal vibrations

Fig. 30 – Peak acceleration limits according to ISO 2631 [87] (left) and SETRA guidelines for footbridges [77](right).

More present in the regulation are Root Mean Square RMS methods, regarding both velocities and accelerations (Equation 33 and 34).

$$a_{RMS} = \sqrt{\frac{1}{T}\int_0^T a^2(t)dt} \tag{33}$$

$$v_{RMS} = \sqrt{\frac{1}{T}\int_0^T v^2(t)dt} \tag{34}$$

Methods considering the root mean quad RMQ are instead used for dose methods, rather than direct check:

$$a_{RMQ} = \sqrt[4]{\int_0^T a^4(t)dt} \tag{35}$$

$$v_{RMQ} = \sqrt[4]{\int_0^T v^4(t)dt} \tag{36}$$

Both the RMS and the RMQ depend on the measurement time T (Fig. 31). The larger T becomes, the more the two values decrease, being averages. This conflicts with the perception of vibration, which generally considers the longer it lasts the more unacceptable it is. The definition of T is, thus, crucial. Given the nature of vibrations, however, it is not easy to identify the beginning and end of the measurement time.

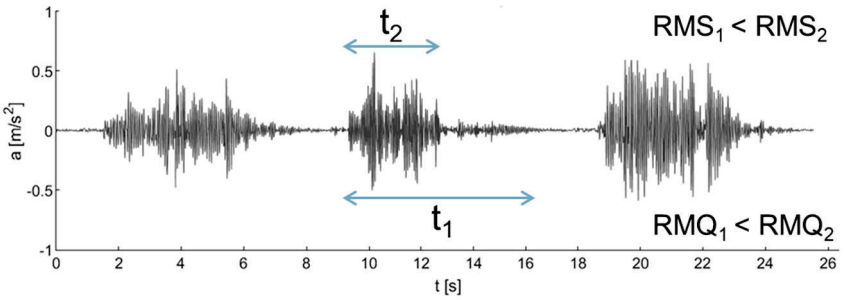

Fig. 31 – Measurement time dependency of RMS and RMQ methods.

However, it is necessary to define if the check has to be performed considering velocity or acceleration. The choice is based on the

assumption that the human body does not perceive all frequencies as uncomfortable in the same way. Acceleration and velocity are thus weighted to create piecewise lines that represent a consistent perception. Therefore, an indication to check is that, under a certain frequency (cut off), the body is more sensible to acceleration. On the other hand, velocity governs the check for higher frequencies.

In Fig. 32, the acceleration and velocity weighted curve are reported from ISO 10137 [37]. The line shows the threshold between acceptable and not acceptable vibration. For higher frequencies, higher vertical RMS acceleration are tolerated, thus the velocity verification is more demanding. On the other hand, the maximum tolerated RMS velocity increase for frequencies lower than 8 Hz.

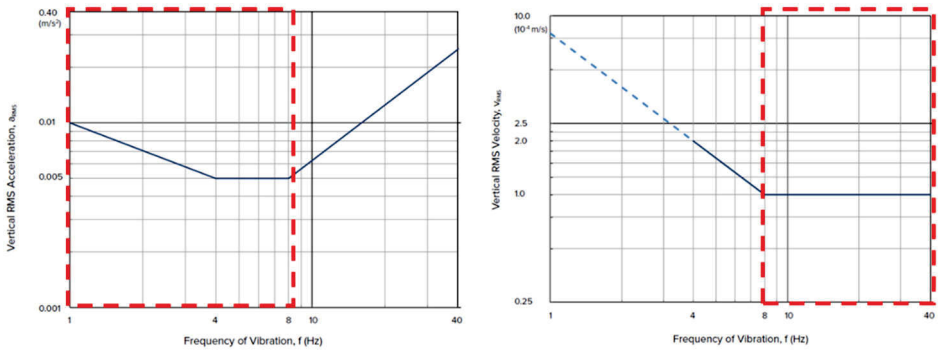

Fig. 32 – Limit values for acceleration and velocity according to ISO 10137 [37].

2.3.3 Vibration Dose Value

Short-duration and infrequent vibration events are likely to be more tolerated than frequent and/or long-duration ones. RMS criteria do not account for the duration and number of vibration events, which can lead to conservative results for some scenarios. Some existing techniques account for the duration and frequency of vibration events; the most common is VDV.

The VDV is given by the fourth root of the integral with respect to time of the fourth power of the weighted acceleration (a_w). (It is effectively an RMQ.) Using the fourth power method makes the VDV more sensitive to peaks in the acceleration waveform. Furthermore, the

VDV accumulates the vibration energy received during the day and night periods.

$$VDV = \sqrt[4]{\int_0^T a_w^4(t)dt} \quad [m/s^{1.75}] \tag{37}$$

Moreover, the VDV is less dependent on the measuring period T with respect to RMS methods (Fig. 33).

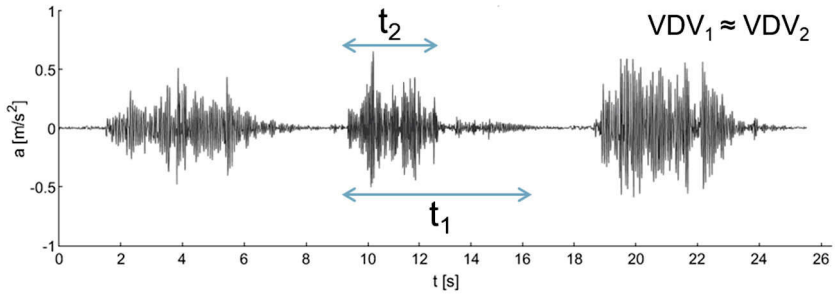

Fig. 33 – Measurement time dependency of VDV method.

The acceleration for the evaluation of the VDV is weighted, based on the different perception of the body to frequencies between 4 and 8 Hz. The weighting curve of ISO 10137 [37] is reported in Fig. 34, showing the weight W_b varying the frequency. It is worth noticing that the value is 1 in correspondence of the aforementioned frequencies.

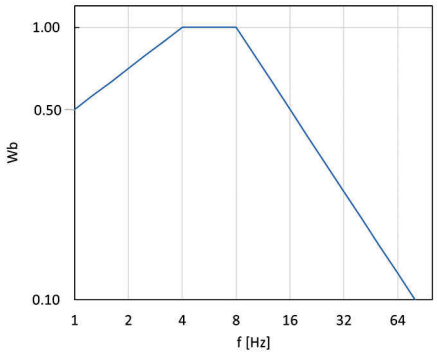

Fig. 34 – Frequency weighting curve for vertical acceleration according to ISO10137 [37].

2.3.4 Crest Factor

The Crest Factor CR is the ratio of the maximum acceleration to the RMS acceleration, both weighted according to Fig. 34.

$$CR = \frac{|a_w|_{max}}{a_{w,RMS}} \tag{38}$$

In standards, the CR is used as a dividing line between the use of RMS-based methods and the use of VDV [86][87][88]. The former, in fact, is less sensitive to local acceleration peaks and is considered suitable for CR<6 [89].

In the literature, authors tried to connect the value of the CR with the selected method of evaluation [89][90]. Passive perception of vibration was investigated in [89], where different dynamical events with crest factor higher than 12 where analysed. The study was made using RMS, MTVV (Maximum Transient Vibration Value, i.e. the maximum of the weighted acceleration over time) and VDV method, and the researchers found that the VDV is the most suitable for signal with high CR. Moreover, in [90] the CR was used to estimate the VDV.

After the focus and discussion of most of the indicators that can be used to evaluate the comfort due to vibrations, the VDV was chosen for the parametric analysis of Chapter 5. The VDV represents the most complete approach available in the current state-of-the-art. The implementation of this parameter is less intuitive with respect to others (maximum or RMS accelerations), since a weighting procedure is needed. For this reason, it is usually not considered in the design practice, but only in academic papers or advanced standards, such as [91][92].

II-3 CODES AND REGULATIONS

Vibration serviceability in timber floors is an issue several centuries years old. In 1820, Thomas Tedgold wrote "Elementary Principles of Carpentry" [93] considering, for the first time, the deflection limit as essential to control excessive vibrations in wooden floors. In the book, a limit of 1/480 of the span was suggested:

"Girders for long bearings should always be made as deep as the timber can be obtained; an inch or two taken from the height of a room is of little consequence compared with a ceiling disfigured with cracks, besides the inconvenience of not being able to move without shaking everything in the room"

From that paragraph, 200 years of deflection control codes began, starting from the adaptation of the 1885 by Kidder [94], which became the north American L/360 suggestion, under a 40 pounds per square foot uniformly distributed load (equivalent to 1.9 kN/m^2).

Herein, available standards and codes are analysed, starting from the Italian one. Then European regulations are discussed, together with useful documents and parallel studies. Finally, some of the most important extra-European codes are reported.

3.1 Italian Building Code

In the Italian Building Code [95], chapter 4.4 contains all regulation to be applied on timber structure under static loads (earthquake actions

are described in section 7 of the standard). However, chapter 4.4 does not include a specific "vibration check", but only a sentence stating that *"Le deformazioni di una struttura […] devono essere contenute entro limiti accettabili"*, i.e. *"deformation of a structure […] must be contained within acceptable limits"*. Though, in chapter 2.2.2 "Stati Limite di Esercizio (SLE)", i.e. Serviceability Limit States, the vibration limit state is enlisted and, thus, has to be considered in the design process (Fig. 35).

2.2.2. STATI LIMITE DI ESERCIZIO (SLE)

I principali Stati Limite di Esercizio sono elencati nel seguito:

a) danneggiamenti locali (ad es. eccessiva fessurazione del calcestruzzo) che possano ridurre la durabilità della struttura, la sua efficienza o il suo aspetto;

b) spostamenti e deformazioni che possano limitare l'uso della costruzione, la sua efficienza e il suo aspetto;

c) spostamenti e deformazioni che possano compromettere l'efficienza e l'aspetto di elementi non strutturali, impianti, macchinari;

d) vibrazioni che possano compromettere l'uso della costruzione;

e) danni per fatica che possano compromettere la durabilità;

f) corrosione e/o degrado dei materiali in funzione del tempo e dell'ambiente di esposizione che possano compromettere la durabilità.

Altri stati limite sono considerati in relazione alle specificità delle singole opere; in presenza di azioni sismiche, gli Stati Limite di Esercizio comprendono gli Stati Limite di Operatività (SLO) e gli Stati Limite di Danno (SLD), come precisato nel § 3.2.1.

Fig. 35 – Extract from the IBC [95] regarding the serviceability limit states (Stati Limite di Esercizio SLE).

To have a more detailed quantification of the vibration check, the applicative circular of the Italian building code can be consulted [96]. In paragraph C4.4 of the applicative document, there is the indication to refer directly to the UNI EN 1995-1-1 (EC5)[38]. For accurate verifications, proven validity codes, guidelines or standard are necessary. The National Research Council, in the CNR DT 206 [97], in fact, suggest the ISO 10137 [37] to perform accurate vibration checks on timber floor. The old version of the CNR DT 206 recommended only a frequency check, i.e. a fundamental vertical frequency of the floor > 6 Hz, in order to avoid the resonant response of the structure.

3.2 Eurocode 5

UNI EN 1995-1-1 [38] vibration check refers to Ohlson's findings [52]. The proposed methodology, in fact, is based on three separate checks on deflection, frequency and velocity, and its validity include BxL

timber floor, simply supported along all the edges. Moreover, the frequency had to be greater than 8 Hz, since for resonant response no guidance is given, and special investigations are necessary. However, no specifications are included in the code.

The inequalities to be checked according to the Eurocode are herein reported:

$$f_1 > 8\ Hz \tag{39}$$

$$\frac{w}{F} \leq a\ [mm/kN] \tag{40}$$

$$v \leq b^{(f_1 \xi - 1)} \quad [m/(Ns^2)] \tag{41}$$

Where f_1 is the fundamental frequency of the floor, w is the deflection caused by a force F applied in the most unfavourable place of the floor, v is the velocity induced by a unitary impulse and ξ is the damping. The parameters a and b are linked to the comfort level to be achieved, following Fig. 36. High quality comfort is achieved moving toward "1". Limited and poor comfort floors are collocated toward the "2". Typically, a=1 mm/kN and b=120 are used for residential building according to current design practice.

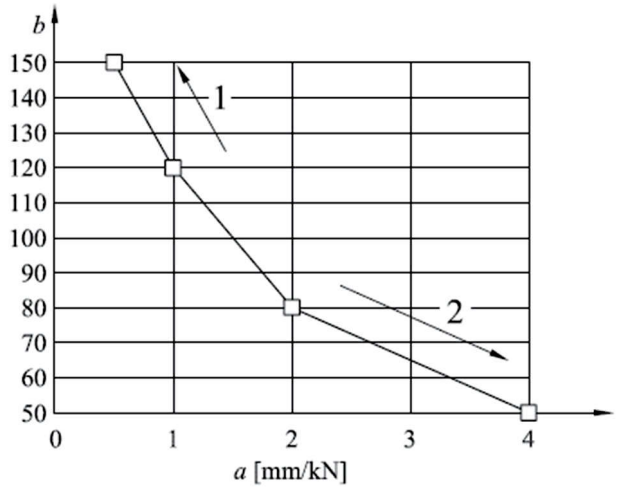

Fig. 36 – Definition of a and b parameters linked to the performance of the timber floor (1: better – 2: worse) according to EC5 [38].

Eurocode 5 proposes a formulation to evaluate the fundamental vertical frequency of the floor, assuming a beam behaviour; the formulation, in fact, do not take into account the transversal collaboration of boards or screed layers.

$$f = \frac{\pi}{2L^2}\sqrt{\frac{(EJ)_l}{m}} \tag{42}$$

Where L is the floor span, m the mass of the floor [kg/m^2] and $(EJ)_l$ is the equivalent plate flexural stiffness of the floor, considering an axis perpendicular to the joists' direction [Nm^2/m]. The deflection check is based on the aforementioned defined longitudinal stiffness, and can follow equation 43. The formulation, in fact, represents the deflection of a simply supported beam under a mid-span concentrated load F. Considering EC5 suggestion, the load F has to be applied in the most unfavourable position on the floor but, given the simply support on all edges, the midspan point can be selected.

$$w = \frac{FL^3}{48(EJ)_l\, b_{eff}} \leq a \tag{43}$$

Where F = 1 kN and b_{eff} is the effective width of the one-way stripe of the floor, considered for the deflection calculation. Since the EC5 do not give formulation to evaluate the effective width, prove validity literature is needed.

For floors with a fundamental frequency above 8 Hz (cut-off frequency), EC5 proposes to check the velocity caused by a unitary impulse, i.e. an ideal impulse equal to 1 Ns applied in the most unfavourable point of the floor. The obtained value has to be lower than threshold value v_{lim}. Furthermore, vibration modes with frequency higher than 40 Hz can be neglected.

The velocity and the number of modes under 40 Hz can be estimated thanks to equation 44 and 45:

$$v = \frac{4(0.4 + 0.6n_{40})}{mBL + 200} \leq v_{lim} \tag{44}$$

$$n_{40} = \left\{ \left(\left(\frac{40}{f_1} \right)^2 - 1 \right) \left(\frac{b}{l} \right)^4 \frac{(EJ)_b}{(EJ)_l} \right\}^{0.25} \tag{45}$$

Where B and L are the width and the span of the floor, m is the mass of the floor (kg/m^2), f_1 is the vertical fundamental frequency of the floor (Hz) and EJ_b and EJ_l are the flexural stiffness in transversal and longitudinal directions respectively. Finally, the limit value of the velocity can be obtained according to formulation 46:

$$v_{lim} = b^{(f_1 \xi - 1)} \tag{46}$$

The EC5 suggest a value of ξ equal to 1% for the evaluation.

The draft of the new EC5 enhanced the former verification procedure, considering both acceleration and velocity check. A Root-Mean-Square rather than a peak approach was introduced, following both a stiffness criterion and a frequency criterion.

The verification, in fact, is based on two sequential criteria. The first step, see Fig. 37, is the classical floor deflection check, where the deflection is evaluated under a concentrated 1 kN load (w_{1kN}) positioned in the most unfavourable position. The limit value is given for different comfort levels, from the highest (level I & II) to the lowest (VI). If this criterion is satisfied, the designer must also check if the first natural frequency of the floor is above a certain threshold f_{lim}, representing the cut-off frequency, i.e. the limit between the resonant and the transient response. The cut-off frequency is still debated topic, and varies between from 7.5 to 10 Hz, depending on the authors (See Section 1.3). Moreover, a minimum frequency of 4.5 Hz has to be achieved, in order to avoid significant resonance effects under human induced loads.

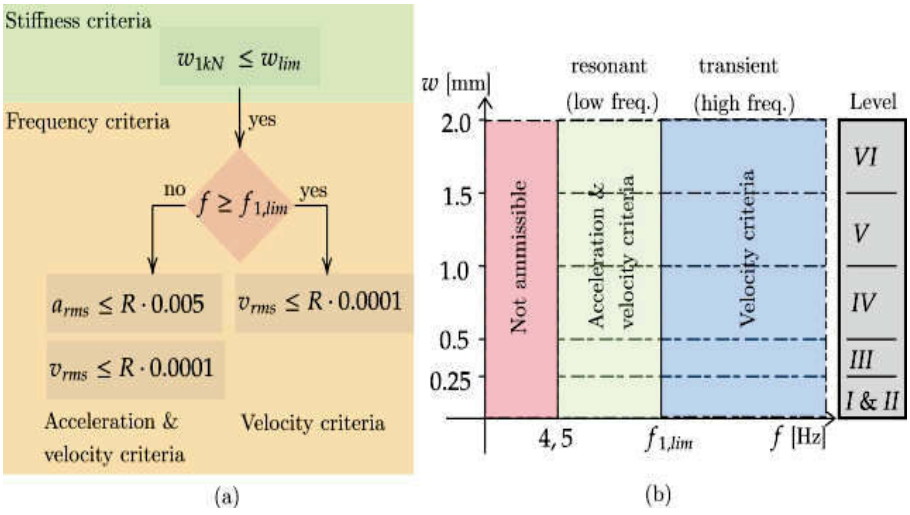

Fig. 37 – Design flowchart for timber floors according to the draft of the new EC5 (from [98]).

After the frequency check, the rms acceleration and/or velocity need a further check. If the response of the floor is "resonant", the vertical rms acceleration has to be checked, since the sensitivity toward resonance of these kind of floors. To evaluate the limit conditions for both acceleration and velocity, a Response Factor R is applied. The Response factor is defined as the ratio between the rms value and the base curve value, indicating the level of vibration perceptible to an average human [37][86][87]. The higher R is considered, lower are the comfort levels, since a high vibration response is tolerated (see Table 13).

Table 13 – Floor criteria according to the new EC5 draft (from [98]).

Criteria	Floor Performance level					
	I	II	III	IV	V	VI
Response factor R	4	8	12	24	36	48
Deflection limit w_{lim} [mm]	0.25	0.25	0.5	1	1.5	2
Frequency criteria (all floors)	f>4.5 Hz					
Acceleration criteria (resonant floor)	$a_{rms} \leq 0.005R$ m/s2					
Velocity criteria (all floors)	$v_{rms} \leq 0.0001R$ m/s					

Furhermore, the new draft of EC5 contains simplified formulations to evaluate the effective width of the floor and the frequency, taking into account the transveral stiffness [98]. It is Worth noticing that the DIN

1052 of 2008 [99]already presented this procedure, considering an acceleration verification for resonant floors below 8 Hz (Fig. 38)

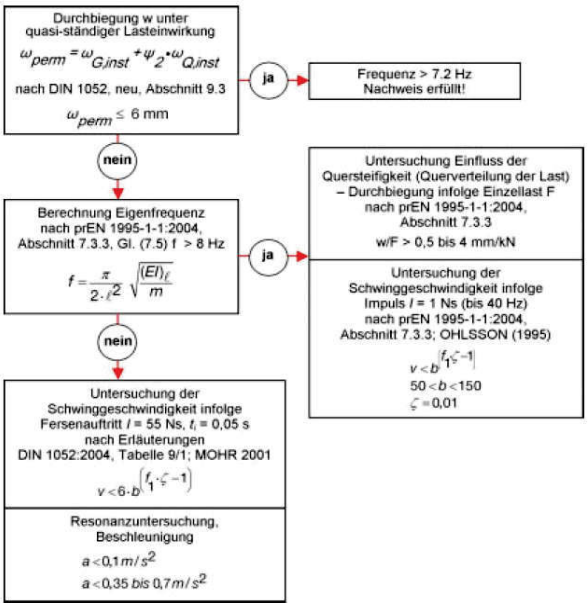

Fig. 38 – Flowchart for timber floors verification according to DIN 1052 [99].

3.2 Available technical documents

3.2.1 ISO 2631

In the ISO 2631-1 [86], information about possible effects of vibration on health, comfort, and perception for frequencies between 0.5 Hz and 80 Hz are reported. Moreover, the standard defines evaluation base methods to check the acceleration limits. ISO 2631-1, in fact, suggests that the vibration magnitude be measured in the form of acceleration. Nonetheless velocity is acceptable for low vibration magnitude, such as in buildings.

In order to evaluate the vibration, the weighted acceleration a_w need to be calculated:

$$a_w = \sqrt{\frac{1}{T}\int_o^T a_w(t)^2 dt} \tag{47}$$

where a_w (t) is the weighted acceleration (m/s^2), and T is the duration of the measurement (s).

Since the frequency content influences the perception and the comfort, acceleration needs to be frequency-weighted. The human body, in fact, has high sensitivity in the range 4-8 Hz, that is typical of low frequency timber floors. Weights from ISO 2631-1 [86] are reported in Fig. 39, W_k for vertical and W_d for horizontal vibration. It is worth noticing that 50 percent of alert and fit persons can just detect a W_k weighted vibration with a peak acceleration of 0.015 m/s^2 [86].

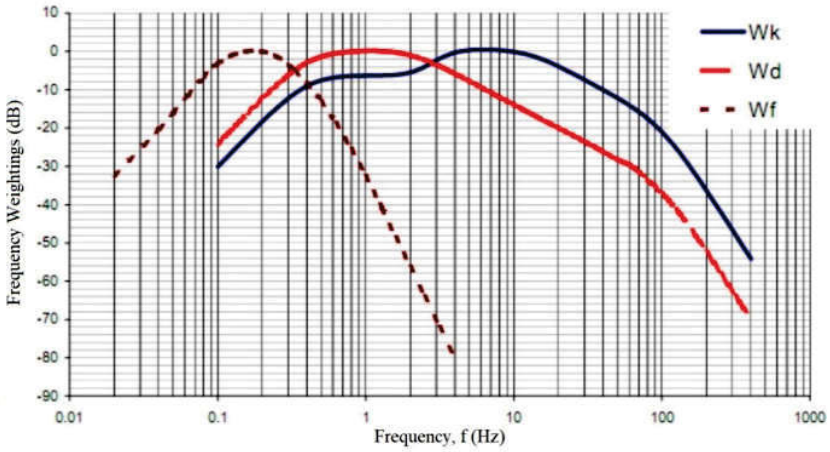

Fig. 39 – Frequency weight according to ISO 2631 [86](W_k vertical, W_d horizontal vibrations).

Following ISO 2631, equation 47 is suitable for steady state resonant response (frequency lower than the cut-off frequency) with low Crest Factor (the ratio between maximum acceleration and RMS value, see Section 2.3.4). When the CR is higher than 9 [86] or 6 [37], running RMS and VDV are recommended. Running (or Rolling) RMS at time t_0 is defined for an interval τ, typically chosen as 1 or 0.5 s, as:

$$a_w(t_0) = \sqrt{\frac{1}{\tau}\int_{t_0-\tau}^{t_0} a_w(t)^2 dt} \tag{48}$$

The maximum value of the running rms is called maximum transient vibration value (MTVV)

The fourth power vibration dose method uses the fourth power instead of the second power, thus is more sensitive to peaks, see Section 2.3.3.

According to ISO 2631-1 [86], MTVV and VDV should be used instead of RMS acceleration if the following inequalities are exceeded:

$$\frac{MTVV}{a_w} > 1.5 \qquad \frac{VDV}{a_W T^{0.25}} > 1.75 \tag{49}$$

ISO 2631-2 [87], contains also peak acceleration boundaries, different for different uses of the floors, depending on the fundamental frequency. For example, a residential floor needs a maximum peak acceleration of 0.5% of g, i.e. 0.05 m/s^2, in order to be acceptable, see Fig. 40.

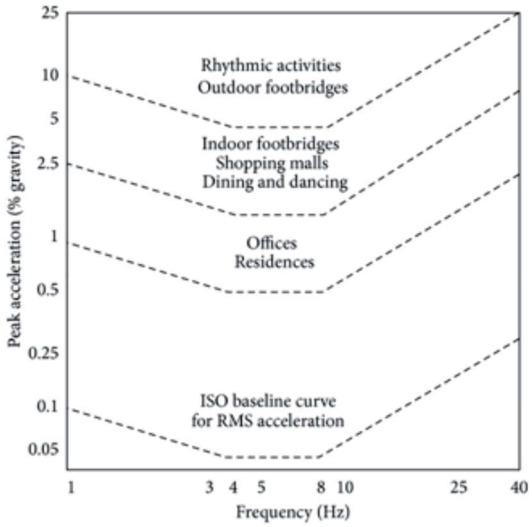

Fig. 40 – Peak acceleration boundaries according to [87].

3.2.2 ISO 10137

According to the ISO 10137 [37] three occupancy categories for human reactions to vibrations can be considered: (1) sensitive (such as hospital operating rooms), (2) regular (offices and residential areas), and (3) active (such as exposure to heavy industrial work).

The standard uses the weighted vibration acceleration and the VDV and compare them with base curves and/or reference limit values. As an example, Fig. 41 reproduce the baseline for the rms acceleration. In red, the residential line is highlighted, considering a multiplying factor of 2.

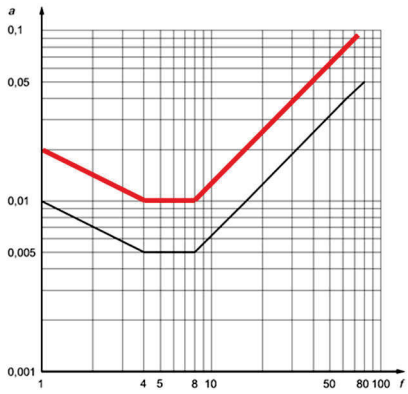

Place	Time	Multiplying factors to base curve (Figures C.1, C.2 and C.3) [a]	
		Continuous vibration and intermittent vibration [b]	Impulsive vibration excitation with several occurrences per day
Critical working areas (e.g. some hospital operating-theatres, some precision laboratories, etc.)	Day	1	1
	Night	1	1[c]
Residential (e.g. flats, homes, hospitals)	Day	2 to 4 [d]	30 to 90 [d, e, f]
	Night	1,4	1,4 to 20
Quiet office, open plan	Day	2	60 to 128 [g]
	Night	2	60 to 128
General office (e.g. schools, offices)	Day	4	60 to 128 [g]
	Night	4	60 to 128
Workshops [h]	Day	8	90 to 128 [g]
	Night	8	90 to 128

Fig. 41 – ISO 10137 RMS acceleration limits for residential floors [37].

Tolerance limit for the VDV are reported in Fig. 42 for residential and offices, according to [37][100]

Multiplying Factors to Base Curves			
Building Usage	**Time**	**Continuous and Intermittent Vibration**	**Impulsive Vibration**
Residential	Day	2–4	30–90
	Night	1.4	1.4–20
Office and School	Day	4 *	60–128
	Night	4 *	60–128
Vibration Dose Values ($m/s^{1.75}$) in Equation (4) from BS 6472			
Building usage	Adverse comment unlikely	Adverse comment possible	Adverse comment probable
Residential 16 h day	0.2–0.4	0.4–0.8	0.8–1.6
Residential 8 h night	0.13	0.26	0.51
* A value of 2 is recommended for a quiet office.			

Fig. 42 – VDV values according to ISO [37] and BS [100].

3.2.3 Guidelines

Since few guidelines for timber floors were specifically written, those of other material are commonly used. The most implemented in current design practice are CCIP-016 by the Cement and Concrete Industry [36], SCI-P354 by the Steel Construction Institute [32], and the Steel Design Guide Series AISC/CISC DG 11 by the American Institute of Steel Construction [35]. The comfort limits of SCI-P354 are taken from the British standard BS 6472 [92], and those of CCIP-016 and AISC/CISC DG 11 are represented in Table 14 and Table 15. For each floor use, the acceleration/velocity and he Response Factor are provided, depending on the resonant (low frequency) or transient (high frequency) response.

Table 14 – Comfort limits according to CCIP-016 [36].

Floor Use	Low frequency		High Frequency	
	Peak acceleration	Response Factor R	V_{RMS} (m/s)	Response Factor, R
Commercial	0.0057g	8	$8 \cdot 10^{-4}$	8
Residential (day)	0.0028g-0.0057g	4 to 8	$4\text{-}8 \cdot 10^{-4}$	4 to 8
Premium quality offices	0.0028g	4	$4 \cdot 10^{-4}$	4
Residential (night)	0.002g	2.8	-	-
Hospitals and critical work areas	0.00071g	1	-	-

Table 15 – Comfort limits according to AISC DG 11 [35].

Floor Use	Low frequency		High Frequency	
	Peak acceleration	Response Factor R	V_{RMS} (m/s)	Response Factor, R
Pedestrian bridges (outdoor)	0.050g	70	-	-
Pedestrian bridges (indoor), malls	0.015g	21	-	-
Residential, offices, quiet areas	0.005g	7	-	-
Ordinary workshops	-	-	$8 \cdot 10^{-4}$	8
Offices	-	-	$4 \cdot 10^{-4}$	4
Residential	-	-	$2 \cdot 10^{-4}$	2
Hospital	-	-	$1.5 \cdot 10^{-4}$	1.5

The SCIP354 method [32] is based on finding RMS acceleration or VDV response from a range of step and floor frequencies, given a cut-

off frequency of 10 Hz for general floors. For frequency higher than the cut-off frequency, a transient response needs to be checked. On the other hand, low frequency floors need both resonant and transient verifications. In this method, the weighted RMS acceleration response of each force harmonic at each mode is calculated at the centre of the floor. Then, the total acceleration is evaluated summing up RMS of each mode, assuming that peaks occurs at the same time (simplified and conservative choice).

Another guideline is worth mention. The ISO/TR 21136 method [101] contains a simple check for the vibration of timber floors, involving the relation between fundamental frequency and deflection under 1 kN static force. Equation 50, was developed from a logistic regression on the database of field frame timber floors in Canada occupants' survey and testing, thus may not be accurate for European or specifically Italian floors:

$$d_{1kN} = \frac{f^{2.56}}{1090.31} \tag{50}$$

Finally, the HIVOSS method is reported [46]. The method was developed by ArcelorMittal (Steel manufacturer). Load walking functions combines coefficients up to the 8th order, based on the step frequency. Moreover, on the basis of a single-step load function, the design value OS-RMS90 called the "one step root mean square 90", was considered, covering the response velocity of the floor filtered using the weighting functions for a significant step with the intensity of 90% of people's walking normally. In the HIVOSS method, the fundamental vertical frequency and the corresponding modal mass are calculated from FEM analysis or simple equations. Set the critical damping, diagrams can be used to evaluate the classification of the floor from F (worse) to A (best). An example of diagram is reported in Fig. 43 for a 3% damping. A table to check the suitability of the floor is also provided (Fig. 44).

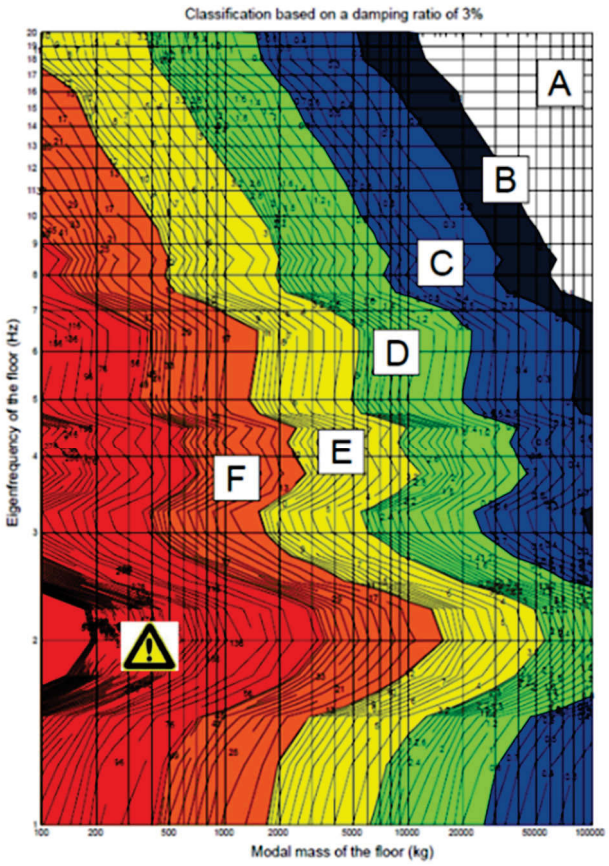

Fig. 43 – HIVOSS performance levels for floor having a 3% damping (from [46]).

Class	$OS\text{-}RMS_{90}$		Usage of the floor structure									
	Lower limit	Upper limit	Critical areas	Hospitals, surgeries	Schools, training centers	Residential buildings	Office buildings	Meeting rooms	Senior citizens' Residential building	Hotels	Industrial Workshops	Sports facilities
A	0.0	0.1										
B	0.1	0.2										
C	0.2	0.8										
D	0.8	3.2										
E	3.2	12.8										
F	12.8	51.2										

Recommended
Critical
Not recommended

Fig. 44 – Checking table containing the limits for each floor class and usage (from [46]).

3.2.4 Extra-European standards

In order to conclude the chapter about standards and guidelines, two of the most used extra-European standards are herein presented. Since they are current design standard, a simplified way to assess the vibration performance is proposed.

The Australian standard [88] refers to a deflection control criterion in order to avoid vibration adverse comments by occupants. The first check is done on the static deflection under dead load plus the 40% of live load, considering a maximum of L/300 deflection, with L the span of the floor. Moreover, a deflection less than 1 or 2 mm is suggested for vibration serviceability, calculated under a F =1 kN vertical load.

The Canadian standard CSA 086:2019 [102], on the other hand, has a "span approach" for single-span timber joisted floor systems with prefabricated wood I-joists and wood structural panel subfloor. The maximum suggested span l_v (m) is:

$$l_v = \frac{0.122(EJ_{eff})^{0.284}}{k_{tss}^{0.14} m_L} \tag{51}$$

$$k_{tss} = 0.0294 + 0.536k_1^2 + 0.516k_1^{0.5} + 0.31k_1^{0.75} \tag{52}$$

where EI_{eff} (Nm^2) is the effective flexural stiffness of the floor system in the span direction, k_{tss} is a factor that accounts for the flexural stiffness in the transverse direction, and m_L is the mass per unit length (kg/m) of the composite floor system.

II-4 EXPERIMENTAL TESTS

In this chapter, a full-scale timber floor was assembled and dynamically tested under human induced vibration, in a joint research project with the University of L'Aquila. The tests were performed recording the data both with force-balance accelerometers and smartphone, in order to estimate corrective coefficient to be applied and minimize the difference between smartphone and professional accelerometers records. Furthermore, a test protocol for in-situ tests is proposed, based on the minimum number of walks obtained by the laboratory tests.

4.1 Specimen geometry

To perform the non-destructive dynamic tests, a full-scale timber floor was built at the Laboratory of Materials and Structures of the University of L'Aquila, Department of Civil, Construction-Architectural, and Environmental Engineering (Fig. 45).

According to Fig. 45, the specimen was assembled to have a nominal span L=4000 mm and a distance between supports of 3700 mm. The resisting cross-section of the floor consisted of three glulam longitudinal beams (130×240mm, their section), spaced 530 mm apart (Fig. 46).

A single solid wood plank layer, 40mm in thickness, was placed on the top of the beams to create the pedestrian surface. A set of 12 boards (arranged 4 in width × 3 in span), with a width of 265 mm and a length of 1600mm (800mm at mid-span), was used to cover the floor surface.

Fig. 45 – Assembling phases of the full-scale timber floor (up) and particular of the secondary joists (down).

In addition, secondary transversal beams made of solid wood, with an 80×80mm cross-section and a total length of 400 mm, were placed 783 mm apart from each other orthogonally to the longitudinal beams to provide a lateral restrain and support for the planks. Finally, the mechanical connection between the plank layer and the longitudinal glulam beams was obtained using 45° inclined screws (9 mm in diameter and 160mm in length), spaced 200 mm apart.

Regarding the mechanical boundaries, simply supported restraints were reproduced with bespoke steel rollers, placed 180 mm apart from the ends (Fig. 46).

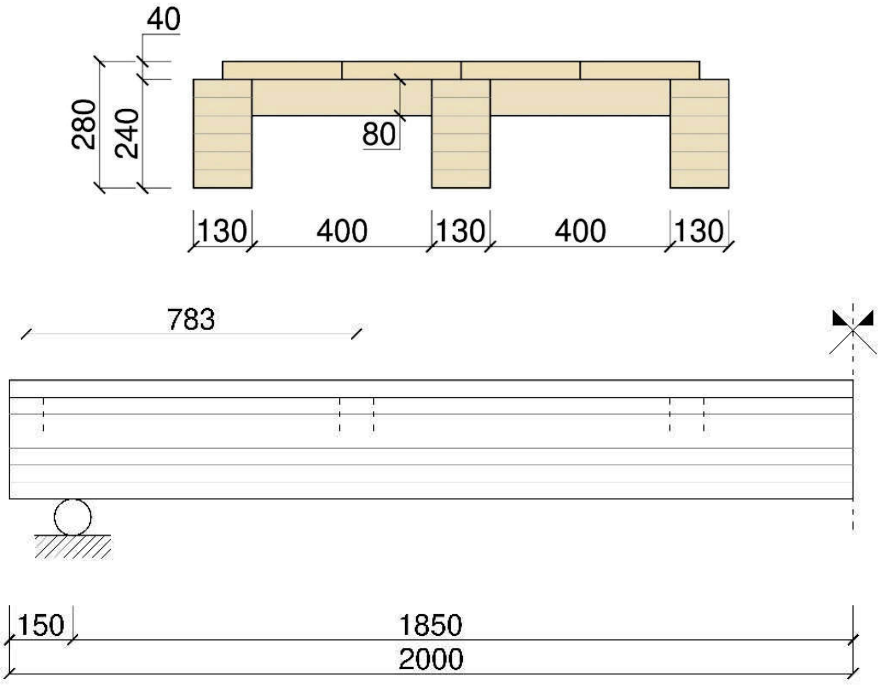

Fig. 46 – Section (up) and profile (down) of the timber floor specimen.

4.2 Material properties

Each component used to assemble the full-scale specimen was previously tested by the Laboratory of Tests, Materials and Structures of the Department of Civil, Building and Architecture and Environmental Engineering of the University of L'Aquila [103][104]. Herein, an overview of the test that were performed is reported, focusing on beams, secondary joists, boards and screwed connection.

4.2.1 Glulam beams

Principal joists are six-layered glue-laminated timber beams made of homogeneous beech. Timber boards are 40 mm thick and were overlapped and glued together by a Melamine Urea Formaldehyde (MUF). According to EN 408 [105], the bending strength and the elastic (local and global) moduli were evaluated by means of a four-point bending test campaign on simple supports, carried out on 9 specimens for bending and 4 for shear (Fig. 47).

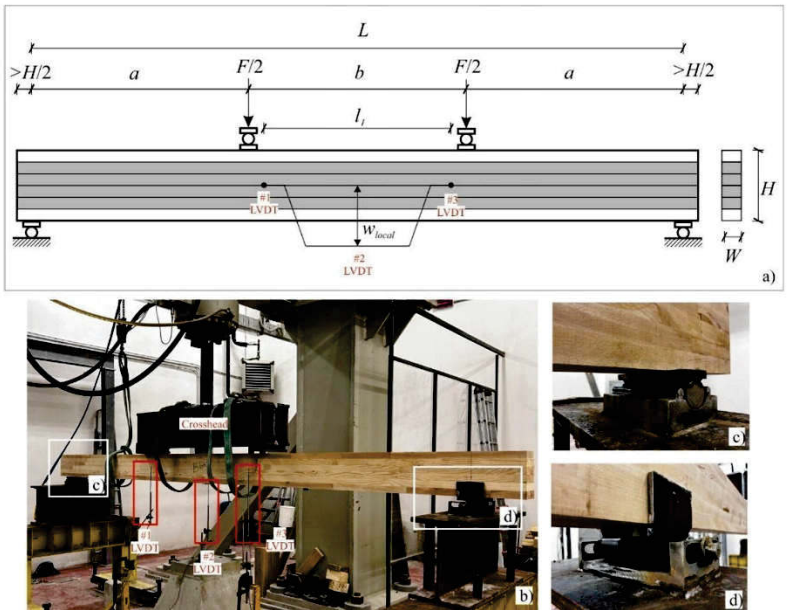

Fig. 47 – a) Geometrical representation of the setup; b) Test setup; c) Hinge detail; d) Carriage 157 detail. W_{local} = local deformation; W = width; H = height; L = test span (18H for bending and 9 H for shear tests); a = b = 6 H for bending and 3 H for shear tests; l1 = distance for the measure of the local deformation = 5 H; F = load.

Following EN 408 [105], bending strength f_m and local modulus of elasticity $E_{m,l}$ were calculated for each sample according to equation 53 and 54.

$$f_m = \frac{3Fa}{WH^2} \tag{53}$$

$$E_{m,l} = \frac{al_1^2(F_2 - F_1)}{16\, I\, (w_2 - w_1)} \tag{54}$$

where F is the maximum recorded force, W is the width of the specimen, H is the height of the specimen, a= 6H, F_1 and F_2 are the 10% and the 40% of the maximum recorded force respectively, w_1 and w_2 are the 10% and the 40% of the maximum average deflection recorded by transducers placed at 2.5h from the centre and I is the moment of Inertia.

Finally, the global elastic modulus can be evaluated by means of equation 55 of EN 408 [105], after obtaining average value, standard deviation and characteristic values of each parameters.

$$E_{m,gl} = \frac{3al^2 - 4a^3}{2WH^3\left(2\frac{w_2 - w_1}{F_2 - F_1} - \frac{6a}{5GWH}\right)} \quad (55)$$

where G is the average value of the shear modulus obtained from the tests.

The tests resulted in mean and characteristic value of $f_{m,k}$=40MPa, $E_{0,mean}$=14,360 MPa, and mean mass density ϱ_m=695 kg/m^3 (Fig. 48). For further detail on the experimental campaign, see [104].

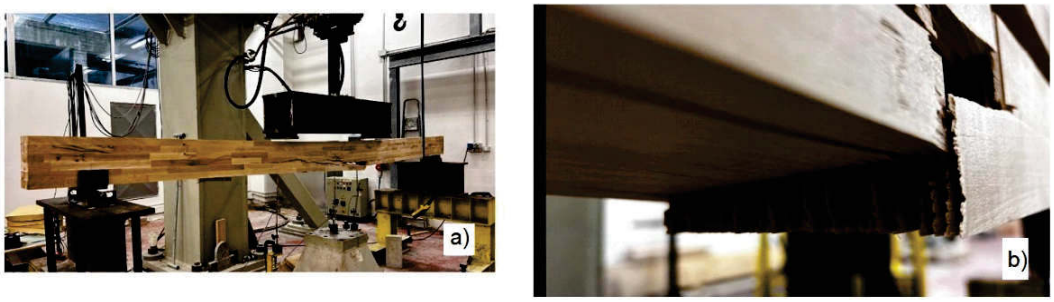

Fig. 48 – a) homogeneous beam failure for bending; b) aligned finger-joints detail.

4.2.2 Upper boards and secondary joists

The upper layer of boards and the secondary joist are made of solid wood, and were visually classified. Since the visual classification of the timber planks resulted in the LS2 class, the strength class was assumed as D24 according to UNI EN 338:2016 [106], which provides also their strength, stiffness and density values. Thus, the following mechanical properties were taken: $f_{m,k}$=24.00 MPa, $E_{0,mean}$=10000 MPa, ϱ_m=580 kg/m^3. For further details, see [103].

4.2.3 Screwed Connection

The connection between principal beams and plank layer was preliminary investigated through 5 pushout tests. The specimen consists of a central timber element and two solid timber elements, symmetrically

arranged and connected by 45° inclined 9x160 mm screws (Fig. 49). The central timber element was obtained by cutting the previously manufactured glulam beech beams, the same structural elements subjected to four-point bending tests. The beam was cut to obtain 560 mm long specimen. The side elements are D24 solid beech boards, the same used for the upper layer of the floor.

Fig. 49 – Pushout test geometrical configuration.

The experimental campaign was carried out at the laboratory of the Department of Civil, Building-Architectural and Environmental Engineering (DICEAA) of the University of L'Aquila. The test setup is shown in Fig. 50.

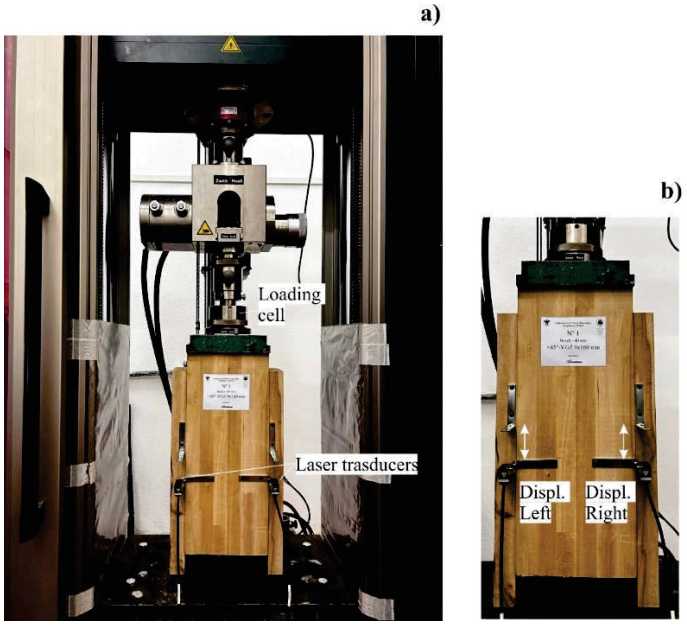

Fig. 50 – Pushout test setup.

The connection performance parameters (i.e. yield point, secant stiffness, ultimate conditions and static ductility) were estimated according to EN 12512 [107] and EN 26891 [108]. The fundamental parameter for the dynamic tests on the floor is the slip modulus K_s of the connections (corresponding to the slip modulus K_{ser} provided by EN 1995-1-1) [38]. It was calculated by means of the following equation:

$$K_s = \frac{0.4F_{est}}{\frac{4}{3}(v_{04} - v_{01})} \tag{56}$$

where v_{01} and v_{04} are the connection slips (evaluated for each specimen) corresponding to loading equal to $0.1 \cdot F_{\text{est}}$ and $0.4 \cdot F_{\text{est}}$ respectively; F_{est} is the estimated maximum load for each configuration based on preliminary tests. The result of the five pushout tests is reported in Fig. 51. In conclusion, for the configuration 9x160 mm 45° degrees inclined screws, K_{ser}=5.97 kN/mm was obtained. For further detail on the test campaign, see [103].

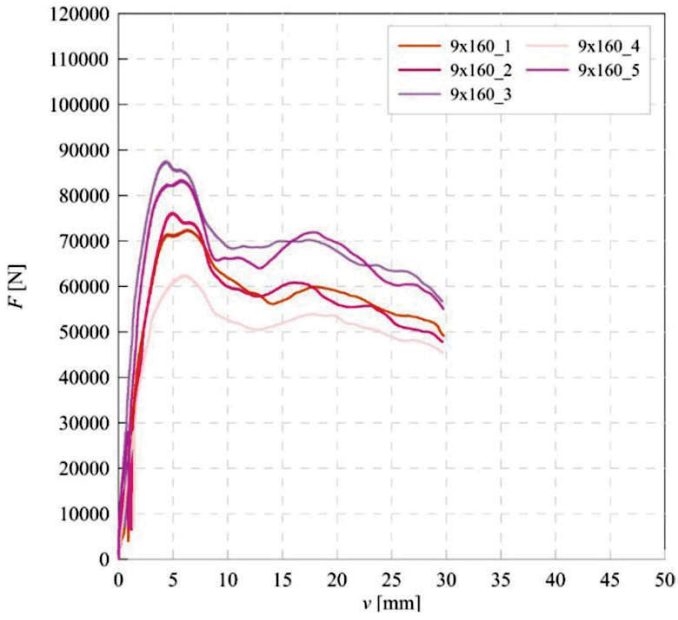

Fig. 51 – Pushout tests curves load vs displacement for 9x160 screws.

4.3 Experimental Setup

The experimental program was carried out according to the test setup schematised in Fig. 52 and Fig. 53. To perform the dynamic tests, the floor was instrumented with three force balance accelerometers, 1.5 kg in weight each, placed in the A0 and A2 positions (¼L and ¾L) and in A1 (the mid-span section). The digital array accelerometric measurement chain was composed by FB SA10 accelerometers produced by Sara Electronic Instruments (Italy), see Fig. 54. The accelerometer had a dynamic range higher than 165 dB from 0.1 Hz to 200 Hz, with a 1 g-full scale. Moreover, the chain was driven by a master recording unit (A0) connected to a Wi-Fi access point and synchronized by GPS receivers to the other receivers. The sample rate of these accelerometers was set at 200 Hz. Furthermore, a smartphone (S0 sensor) was fixed to the floor for the whole experimental campaign, close to the central accelerometer A1, in order to record the vertical acceleration data with a sample frequency of 250 Hz. The S0 sensor consisted of a Xiaomi Redmi Note 7 device with 4 GB RAM and an octa-core processor (2.20 GHz maximum), equipped with a MEMS accelerometer ICM-20607 (Fig. 55).

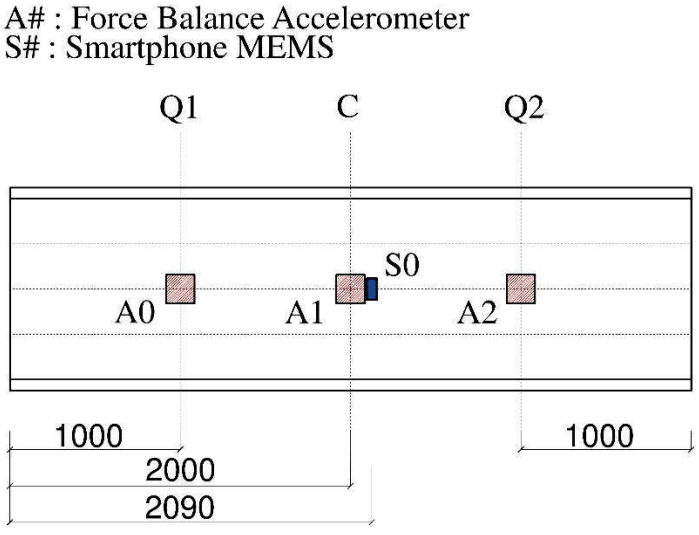

Fig. 52 – Accelerometers and Smartphone setup – plan view.

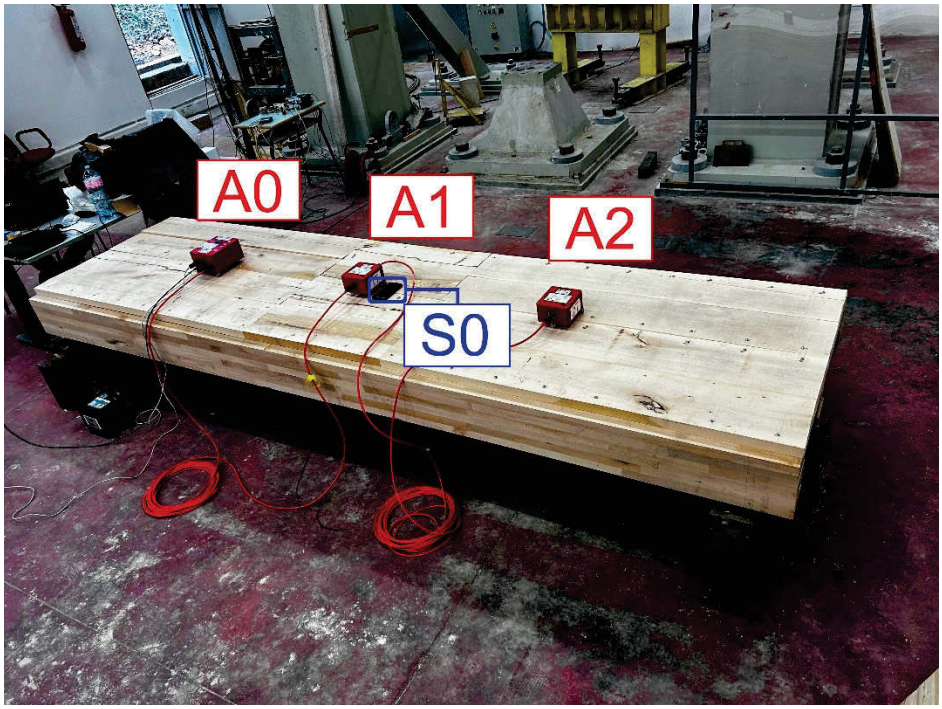

Fig. 53 – Accelerometers and smartphone setup – laboratory view.

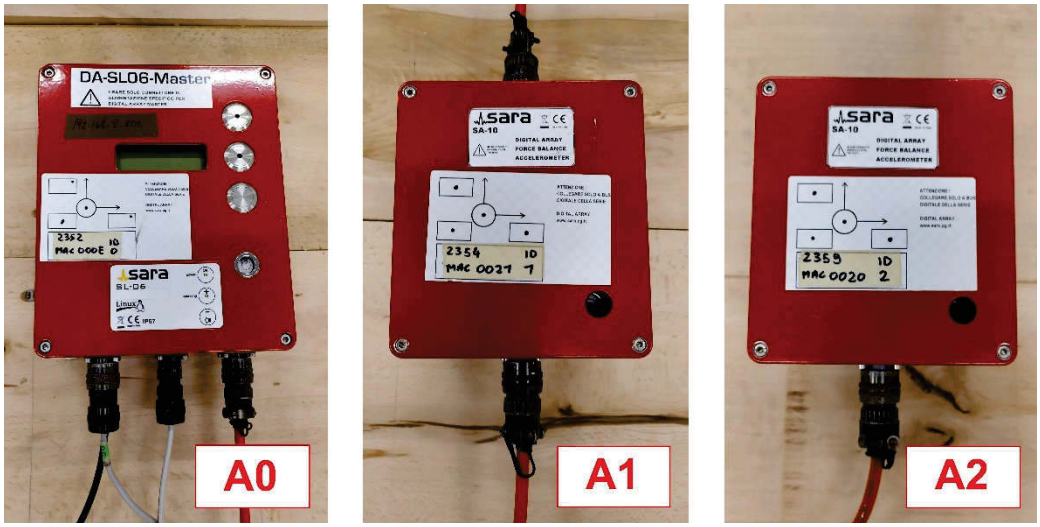

Fig. 54 – Force-Balance accelerometers A0-A1-A2 by SARA.

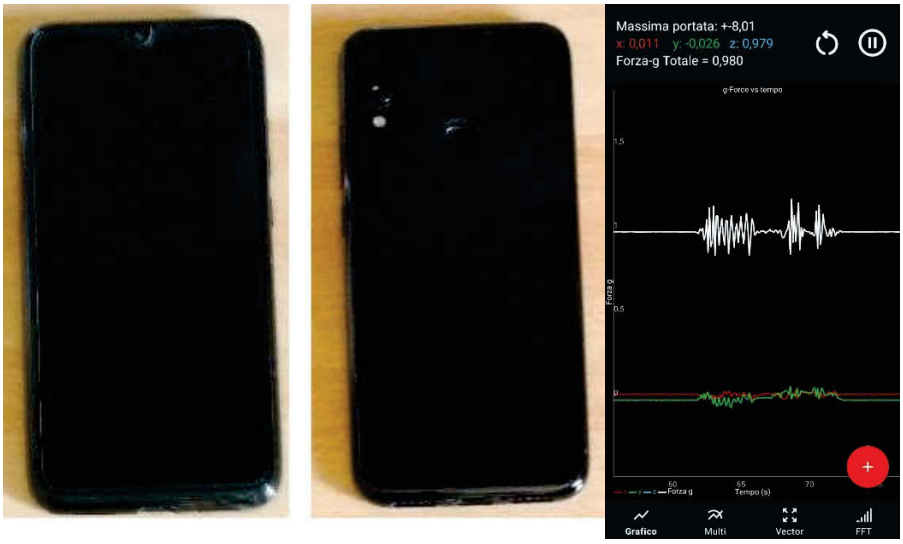

Fig. 55 – Xiaomi Redmi note 7 smartphone and screenshot from "Physics Toolbox Suite" app.

To record the vertical acceleration through the smartphone the free version of the app "Physics Toolbox Suite" was used. This application allows to collect raw data from the accelerometer, up to the maximum frequency supported by the device. With respect with other app tested during this research and in other literature works [12], this solution avoids non-clear manipulation of the data by the app, and "black box" effect due to unknown algorithms. The data collected, in fact, was successively postprocessed by a custom MATLAB script, developed to filter and evaluate comfort parameters starting from raw signals.

Moreover, a 250 Hz sampling frequency was set, higher than the 200 Hz used for the FB accelerometers. The choice aims to mitigate the down sampling of the signal. While an accelerometer is entirely dedicated to the signal collection, a smartphone has background processes than can slow down the sampling [109][110]. Using a higher frequency allows to reduce the cases where a frequency <200 Hz occurs. The signal from the smartphone will need a postprocessing phase of resampling, to make the sample rate constant at 250 Hz.

4.4 Loading protocol

A complete test-schedule was developed, to achieve 33 different load combination.

Two main volunteers were chosen, with different mass M, height H, and height of the center of mass H_G (Table 16). A third volunteer was recruited at the end of the tests to perform a linear path walk.

Table 16 – Pedestrian volunteers mass M, total height H and approximate height of the center of mass H_G.

ID	M [kg]	H [m]	H_G [m]
1	70	1.82	1.07
2	78	1.70	0.96
3	70	1.75	0.97

Furthermore, three walking frequencies were selected for the experimental configurations (1.0-1.5-2.0 Hz). The number of pedestrians walking simultaneously was also varied, considering five possible scenarios:

- a single volunteer walking alone;
- one volunteer walking, with the other standing at midspan;
- two pedestrians;
- a single volunteer jumping alone;
- one volunteer jumping, with the other standing at midspan.

Finally, different walking path were considered (linear and random patterns respectively). The complete set of tests is reported in Table 17 and Fig. 56.

Table 17 – Description of performed walking/jumping tests.

Test	Description
A	Linear path – 1 pedestrian
B	Random path – 1 pedestrian
C	Linear path – 1 ped. + 1 ped.
D	Random path – 1 ped. + 1 ped.
E	Linear path – 2 pedestrians opposite
F	Linear path – 2 pedestrians following
G	Jump – 1 pedestrian
H	Jump – 1 ped. + 1 ped. standing

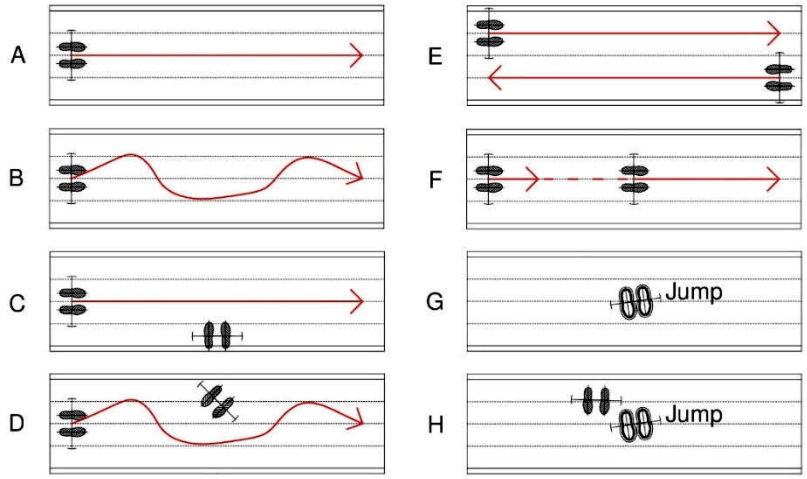

Fig. 56 – Plan view of the performed walking/jumping tests.

4.5 Results

A total of 33 single test were organized, 28 walking and 5 jumping sessions. Each walking session is composed by an average of 10 single walk sequences. Photos from the test program are reported in Fig. 57, showing a typical walk (a) and jump (b).

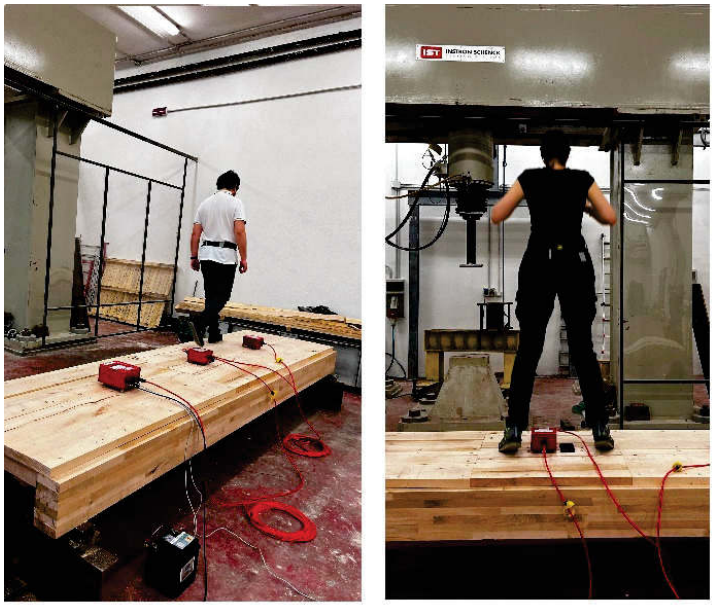

Fig. 57 – Walking (a) and jumping (b) session during the tests.

Table 18 reports all the 33 tests. Provided details are in accordance with the previous paragraph. The Test ID, varying from A (linear path) to H (jumping) is shown together with the pedestrian volunteer ID and the indicative step frequency of walk. The frequencies 1.0-1.5-2.0 Hz are, in fact, only indicative of a slow, normal and fast walk respectively. The metronome was not used to measure the steps, in order to avoid unnatural walking of the volunteers, as observed in [46].

Table 18 – Detail of the 33 performed dynamic walking/jumping tests.

		Pedestrian ID and type:		
Test N.	Test ID	Walking/Jumping	Standing	Step freq. [Hz]
1	A	1		1
2	A	1		1.5
3	A	1		1.5
4	A	1		2
5	G	1		
6	B	1		1.5
7	C	1	2	1
8	C	1	2	1.5
9	C	1	2	1.5
10	C	1	2	2

Test N.	Test ID	Pedestrian ID and type: Walking/Jumping	Standing	Test N.
11	H	1	2	
12	D	1	2	1.5
13	A	2		1
14	A	2		1.5
15	A	2		1.5
16	A	2		2
17	G	1		
18	B	1		1.5
19	C	2	1	1
20	C	2	1	1.5
21	C	2	1	1.5
22	C	2	1	2
23	H	2	1	
24	D	2	1	1.5
25	E	1, 2		1.5
26	F	1, 2		1.5
27	A	1		1
28	A	1		1.5
29	A	1		1.5
30	A	1		2
31	G	1		
32	B	1		1.5
33	A	3		1.5

The vertical acceleration was collected simultaneously by the FB accelerometers and the smartphone sensor. In Fig. 58, an example of data acquisition is reported, overlapping the signals of the S0 and A1 sensors. In particular, the test showing the three indicative step frequencies (Test 1 – 1.0 Hz, Test 2 – 1.5 Hz and Test 3 – 2.0 Hz) and a jump session are reported.

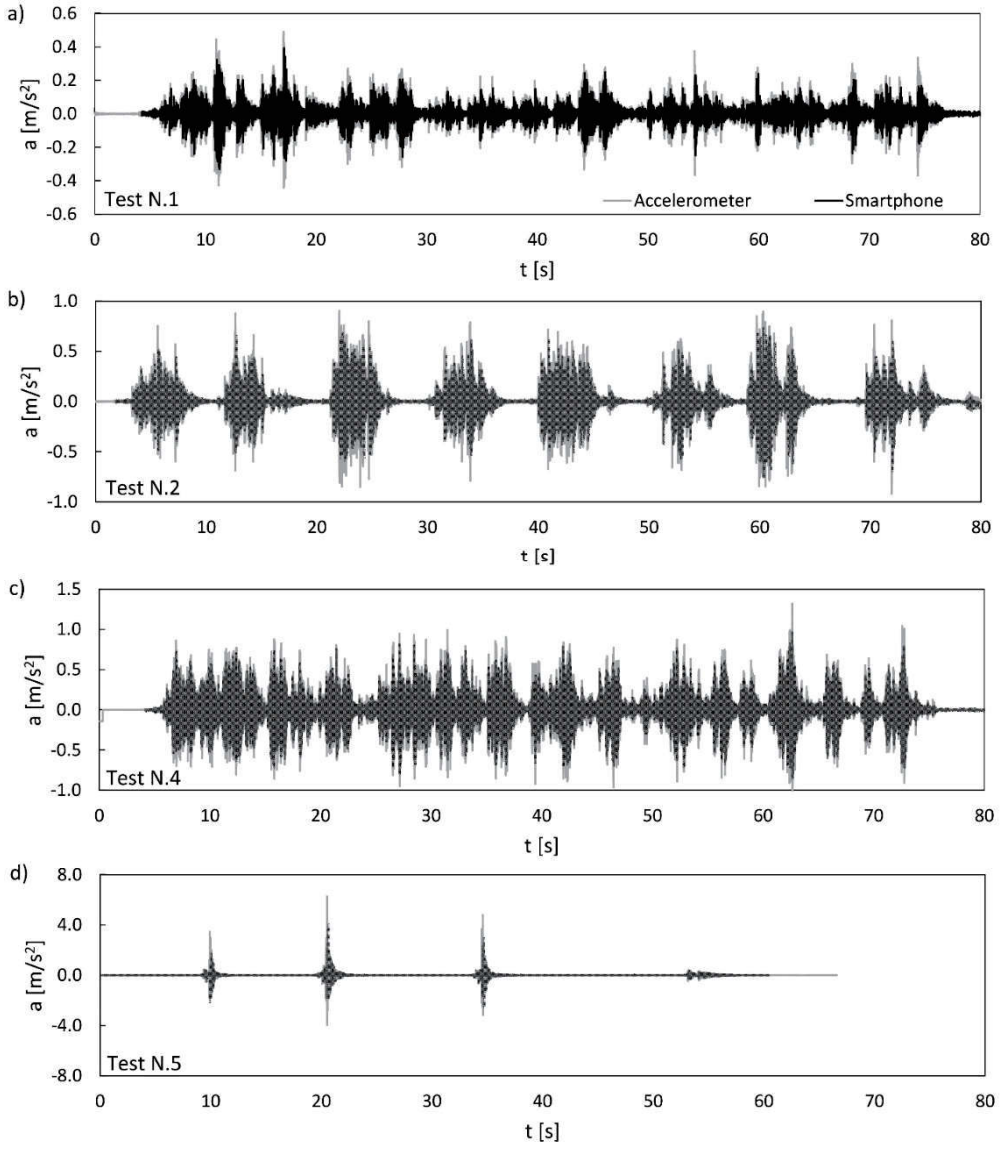

Fig. 58 – Example of recordings obtained during the tests. Slow (a), Normal (b) and Fast (c) walk; Jumping (d).

As mentioned before, to compare the signals, it was necessary to resample the smartphone record. Even if a 250 Hz sample frequency was set, background process in the device caused an irregular sampling between 200 and 250 Hz, with isolated cases with frequency lower than 200 Hz.

To resample the signal, a MATLAB script was developed, which took in input the irregular signal and gave in output the regular 250 Hz record. A linear interpolation resampling was used where necessary. The implementation of polynomial fitting, in fact, led to acceleration peaks showing a numerical rather than physical meaning. A linear interpolation, however, can introduce an error in the maximum acceleration evaluation, since peak can be cut during the resampling. Nonetheless, this passage was necessary to further proceed, and the discrepancy introduced will be englobed in the correction coefficient.

Successively, the signal of sensor A1 and S0 were synchronized. It is worth noticing that the Toolbox app needs a starting input given by a volunteer, and, thus signal have a lag of some seconds. To synchronize the records, the peak accelerations were aligned, processing the data by means of a MATLAB code. Finally, the single walks were isolated, by individuating the minimums between each session. For example, test n. 2 of Fig. 58b was divided in eight single walks (Fig. 59). A total of 237 walking sequences and 26 single jumps were isolated.

Then, the data was further elaborate to obtain the required comfort parameters. In accordance with Section 2.3, the following values were considered:

- Peak acceleration a_{max};
- Root-Mean-Square acceleration a_{rms} (Equation 33)
- Maximum rolling RMS acceleration $a_{R,rms}$ (Equation 48)
- Vibration Dose Value VDV (Equation 37)

To this aim, another MATLAB code was developed, involving all the aforementioned parameters.

To evaluate the maximum peak acceleration, it was sufficient to search for the highest value of the vertical acceleration, in absolute value.

On the other hand, RMS was calculated according to equation 33 and, for the rolling RMS a moving interval of 0.5 s was used, according to [111]. Then, the maximum value of the rolling RMS was taken. To estimate the VDV, a first phase involved the weighting of the vertical recorded acceleration, in accordance to weigh curves of Fig. 34. A pass-band filter was implemented in MATLAB and the VDV was obtained integrating the weighed acceleration according to equation 37.

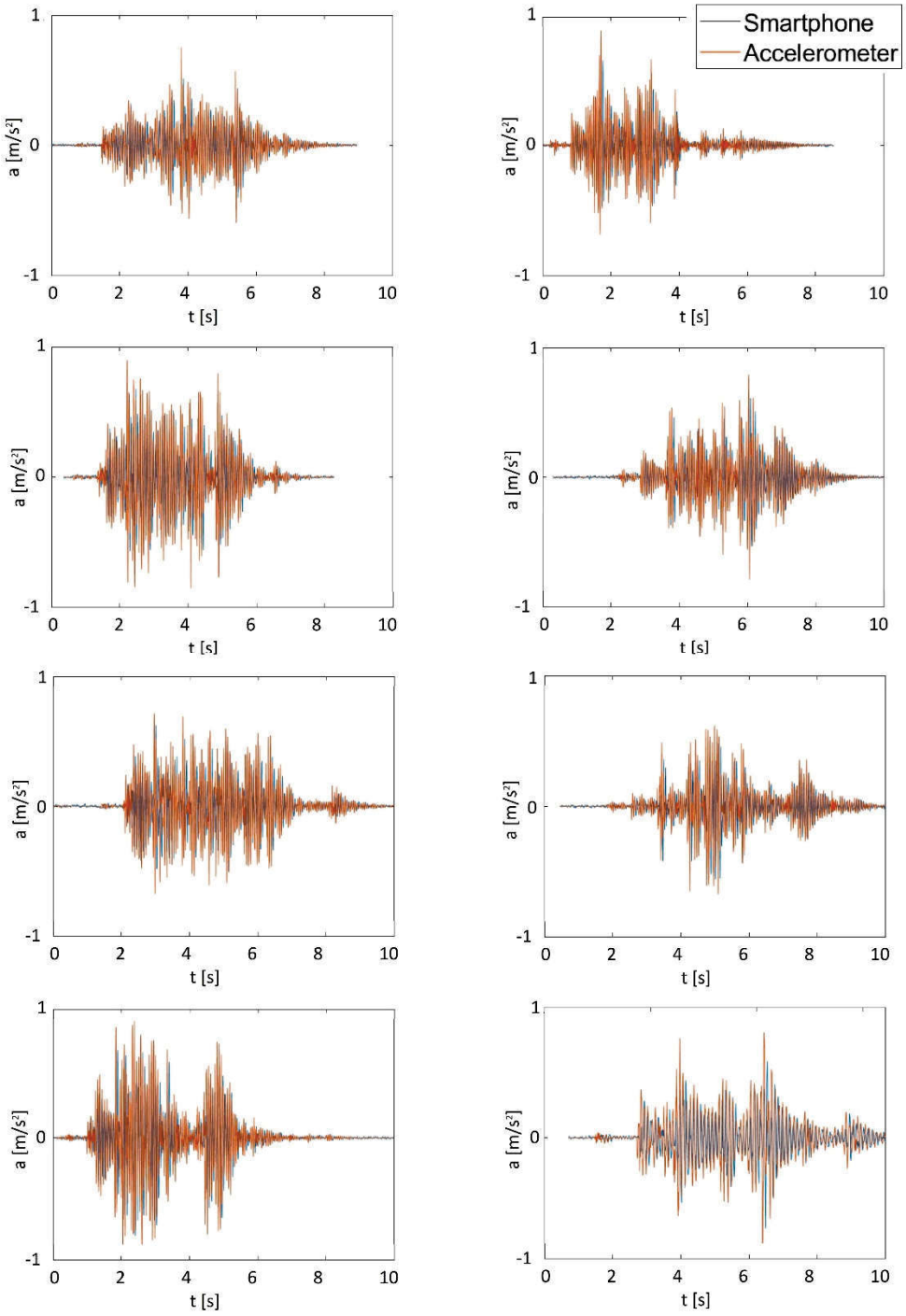

Fig. 59 – Example of test subdivision in single walking segments. Test N.2 is here shown.

The results divided for number of pedestrian volunteers and indicative frequency are herein proposed. Jumps will be postprocessed separately, in the next section. Fig. 60 reports the peak acceleration results for each scenario. Black crosses and black diamonds are the FB accelerometer and smartphone peak accelerations respectively, as obtained for each single walking sequence. A red marker highlights the mean value. A higher sensibility to peak values of the FB devices can be noted, with respect to the smartphone. It is worth noticing that FB are built for ambient excitation measurement, which magnitude is extremely low and, thus, a high sensitivity is necessary. On the other hand, smartphone MEMS do not have the sensitiveness to be used in ambient dynamic identification, since a noise level of ±0.010 m/s2 has been detected. Thus, particular caution has to be used when collecting data of very stiff floor (e.g. concrete slabs). Timber floors are generally flexible, and peak accelerations higher than 0.01 m/s^2 are expected.

A first comparison between the collected data was performed in terms of difference, applying equation 57 to the parameters obtained from FB accelerometers and smartphone:

$$Diff = \frac{p_s - p_a}{p_a} \tag{57}$$

Where p assumes the value of each parameter (a_{max}, a_{rms}, $a_{R,rms}$, VDV) and the subscript s and a stand for smartphone and accelerometer respectively.

From the data, difference between 18% and 27% were found for one pedestrian walking. Difference of -22/-29% and -16/-24% were instead evaluated for one pedestrian walking while one standing, and two volunteers walking respectively (Fig. 60).

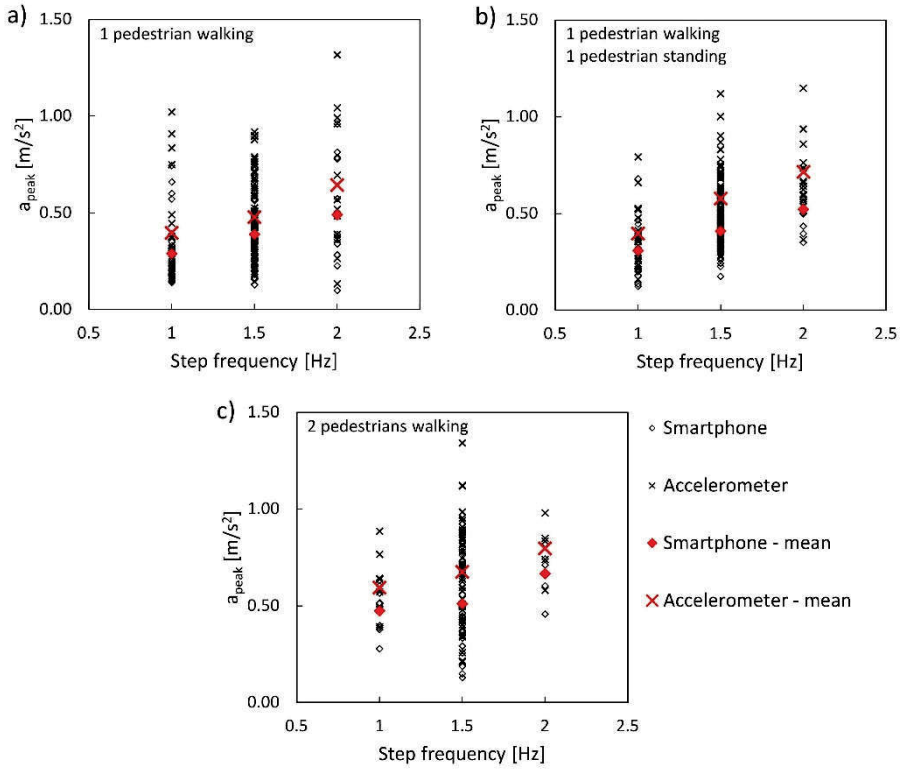

Fig. 60 – Maximum vertical acceleration recorded from FB accelerometer and smartphone sensor – comparison. Mean value are reported in red.

Similarly, the differences between the average values were obtained for RMS (Fig. 61) and maximum rolling RMS acceleration (Fig. 62). Mean differences are slightly lower, since the two parameters are averaged on time. In particular, differences of -19/-22% for one pedestrian, -22/-23% for one pedestrian walking and one standing and -19/-22% for 2 walking volunteers were obtained in terms of RMS. On the other hand, for the RRMS the differences were -19/-22%, -21/-23% and -19/-21% for each case respectively.

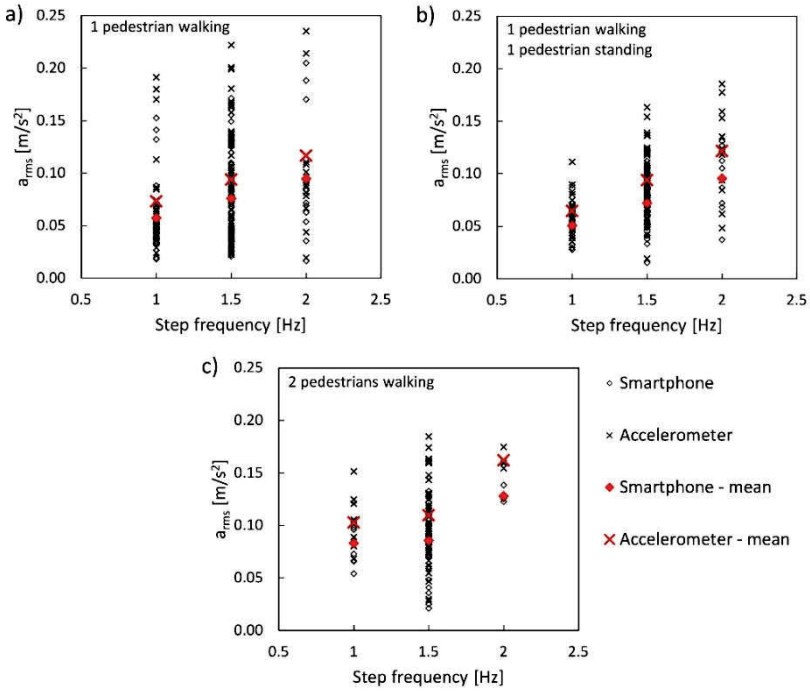

Fig. 61 – RMS acceleration recorded from FB accelerometer and smartphone sensor – comparison. Mean value are reported in red.

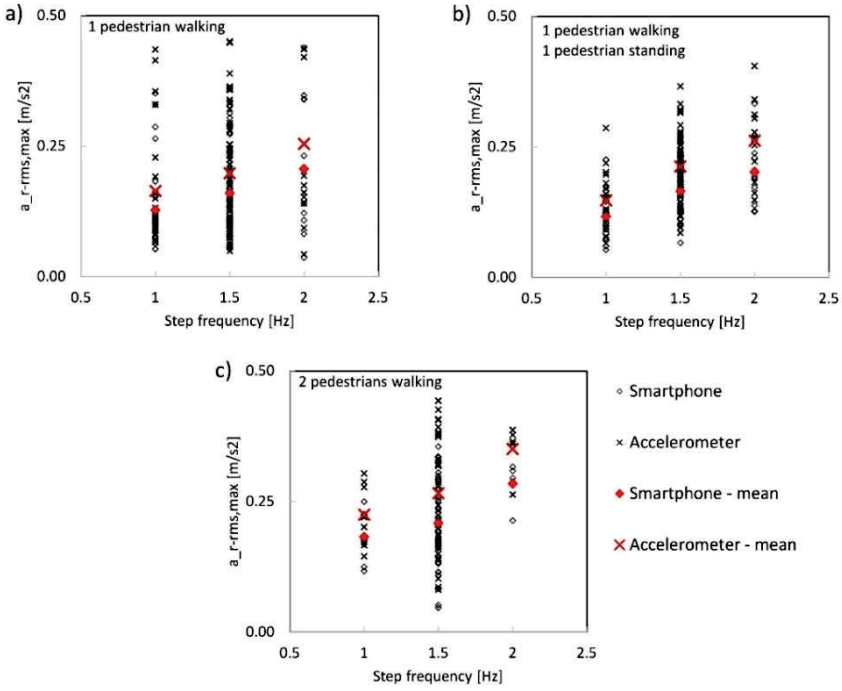

Fig. 62 – Maximum Rolling RMS acceleration recorded from FB accelerometer and smartphone sensor – comparison. Mean value are reported in red.

Finally, the VDV was calculated on the sequences obtained dividing each test (Fig. 63). The mean differences vary between -18% and -20% for one pedestrian, between -14% and -20% for one pedestrian walking and one pedestrian standing and, finally, between -18% and -19% for two pedestrian walking simultaneously. These results highlight that the VDV is the best estimated parameter between the four proposed.

Moreover, the smartphone underestimates the response of the floor, giving results that are typically lower than those from the FB balance accelerometer. In order to use the smartphone for fast assessment a slight overestimation is preferable, to work in sake of security.

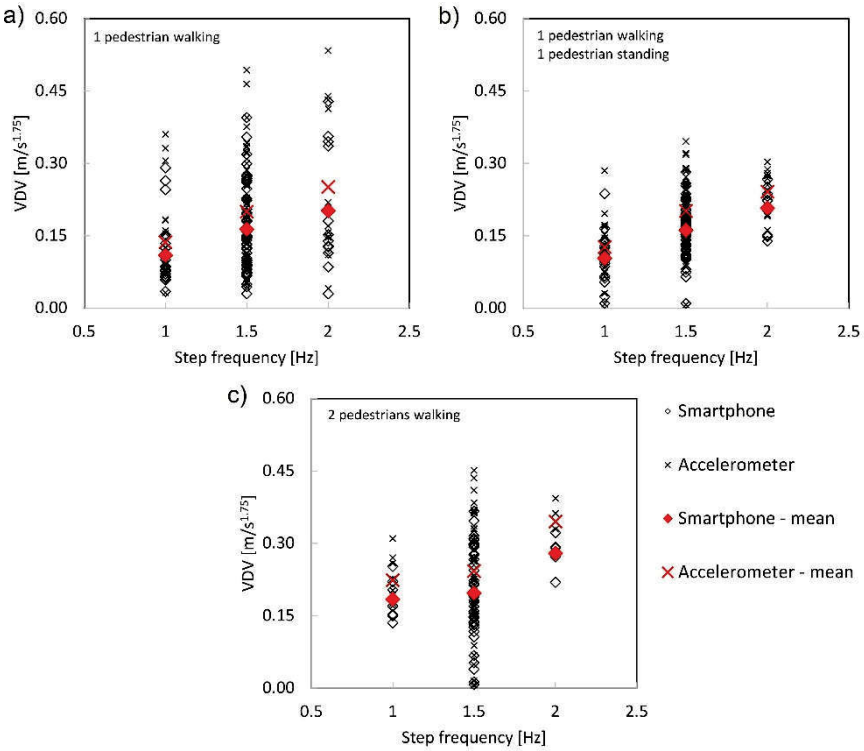

Fig. 63 – VDV calculated from FB accelerometer and smartphone sensor – comparison. Mean value are reported in red.

The jumps were similarly post-processed. They were further divided by number of pedestrians simultaneously on the floor (Fig. 64). In both cases, in fact, only one volunteer jumped and when two are on

the floor, one is considered only as added mass. With respect to the walking results, the parameter obtained from the jumps are more scattered, due to the lower amount of data. Mean differences of -18%/-31% were obtained for peak acceleration (1 and 2 volunteers respectively), -18%/-27% for RMS, -19%/-28% for maximum RRMS and, finally, -16%/-16% for the VDV. Once again, the VDV is the most performant parameter in terms of differences with the FB accelerometers.

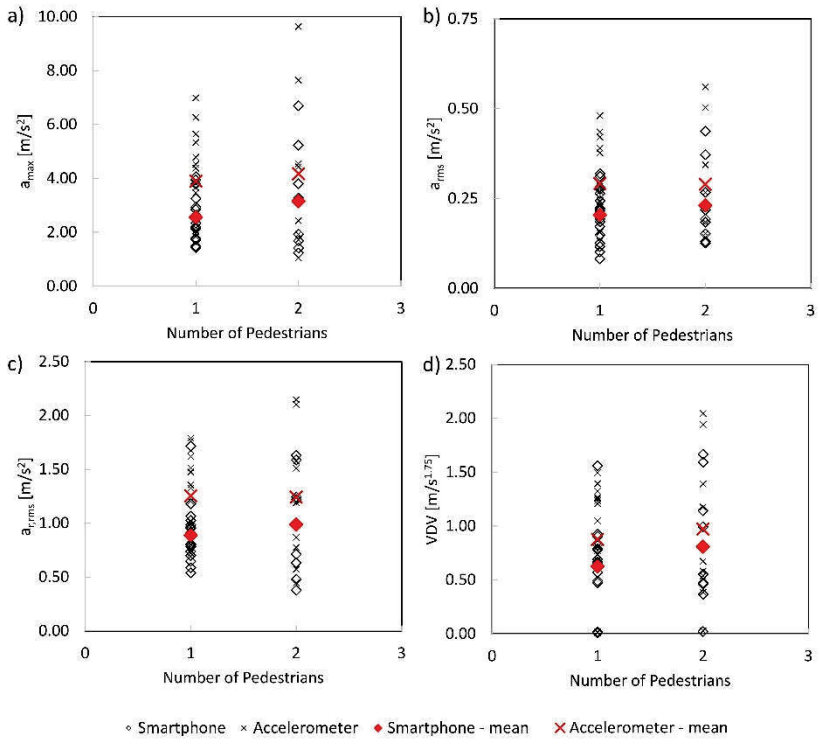

Fig. 64 – Comfort parameters a_{max} (a), a_{rms} (b), $a_{R,rms}$ (c) and VDV (d) for jumps, varying the number of pedestrian simultaneously on the floor. Mean values are reported in red.

4.6 Calibration of correction coefficients

In this section, all the collected data from walking and jumping were statistically analysed, considering each whole sample (237 walking sequences and 26 single jumps).

First, the difference between FB accelerometers and smartphone was computed for the entire sample according to equation 57.

Furthermore, the results will be used to evaluate a set of three coefficient for each comfort parameter. A statistical fit was performed, in order to calculate k_{10}, k_{50} and k_{90}, corresponding to a cumulative probability of 10%, 50% and 90% respectively. The main goal is to obtain a simple-to-use k parameter to be applied during an in-situ test using a smartphone to evaluate the corrected value p as:

$$p_{s,c,n} = k_{y,n} p_s \tag{58}$$

Where p assumes the values as in equation 57, the subscript s stands for smartphone and n assumes the values 10, 50 or 90, depending on the probability chosen. The subscript y can stand for walk (w) or jump (j). The values of k were evaluated in the next paragraph for each parameter, considering the ratio between accelerometer and smartphone recording.

4.6.1 Walking coefficients

To analyse the walking recorded signals, the logistic curve was used. The fit was performed in MATLAB distribution fitter toolbox. Among the normal, lognormal, extreme-value and logistic distribution, the last gave the better results.

Logistic distribution is defined as a continuous distribution function characterized by wider tails than a normal distribution (higher kurtosis). It useful in several applications such as logistic regression, logit models, and neural networks to better predict extreme events.

Cumulative distribution function CDF and probability density function pdf are given in equation 59 and 60:

$$CDF = F(x;\, \mu, s) = \frac{1}{1 + e^{-(x-\mu)/s}} \tag{59}$$

$$pdf = \frac{\partial F(x;\mu,s)}{\partial x} f(x;\, \mu, s) = \frac{e^{-(x-\mu)/s}}{s(1 + e^{-(x-\mu)/s})^2} \tag{60}$$

In which x is the variable, μ is the mean value and s is a scale factor, linked to the variance σ by equation:

$$\sigma^2 = \frac{1}{3}\pi^2 s^2 \tag{61}$$

Complete tables containing each walking segment are reported in Appendix A, for sake of brevity. In the following paragraph, each comfort parameter has been analysed, fitting the results in terms of difference and ratio, and the corrective coefficient k are estimated.

Maximum Acceleration

Equation 57 was applied to evaluate the difference between force-balance and MEMS maximum acceleration. The logistic distribution in terms of density and cumulative probability was overlapped to the experimental data in Fig. 65. The distribution highlights a mean value of -18.7% and a standard deviation of 5.6%.

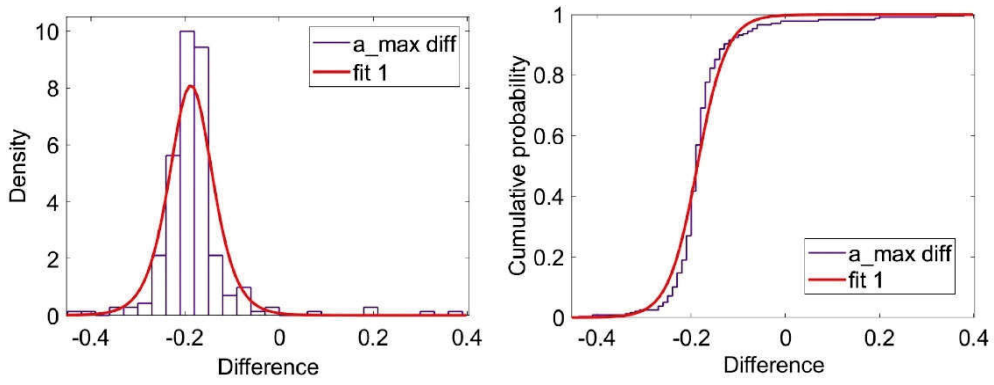

Fig. 65 – Pdf and CDF for the difference between FB and smartphone maximum acceleration.

Furthermore, the ratio A/S between the experimental outcomes of FB accelerometers (A) and smartphone MEMS (S) was also evaluated, showing a mean ratio of 1.31 and a standard deviation of 0.20 (Fig. 66). The quite high standard deviation means scattered results. It is an expected outcome, due to the high sensibility of force-balance accelerometers.

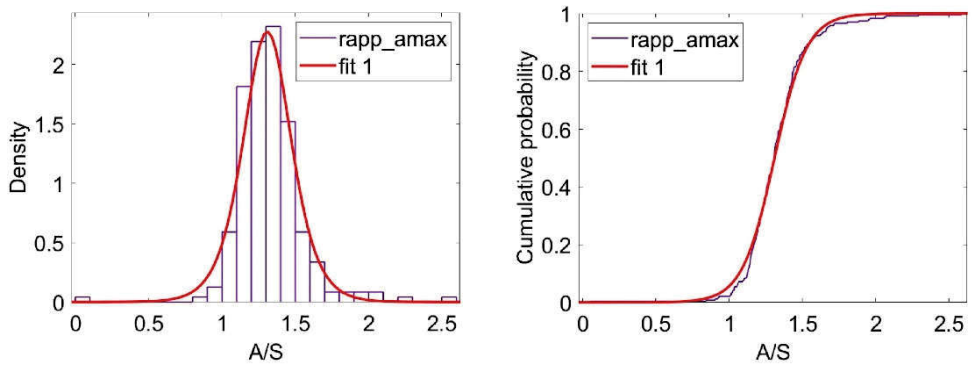

Fig. 66 – Pdf and CDF for the ratio A/S between FB and smartphone maximum acceleration.

The cumulative distribution function of the ratio A/S was used to evaluate the k value at 10%, 50% and 90% of probability, obtaining the values of 1.07, 1.31 and 1.55 respectively.

RMS acceleration

The difference between the root-mean-square acceleration of each signal recorded by the accelerometer was compared to the smartphone recordings (Fig. 67). Choosing the logistic distribution, a -21.2% mean difference was evaluated, with a standard deviation of 4.4%.

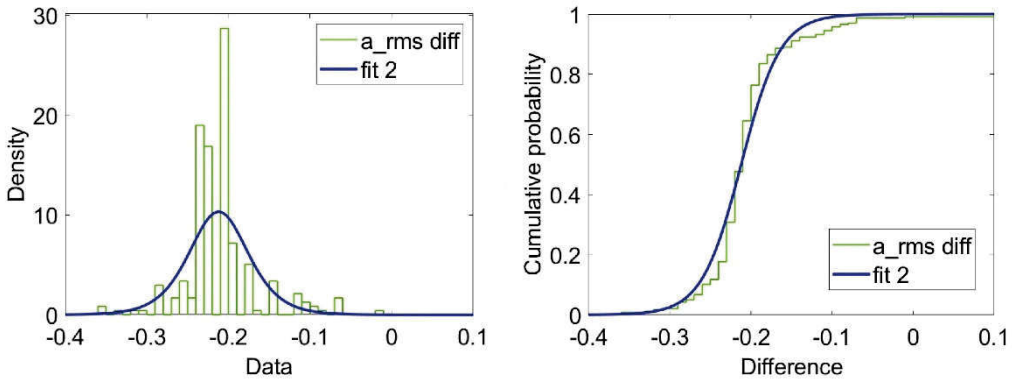

Fig. 67 – Pdf and CDF for the difference between FB and smartphone RMS acceleration.

Moreover, the ratio A/S was calculated, reporting an average of 1.27 and a standard deviation of 0.07 (Fig. 68). As expected, using an

"average method" as the RMS allow to reduce the dispersion of the data, since the acceleration is evaluated on the entire signal duration.

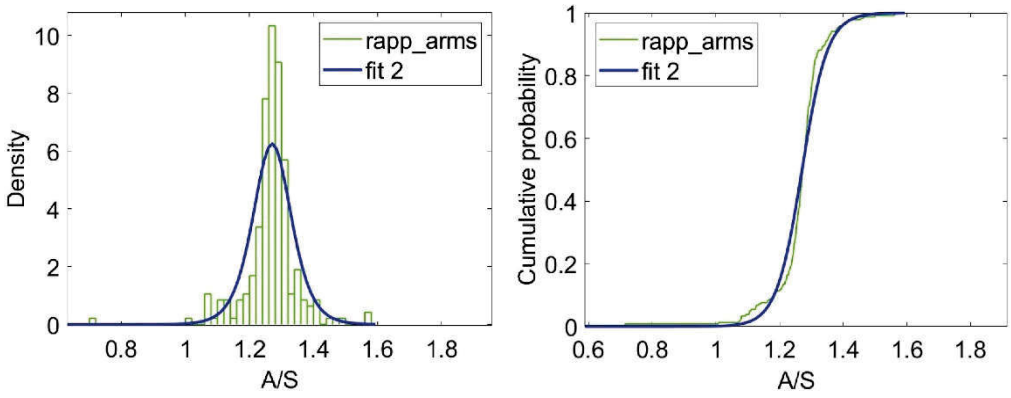

Fig. 68 – Pdf and CDF for the ratio A/S between FB and smartphone RMS acceleration.

The values of k were the evaluated, obtaining 1.18, 1.27 and 1.36 for a cumulative probability of 10%, 50% and 90% respectively.

Rolling RMS maximum acceleration

The maximum values of the rolling root-mean-square acceleration were also compared, using the logistic distribution (Fig. 69). A mean difference of 20.1% and standard deviation of 5.8% were found.

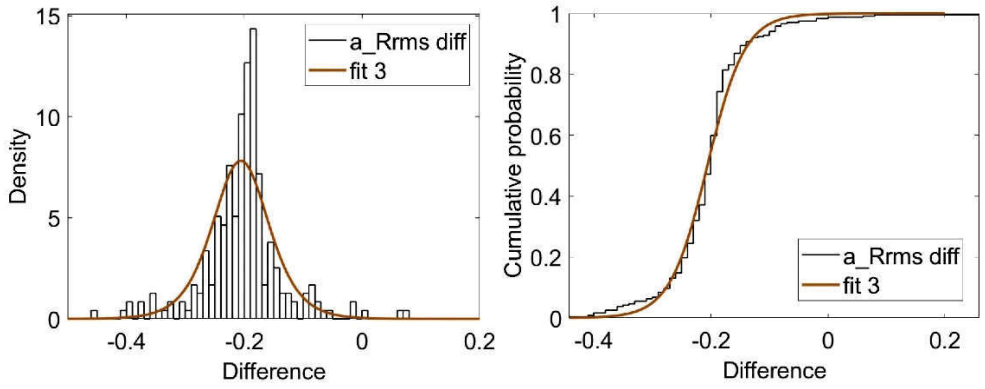

Fig. 69 – Pdf and CDF for the difference between FB and smartphone maximum Rolling RMS acceleration.

However, considering the ratio between the recorded signals, an average value of 1.26 was found, with a standard deviation of 0.10, giving

a better result compared to the maximum vertical acceleration but worse than the rms parameter (Fig. 70).

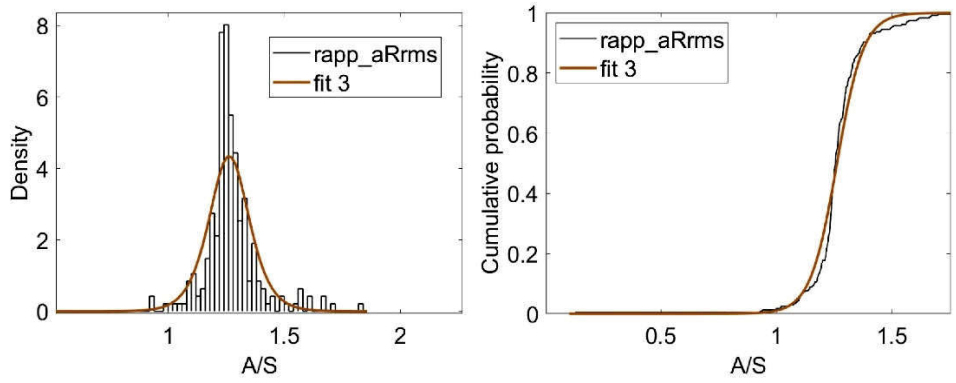

Fig. 70 – Pdf and CDF for the ratio A/S between FB and smartphone maximum Rolling RMS acceleration.

As for the other cases, the cumulative probability function was used to evaluate the correction k. The values 1.14, 1.26 and 1.39 were obtained, for a probability of 10%, 50% and 90%.

Vibration Dose Value

Finally, the evaluation was performed in terms of Vibration Dose Value. The global differences between accelerometer and smartphone were calculated, obtaining an average of -18.7% and a standard deviation of 5.3% (Fig. 71). Compared to the other parameters, the VDV appears to be the better parameter to perform smartphone in-situ tests.

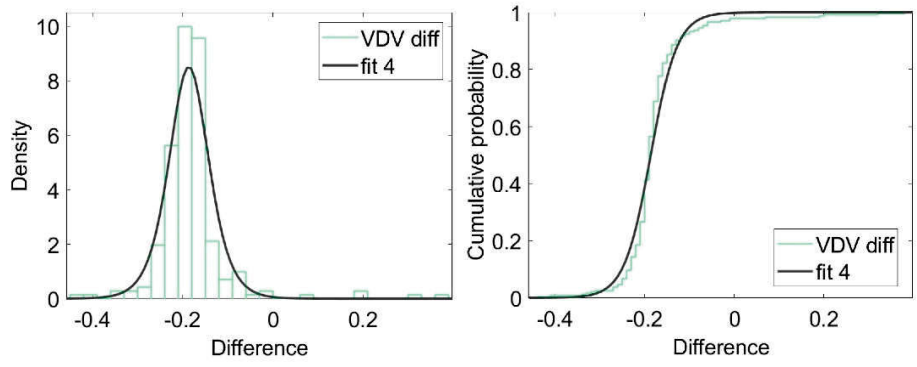

Fig. 71 – Pdf and CDF for the difference between FB and smartphone VDV.

Furthermore, the ratio A/S were calculated and then fitted with a logistic distribution (Fig. 72). A mean ratio of 1.23 was found, the smaller among all the analysed parameters, and a standard deviation of 0.07 was observed, confirming the VDV as best parameter.

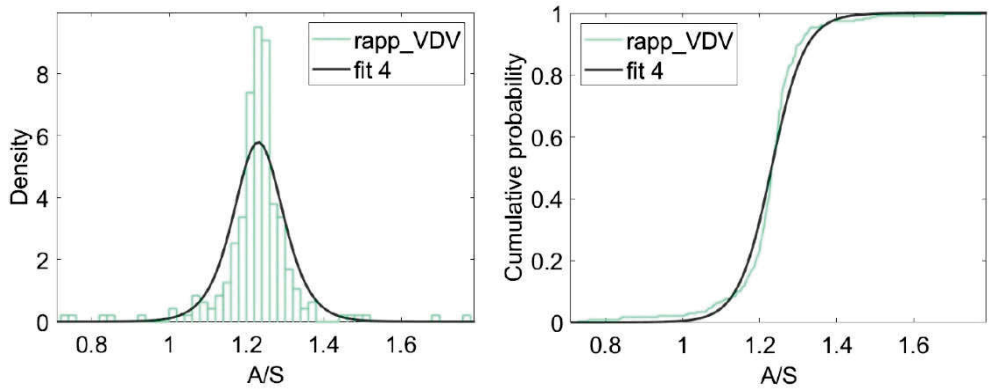

Fig. 72 – Pdf and CDF for the ratio between FB and smartphone VDV.

In conclusion, the correction factors k were obtained from the cumulative distribution. Values equal to 1.14, 1.23 and 1.33 were calculated for probability 10, 50 and 90%.

4.6.2 Jumping coefficients

Similarly to the walking data, the jumping dataset was fitted using MATLAB. The best distribution for the sample was the Generalised Extreme Value distribution, whose probability density function is:

$$pdf = f(x;k,\mu,\sigma) = \frac{1}{\sigma} e^{-\left(1+k\frac{x-\mu}{\sigma}\right)^{\frac{1}{k}}\left(1+k\frac{x-\mu}{\sigma}\right)^{-1-\frac{1}{k}}} \quad (62)$$

For:

$$1 + k\frac{x-\mu}{\sigma} > 0$$

In which k is the shape parameter, μ is the location parameter and σ the scale parameter.

The generalized extreme value distribution is frequently used to model the smallest or largest value among a large set of independent, identically distributed random values. The generalized extreme value combines three simpler distributions into a single form, allowing a continuous range of possible shapes. The distribution can be used to model dataset of block maxima and automatically fit the appropriate distribution among the three, based on provided dataset. The three distributions included in the generalised are referred to as the Types I, II, and III. Exponentially decreasing tail distribution (e.g. normal) lead to the Type I, while distributions whose tails decrease as a polynomial (e.g. Student's) lead to the Type II. Finally, finite tail distributions (e.g. beta) lead to the Type III.

The values obtained analysing the jumping data could be useful to correct in-situ test related to impulsive force as jumping but also heel drop.

Maximum Acceleration

As for the walking signals, the data related to jumps were also analysed in terms of difference between force-balance and MEMS recording. Applying a GEV distribution fitting to the data, for the maximum acceleration a mean value of -26.6% and a standard deviation of 15.3% (Fig. 73). The results are highly dispersed. A first reason is related to the lower amount of recording with respect to the walking test. Moreover, the force balance accelerometer is very sensitive to peak signals, recording much higher values than the smartphone accelerometers.

In terms of ratio A/S, the mean value of 1.40 was obtained, together with a standard deviation of 0.27, thus confirming the aforementioned observation linked to the difference between results (Fig. 74). The k value was finally evaluated: 1.10, 1.43 and 1.70 for a cumulative probability of 10, 50 and 90% respectively.

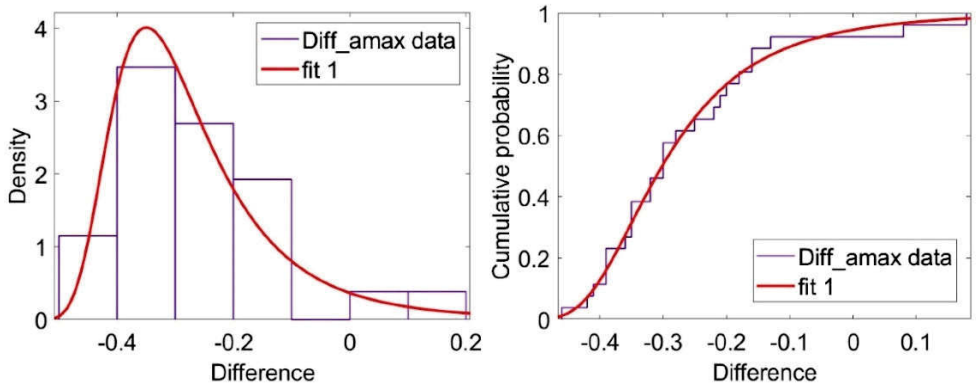

Fig. 73 – Pdf and CDF for the difference between FB and smartphone maximum acceleration - jumps.

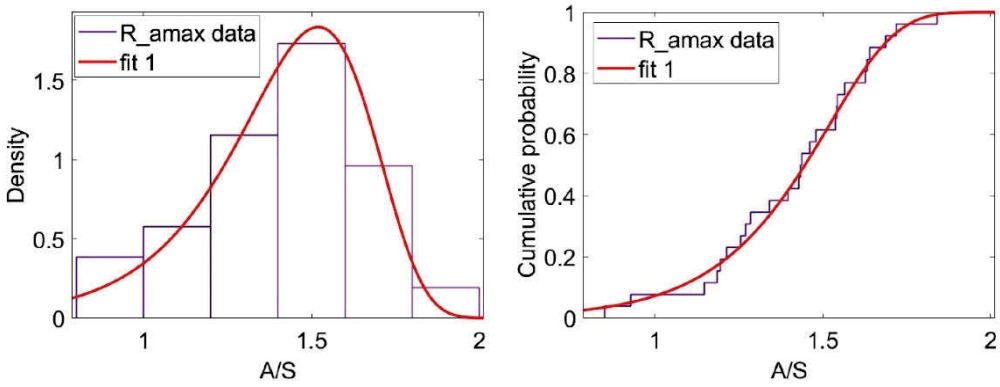

Fig. 74 – Pdf and CDF for the ratio A/S between FB and smartphone maximum acceleration - jumps.

RMS acceleration

Root-mean-square data are more incomplete then maximum acceleration, showing some empty bins in the histogram. The GEV curve was the best found fit to the data (Fig. 75). An average difference of -23.9% was found, and a standard deviation of 12.6% evaluated, thus confirming the high scattering of the records.

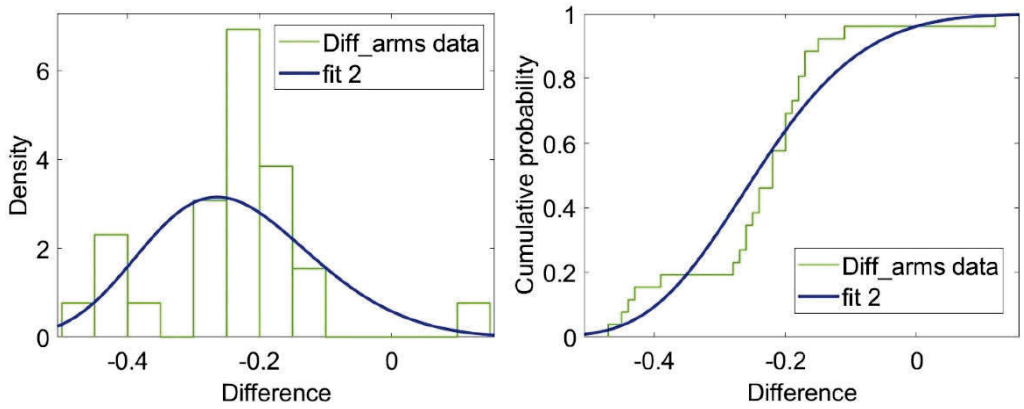

Fig. 75 – Pdf and CDF for the difference between FB and smartphone RMS acceleration - jumps.

The mean ratio of 1.35 and standard deviation of 0.22 show a better result of this parameter with respect to the maximum acceleration (Fig. 76). From the cumulative probability function the value of 1.09, 1.33 and 1.65 were extracted, corresponding to a probability of 10, 50 and 90%.

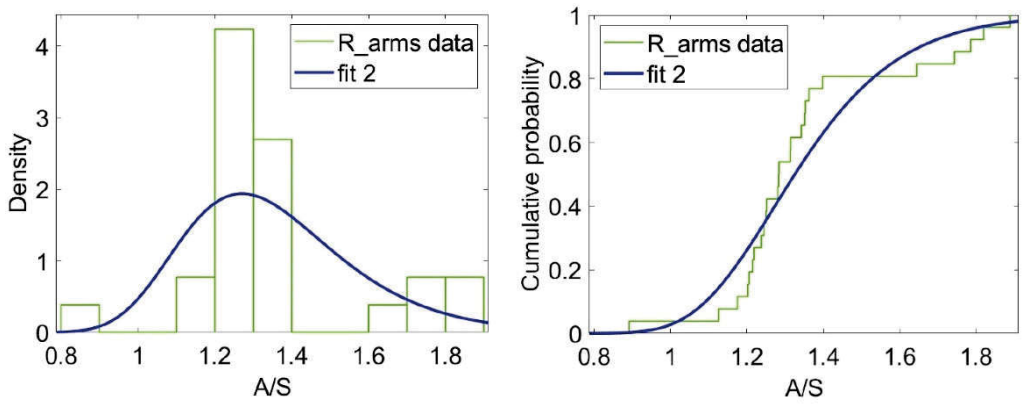

Fig. 76 – Pdf and CDF for the ratio A/S between FB and smartphone RMS acceleration - jumps.

Rolling RMS maximum acceleration

Empty bins were also observed in the evaluation of the difference between maximum rolling rms. In particular, the GEV distribution gave an average difference of -24.5% and a standard deviation of 13.3%, results that match with the rms evaluation of the previous paragraph (Fig. 77).

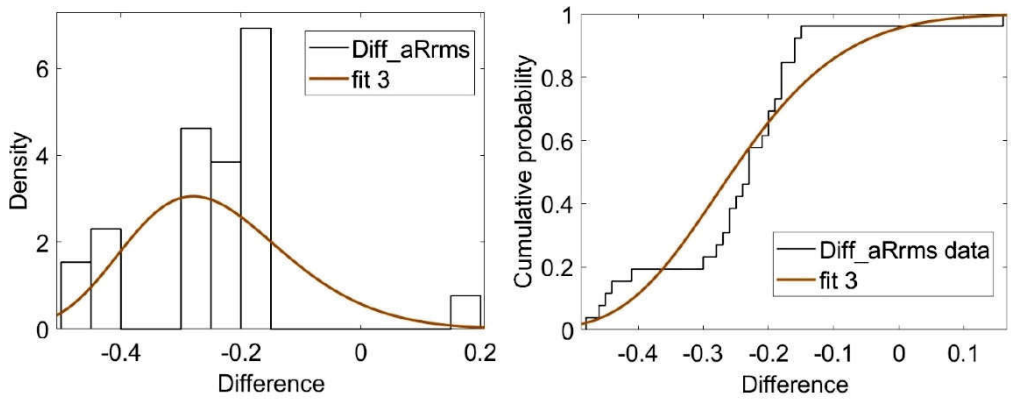

Fig. 77 – Pdf and CDF for the difference between FB and smartphone maximum Rolling RMS acceleration - jumps.

Moreover, also the ratio A/S gave result comparable to the rms values, highlighting an average ratio of 1.37 and a standard deviation of 0.24 (Fig. 78). The k values are then evaluated following the cumulative probability GEV distribution: 1.09, 1.34 and 1.69 for 10, 50 and 90% respectively.

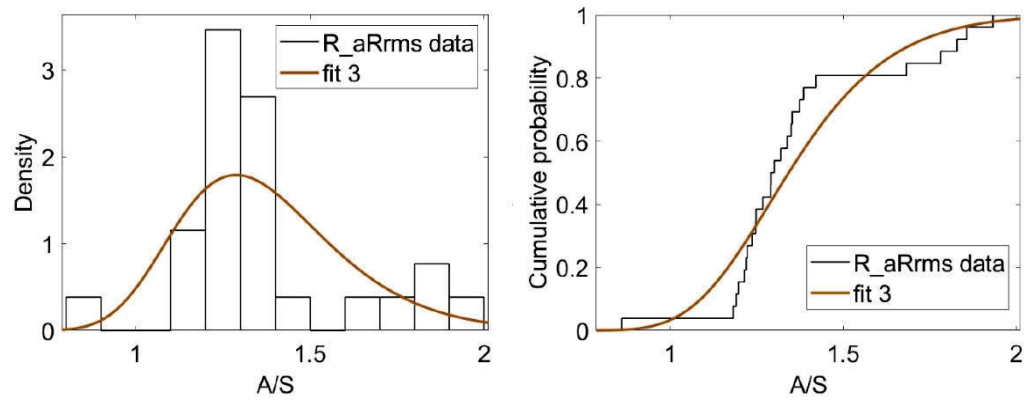

Fig. 78 – Pdf and CDF for the ratio A/S between FB and smartphone maximum Rolling RMS acceleration - jumps.

Vibration Dose Value

Finally, the VDV differences were evaluated for the jumping tests. As for the walking recordings, also for the jump the VDV gave the best

results (Fig. 79), showing the smaller average difference of -20.9%. Nonetheless, the standard deviation is high (15.2%).

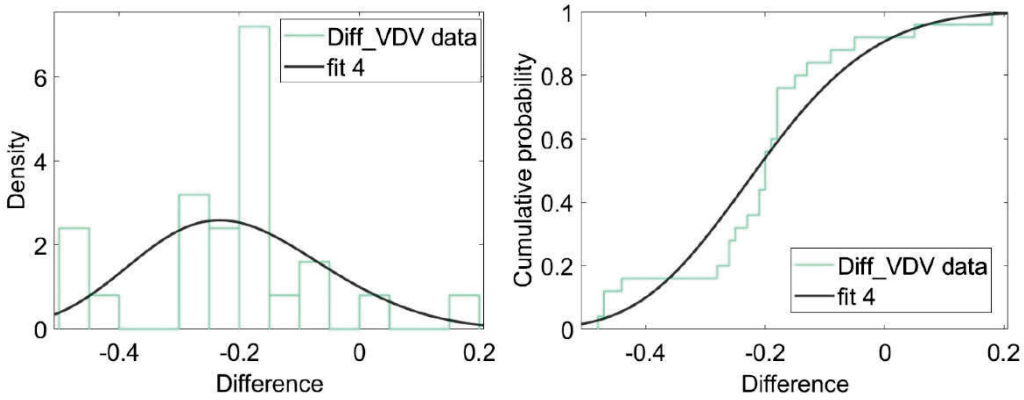

Fig. 79 – Pdf and CDF for the difference between FB and smartphone VDV - jumps.

The ratio A/S, on the other hand, gave an average of 1.32 with a standard deviation of 0.26 (Fig. 80). Finally, the correction factors were evaluated. A k equal to 1.02, 1.28 and 1.67 were obtained for a cumulative probability of 10, 50 and 90%.

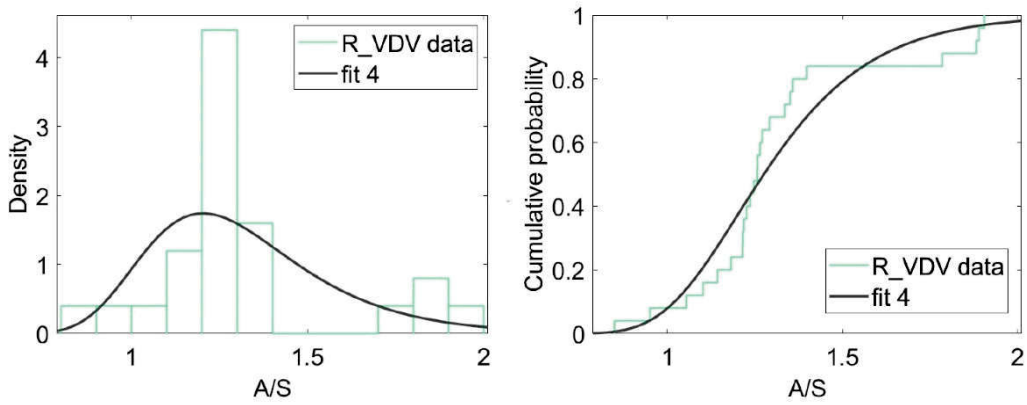

Fig. 80 – Pdf and CDF for the ratio A/S between FB and smartphone VDV - jumps.

4.6.3 Summary

The major outcomes of the data analysis are herein reported. Table 19 shows the k_w values obtained for the walking correction of

smartphone recordings. It is worth noticing that this procedure is related to one smartphone only, but the process can be replicated to other devices. The aim of the work is to demonstrate that modern smartphone can substitute professional accelerometer for fast in-situ comfort tests.

The value corresponding to the 50% of the probability should be used to correct the smartphone recording, since a balance between accuracy and slight overestimation can be achieved. Using the $k_{w,10}$ could lead to better results, but there is the possibility of underestimation of the signals. Since a fast in-situ strategy is the goal, a conservative overestimation is pursued. On the other hand, the use of $k_{w,90}$ seems to be too conservative.

The validity of the k_w will be tested in different case study at the end of the thesis.

Table 19 – Corrective coefficient $k_{w,p}$ for walking signals recorded by smartphone, where p is the cumulate probability 10-50-90.

	$k_{w,n}$		
CP (%):	10	50	90
a_{max}	1.07	1.31	1.55
a_{rms}	1.18	1.27	1.36
$a_{R,rms}$	1.14	1.26	1.39
VDV	1.14	1.23	1.33

Furthermore, the optimal number of walks was evaluated, in order to give a protocol to follow during in-situ tests. To this aim, eight scenarios were built, considering the possibility of performing 5, 10, 20, 30, 40, 50, 60 or 70 walks on the floor. For each scenario, 2000 possible combination of single walks were extracted from the laboratory test database for each type of scenario. The corrected mean ratio between accelerometer and smartphone records was evaluated for each combination and the results are proposed in Fig. 81.

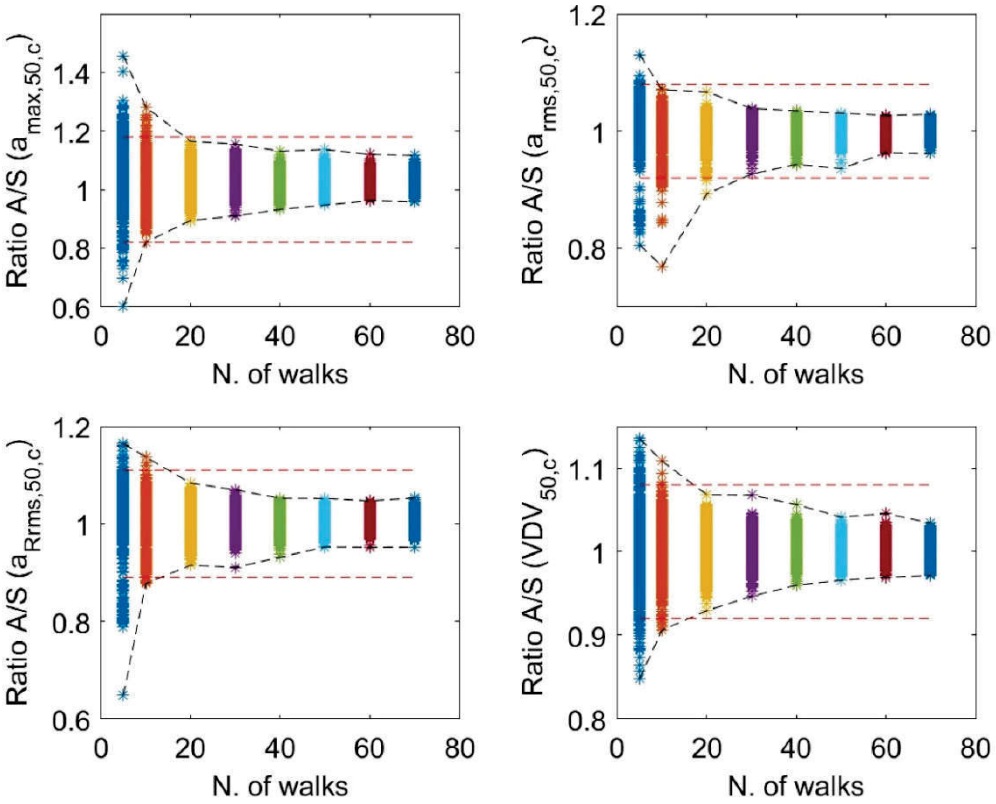

Fig. 81 – Statistical evaluation of the minimum number of walks needed to have a mean value of the parameter inside the ±1 standard deviation (highlighted by the red dashed lines).

The red dashed line represents the boundary mean ± one standard deviation, where the mean and the standard deviation were based on the entire laboratory test database of walks. The main goal was to not exceed those boundaries, thus having a number of walks which gave a reliable output with respect to the laboratory programme. The results are reported in Table 20.

Since 30 walks are borderline with the threshold, a total of 40 walks can be chosen. The programme should follow the given schedule:

- 10 Normal walk (1.0-1.5 Hz) Longitudinal;
- 10 Fast walk (2.0 Hz) Longitudinal;
- 10 Normal walk (1.0-1.5 Hz) Transversal;
- 10 Fast walk (2.0 Hz) Transversal.

Table 20 – Result of the statistical simulation of the minimum number of walks. In yellow the combinations which were inside the target boundaries.

Ratio A/S N. Walks	a_{max}			a_{rms}			a_{Rrms}			VDV		
	mean	**max**	**min**	**mean**	**max**	**min**	**mean**	**max**	**min**	**mean**	**max**	**min**
5	1.03	1.46	0.60	1.01	1.13	0.81	1.01	1.17	0.65	1.00	1.14	0.85
10	1.03	1.28	0.82	1.00	1.07	0.77	1.01	1.14	0.88	1.00	1.11	0.91
20	1.03	1.17	0.89	1.00	1.07	0.89	1.01	1.08	0.92	1.00	1.07	0.93
30	1.03	1.16	0.91	1.00	1.04	0.93	1.01	1.07	0.91	1.00	1.07	0.95
40	1.03	1.13	0.93	1.00	1.03	0.94	1.01	1.05	0.93	1.00	1.06	0.96
50	1.03	1.14	0.95	1.00	1.03	0.94	1.01	1.05	0.95	1.00	1.04	0.97
60	1.03	1.12	0.96	1.00	1.03	0.96	1.01	1.05	0.95	1.00	1.05	0.97
70	1.03	1.12	0.96	1.00	1.03	0.96	1.01	1.05	0.95	1.00	1.03	0.97
	Target:	**1.18**	**0.82**	**Target:**	**1.08**	**0.92**	**Target:**	**1.11**	**0.89**	**Target:**	**1.08**	**0.92**

Where the longitudinal direction coincides with the principal joists' orientation. Forty walks may seem excessive or time consuming. However, it is worth to know that each walk lasts between 5-10 seconds, depending on the floor. Thus, ten minutes are needed.

Table 21 presents the k_j values obtained for the impulsive in-situ test. Given the strategy described for k_w regarding the choice of the best cumulative probability, it is worth noticing that the results of the jumping tests were quite scattered, and worst fit and standard deviation were obtained. Thus, the coefficients have limited validity.

Table 21 – Corrective coefficient $k_{j,p}$ for jumping signals recorded by smartphone, where p is the cumulate probability 10-50-90.

		$k_{j,n}$		
(%):	CP	10	50	90
	a_{max}	1.10	1.43	1.70
	a_{rms}	1.09	1.33	1.65
	$a_{R,rms}$	1.09	1.34	1.69
	VDV	1.02	1.28	1.67

An analogous procedure was followed to individuate the minimum jumps needed to reproduce the laboratory test. Eight jumping scenarios were created (3, 5, 8, 10, 12, 15, 18, 20 jumps) and 500 combinations were randomly generated. Corrected ratio between accelerometer and smartphone are reported in Fig. 82.

The minimum jumps to not trespass the threshold are reported in Table 22.

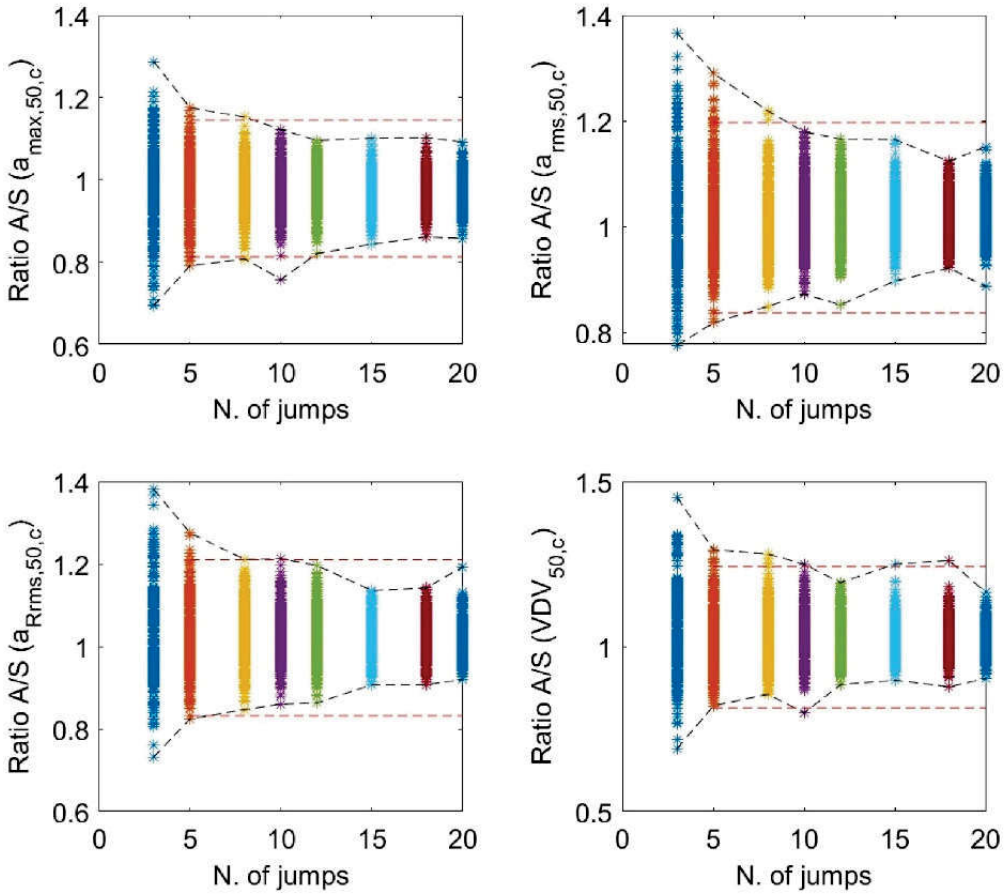

Fig. 82 – Statistical evaluation of the minimum number of jumps needed to have a mean value of the parameter inside the ±1 standard deviation (highlighted by the red dashed lines).

Table 22 – Result of the statistical simulation of the minimum number of jumps. In yellow the combinations which were inside the target boundaries.

Ratio A/S N. Jumps	a_{max}			a_{rms}			a_{Rrms}			VDV		
	mean	max	min	mean	max	min	mean	max	min	mean	max	min
3	0.98	1.29	0.70	1.01	1.37	0.78	1.02	1.38	0.73	1.04	1.45	0.69
5	0.98	1.18	0.79	1.02	1.29	0.82	1.02	1.28	0.82	1.02	1.29	0.82
8	0.99	1.15	0.81	1.02	1.22	0.85	1.03	1.21	0.85	1.03	1.28	0.86
10	0.98	1.12	0.76	1.02	1.18	0.87	1.03	1.21	0.86	1.03	1.25	0.80
12	0.98	1.10	0.82	1.02	1.17	0.85	1.02	1.20	0.86	1.03	1.19	0.88
15	0.98	1.10	0.84	1.02	1.16	0.90	1.02	1.14	0.91	1.03	1.25	0.90
18	0.98	1.10	0.86	1.02	1.12	0.92	1.02	1.14	0.91	1.03	1.26	0.88
20	0.98	1.09	0.86	1.02	1.15	0.89	1.02	1.19	0.92	1.02	1.16	0.90
	Target:	**1.15**	**0.81**	**Target:**	**1.20**	**0.84**	**Target:**	**1.21**	**0.83**	**Target:**	**1.24**	**0.82**

Thus, a minimum of 12 jumps should be taken, in the centre of the tested floor. It is worth noticing that the dimension of the data of the test is limited (since the aim was walking testing the floor) and the number of single tests could be not sufficient.

In conclusion the testing protocol is here summarized in Fig. 83:

4.7 Final remarks

In this context, it is also important to remind that the presently reported laboratory tests were performed on a 1-way, three joist floors prototype only, which may not be representative of the response of a full-scale timber floor.

For this reason, a finite element model of the same full-scale specimen was developed SAP2000 [112], according to the geometrical and mechanical properties of its timber components (Fig. 84). Frame elements were used for primary and secondary joist, and a thin-shell was implemented for the boards covering. Furthermore, elastic link elements were used at the interface, to describe the effect of screwed connections. A simply supported boundary condition was finally taken into account.

Phase 1 - Preparing

Open the app to record vertical acceleration and set the sampling frequency to 200Hz/250Hz.

Fix the smartphone to the surface at midspan. Avoid unstable positioning, such as broken tiles or deformed parquet. Use strong bi-adhesive tape.

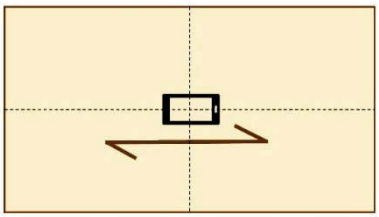

Phase 2 -Testing - Walks

Start the acquisition on the smarphone and go to the starting position for longitudinal walks.

Wait a couple of seconds, drop the heel and wait another couple of seconds (the heel drop signals the beginning of the test

Perform 10 walks at normal pace (1.0-1.5 Hz).

Perform 10 walks at fast pace (2.0 Hz).

Wait a couple of seconds, drop the heel and wait another couple of seconds (the heel drop signals the end of the test phase).

Stop the acquisition.

Start the acquisition on the smarphone and go to the starting position for transversal walks.

Wait a couple of seconds, drop the heel and wait another couple of seconds (the heel drop signals the beginning of the test

Perform 10 walks at normal pace (1.0-1.5 Hz).

Perform 10 walks at fast pace (2.0 Hz).

Wait a couple of seconds, drop the heel and wait another couple of seconds (the heel drop signals the end of the test phase).

Stop the acquisition.

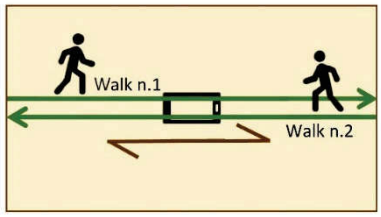

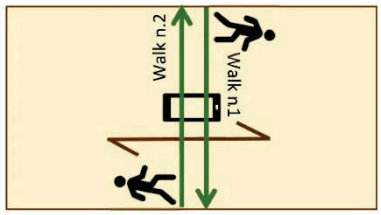

Phase 3 -Testing - Heeldrops

Start the acquisition on the smarphone and stand 20-30 cm aside, in proximity of midspan.

Perform 12 heeldrops, waiting a couple of second between each one.

Wait a couple of seconds after the last one.

Stop the acquisition.

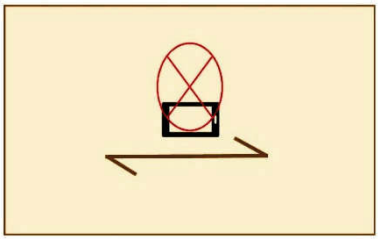

Phase 4 - Postprocessing

Manual processing: extract the data from the files corresponding to the tests and evaluat the needed parameters. Apply the k_{50} coefficient to the parameter to have the corrected values.

Automated processing: Extract the three files corresponding to the tests and apply the MATLAB routine to analyse them; the correction is applyed automatically.

	k_w				k_j		
CP (%):	10	50	90	CP (%):	10	50	90
a_max	1.07	1.31	1.55	a_max	1.1	1.43	1.7
a_rms	1.18	1.27	1.36	a_rms	1.09	1.33	1.65
a_Rrms	1.14	1.26	1.39	a_Rrms	1.09	1.34	1.69
VDV	1.14	1.23	1.33	VDV	1.02	1.28	1.67

Fig. 83 – Loading protocol for the in-situ fast assessment of timber floors.

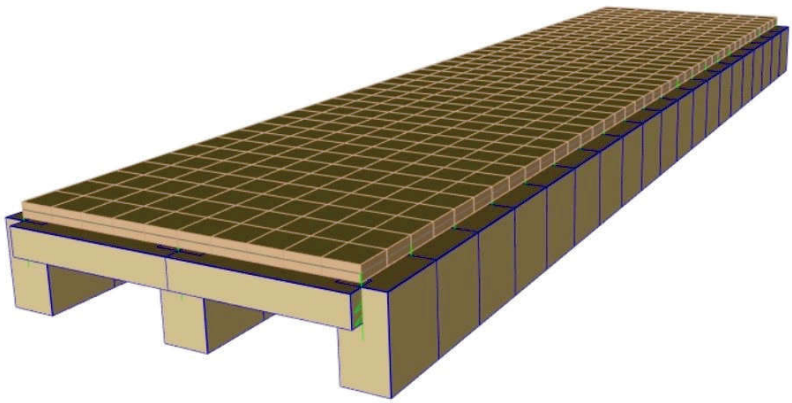

Fig. 84 – FEM model of the full-scale timber floor.

Through the parametric analysis, the aspect ratio of the floor was changed modifying the number of timber joist, keeping fixed the span L=4.00 m. Overall, 7 configurations were analysed for a B/L ratio from 0.125 (single joist configuration) to 3 (corresponding to 25 joists). The parametric numerical results were again compared in terms of peak/rms acceleration and VDV. Since the rolling rms acceleration gave similar results to the rms acceleration, the parameter was not considered for the parametric analysis.

The parametric numerical analysis was performed by simulating possible walking scenarios and by varying the step frequency of a single pedestrian from 1.5 to 2.5 Hz. This loading configuration was reproduced by using the consolidated deterministic analytical model proposed in [75][32], described in section 2.2.1 of the thesis. This deterministic approach models the typical footfall effects F(t) due to a single pedestrian as:

$$F(t)/W = \sum_{i=1}^{8} K_i t^i \tag{63}$$

In (63), W is the weight of the pedestrian (N), K_i are specific coefficients listed in Table 5 and t is the time (in seconds) within a single footfall.

As an example, Fig. 85 shows the vertical acceleration at midspan for B/L=1 and an imposed step frequency 1.50 Hz. The rolling rms acceleration over time was also overlapped.

Fig. 86 shows the results of the parametric analysis for a_{max} (a), a_{rms} (b) and VDV (c), normalized to B/L=0.25, which represents the 3-joist specimen.

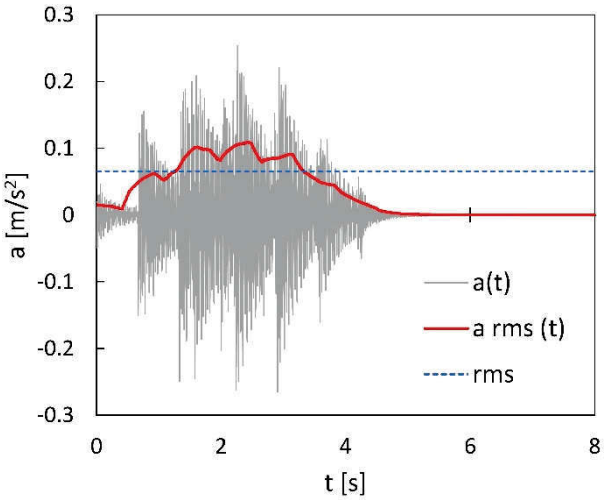

Fig. 85 – Midspan vertical acceleration for B/L=1 and step frequency 1.50 Hz. In red the rolling rms is reported; the rms is shown in blue dashed line.

The numerical outcomes highlight that aspect ratio has an important impact for B/L < 1.0, where the performance indicators are 1.3÷2.3 times higher than the tested configuration, indicating that an assessment procedure on a simplified model made of only one joist is in general not able to reproduce a realistic behaviour. However, it is worth noticing that the 3-joist configuration (B/L=0.25) still overestimates the selected comfort indicators. The peak acceleration ratio reduces to nearly 0.5 for B/L>1, whereas rms and VDV are close to 0.25. For B/L>1, the variation of these indicators tends in fact to stabilize.

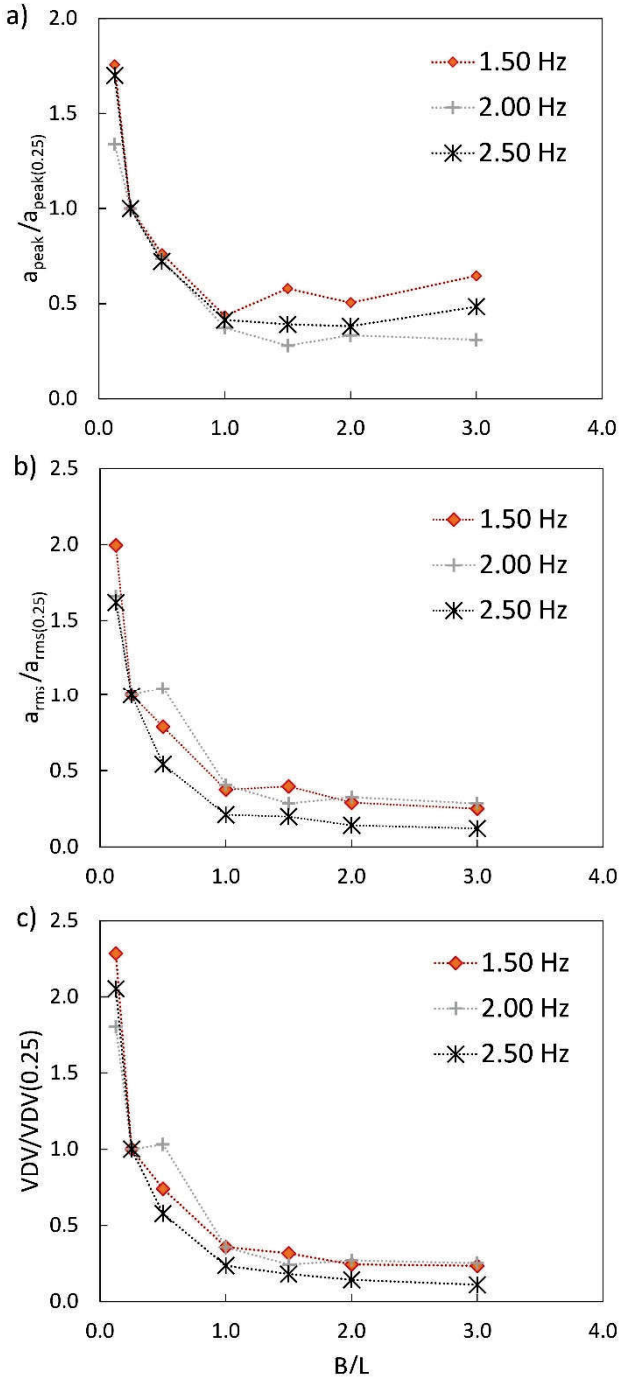

Fig. 86 – Parametric analysis results in terms of a_{max} (a), a_{rms} (b) and VDV (c) varying the step frequency and the aspect ratio B/L.

11-5 PARAMETRIC ANALYSIS

Starting from the modelling approach used for the tested floor in section 4.7, a parametric analysis was carried out, in order to investigate the influence of several parameters (e.g. span, connections, presence of screed, …) on the dynamic response of timber joisted floors.

The aim of the analyses was to verify if code conforming joisted floors are adequate to satisfy also comfort vibrational requirements, such as VDV limit values, and to propose further checks to ensure the verification.

First, a set of parameters was decided, in order to create a large sample of configuration. However, to avoid under- or over-designed floors, an EC5 [38] check was applied, neglecting not verified structures and floor with a ratio demand/capacity below 0.85. This check was set only to avoid not-optimized floor (e.g. section height equal to 60 cm for 3 m span floors). The check process followed deflection criteria for residential buildings and vibration check according to section 3.1 and 3.2 of the dissertation.

Set a live load of 2.00 kN/m^2 according to IBC [95] and EC5 [38], the following deflection checks were performed, with w the deflection and L the floor span:

- w < L/300 for instantaneous deflection under live load;
- w < L/200 for final deflection under live load;
- w < L/250 for final deflection under permanent and live loads.

Verification were performed according to EC5 [38], considering a k_{def}=0.6 (service class 1) and simply support boundary conditions. The

connection between beam and top layer was considered, thus taking into account composite action by means of gamma-method contained in [38](see section 5.2.2 for the gamma evaluation).

Verification checks were performed according to EC5 approach, described in section 3.2 of the thesis. However, if the fundamental frequency f_1 of the floor was <8 Hz, an acceleration verification was carried out, since no suggestion are provided by the code. The acceleration was evaluated through equation [57]:

$$a_{max} = 0.4 \frac{P_0 \cdot \alpha(f_1)}{M^*} \beta \leq a_{lim} \tag{64}$$

$$\beta = \frac{1}{\sqrt{((\frac{f_1}{f_F})^2 - 1)^2 + (2\xi \frac{f_1}{f_F})^2}} \tag{65}$$

Where:
P_0: weight of the pedestrian (700 N);
M*: modal mass of the floor [kg];
α: see Table 23;
f_F: frequency of external force;
ξ: modal damping.

Table 23 – Parameters α and f_F depending on f_1.

f_1 (Hz)	$\alpha(f_1)$	f_F (Hz)
≤ 5.1	0.2	f_1
>5.1 e ≤ 6.9	0.06	f_1
>6.9	0.06	6.9

Limit values were taken from ISO 2631-2 [37]. For residential floors with standard requirements, a maximum acceleration of 0.1 m/s^2 was considered.

5.1 Description of the parameters

To obtain a high variety of timber joisted floors, 13 variables were considered: Section, Material, Span, Number of Beams, Beam Spacing, Plank layer height, Connection stiffness, Screw spacing, Screed height, Non-structural weight, Damping, mean walking frequency. All variables are reported in Table 24. A total of 259,300 possible configurations can be obtained. Preliminary deflection/vibration checks were performed. In this way, the total analysed geometries were reduced to 14,992. Herein, each parameter is discussed.

Table 24 – Variables for the parametric analysis.

Variable	Key	Number of cases	Values
Sections	Sec	10	*
Materials	Mat	3	C16 - C24 - D24
Spans	L	5	3.0 - 5.0 m @0.5m
Number of beams	Nb	4	7, 13, 19, 25
Beam spacing	Sb	3	0.4-0.5-0.6 m
Plank layer height	hp	2	0.02 - 0.04 m
Connection Stiffness	ks	4	0 - 2500 - 5000 - 15000 kN/mm
Screw spacing	ss	2	0.10 - 0.20 m
Screed	hs	3	0 - 0.05 - 0.10 m
Non-structural weight	G2	3	0.5 - 1.0 - 1.5 kN/m^2
Damping	d	3	0.01 - 0.02 - 0.04
Mean walking frequency	fm	3	1.0 - 1.5 - 2.0 Hz
Total configurations:		259,200	
Total analysed configurations:		14,992	

Ten sections (Table 25) and three material were taken into account. To reduce the number of analyses, only solid wood C16 (E = 8000 MPa), C24 (E=11000 MPa) and D24 (E=10000 MPa) were chosen, and typically commercial section were taken. However, several section match with glulam commercial ones (e.g. 100x120, 120x200, 120x240). Besides, Gl24 has an elastic modulus and mass similar to C24, thus allowing post-analysis parallelisms. In this work, in fact, no long-span floors were studied, since the aim was to analyse typically residential joisted floors.

Table 25 – Beam sections for the parametric analysis.

Section ID	BxH [mm]
1	60x120
2	60x160
3	80x120
4	80x160
5	80x200
6	100x120
7	100x200
8	120x120
9	120x200
10	120x240

Actually, five spans were considered from 3 to 5 m, with increments of 0.5 m. These measures are typical of residential spaces. Moreover, the spacing of beams was varied, considering 0.4-0.5-0.6 m.

Usually, design practice considers a one-way strip of the floor to perform checks. However, the width of the floor could have a high impact on the dynamic response, as seen in section 4.7 for the laboratory test. Thus, a variable number of beams between 7 and 25 was considered, in order to build floor with different width/span ratios.

To simulate the presence of an upper layer of boards, two thickness were considered (2 and 4 cm) and the connection with the beams was properly taken into account, varying the stiffness of the single screw (from 0 to 15000 kN/mm) and the spacing between connectors (10 or 20 cm). The 0 kN/mm stiffness simulate the absence of connection between the layers, while the other values are based on preliminary test performed [113].

The screed presence has a not-negligible influence on the dynamic response of the floor, even if it is considered as a non-structural element. For this reason, a screed of 0 cm (absence), 5 cm or 10 cm was considered on top of the plank layer, with a young modulus of 25 GPa and a weight of 16 kN/m^3.

To the self-weight of the floor (timber structure and screed, if present), a non-structural weight was also added, to simulate finishing and furniture. The mass is, in fact, a fundamental parameter describing

the dynamic response of the floor. Three non-structural G_2 loads were taken, equal to 0.5-1.0-1.5 kN/m^2.

As discussed in section 1.3.3, damping is still a debated issue, since it is complex to estimate. Thus, three damping classes were considered (1%, 2% and 4%), in order to investigate their influence on the comfort checks.

Finally, the floors were analysed under human induced loads. Three mean walking frequency were chosen, representing slow, normal and fast walk, 1.0-1.5-2.0 Hz respectively. As said, these are mean frequency: to perform the analyses, in fact, the probabilistic model proposed by Chen [45] was applied, thus varying step frequency, length and superposition according to intra- and inter-subject variability. Moreover, five pedestrians of different weight were considered for each frequency.

Considering also the damping classes (3), the different step frequencies (3) and pedestrian involved (5), each floor geometry was analysed 45 times. Thus, a total of 14,992 x 45 = 674,640 dynamic analyses were performed for the parametric study.

5.2 Modelling approach

Modelling approach follows the strategy adopted in Section 4.7 for the tested floor in SAP2000 [112](Fig. 87). To the beams, simply supported frame elements were assigned, while the upper layers where modelled by means of shell-thin elements, thus neglecting the influence of discrete boards. Only a vertical restraint was applied to the top layers, while rotations were left free, in order to simulate a simply support condition on each edge. The approach wants to simplify the geometry of the models, given the amount of analyses. Nonetheless, three critical issues emerge, involving the connection system, the modelling of the screed and the application of the pedestrian load.

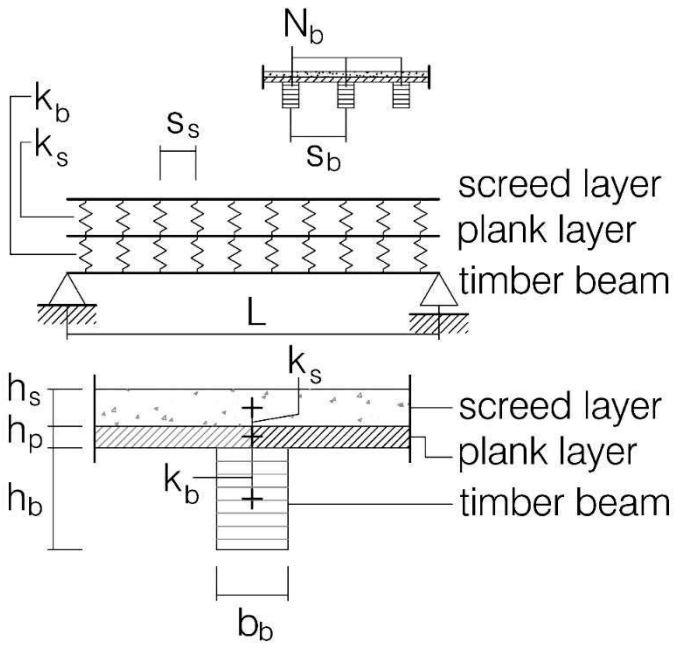

Fig. 87 – FEM modelling approach for timber floors.

5.2.1 Beam-boards connection

The connection between boards and beams was obtained by means of discrete linear links representing each screw, connecting the centres of mass of beams and plank. To each link, a transversal stiffness k_b was assigned, to reproduce the shear rigidity of the connection according to table. The axial degree of freedom was fixed, in order to replicate a rigid connection. The beams and the top shell layer were meshed to match the nodes of the links.

5.2.2 Presence of the screed

The screed was modelled as shell elements with thickness derived from Table 24. No shear connections are present between beam/planks and screed, since it is a non-structural layer. However, vibration under human induced load condition, a low but not negligible interaction take

place. At the date, no data is available to model this interaction without explicitly introduce friction in the FEM modelling. It is a complex and time-consuming approach, not suitable to assess over 600,000 analysis.

To overcome the issue, a discrete modelling approach was considered, inverting the γ-method [38] to obtain an equivalent stiffness k_s for an equivalent spacing s of discrete connectors.

From the γ-method, it is known that the γ value takes the form:

$$\gamma = \left[1 + \frac{\pi^2 EAs}{(kL^2)}\right]^{-1} \tag{66}$$

Where, γ represent the grade of composite action, E and A are the young modulus and the area section of the concrete screed, s and K are the spacing and the stiffness of connectors and L is the span of the floor. The formulation can be inverted to obtain the stiffness k_s, which represent the equivalent shear stiffness of the connector simulating screed-boards interaction.

$$k_s = \frac{\pi^2 EAs}{L^2(\frac{1}{\gamma} - 1)} \tag{67}$$

The geometrical and mechanical parameters are known (E, A and L). To simplify the modelling of the floor, the spacing s can be taken equal to the screw spacing s_s, according to Table 24. To quantify the value of gamma, to the author's knowledge no studies are available. A suitable range can be found in Fig. 88 [35], where a value between 0.05 and 0.15 is suggested for concrete topping on mass timber floors. In this case, the screed is considered cast directly on timber boards, thus allowing a parallelism. A coefficient gamma = 0.05 was considered.

Case		Partial Composite Action Factor (γ)	
		Strength & Deflection	Vibration Design
Concrete topping on mass timber panel detailed as a TCC system with explicit composite action		From testing or detailed analysis	Potentially higher than for strength & deflection
Incidental Composite Action	Concrete topping cast directly on mass timber floor with nominal connection	N/A[1]	0.15-0.50[2]
	Concrete topping cast directly on mass timber floor with no connection	N/A[1]	0.05-0.15[2]
	Concrete topping on acoustic mat or slip-sheet on mass timber panel	N/A[1]	0-0.05[2]
	Mass timber panel in direct contact with timber beam with clamping connection	N/A[3]	0.5-1.0[2]

[1] Only the mass timber panel is considered; the cementitious topping layer is ignored.
[2] Values are based on limited testing and field observations.
[3] Only the beam is considered; potential contribution from the mass timber panel and topping is ignored.

Fig. 88 – Value of γ from [35].

5.2.3 Pedestrian load

The human induced loading was applied as pointed forces acting in correspondence of each step. The coordinates of each force, like the magnitude-time law representing each step, was obtained from Chen et al. [45] probabilistic model described in section 2.2.1 of the manuscript.

For each individual walk, a pedestrian weight was randomly generated with a normal distribution with mean 750 N and standard deviation of 150 N, in order to cover a high variety of people. 750 N is usually taken as an average weight for people [32][46]. Moreover, according to Chen model, the first contact between foot and support can be drawn from a normal distribution between 0 and the step length. In this study, a minimum of 0.1 m for the edge of the floor was kept, avoiding the first load on the boundary.

A linear path passing on the central beam through midspan was considered, walking parallel to the joists. A constant transversal distance of 20 cm was used between the steps, in order to not add another (negligible) parameter. The overlap time of each step, i.e. the double support time DS, was calculated for each step j according to $DS(j) = T(j) - 1/fp(j)$ [45], where f_p is the step frequency that considers both intra- and inter- subject variability, while the step length was taken from a normal

distribution with mean 0.74 m and standard deviation 0.08 [45]. The number of steps for each walk was calculated starting from the span of the floor and the step frequency.

Inter- and intra-subject variabilities were obtained for each walk/step from equations 29 and 30, and Table 9, 10 and 11, thus evaluating 15 walks for each model to be analysed. The flow-chart of the walking simulator is reported in Fig. 89.

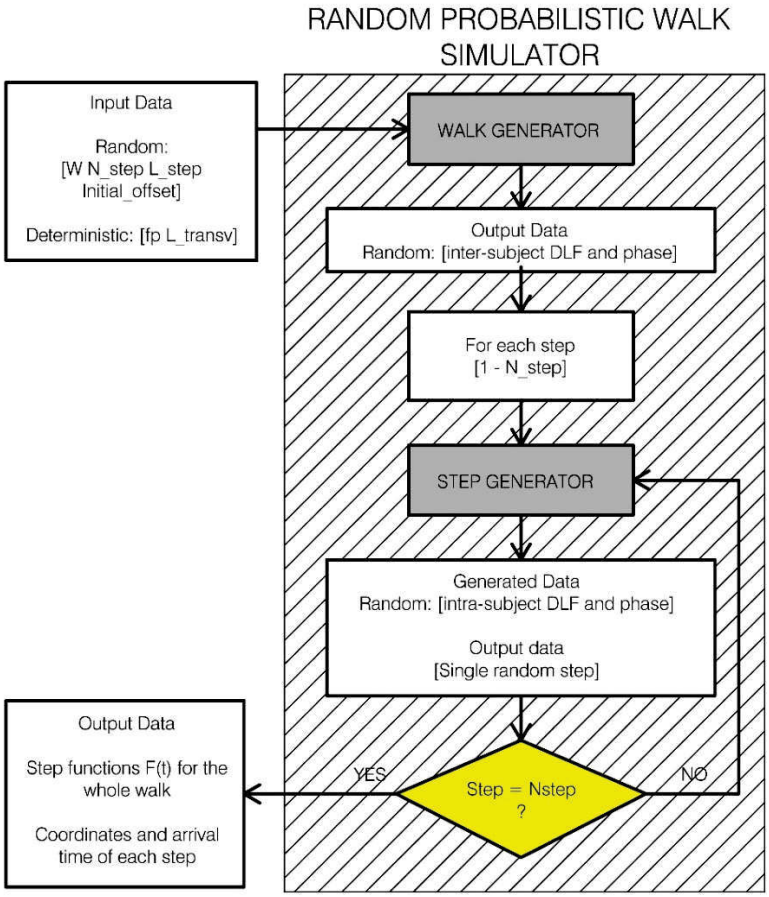

Fig. 89 – Algorithm to generate random walks, assembled according to Chen.

The "Walk generator" creates the DLFs and the phase angles accounting for the inter-subject variability. In input, random variable are given: the weight of the pedestrian (W), the number of step (Nstep), the length of the step (L_step) and the initial position of the first step (initial_offset). Moreover, deterministic variables are also given: the mean frequency of the steps (f_p) and the transversal distance between steps (L_transv). The output DLFs and phase angle are elaborate in the

"Step simulator", which creates Nstep functions describing the force-time laws and the positioning on the floor, taking into account the intra-subject variability. The "Random probabilistic walk simulator" code was inserted in the complete code for the parametric analysis.

5.2.4 Analysis algorithm

To execute the parametric analysis, a MATLAB code was written (Fig. 90). The "floor generator" assembles each floor geometry starting from the input parameters of Table 24. Each floor is checked according to EC5.

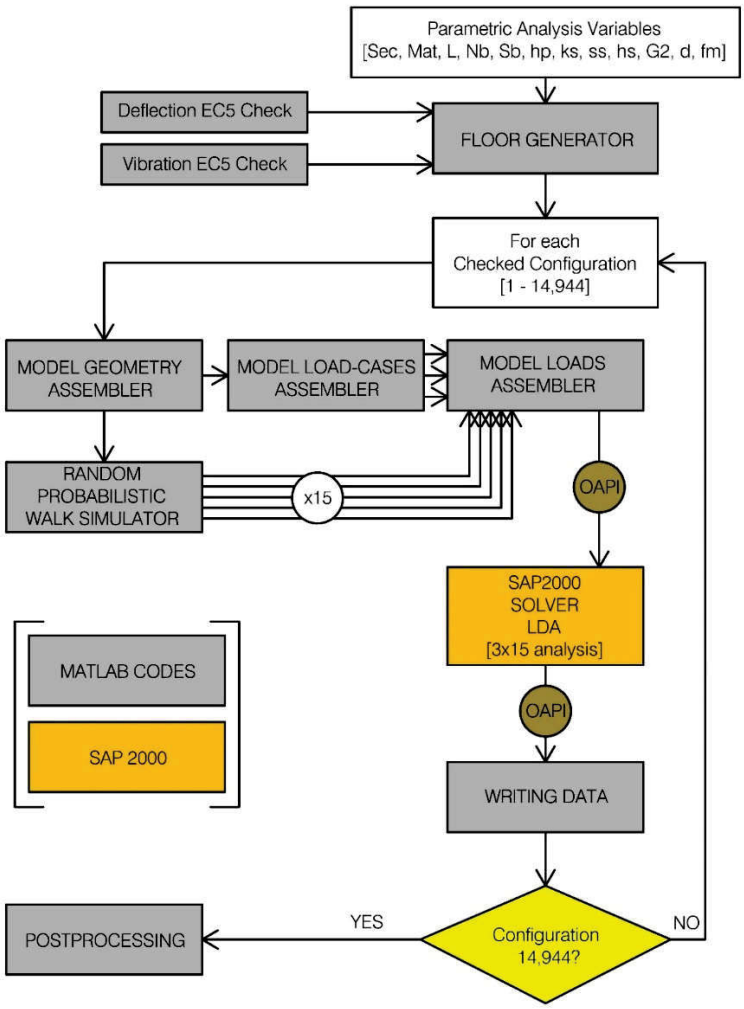

Fig. 90 – Algorithm to perform Parametric floor analysis (MATLAB/SAP2000).

To analyse the configurations, the OAPI of SAP2000 were used, writing MATLAB codes. The geometry, the load cases and the loads were generated, using the Random Probabilistic Walking Simulator to simulate each random walk for each model.

Furthermore, each configuration was analysed via Linear Dynamic Analysis LDA, and the output was written to disk. Finally, the data was post-processed to evaluate the comfort parameters.

5.3 Results

The vertical accelerations at midspan point were processed to evaluate the Vibration Dose Value (VDV), and the influence of the chosen parameters on the comfort verification was studied. The comfort check was performed according to ISO10137 [37] and BS standard [100], considering the maximum comfort class for VDV < 0.2 $m/s^{1.75}$ and setting the maximum desirable VDV = 0.4 $m/s^{1.75}$, in order to avoid adverse comments (Table 26). Since the huge amount of points from the analysis (over 600,000), only mean and standard deviation are herein reported.

Table 26 – VDV limits according to [37] and [100].

Building Usage	Adverse comments unlikely	Adverse comment possible	Adverse comment probable
Residential 16h day	0.2-0.4	0.4-0.8	0.8-1.6
Residential 8h night	0.13	0.26	0.51

In Fig. 91, the influence of the stiffness K_{ser} is presented. Each value of K_{ser} is shown with different coloured cross markers, which represent the mean value obtained over 600,000 configurations. From the data, increasing the stiffness of the connection has a positive effect on the vibration performance, decreasing the VDV. The influence of K_{ser} is higher for longer spans, see Table 27. However, Table 28 shows that high standard deviation was detected. Even if an average improvement of the vibrational performance can be achieved increasing the stiffness, it cannot be considered a valid solution, since the large dispersion of the results.

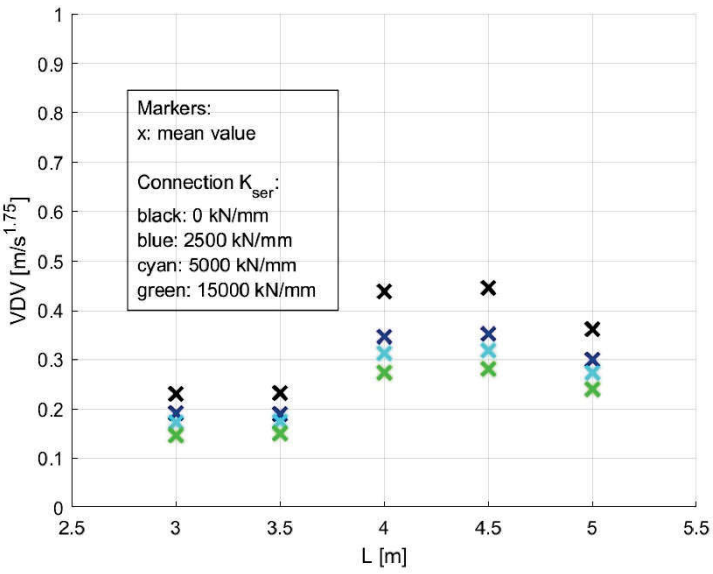

Fig. 91 – Effect on the VDV of span length and connection stiffness K_{ser}.

Table 27 – Mean VDV varying span and connection stiffness K_{ser}.

	L [m]				
Kser [kN/mm]	3	3.5	4	4.5	5
0	0.231	0.233	0.438	0.445	0.362
2500	0.192	0.189	0.346	0.352	0.300
5000	0.173	0.174	0.312	0.319	0.274
15000	0.147	0.151	0.274	0.282	0.240

Table 28 – Standard Deviation associated to VDV varying span and connection stiffness K_{ser}.

	L [m]				
Kser [kN/mm]	3	3.5	4	4.5	5
0	0.292	0.324	0.406	0.419	0.370
2500	0.233	0.243	0.301	0.296	0.299
5000	0.204	0.217	0.272	0.271	0.267
15000	0.165	0.180	0.241	0.239	0.227

Furthermore, the influence of the screed is herein considered. Fig. 92 shows the mean VDV for each span length (3.0 – 5.0 m @0.5m) and

for each screed thickness h_s (0.00 – 0.05 – 0.10 m). Moreover, the standard deviation is reported for each point. The absence of the screed has high negative effect on the VDV, causing high values that exceed the threshold of 0.4 $m/s^{1.75}$. The presence of a screed reduces significantly the vertical acceleration, since stiffness and mass are added. Moreover, the standard deviation decreases considerably adding a screed, meaning that a floor with a light concrete layer has a more predictable behaviour under human induced vibrations (Table 29). Form Table 29, a 0.05 m thick screed reduces the mean VDV from 0.366-0.531 $m/s^{1.75}$ (possible adverse comments of occupants) to 0.150-0.192 $m/s^{1.75}$ (unlikely adverse comments). The standard deviation varies from 0.279-0.349 to 0.095-0.129 (Table 30). The presence of a high thickness screed (0.10 m) is sufficient to verify the floor for each span length, reducing significantly the standard deviation. Furthermore, according to Fig. 92 the screed has comparable effect independently from the span length.

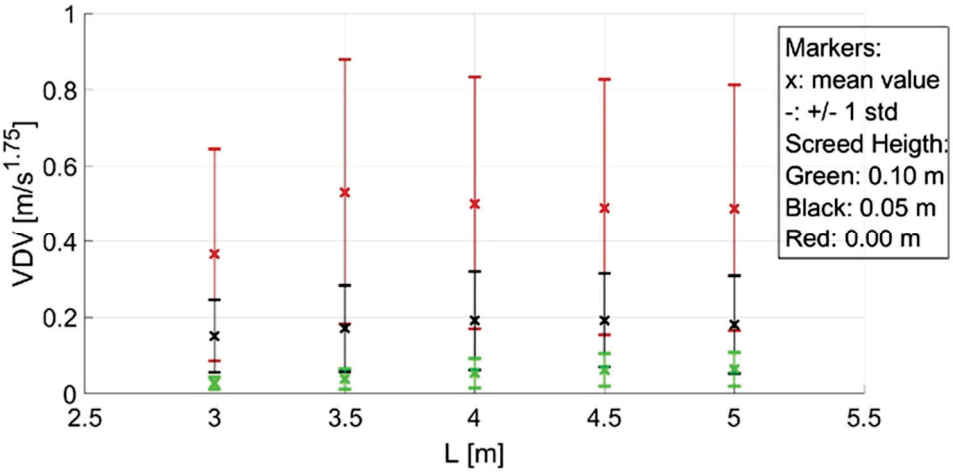

Fig. 92 – Influence of span length and screed height on the VDV.

Table 29 – Mean VDV varying span and screed height h_s.

	L [m]				
h_s [m]	3	3.5	4	4.5	5
0.00	0.366	0.531	0.502	0.491	0.489
0.05	0.150	0.171	0.191	0.192	0.181
0.10	0.027	0.038	0.054	0.062	0.064

Table 30 – Standard Deviation associated to VDV varying span and screed height h_s.

	L [m]				
h_s [m]	3	3.5	4	4.5	5
0.00	0.279	0.349	0.331	0.337	0.324
0.05	0.095	0.113	0.129	0.122	0.127
0.10	0.016	0.027	0.038	0.042	0.044

The relation between frequency and VDV is reported in Fig. 93, marking average values and standard deviation. Increasing the frequency not only allows to decrease the mean VDV recorded on the floor, but also significantly decrease the standard deviation.
From the graph, it emerges that simple requirements of frequency check (e.g. DIN1052 [99], old CNR-DT 206 [97]) are not sufficient. For frequency between 8 Hz and 15 Hz, floors are not verified under human induced vibrations, exceeding the VDV boundaries. Current codes, in fact, require further checks in terms of velocity and acceleration (EC5 [38]), considering that frequency is not sufficient to ensure the comfort, as seen in [57]. Nonetheless, it is worth noticing that all the tested structures in the parametric analysis were previously checked according to the Eurocode.

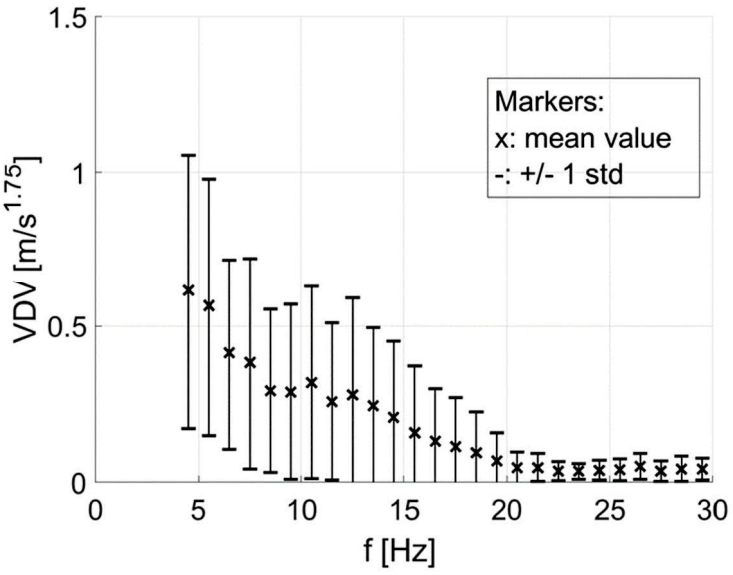

Fig. 93 – Frequency-VDV relationship from the parametric analysis.

To further inspect the behaviour of joisted timber floors, the weight of the structural components (beams, board, screed) was increased adding a non-structural load of 0.5-1.0-1.5 kN/m^2, in order to represent finishing and/or furniture. The VDV obtained varying the weight of the floor W_{fl} and the added load is reported in Fig. 94. Three classes of floors emerged from the parametric analysis. A first class shows a weight up to 0.50 kN/m^2, meaning light floors, typically without screed. Even if the floors pass the Eurocode checks, the results are very unstable, with high dispersion. A slight increase in performance can be noted adding loads. A second class of floor weights between 1.0 and 1.5 kN/m^2, and a third class weights from 2.0 to 2.5 kN/m^2. The larger mass has a consistent positive effect on the response of the floors, ensuring the verification for maximum requirement (VDV<0.2 m/s$^{1.75}$). Heavier floors show also a reduced standard deviation with respect to the other cases.

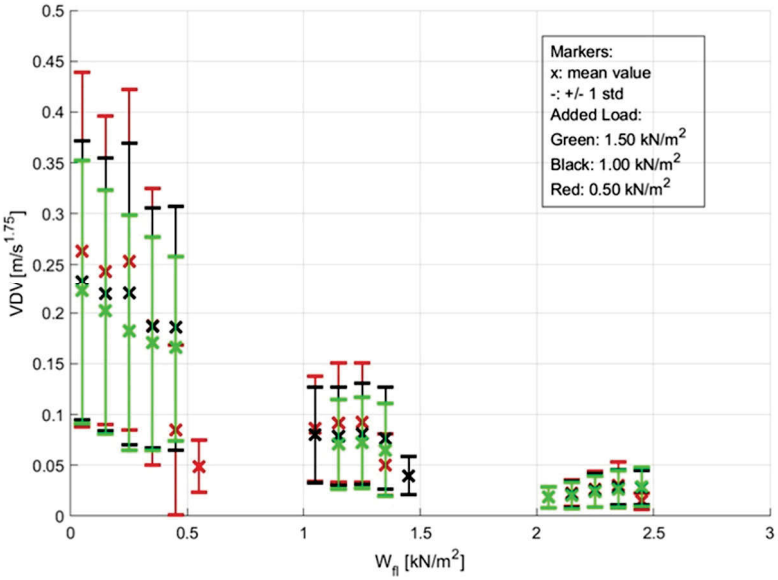

Fig. 94 – Influence on VDV of the added non-structural load with respect to the weight of the floor W_{fl}.

The analysis of the influence of the weight of the floor was reproduced also varying the number of beams (i.e. the width of floor, and thus the aspect ratio), considering the ratio between the weight of

the walking pedestrian and the floor W_{ped}/W_{fl}. Moreover, the results were divided for span lengths, see Fig. 95.

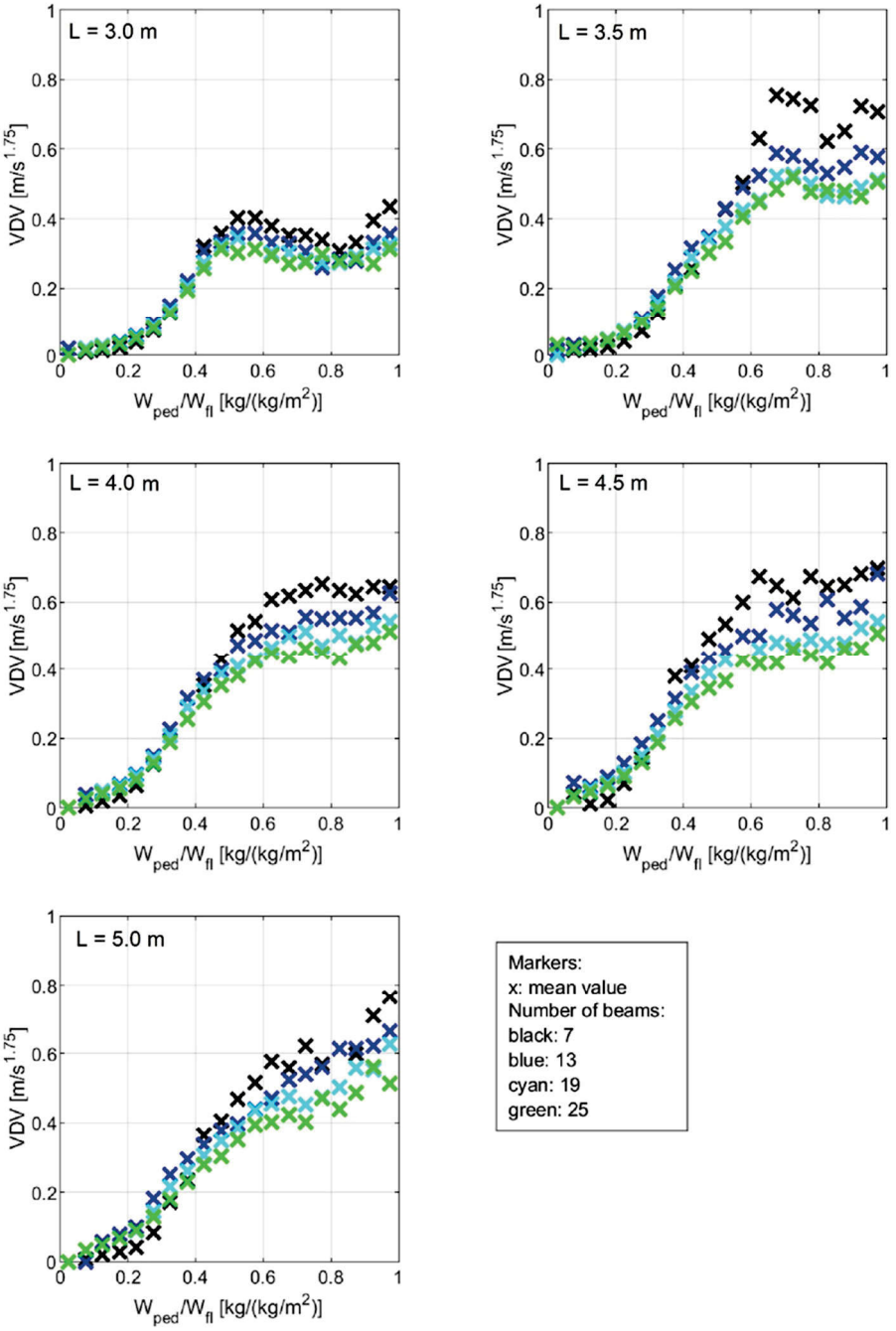

Fig. 95 – Influence of number of beams and ratio W_{ped}/W_{fl} on VDV.

The results highlighted that a wider floor responds better to vibration for high W_{ped}/W_{fl} ratio, since the stiffness of the floor is provided by more beams working together thanks to the board and screed layers. The influence of the number of beam is instead slight for low W_{ped}/W_{fl} (i.e. heavier floors).

Moreover, analysing Fig. 95, floors with a ratio below 0.4 highlight a mean response under 0.20 $m/s^{1.75}$. Thus, considering a pedestrian of 70 kg, floors having a self-weight of 1.70 kN/m^2 satisfy the comfort requirements. When the floor shows a self-weight over square meter comparable to the pedestrian weight, the response produces high vertical acceleration and, consequently, high VDV values. However, a stabilization can be observed for higher ratio, where the response does not get worse event if the ratio furtherly increases. For example, in the L=3.0 m case, the mean response for $W_{ped}/W_{fl} > 0.4$ are quite constant between 0.3-0.4 $m/s^{1.75}$. Analogous considerations can be made for the others spans. Only the case L=5.0 m does not show the same trend, but only because the graph is cut at 1.0.

Since the mass has a strong influence on the final response of the floors, the configurations were plotted varying the ratio W_{ped}/W_{fl}. Each configuration was associated to an interval: VDV≤0.2 (green), 0.2<VDV≤0.4 (yellow) and VDV>0.4 (red). Then, the ratio W_{ped}/W_{fl} were obtained, setting the 95% of configuration that verify VDV<0.2 and VDV<0.4. To compute W_{fl}, both structural elements (beams, boards and screed) and added masses were considered. Fig. 96 shows the results for floor with frequency f < 8 Hz, while f >= 8 Hz are reported in Fig. 97. Moreover, the graphs are reported for each damping class (1%, 2% and 4%).

It is worth noticing that, according to Fig. 96, only the 20%, 27% and 39% of configurations showed response under 0.2 $m/s^{1.75}$, thus avoiding possible adverse comments. For transient response floors (f ≥ 8 Hz), on the other hand, 60%-70% of floors satisfy the VDV maximum comfort requirement.

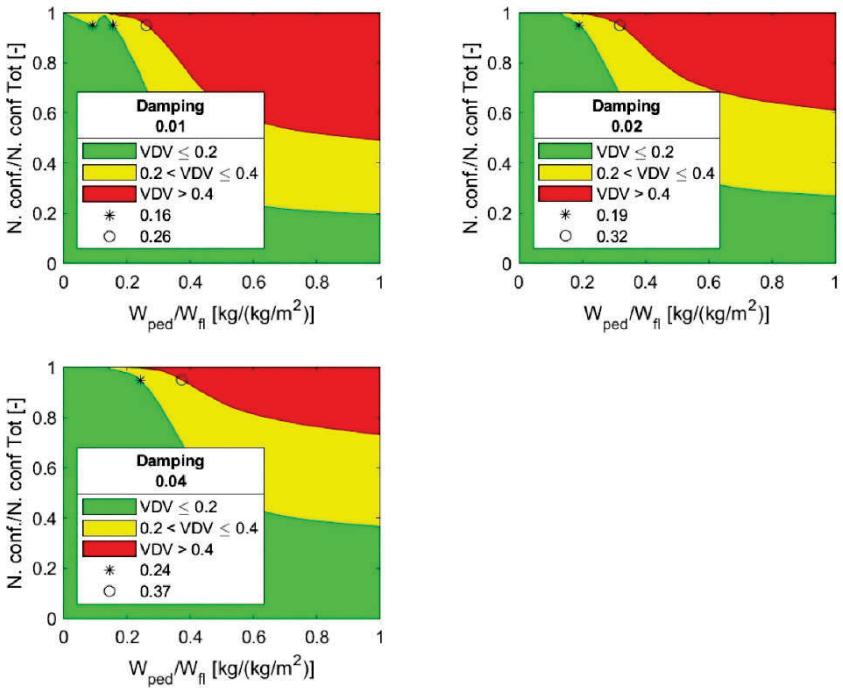

Fig. 96 – Cumulative number of configurations that fall within the three VDV ranges varying the W_{ped}/W_{fl} ratio for floor frequency f < 8Hz (VDV≤0.2: green, 0.2<VDV≤0.4: yellow, VDV>0.4: red).

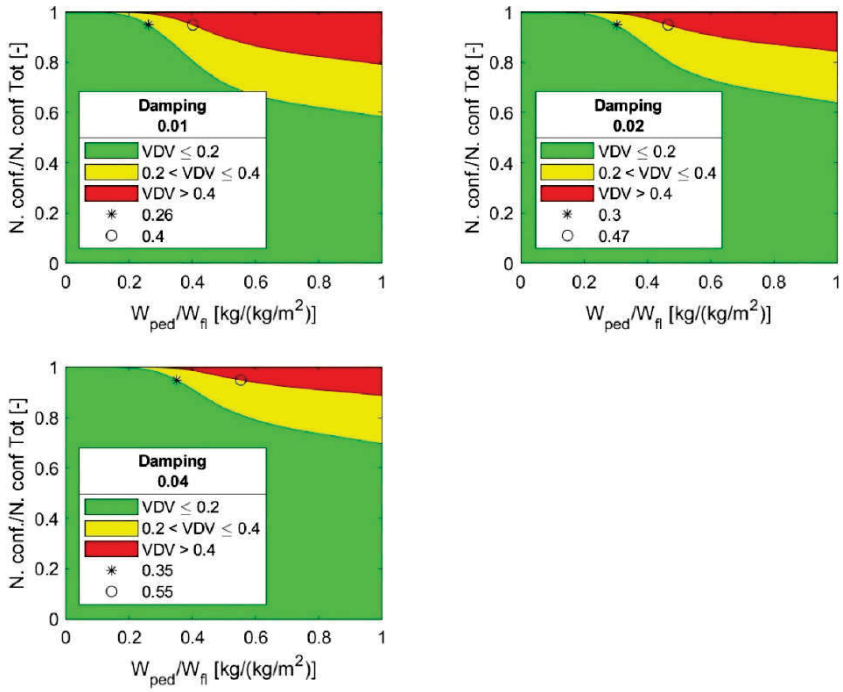

Fig. 97 – Cumulative number of configurations that fall within the three VDV ranges varying the W_{ped}/W_{fl} ratio for floor frequency f ≥ 8Hz (VDV≤0.2: green, 0.2<VDV≤0.4: yellow, VDV>0.4: red).

In Fig. 98, all the configurations are reported together, in order to evaluate the 95% of configuration satisfying the maximum (green) and minimum (yellow) comfort check. Among all the 600,000 tests performed, 50%-63% of the floors are compatible with the "Adverse comments unlikely – VDV < 0.2 $m/s^{1.75}$ class". To rise the percentage to 95%, a ratio between pedestrian and floor mass (kg/m^2) lower than 0.24 (1% damping), 0.28 (2% damping) and 0.32 (4% damping) is necessary. Considering a 70 kg pedestrian, the floor needs a total distributed mass of 292 kg/m^2, 250 kg/m^2 and 219 kg/m^2. Considering a VDV in the yellow interval, the floors need a mass of 194 kg/m^2, 171 kg/m^2 and 143 kg/m^2 respectively. It is worth noticing that the mass check would be a further verification, to be used together with Eurocode suggestions.

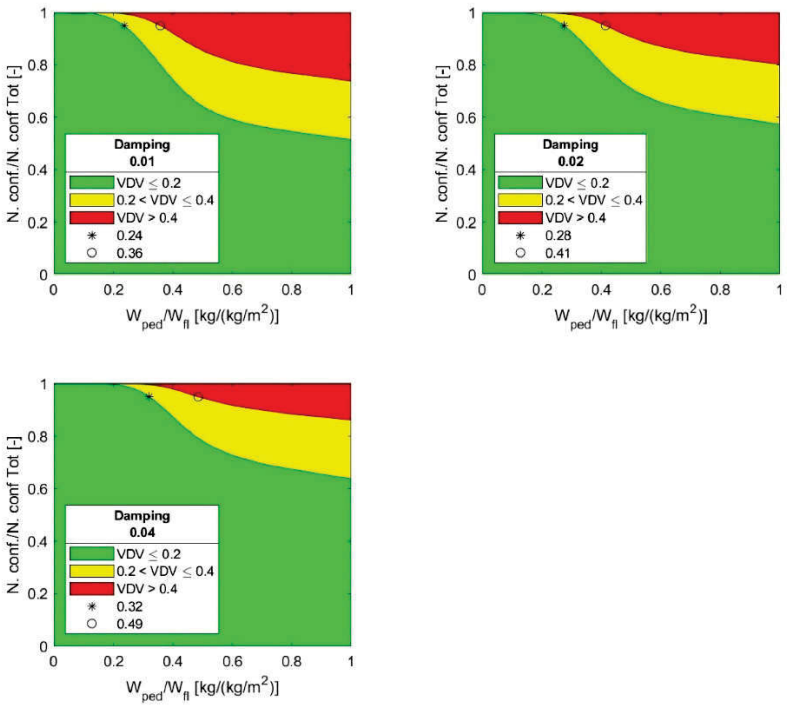

Fig. 98 – Cumulative number of configurations that fall within the three VDV ranges varying the W_{ped}/W_{fl} ratio for all analysed floors (VDV≤0.2: green, 0.2<VDV≤0.4: yellow, VDV>0.4: red).

Finally, Table 31 summarizes the outcomes in term of mass ratio for resonant (f<8 Hz) and transient (f>8) floors, and for all configurations.

Table 31 – Minimum distributed mass (kg/m^2) of timber joisted floor to satisfy the VDV requirements. The mass includes both self-mass and added masses.

	VDV ≤ 0.2 m/s$^{1.75}$			VDV ≤ 0.4 m/s$^{1.75}$		
damp [%]:	1	2	4	1	2	4
f < 8 Hz	438	368	292	269	219	189
f ≥ 8 Hz	269	233	200	175	149	127
all	292	250	219	194	171	143

The requirements for a resonant floor are quite high considering 1% damping. However, it is worth noticing that 1% is a conservative choice proposed by current codes. Moreover, a VDV≤0.4 m/s$^{1.75}$ is considered acceptable to avoid adverse comments by occupants, thus a 269 kg/m^2 distributed mass can be taken into account. A lighter floor can, in fact, give a response not compatible with occupants' comfort requirements.

II-6 CASE STUDIES

The vibration comfort assessment protocol developed in chapter 4 was tested on site in three case studies in L'Aquila (Italy), thanks to the collaboration with the University of L'Aquila and the municipality. In all the case studies, the floor was equipped with both force-balance accelerometer and smartphone sensor, in order to record vertical acceleration simultaneously. The test performed gave generally largely more data than the minimum number set during calibration. Thus, to test the assessment protocol, the scenarios were successively simulated. The results were post-processed considering the correction coefficient found in laboratory and then a comparison between force-balance and MEMS was performed.

6.1 Case study 1 – Meraviglia 1st floor

The first case study consists in a residential building belonging to the CASE project in L'Aquila. The structure is made of timber columns and beams. The analysed floor is located at the first level. It is 3.00 x 4.05 m in plan, with beams oriented along the smaller dimension. Floor beams are 120 x 200 mm, 3.00 m long. Fig. 99 shows the plan view of the building and reports the analysed floor. Infiltration of water were detected, coming from the upper storey. The apartment is not inhabited.

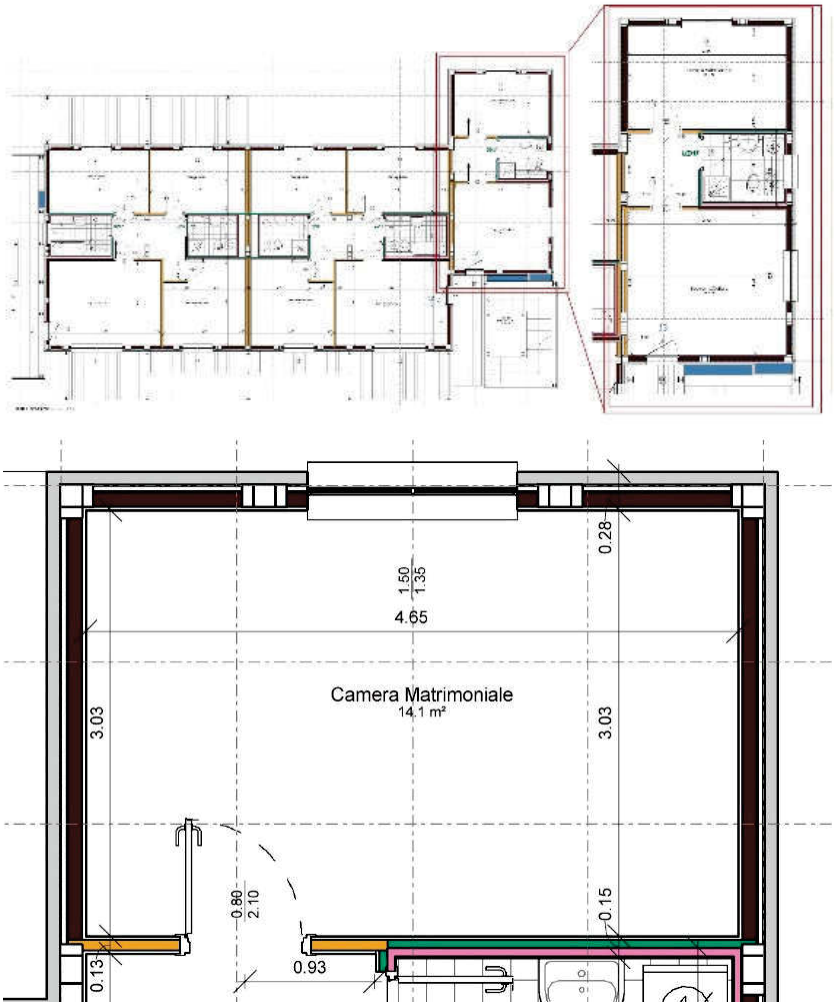

Fig. 99 – Plan view of the building (up) and the bedroom analysed during the in-situ tests (down).

The floor was equipped with 5 force-balance accelerometer SARA (the same used during laboratory test). They were positioned at midspan and at ¼ of the span in both longitudinal and transversal direction. A 200 Hz sampling frequency was chosen, as the maximum supported by the instrumentation. The battery and the wi-fi connection were set, in order to collect data from a PC station located in the adjacent room. Furthermore, the smartphone was fixed next to the midspan accelerometer, to record the vertical acceleration. To avoid slip between the device and the floor, an industrial bi-adhesive was used, after cleaning the surface. A sampling frequency of 250 Hz was set, in order to avoid

down-sampling <200 Hz due to background processes in the smartphone.

Two paths selected for the walking tests. The longitudinal path follows the orientation of the beams, the transversal one is orthogonal. See Fig. 100 and Fig. 101 for the complete test setup.

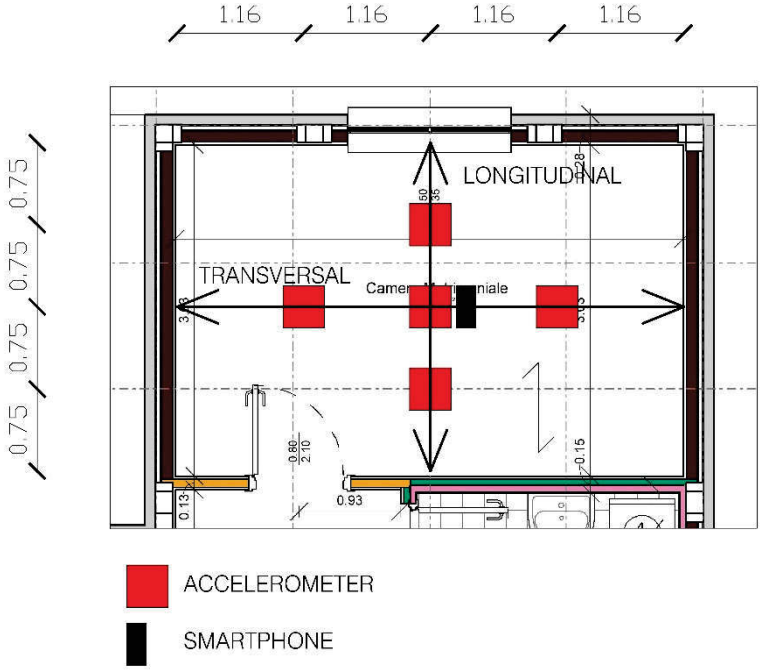

Fig. 100 – Test setup reporting FB accelerometers in red and the smartphone in black.

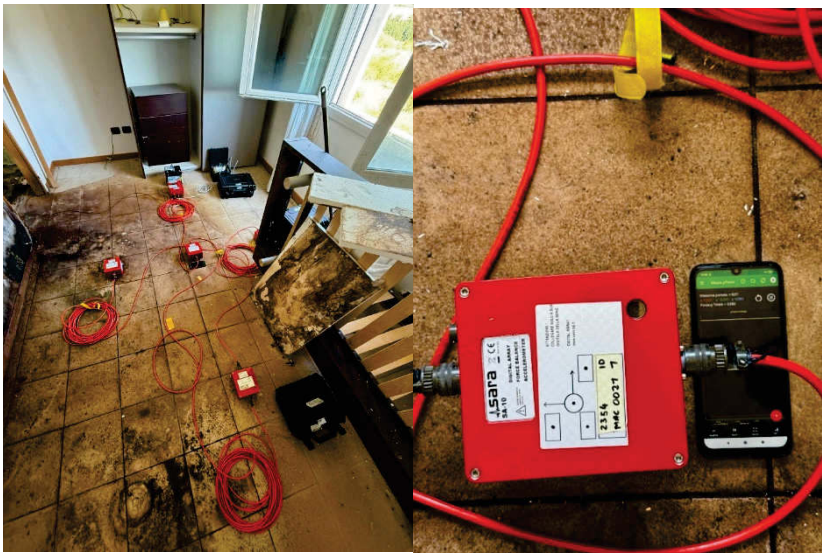

Fig. 101 – Overviews of the bedroom and the setup.

A total of seven test of about 4 minutes each were carried out, varying the step frequency. The indicative frequency of 1.5 Hz was considered to simulate a normal walk, 2.0 Hz was used to perform a fast walk. Furthermore, test 5 consisted in several heel-drops in three different points of the floor (midspan and ±1/4L), see Table 32.

Table 32 – Characteristics of the onsite test.

Test ID	Type	Frequency	Path
1	Walk	1.5	Longitudinal
2	Walk	2.0	Longitudinal
3	Walk	1.5	Transversal
4	Walk	2.0	Transversal
5	Heel drop	-	-
6	Walk	1.5	Longitudinal
7	Walk	2.0	Longitudinal

6.1.1 Walking tests

The walking test followed the longitudinal and transversal path displayed in Fig. 100. The starting point of each walking session is reported in Fig. 102, together with an image taken during the tests. A total of 279 walks were recorded, divided in 6 tests of about 4 minutes each.

Herein, an example of data processing is reported for Test n. 2. An example of recorded data is proposed in Fig. 103. A zoom-in is reported in Fig. 104. The records were synchronised, matching the occurring peaks of vertical acceleration. The superposition of the signal denotes a good overlap, showing that the smartphone underestimated the maximum peaks. Nonetheless, this aspect was noted also during laboratory tests.

The complete test, corresponding to 36 single walks was divided into single signals, to isolate each walk. For example, Fig. 104 reports three walks in the transversal direction. A step frequency between 1.52 and 1.92 Hz was detected successively (2.00 Hz was the indicative fast walk frequency for the tests).

Fig. 102 – Starting position of walking tests (left) and photo from the walking test (right).

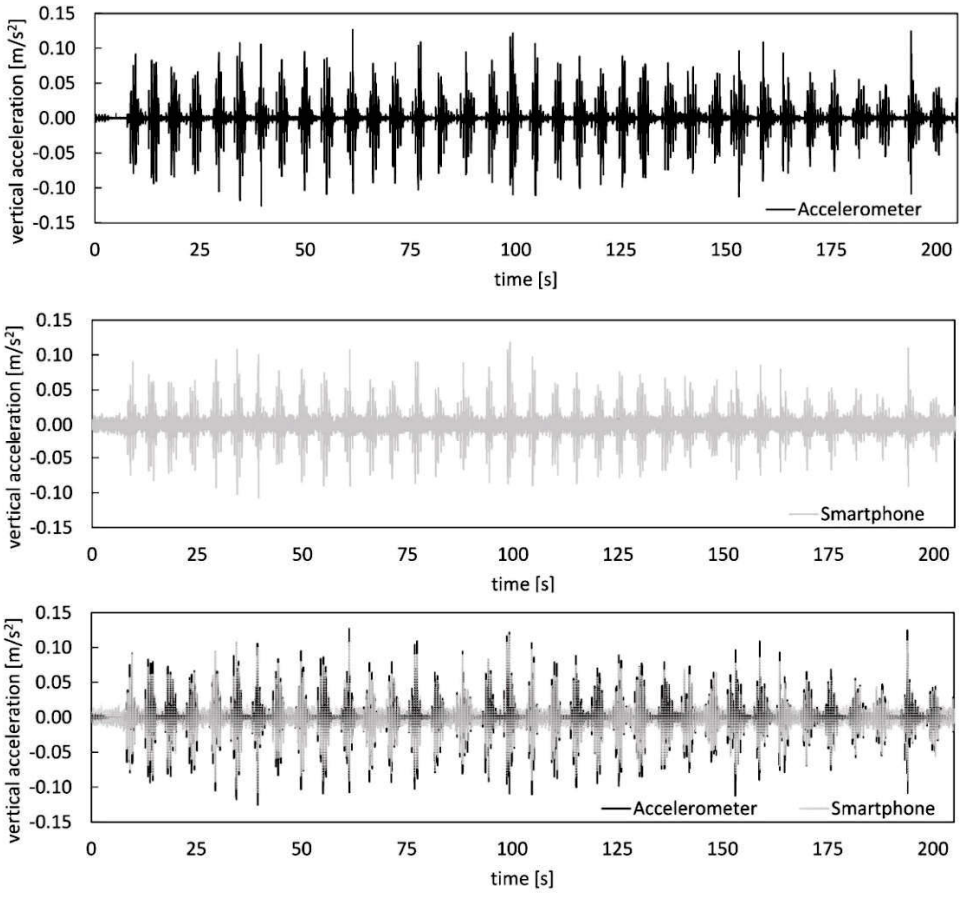

Fig. 103 – Example of recorded signal form the tests, from accelerometer, smartphone and finally overlapping the records.

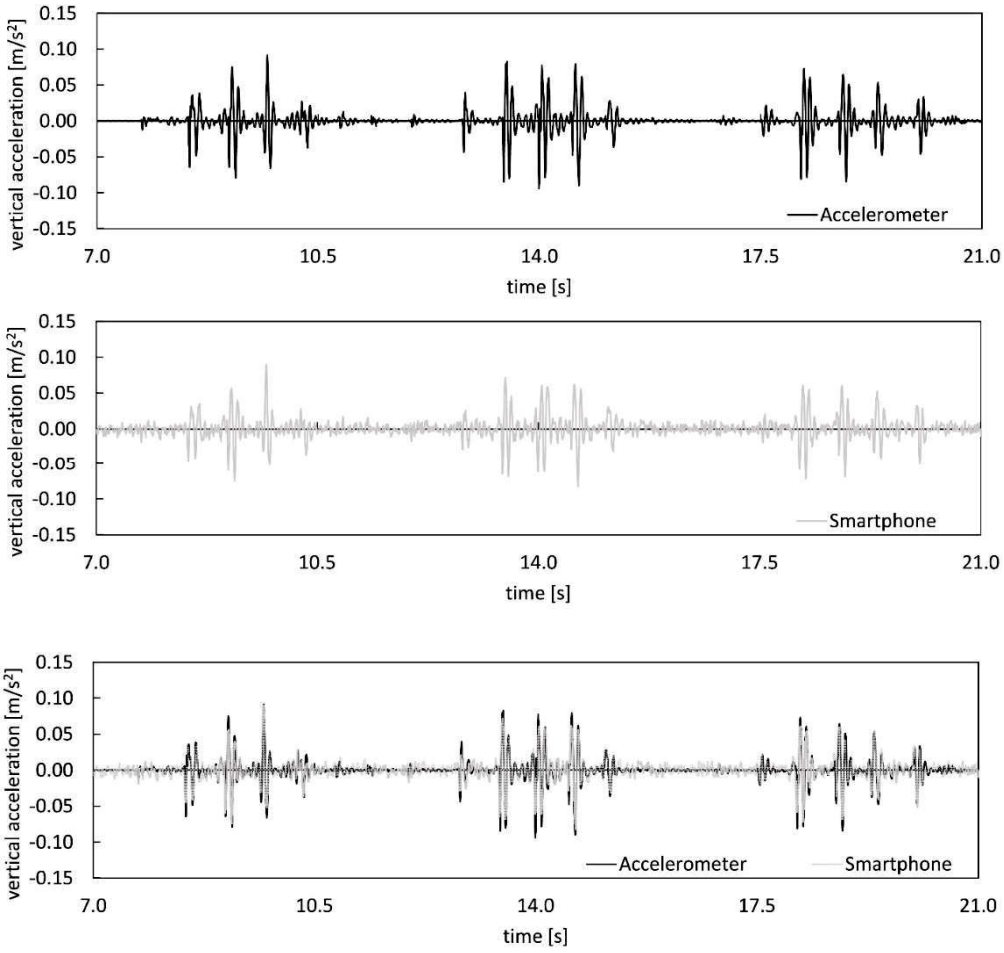

Fig. 104 – Zoom on three walks of tests 2, from accelerometer, smartphone and finally overlapping the records.

For each of the 36 walks in the test, four parameters were calculated, according to the evidence in chapter 4. In particular, maximum vertical acceleration a_{max}, root-mean square acceleration a_{rms}, maximum rolling root mean square acceleration $a_{R,rms}$ and Vibration Dose Value VDV. The raw (not corrected) results are reported in Table 33 and Table 34. Moreover, the ratio A/S between the parameter obtained from the Accelerometer (A) and the Smartphone (S) is also reported.

Table 33 – Raw results from Test n. 2 in terms of ratio A/S for maximum and rms acceleration.

Seq	$a_{max,A}$	$a_{max,S}$	Ratio A/S	$a_{rms,A}$	$a_{rms,S}$	Ratio A/S
	m/s^2	m/s^2	-	m/s^2	m/s^2	-
1	0.092	0.090	1.02	0.014	0.014	1.06
2	0.094	0.083	1.14	0.019	0.018	1.06
3	0.084	0.072	1.17	0.016	0.014	1.13
4	0.080	0.068	1.17	0.013	0.012	1.08
5	0.105	0.093	1.13	0.016	0.015	1.06
6	0.118	0.108	1.10	0.019	0.017	1.11
7	0.125	0.107	1.17	0.015	0.014	1.07
8	0.083	0.077	1.08	0.015	0.012	1.19
9	0.103	0.084	1.23	0.015	0.015	1.02
10	0.109	0.090	1.21	0.017	0.014	1.20
11	0.127	0.107	1.18	0.016	0.016	1.02
12	0.093	0.075	1.24	0.015	0.013	1.17
13	0.093	0.080	1.17	0.015	0.014	1.10
14	0.109	0.090	1.22	0.018	0.015	1.20
15	0.079	0.077	1.03	0.013	0.013	0.96
16	0.094	0.088	1.07	0.012	0.011	1.06
17	0.092	0.086	1.07	0.016	0.014	1.12
18	0.122	0.118	1.03	0.020	0.019	1.07
19	0.110	0.097	1.14	0.015	0.015	1.02
20	0.088	0.075	1.18	0.016	0.015	1.06
21	0.100	0.087	1.16	0.016	0.016	1.00
22	0.095	0.077	1.24	0.015	0.013	1.17
23	0.099	0.079	1.25	0.016	0.015	1.08
24	0.085	0.077	1.10	0.017	0.016	1.11
25	0.079	0.068	1.16	0.013	0.012	1.07
26	0.079	0.069	1.14	0.013	0.013	0.99
27	0.064	0.064	1.01	0.013	0.013	1.07
28	0.112	0.081	1.39	0.015	0.013	1.16
29	0.109	0.085	1.28	0.014	0.012	1.14
30	0.093	0.080	1.17	0.013	0.012	1.05
31	0.069	0.068	1.02	0.011	0.010	1.03
32	0.076	0.067	1.13	0.012	0.011	1.09
33	0.058	0.053	1.08	0.010	0.010	0.98
34	0.055	0.053	1.03	0.009	0.009	1.07
35	0.125	0.110	1.14	0.014	0.014	1.00
36	0.053	0.055	0.96	0.011	0.010	1.04
		mean	**1.14**		**mean**	**1.08**
		std	**0.09**		**std**	**0.06**

Table 34 – Raw results from Test n. 2 in terms of ratio A/S for maximum rolling rms acceleration and VDV.

Seq	$a_{Rrms,A}$	$a_{Rrms,S}$	Ratio A/S	VDV_A	VDV_S	Ratio A/S
	m/s^2	m/s^2	-	$m/s^{1.75}$	$m/s^{1.75}$	-
1	0.029	0.025	1.14	0.043	0.039	1.10
2	0.032	0.030	1.09	0.050	0.043	1.17
3	0.031	0.029	1.08	0.043	0.038	1.14
4	0.026	0.022	1.16	0.038	0.033	1.15
5	0.036	0.035	1.03	0.048	0.044	1.08
6	0.041	0.039	1.05	0.054	0.049	1.11
7	0.040	0.036	1.12	0.052	0.045	1.15
8	0.028	0.024	1.16	0.041	0.035	1.15
9	0.037	0.029	1.27	0.050	0.041	1.21
10	0.034	0.029	1.16	0.048	0.041	1.16
11	0.044	0.038	1.17	0.055	0.047	1.17
12	0.029	0.025	1.14	0.041	0.035	1.16
13	0.030	0.025	1.21	0.041	0.035	1.19
14	0.038	0.033	1.13	0.054	0.045	1.19
15	0.028	0.026	1.09	0.039	0.035	1.13
16	0.034	0.029	1.20	0.043	0.035	1.21
17	0.034	0.031	1.08	0.044	0.041	1.08
18	0.044	0.038	1.15	0.062	0.054	1.13
19	0.038	0.033	1.15	0.052	0.045	1.17
20	0.030	0.028	1.07	0.044	0.040	1.12
21	0.034	0.028	1.21	0.045	0.039	1.17
22	0.027	0.023	1.17	0.041	0.035	1.17
23	0.034	0.031	1.09	0.048	0.041	1.15
24	0.031	0.027	1.14	0.047	0.040	1.16
25	0.027	0.023	1.16	0.038	0.033	1.15
26	0.027	0.025	1.09	0.038	0.034	1.12
27	0.023	0.021	1.13	0.036	0.031	1.15
28	0.037	0.031	1.18	0.047	0.040	1.18
29	0.034	0.029	1.18	0.043	0.036	1.19
30	0.032	0.027	1.18	0.041	0.035	1.18
31	0.025	0.023	1.11	0.032	0.028	1.15
32	0.028	0.025	1.15	0.036	0.032	1.15
33	0.022	0.021	1.03	0.029	0.028	1.04
34	0.022	0.019	1.15	0.028	0.025	1.11
35	0.042	0.037	1.13	0.052	0.047	1.12
36	0.021	0.019	1.06	0.029	0.026	1.11
		mean	**1.13**		**mean**	**1.15**
		std	**0.05**		**std**	**0.04**

The ratio between maximum vertical accelerations varies between 0.96 and 1.39, with a mean value of 1.14 and a standard deviation of 0.09. The smartphone, as expected, gave lower results in terms of amplitude, thus providing underestimation of the parameter. Similar results, but with lower standard deviation, were observed for the other chosen parameters. Nevertheless, a good quality output was obtained, with differences of about 20%, as denoted by the laboratory tests.

Successively, the factors $k_{w,50}$ were used to correct the values obtained with the smartphone. The coefficients are recalled in Table 35, with their standard deviation.

Table 35 – Corrective coefficient $k_{w,50}$ to be applied to smartphone records and standard deviation.

a_{max}	a_{rms}	a_{Rrms}	VDV
1.31 ± 0.20	1.27 ± 0.07	1.26 ± 0.10	1.23 ± 0.07

The coefficients were applied to each parameter of each sequence. Then, the mean and standard deviation were calculated once again. The results are reported in Table 36 and Table 37 for Test n.2.

The ratios are now all below the unity, as pursued. A ratio A/S <1 means an overestimation of the selected parameter and, thus, allow to work in favour of safety. The most performing parameter is the VDV, with a mean ratio of 0.93 and a standard deviation of 0.03.

However, this was an elaboration of a single test. The global test program, consisting in 6 test and 279 walks, was also processed. The complete tables with all the data was reported in Appendix B, in order to make the present section more concise. To this aim, only the final results are herein reported in Table 38. The first part of the table reports the raw value, thus not corrected by means of coefficient of Table 35. The second half of Table 38, on the other hand, shows the values of the parameter after the correction.

Table 36 – Corrected results from Test n. 2 in terms of ratio A/S for maximum and rms acceleration.

Seq	$a_{max,A}$	$a_{max,S,c,50}$	Ratio A/S	$a_{rms,A}$	$a_{rms,S,c,50}$	Ratio A/S
	m/s²	m/s²	-	m/s²	m/s²	-
1	0.092	0.118	0.78	0.014	0.017	0.83
2	0.094	0.108	0.87	0.019	0.023	0.83
3	0.084	0.094	0.90	0.016	0.018	0.89
4	0.080	0.089	0.89	0.013	0.015	0.85
5	0.105	0.122	0.86	0.016	0.019	0.83
6	0.118	0.141	0.84	0.019	0.022	0.87
7	0.125	0.141	0.89	0.015	0.018	0.84
8	0.083	0.101	0.83	0.015	0.016	0.94
9	0.103	0.110	0.94	0.015	0.019	0.80
10	0.109	0.118	0.92	0.017	0.018	0.95
11	0.127	0.140	0.90	0.016	0.020	0.81
12	0.093	0.098	0.95	0.015	0.016	0.92
13	0.093	0.104	0.89	0.015	0.017	0.86
14	0.109	0.117	0.93	0.018	0.019	0.94
15	0.079	0.100	0.79	0.013	0.017	0.76
16	0.094	0.116	0.81	0.012	0.014	0.83
17	0.092	0.112	0.82	0.016	0.018	0.88
18	0.122	0.155	0.79	0.020	0.024	0.84
19	0.110	0.127	0.87	0.015	0.019	0.80
20	0.088	0.098	0.90	0.016	0.019	0.84
21	0.100	0.113	0.89	0.016	0.020	0.79
22	0.095	0.100	0.95	0.015	0.016	0.92
23	0.099	0.103	0.95	0.016	0.019	0.85
24	0.085	0.101	0.84	0.017	0.020	0.87
25	0.079	0.089	0.89	0.013	0.015	0.84
26	0.079	0.090	0.87	0.013	0.016	0.78
27	0.064	0.084	0.77	0.013	0.016	0.84
28	0.112	0.106	1.06	0.015	0.017	0.91
29	0.109	0.111	0.98	0.014	0.015	0.90
30	0.093	0.104	0.89	0.013	0.016	0.83
31	0.069	0.089	0.78	0.011	0.013	0.82
32	0.076	0.088	0.86	0.012	0.014	0.86
33	0.058	0.070	0.83	0.010	0.012	0.78
34	0.055	0.070	0.79	0.009	0.011	0.84
35	0.125	0.144	0.87	0.014	0.017	0.79
36	0.053	0.072	0.73	0.011	0.013	0.82
		mean	**0.87**		**mean**	**0.85**
		std	**0.07**		**std**	**0.05**

Table 37 – Corrected results from Test n. 2 in terms of ratio A/S for maximum rolling rms acceleration and VDV.

Seq	$a_{Rrms,A}$	$a_{Rrms,S,c,50}$	Ratio A/S	VDV_A	$VDV_{S,c,50}$	Ratio A/S
	m/s^2	m/s^2	-	$m/s^{1.75}$	$m/s^{1.75}$	-
1	0.029	0.032	0.90	0.043	0.048	0.90
2	0.032	0.037	0.86	0.050	0.053	0.95
3	0.031	0.036	0.85	0.043	0.046	0.92
4	0.026	0.028	0.92	0.038	0.041	0.93
5	0.036	0.044	0.82	0.048	0.054	0.88
6	0.041	0.049	0.83	0.054	0.060	0.91
7	0.040	0.045	0.89	0.052	0.055	0.94
8	0.028	0.030	0.92	0.041	0.044	0.93
9	0.037	0.037	1.01	0.050	0.050	0.98
10	0.034	0.037	0.92	0.048	0.051	0.94
11	0.044	0.047	0.92	0.055	0.058	0.95
12	0.029	0.032	0.91	0.041	0.043	0.94
13	0.030	0.031	0.96	0.041	0.043	0.97
14	0.038	0.042	0.90	0.054	0.056	0.97
15	0.028	0.033	0.86	0.039	0.043	0.92
16	0.034	0.036	0.95	0.043	0.043	0.98
17	0.034	0.039	0.86	0.044	0.050	0.88
18	0.044	0.048	0.91	0.062	0.067	0.92
19	0.038	0.041	0.92	0.052	0.055	0.95
20	0.030	0.035	0.85	0.044	0.049	0.91
21	0.034	0.035	0.96	0.045	0.047	0.95
22	0.027	0.029	0.93	0.041	0.043	0.95
23	0.034	0.039	0.86	0.048	0.051	0.94
24	0.031	0.034	0.91	0.047	0.049	0.95
25	0.027	0.029	0.92	0.038	0.040	0.93
26	0.027	0.031	0.87	0.038	0.042	0.91
27	0.023	0.026	0.89	0.036	0.038	0.94
28	0.037	0.039	0.93	0.047	0.049	0.96
29	0.034	0.036	0.93	0.043	0.044	0.97
30	0.032	0.034	0.94	0.041	0.043	0.96
31	0.025	0.028	0.88	0.032	0.035	0.94
32	0.028	0.031	0.91	0.036	0.039	0.93
33	0.022	0.026	0.82	0.029	0.034	0.84
34	0.022	0.024	0.91	0.028	0.031	0.90
35	0.042	0.047	0.89	0.052	0.057	0.91
36	0.021	0.024	0.84	0.029	0.032	0.90
		mean	**0.90**		**mean**	**0.93**
		std	**0.04**		**std**	**0.03**

The corrected parameters – a_{max}, a_{rms}, $a_{R,rms}$ and VDV - show a difference of 12%, 17%, 10% and 7% with respect to the accelerometer value respectively, thus confirming the outcome of the single test post-processing previously presented. Once again, the standard deviation (std) remains high for the maximum vertical acceleration, given the limited capacity of the smartphone of capturing peaks.

Table 38 – Results of the Meraviglia P1 case study in terms of absolute raw and corrected values.

	Raw values - Absolute values							
	$a_{max,A}$	$a_{max,S}$	$a_{rms,A}$	$a_{rms,S}$	$a_{Rrms,A}$	$a_{Rrms,S}$	VDV_A	VDV_S
	m/s^2	m/s^2	m/s^2	m/s^2	m/s^2	m/s^2	$m/s^{1.75}$	$m/s^{1.75}$
mean	0.095	0.081	0.015	0.014	0.032	0.028	0.044	0.038
std	0.030	0.027	0.004	0.004	0.011	0.009	0.014	0.012
	Corrected values - 50% - Absolute Values							
	$a_{max,A}$	$a_{max,S,c,50}$	$a_{rms,A}$	$a_{rms,S,c,50}$	$a_{Rrms,A}$	$a_{Rrms,S,c,50}$	VDV_A	$VDV_{S,c,50}$
	m/s^2	m/s^2	m/s^2	m/s^2	m/s^2	m/s^2	$m/s^{1.75}$	$m/s^{1.75}$
mean	0.095	0.107	0.015	0.018	0.032	0.035	0.044	0.046
std	0.030	0.035	0.004	0.005	0.011	0.011	0.014	0.015

Furthermore, Table 39 reports the ratio between accelerometric and smartphone values A/S. Also in this case, the value before and after the application of $k_{w,50}$ coefficients are shown. In accordance to Test n.2 preview, the corrected ratio is < 1.00, thus allowing a safe slight overestimation with the smartphone. The VDV is the most performing parameter, showing a 0.94±0.05 ratio.

Table 39 – Raw and corrected ratio A/S for the Meraviglia P1 case study.

	Raw values - Ratio A/S			
	a_{max}	a_{rms}	a_{Rrms}	VDV
mean	1.17	1.08	1.14	1.15
std	0.11	0.06	0.06	0.06
	Corrected values - 50% - Ratio A/S			
	a_{max}	a_{rms}	a_{Rrms}	VDV
mean	0.89	0.85	0.90	0.94
std	0.09	0.05	0.04	0.05

However, the procedure was applied to a sample of 279 walks, widely larger than the minimum of 40 walks obtained in Section 4.6.3. To this aim, the statistical procedure used during the calibration was here presented again, in order to verify is a sample of 40 is sufficient to obtain a mean value of the parameters that lies inside the threshold of ±1 standard deviation of the 279 samples test. To this aim, 8 walking scenarios were created (from 5 to 70 total walks performed) and 2000 random extraction were done for each scenario, i.e. 2000 random sets of 5 walks were created for the "five walks" scenario, 2000 random sets of 10 walks were created for the "10 walks scenario" and so on. Fig. 105 reports the results. The "40 walks scenario" do not trespass the boundary and so it is suitable to obtain a mean parameter value near to the 279 one.

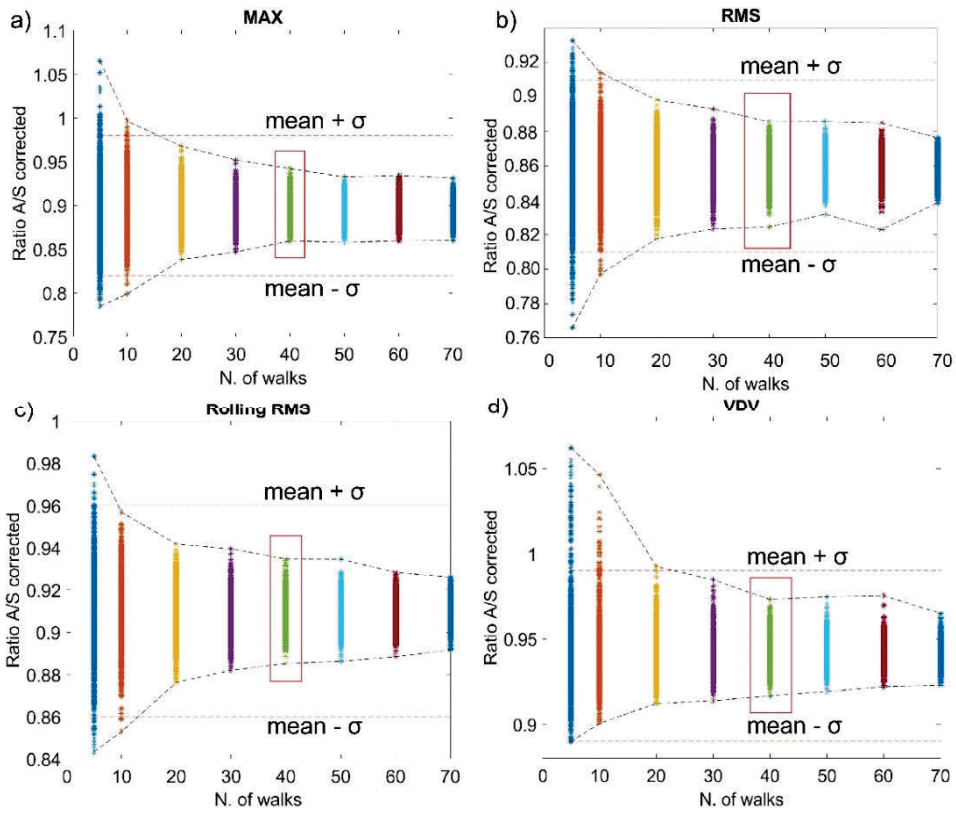

Fig. 105 – Statistical simulation to check if 40 walks are sufficient to respect the ±1 standard deviation boundary.

6.1.2 Heel-drop tests

During test N.5, 17 heel-drops were performed: Six in position 1, five in position 2 and another sequence of six in position 3, see Fig. 106. Moreover, Fig. 107 show the first six heel-drop sequence recorded signal.

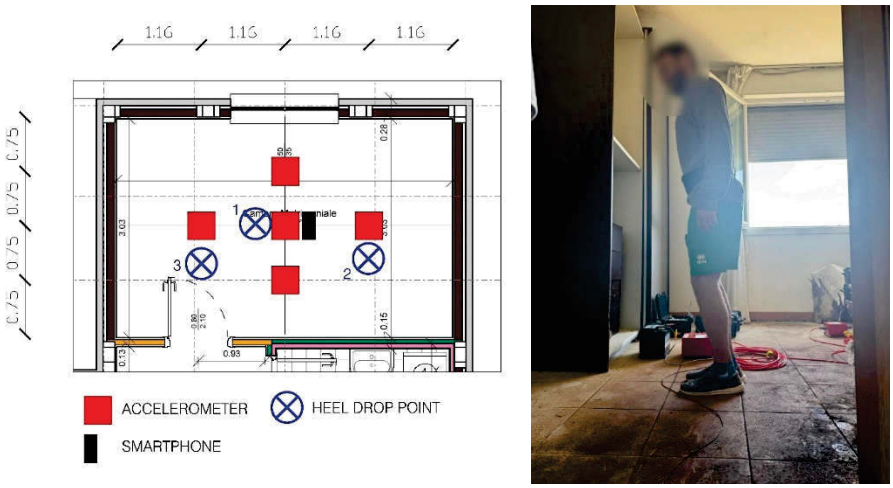

Fig. 106 – Localization of heel-drops (left) and photo from the tests (right).

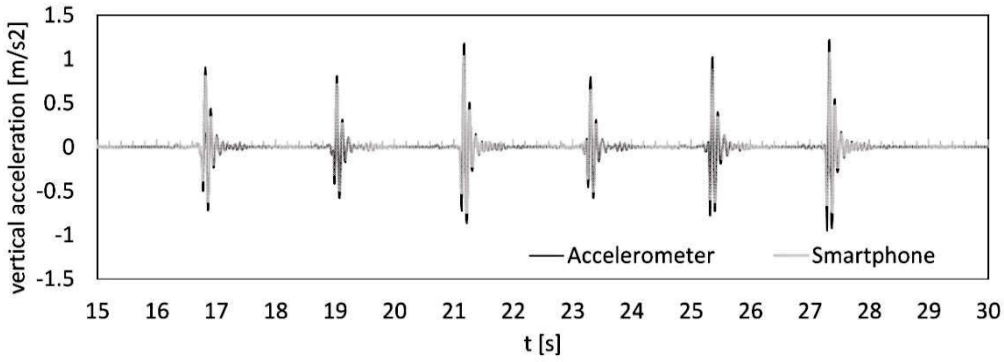

Fig. 107 – Sequence of six heel-drops in position 1.

As for the walk sessions, the raw and corrected mean values are reported in Table 40, allowing a comparison between the parameters. Differences of 22%, 11%, 12% and 8% can be observed for the corrected values, highlighting the great difference in vertical maximum acceleration, with a high standard deviation of 0.30.

Finally, ratio between accelerometric and smartphone data (Ratio A/S) were reported in Table 41, once again confirming the good performance of MEMS device.

Table 40 – Results of the Meraviglia P1 case study in terms of absolute raw and corrected values – heel-drops.

	Raw values - Absolute values							
	$a_{max,A}$	$a_{max,S}$	$a_{rms,A}$	$a_{rms,S}$	$a_{Rrms,A}$	$a_{Rrms,S}$	VDV_A	VDV_S
	m/s^2	m/s^2	m/s^2	m/s^2	m/s^2	m/s^2	$m/s^{1.75}$	$m/s^{1.75}$
mean	0.84	0.72	0.13	0.11	0.27	0.22	0.32	0.27
std	0.22	0.21	0.03	0.03	0.07	0.06	0.11	0.09
	Corrected values - 50% - Absolute Values							
	$a_{max,A}$	$a_{max,S,c,50}$	$a_{rms,A}$	$a_{rms,S,c,50}$	$a_{Rrms,A}$	$a_{Rrms,S,c,50}$	VDV_A	$VDV_{S,c,50}$
	m/s^2	m/s^2	m/s^2	m/s^2	m/s^2	m/s^2	$m/s^{1.75}$	$m/s^{1.75}$
mean	0.84	1.03	0.13	0.14	0.27	0.30	0.32	0.34
std	0.22	0.30	0.03	0.04	0.07	0.08	0.11	0.12

Table 41 – Raw and corrected ratio A/S for the Meraviglia P1 case study – heel-drops.

	Raw values - 50% - Ratio A/S			
	a_{max}	a_{rms}	a_{Rrms}	VDV
mean	1.19	1.20	1.20	1.20
std	0.06	0.04	0.05	0.06
	Corrected values - 50% - Ratio A/S			
	a_{max}	a_{rms}	a_{Rrms}	VDV
mean	0.83	0.90	0.90	0.94
std	0.04	0.03	0.03	0.05

Finally, the minimum number of heel-drops was verified, as for the number of walks. Eight scenarios were developed (from 3 to 20 jumps) and a total of 250 sampling iteration. Twelve heel-drops are sufficient to stay in the boundaries ±1 standard deviation from the mean of the in-situ test (17 heel drops).

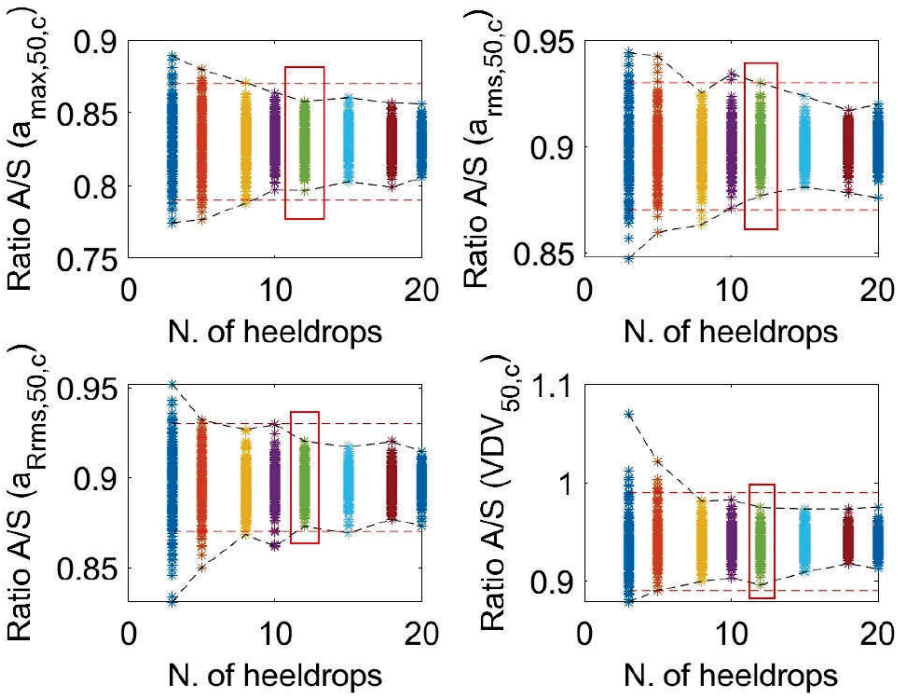

Fig. 108 – Statistical simulation to check if 12 heel-drops are sufficient to respect the ±1 standard deviation boundary.

6.2 Case study 2 – Meraviglia 2nd floor

Since the floor analysed in the previous section highlighted water infiltration from the upper storey, a test campaign was also performed on the balcony form which the water entered, immediately above the first floor. The plan dimension and the setup are reported in Fig. 109. The structure is the same of the previous paragraph, see section 6.1 for the detail.

The five force balance accelerometers and the smartphone were positioned as before, and a longitudinal and a transversal path were defined, according to the direction of the beams. Frequency sampling of 200 Hz for accelerometer and 250 Hz for the MEMS were set.

The floor appears heavily deformed, and the midspan deflection can be visually noticed from Fig. 109, mainly caused by the humidity and water infiltration.

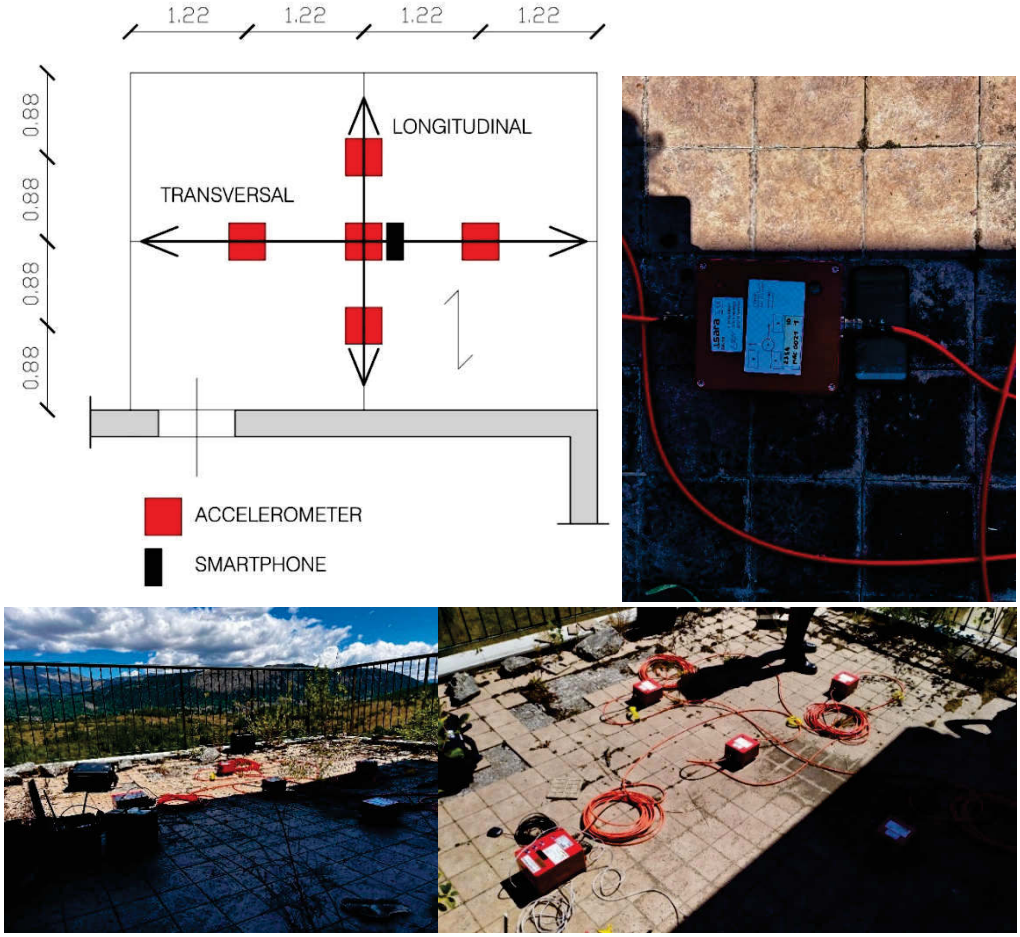

Fig. 109 – Test setup from the Meraviglia P2 case study.

Six tests were performed, according to Table 42. Five walking sessions were carried out, following longitudinal and transversal paths. A sequence of 12 heel-drops was also performed at midspan.

Table 42 – Characteristics of the onsite test.

Test ID	Type	Frequency	Path
1	Walk	2.0	Longitudinal
2	Walk	1.5	Transversal
3	Walk	2.0	Transversal
4	Heel drop	-	-
5	Walk	1.5	Longitudinal
6	Walk	2.0	Transversal

6.2.1 Walking tests

A total of 204 single walks were carried out, starting from the points showed in Fig. 110. The number of single one-way walks was obtained subdividing the signal of each test into single sequences.

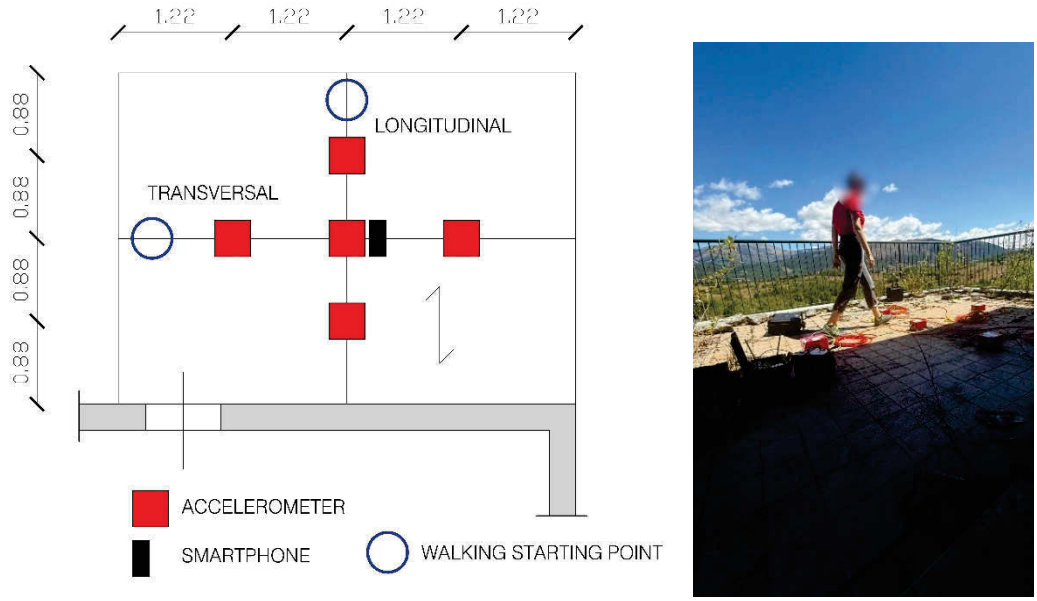

Fig. 110 – Starting position of walking tests (left) and photo from the walking tests (right).

Fig. 111 show, for example, the data collected during test n. 1, which was composed of 46 single walking segments. In Fig. 112, the first five one-way walking sequences are reported. From the peaks, the step frequency can be obtained, showing a variability between 1.65 Hz and 2.29 Hz, thus corresponding to the target of "fast walk at indicative 2.00 Hz".

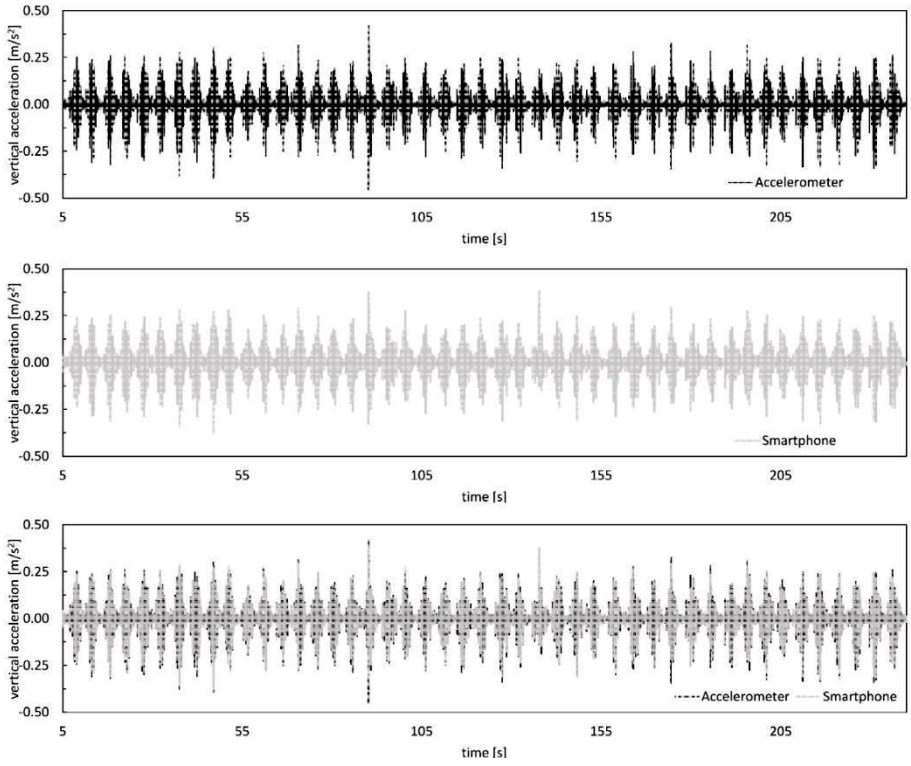

Fig. 111 – Recorded vertical acceleration at midspan during test n.1. Accelerometer and smartphone outcomes are overlapped in the lower tile.

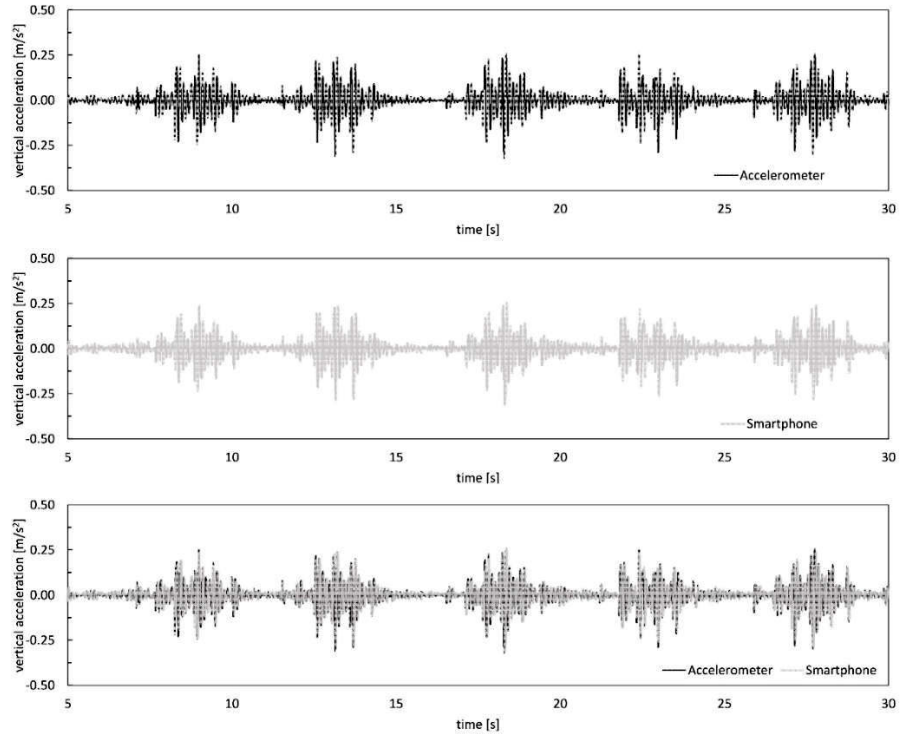

Fig. 112 – Zoom on the first five walks of test n.1. Accelerometer and smartphone outcomes are overlapped in the lower tile.

The complete report is attached in appendix B. Herein, the global results are presented. Table 43 reports the raw and the corrected values for each parameter studied. The corrected outcomes highlight differences of 12%, 17%, 17% and 14% with respect to the accelerometer records. Even if the maximum acceleration gave a better result with respect to the previous tested floor, the standard deviation is high (0.145 m/s^2, compared to a mean value of 0.357 m/s^2).

Table 43 – Results of the Meraviglia P2 case study in terms of absolute raw and corrected values.

	Raw values - Absolute values							
	$a_{max,A}$	$a_{max,S}$	$a_{rms,A}$	$a_{rms,S}$	$a_{Rrms,A}$	$a_{Rrms,S}$	VDV_A	VDV_S
	m/s^2	m/s^2	m/s^2	m/s^2	m/s^2	m/s^2	$m/s^{1.75}$	$m/s^{1.75}$
mean	0.318	0.273	0.054	0.050	0.115	0.106	0.138	0.128
std	0.106	0.111	0.011	0.010	0.027	0.025	0.027	0.026
	Corrected values - 50% - Absolute Values							
	$a_{max,A}$	$a_{max,S,c,50}$	$a_{rms,A}$	$a_{rms,S,c,50}$	$a_{Rrms,A}$	$a_{Rrms,S,c,50}$	VDV_A	$VDV_{S,c,50}$
	m/s^2	m/s^2	m/s^2	m/s^2	m/s^2	m/s^2	$m/s^{1.75}$	$m/s^{1.75}$
mean	0.318	0.357	0.054	0.063	0.115	0.134	0.138	0.157
std	0.106	0.145	0.011	0.013	0.027	0.032	0.027	0.032

Ratio between parameters obtain via force balance accelerometer and smartphone MEMS are also reported in Table 44, both raw and corrected values. Also in this case, the ratio stays below the unity, providing values that – safely – slightly overestimate the parameters with respect to the professional accelerometer.

Table 44 – Raw and corrected ratio A/S for the Meraviglia P2 case study.

	Raw values - Ratio A/S			
	a_{max}	a_{rms}	a_{Rrms}	VDV
mean	0.98	1.09	1.08	1.08
std	0.15	0.06	0.08	0.07
	Corrected values - 50% - Ratio A/S			
	a_{max}	a_{rms}	a_{Rrms}	VDV
mean	0.90	0.85	0.86	0.88
std	0.14	0.05	0.06	0.06

Finally, the statistical procedure to confirm the minimum of 40 walks was performed, in accordance with the scenarios and sampling described for the previous floor (8 scenarios from 5 to 70 walks, 2000 sample for each scenario). The results reported in Fig. 113 show that 40 walks (highlighted in red) are sufficient to not trespass the boundary of one standard deviation around the mean value.

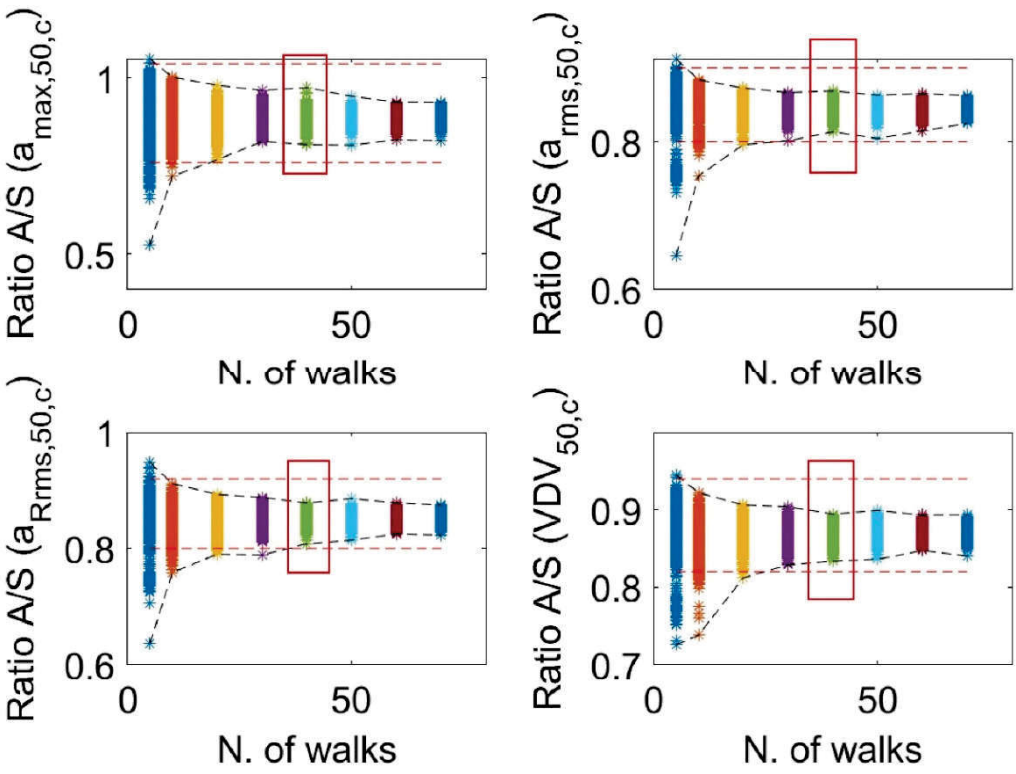

Fig. 113 – Statistical simulation to check if 40 walks are sufficient to respect the ±1 standard deviation boundary.

6.2.2 Heel-drop tests

Then, 12 heel drops were performed, located at midspan (Fig. 114). Differences for corrected values of 9%, 19%, 21% and 16% were detected for a_{max}, a_{rms}, a_{Rrms} and VDV respectively, with respect to the accelerometer outcome. Although the calibration of the coefficients for jumps/heel drops was based on fewer points than for walking, the results obtained are still acceptable for a fast assessment of the timber floor.

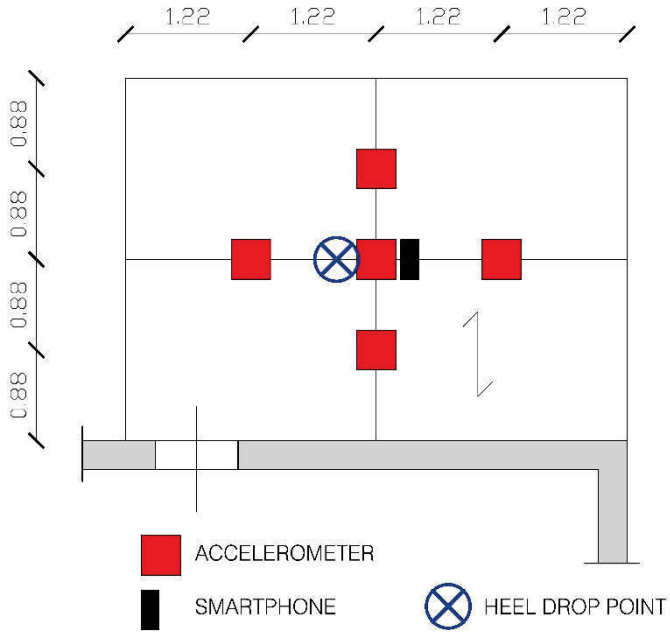

Fig. 114 – Heel-drops localization for the Meraviglia P2 case study.

Table 45 – Results of the Meraviglia P2 case study in terms of absolute raw and corrected values – heel-drops.

	Raw values - Absolute values							
	$a_{max,A}$	$a_{max,S}$	$a_{rms,A}$	$a_{rms,S}$	$a_{Rrms,A}$	$a_{Rrms,S}$	VDV_A	VDV_S
	m/s^2	m/s^2	m/s^2	m/s^2	m/s^2	m/s^2	$m/s^{1.75}$	$m/s^{1.75}$
mean	2.530	1.913	0.346	0.309	0.767	0.684	0.843	0.757
std	0.453	0.325	0.042	0.033	0.059	0.054	0.067	0.063
	Corrected values - 50% - Absolute Values							
	$a_{max,A}$	$a_{max,S,c,50}$	$a_{rms,A}$	$a_{rms,S,c,50}$	$a_{Rrms,A}$	$a_{Rrms,S,c,50}$	VDV_A	$VDV_{S,c,50}$
	m/s^2	m/s^2	m/s^2	m/s^2	m/s^2	m/s^2	$m/s^{1.75}$	$m/s^{1.75}$
mean	2.530	2.736	0.346	0.411	0.767	0.916	0.843	0.969
std	0.453	0.465	0.042	0.044	0.059	0.072	0.067	0.081

Finally, the ratio between accelerometer and smartphone A/S were calculated, and reported in Table 46. Once again, the good performance of smartphone is confirmed, showing differences between -0.16 and -0.07, largely acceptable for a smartphone-based assessment. Moreover, since only 12 heel drops were performed, the statistical procedure to verify the minimum number of heel drops (12) was not carried out.

Table 46 – Raw and corrected ratio A/S for the Meraviglia P2 case study – heel-drops.

	Raw values - Ratio A/S			
	a_{max}	a_{rms}	a_{Rrms}	VDV
mean	1.11	1.12	1.12	1.12
std	0.16	0.06	0.07	0.07
	Corrected values - 50% - Ratio A/S			
	a_{max}	a_{rms}	a_{Rrms}	VDV
mean	0.93	0.84	0.84	0.87
std	0.14	0.05	0.05	0.05

6.3 Case Study 3 – "Historical Palace"

The third case study is an historical palace in the center of L'Aquila. The in-situ tests were carried out on the timber-joisted floor at the upper storey, used as offices. Seven principal beams cover spans between 5.9 and 6.9 m, spaced 2.10 m. The section of the beam was not visible from the lower storey since wood panels hide the elements. The external dimension of the panelled box is 330x490 mm; the measurements were taken using a laser distance meter. Moreover, 8 secondary joists 80x110 mm, 2.10 m span, were placed between each principal beam. Fig. 115 show the floor from the room on the lower storey.

The floor is 17.09 m wide, with a span varying from 5.90 m to 6.90 m, see Fig. 116. Several glass partition walls were installed, dividing the room in three. The office on the right was not accessible, while the central glass curtain did not allow for the walking tests to be performed simultaneously on both sides.

Moreover, another partition wall did not allow longitudinal midspan walks. To overcome the problem, only transversal walks were performed. Furthermore, two paths were considered. The first one, "transversal -partial", starts from the left side and stops near the glass wall. The second one, "transversal – complete", involved two volunteers. The first one started on the left; the second volunteer, positioned near the midspan glass partition wall, started walking after the first one approached midspan, in order to create a unique walk segment. Specular

walk path was followed by the two volunteers to reach again the starting position.

Fig. 115 – Tested timber floor of the historical Palace.

Given the aforementioned boundary condition, only the accessible part of the floor was equipped with force-balance accelerometer (sampling frequency 200 Hz) and the smartphone (sampling frequency 250 Hz), positioned next to the central accelerometer (Fig. 117).

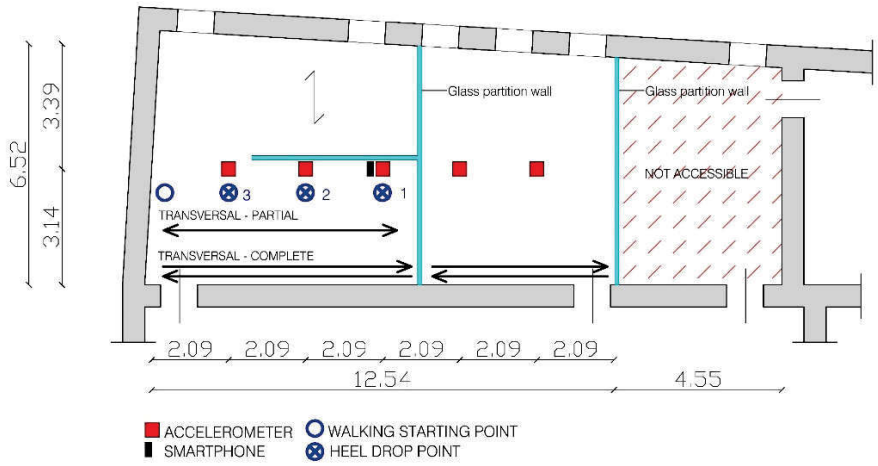

Fig. 116 – Plan view of the tested floor in the historical Palace, showing the test setup.

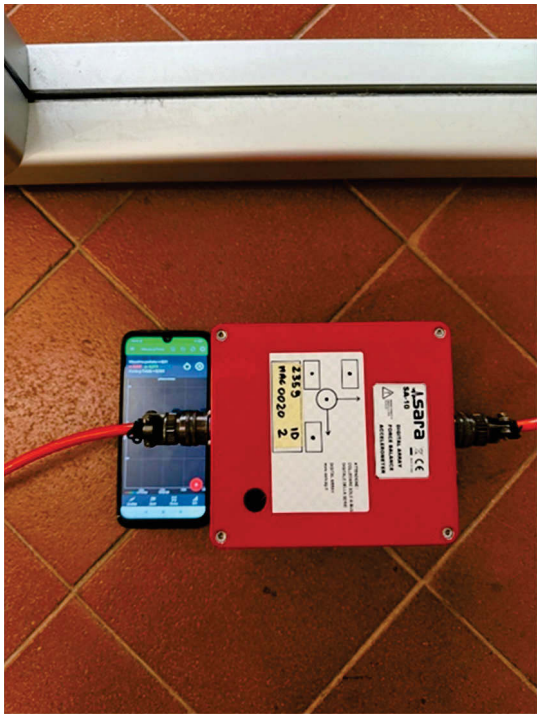

Fig. 117 – SARA FB accelerometer and smartphone positioned at midspan.

The row of instrument was positioned at midspan, not in touch with the glass walls to avoid interferences in vibration.

Eight tests were carried out: 7 walking scenarios and 1 heel drop scenario (Table 47). The step frequency, one again, was varied to simulate a normal (1.5 Hz) and a fast (2.0 Hz) walk. Last walking scenario, with respect to the others, involved 4 volunteers that walked randomly on the floor for 4 minutes.

Table 47 – Characteristics of the onsite test.

Test ID	Type	Frequency	Path
1	Walk	1.5	Transversal - Partial
2	Walk	2.0	Transversal - Partial
3	Walk	1.5	Transversal - Partial
4	Walk	2.0	Transversal - Partial
5	Heel drop	-	-
6	Walk	1.5	Transversal - Complete
7	Walk	2.0	Transversal - Complete
8	Walk	Random	Random

6.3.1 Walking Tests

A total of 133 walks was recorded, subdividing the tested scenarios into single walking sequences (Fig. 118). For example, Fig. 119 reports the vertical acceleration for test n.1, while Fig. 120 shows a zoom of six sequences among the 19 composing the test.

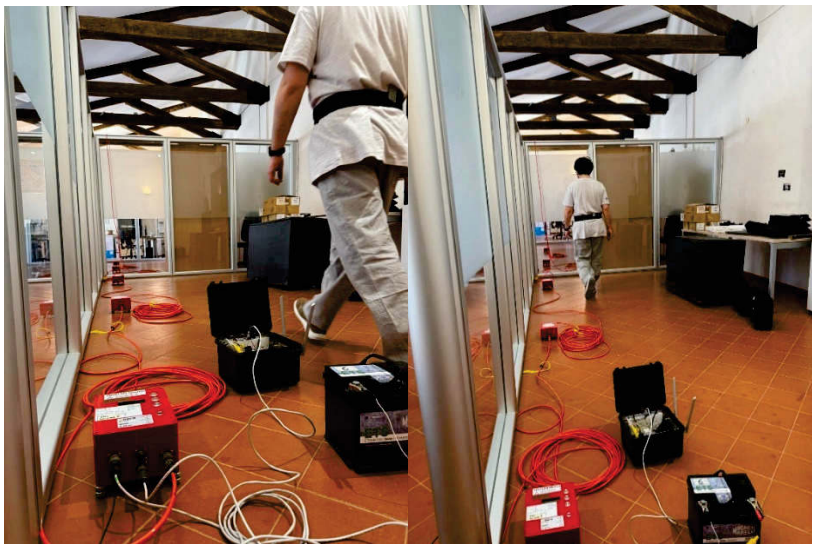

Fig. 118 – Walking tests in the historical palace.

With respect to previous in-situ tests presented, it can be noted that the walk is interrupted at midspan, and then restarted from midspan to reach the starting point. Results are reported for both accelerometer and smartphone, overlapping the signal in the last row. A good superposition can be detected also in this case, with maximum acceleration under 0.05/0.10 m/s^2. It is worth noticing that the smartphone showed a noise signal ±0.012 m/s2, thus not allowing the assessment of stiff floors.

The complete tables of the tests are attached in Appendix B. Herein, the global mean parameters are presented. As for the other case studies, Table 48 enlist the mean value and the standard deviation for a_{max}, a_{rms}, a_{Rrms} and VDV, both raw and corrected. Differences of 20%, 21%, 15% and 15% respectively were found between accelerometer and smartphone corrected parameters.

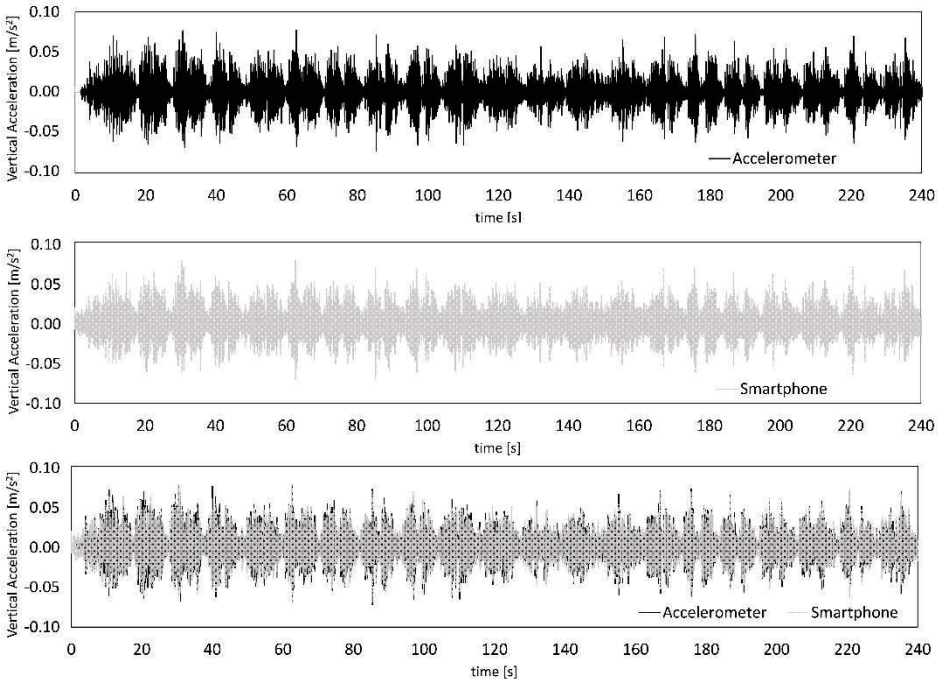

Fig. 119 – Recorded vertical acceleration at midspan during test n.1. Accelerometer and smartphone outcomes are overlapped in the lower tile.

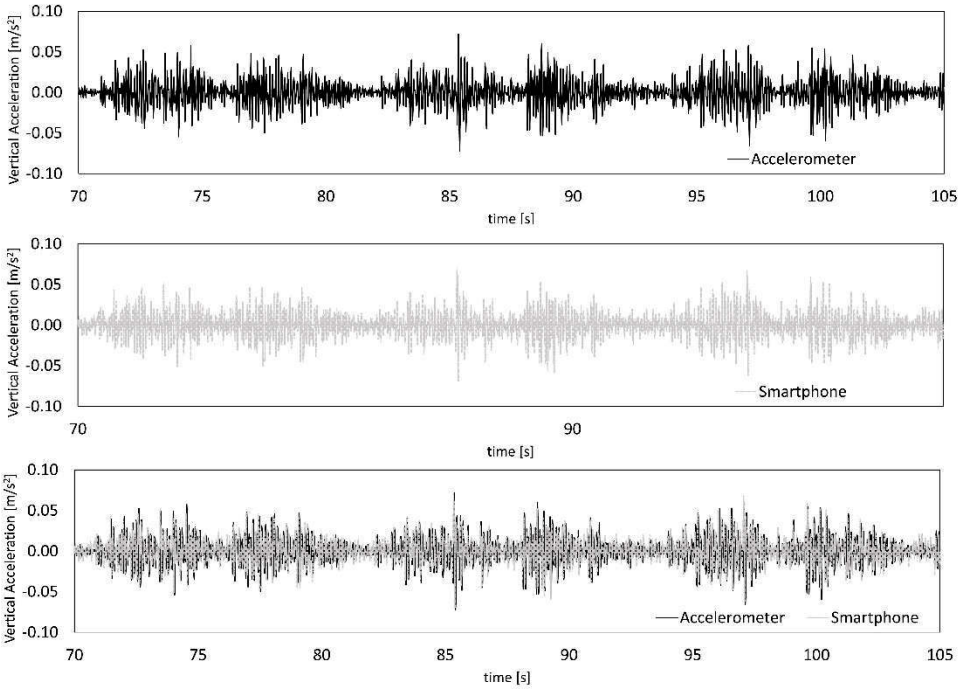

Fig. 120 – Zoom on the first five walks of test n.1. Accelerometer and smartphone outcomes are overlapped in the lower tile.

With respect to the other case studies, this historic floor was stiffer, exhibiting smaller vertical acceleration due to walking. Thus, the lower sensitivity influenced the collected data. Nonetheless, the 20% difference is acceptable, considering the advantages of taking fast in-situ tests through smartphone devices.

Table 48 – Results of the historical palace case study in terms of absolute raw and corrected values.

	Raw values - Absolute values							
	$a_{max,A}$	$a_{max,S}$	$a_{rms,A}$	$a_{rms,S}$	$a_{Rrms,A}$	$a_{Rrms,S}$	VDV_A	VDV_S
	m/s^2	m/s^2	m/s^2	m/s^2	m/s^2	m/s^2	$m/s^{1.75}$	$m/s^{1.75}$
mean	0.073	0.067	0.016	0.016	0.031	0.028	0.039	0.036
std	0.025	0.020	0.004	0.003	0.010	0.008	0.010	0.008
	Corrected values - 50% - Absolute Values							
	$a_{max,A}$	$a_{max,S,c,50}$	$a_{rms,A}$	$a_{rms,S,c,50}$	$a_{Rrms,A}$	$a_{Rrms,S,c,50}$	VDV_A	$VDV_{S,c,50}$
	m/s^2	m/s^2	m/s^2	m/s^2	m/s^2	m/s^2	$m/s^{1.75}$	$m/s^{1.75}$
mean	0.073	0.088	0.016	0.020	0.031	0.036	0.039	0.044
std	0.025	0.027	0.004	0.004	0.010	0.010	0.010	0.010

Furthermore, the good results are also highlighted by the ratio A/S, between accelerometer and smartphone (Table 49). Raw ratio gave values near the unity but, however, the results are not conservative, since an underestimation would be provided. On the other hand, the corrected values are conservative, showing ratio between 0.82 and 0.87.

Table 49 – Raw and corrected ratio A/S for the historical Palace case study.

	Raw values - Ratio A/S			
	a_{max}	a_{rms}	a_{Rrms}	VDV
mean	1.08	1.04	1.08	1.07
std	0.10	0.05	0.07	0.05
	Corrected values - 50% - Ratio A/S			
	a_{max}	a_{rms}	a_{Rrms}	VDV
mean	0.83	0.82	0.86	0.87
std	0.07	0.04	0.05	0.04

Finally, the statistical simulation on 40 walks were carried out, as for the other case studies. For all the parameters, the 40 walks scenario

stays in the threshold, thus confirming that the number of walks is suitable to have a representative mean value.

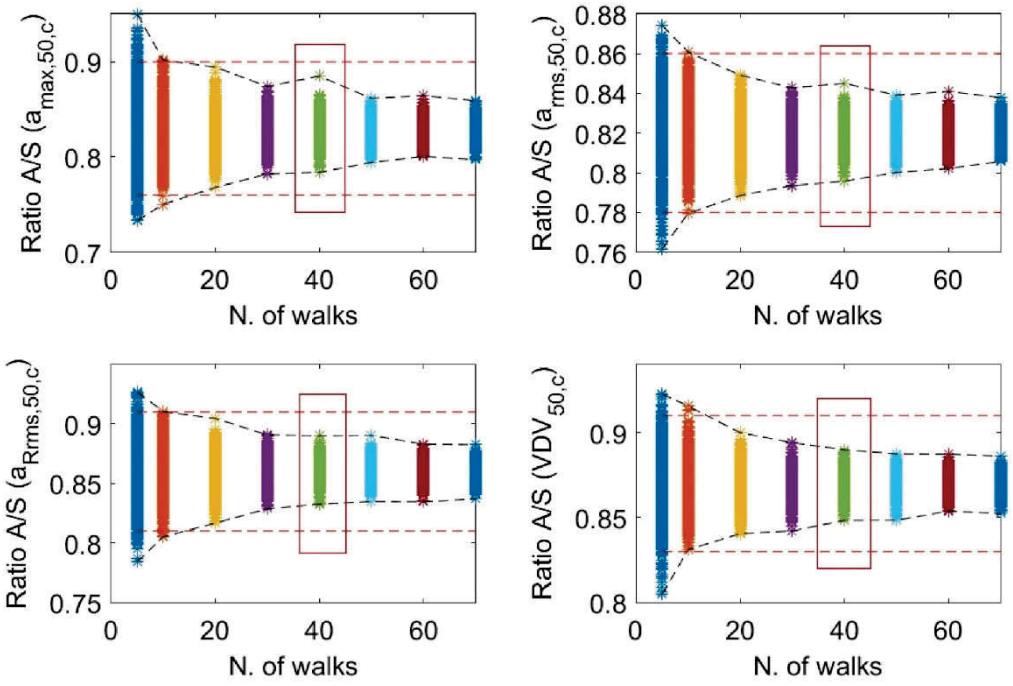

Fig. 121 – Statistical simulation to check if 40 walks are sufficient to respect the ±1 standard deviation boundary.

6.3.2 Heel-drop tests

The same procedure was used to analyse the outcomes of the 17 heel-drops of test n. 5, performed in the positioned shown in Fig. 116. Fig. 122 reports the recorded signals, overlapping the accelerometer and smartphone time histories. Moreover, a zoom in was done in Fig. 123, focusing on the first set of six heel drops.

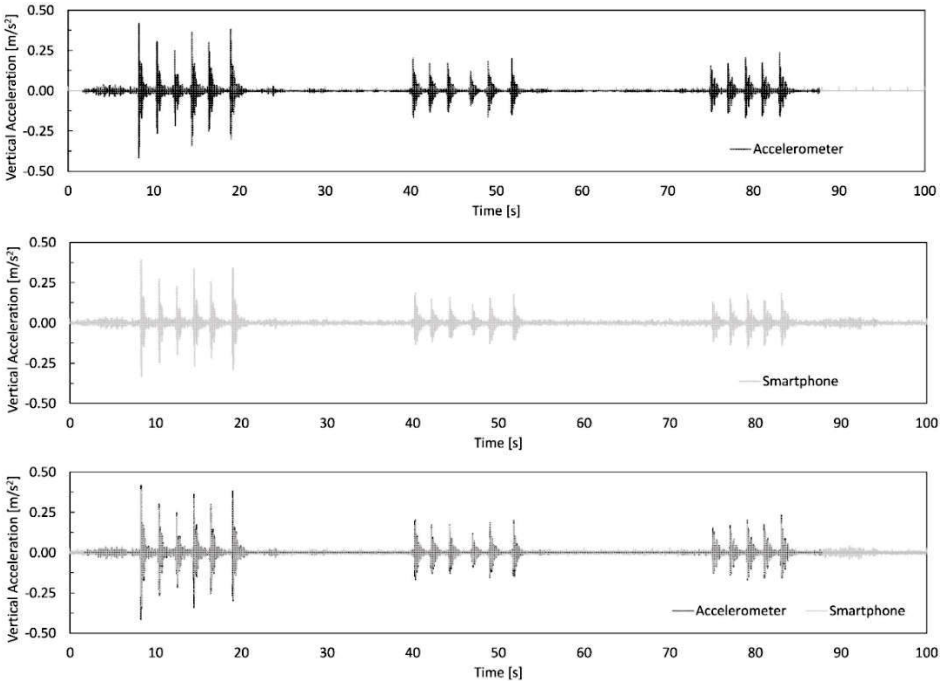

Fig. 122 – Recorded vertical acceleration at midspan during heel-drops. Accelerometer and smartphone outcomes are overlapped in the lower tile.

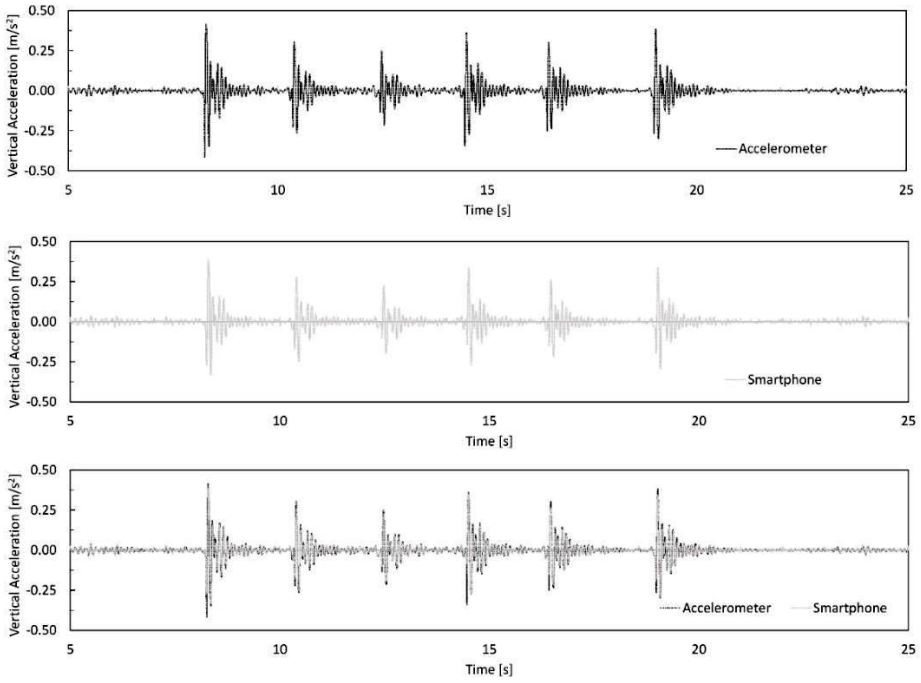

Fig. 123 – Zoom on the first five heel-drops. Accelerometer and smartphone signals are overlapped in the last tile.

Mean and standard deviation are reported for each parameter in Table 50, both raw and corrected values. Differences of 26%, 21%, 22% and 17% were detected for each corrected comfort parameter. The highest value is linked to the maximum vertical acceleration, showing also a high standard deviation of 0.120 m/s^2 compared to the absolute value of 0.303 m/s^2.

Table 50 – Results of the historical palace case study in terms of absolute raw and corrected values – heel-drops.

	Raw values - Absolute values							
	$a_{max,A}$	$a_{max,S}$	$a_{rms,A}$	$a_{rms,S}$	$a_{Rrms,A}$	$a_{Rrms,S}$	VDV_A	VDV_S
	m/s^2	m/s^2	m/s^2	m/s^2	m/s^2	m/s^2	$m/s^{1.75}$	$m/s^{1.75}$
mean	0.240	0.212	0.047	0.043	0.095	0.086	0.105	0.096
std	0.089	0.084	0.018	0.015	0.036	0.031	0.044	0.039
	Corrected values - 50% - Absolute Values							
	$a_{max,A}$	$a_{max,S,c,50}$	$a_{rms,A}$	$a_{rms,S,c,50}$	$a_{Rrms,A}$	$a_{Rrms,S,c,50}$	VDV_A	$VDV_{S,c,50}$
	m/s^2	m/s^2	m/s^2	m/s^2	m/s^2	m/s^2	$m/s^{1.75}$	$m/s^{1.75}$
mean	0.240	0.303	0.047	0.057	0.095	0.116	0.105	0.123
std	0.089	0.120	0.018	0.020	0.036	0.042	0.044	0.050

Ratio between accelerometer and smartphone values are finally reported in Table 51, confirming the outcomes of the previous case studies and proving that the MEMS of smartphone can be reliable in the comfort assessment of typical historical floors.

Table 51 – Raw and corrected ratio A/S for the historical palace case study – heel-drops.

	Raw values - Ratio A/S			
	a_{max}	a_{rms}	a_{Rrms}	VDV
mean	1.14	1.09	1.09	1.09
std	0.07	0.05	0.05	0.04
	Corrected values - 50% - Ratio A/S			
	a_{max}	a_{rms}	a_{Rrms}	VDV
mean	0.80	0.82	0.82	0.85
std	0.05	0.04	0.04	0.03

II-C | CONCLUSIONS

The second part of the thesis focused on the problem of fast assessing the comfort of wooden joisted floors. After an initial overview of the most common historical and modern floors, the dissertation analysed the problem of vibrations in floors, examining codes and guidelines for defining comfort standards.

For the analysis of floors subjected to human induced loads, both deterministic and probabilistic approaches were considered. Nonetheless, only probabilistic approaches allow intra- and inter-subject variability to be taken into account.

To date, the use of smartphones as substitutes for professional accelerometers is becoming increasingly widespread. Although smartphones cannot reach the level of accuracy of professional instruments, they represent a valid alternative in terms of cost, speed of use, and output quality.

The main goal of the study was, in fact, to verify whether smartphones can be implemented as a tool for the comfort fast assessment of wooden floors.

To develop an assessment protocol, a full-scale timber floor prototype was built in laboratory, and successively subjected to human induced vibrations. Two volunteers walked together or separately, at different pacing frequencies, and the vertical accelerations were recorded simultaneously by force-balance accelerometers and built-in sensors of commercial smartphones.

Starting from these results, corrective coefficients were developed, in order to minimize the difference between the two sensors. Moreover,

through a statistical simulation, the minimum number of walks and heel drops was established.

The developed procedure consists in a total of 40 walks (4 sessions of 10 walks each) and 12 heel drops. The walking sessions are performed both longitudinally and transversally to the joist direction, at 1.5 Hz and 2.0 Hz, thus simulating normal and fast walk.

Furthermore, starting from a FEM model of the tested floor, a parametric study was developed for simply supported joisted floors, varying span, beams properties, damping, upper top layers and connection stiffness. Moreover, a probabilistic model was used to evaluate the human induced loads applied to the structures. Over 600,000 linear dynamic analysis were carried out, and the results discussed. Even if all the tested configuration were previously checked according to Eurocode provisions, only 50% (1% damping) and 63% (4% damping) satisfied comfort requirements in terms of VDV. A deeper evaluation showed that using a "mass check" on the floor in addition to Eurocode verifications can rise the percentage to 95%.

Finally, the developed protocol was successfully applied to three case studies in L'Aquila. Two timber floors of a residential building were assessed, highlighting VDV ratios between force balance accelerometer and smartphone of 0.94 ± 0.05 and 0.88 ± 0.06 respectively. Moreover, a wooden floor in an historical palace of L'Aquila was also assessed, obtaining a ratio of 0.87 ± 0.04. In all case studies, the corrected values obtained from smartphone assessment were slightly higher than the effective records from the force balance accelerometers. However, it is worth noticing that a conservative approach is preferable and, thus, a ratio below the unity was seek.

Further development of the protocol will consider more devices to calibrate the corrective coefficients. Moreover, the implementation of a frequency evaluation via smartphone can be taken into account, together with the development of a dedicated application. The application, in fact, can represent an impactful tool for practitioners during decision making process. Nonetheless, the results obtained in laboratory and in situ suggests that the use of smartphones can be a cost-effective alternative for fast assessment of timber floors.

II-R | REFERENCES

[1] Y. C. V. da Costa and T. D. de Araujo, "Evaluation of dynamic behaviour of waffle slab to gym center," *Latin American Journal of Solids and Structures*, vol. 11, pp. 1114–1131, 2014.

[2] C. A. Jones, P. Reynolds, and A. Pavic, "Vibration serviceability of stadia structures subjected to dynamic crowd loads: A literature review," *J Sound Vib*, vol. 330, no. 8, pp. 1531–1566, Apr. 2011, doi: 10.1016/j.jsv.2010.10.032.

[3] S. V. Ohlsson, "Serviceability criteria—Especially floor vibration criteria," in *Proc., Int. Timber Engineering Conf., 1.58–1.65. London: Timber Research and Development Association*, 1991.

[4] I. Smith and Y. H. Chui, "Design of lightweight wooden floors to avoid human discomfort," *Canadian Journal of Civil Engineering*, vol. 15, no. 2, pp. 254–262, Apr. 1988, doi: 10.1139/l88-033.

[5] D. M. Onysko, L. J. Hu, E. D. Jones, and B. Di Lenardo, "Serviceability design of residential wood framed floors in Canada," in *World Conf. on Timber Engineering, 1–8. Vancouver*, 2000.

[6] M. M. Ebadi, G. Doudak, and I. Smith, "Finite-Element Modeling and Parametric Study of Glulam Beam-and-Deck Floors," *Journal of Structural Engineering*, vol. 143, no. 9, Sep. 2017, doi: 10.1061/(ASCE)ST.1943-541X.0001844.

[7] B. M. Basaglia, J. Li, R. Shrestha, and K. Crews, "Response Prediction to Walking-Induced Vibrations of a Long-Span Timber Floor," *Journal of Structural Engineering*, vol. 147, no. 2, Feb. 2021, doi: 10.1061/(ASCE)ST.1943-541X.0002888.

[8] X. Zhao, K. Ri, R. Han, Y. Yu, M. Li, and J. Ou, "Experimental Research on Quick Structural Health Monitoring Technique for

Bridges Using Smartphone," *Advances in Materials Science and Engineering*, vol. 2016, pp. 1–14, 2016, doi: 10.1155/2016/1871230.

[9] G. M. Guzman-Acevedo *et al.*, "GPS, Accelerometer, and Smartphone Fused Smart Sensor for SHM on Real-Scale Bridges," *Advances in Civil Engineering*, vol. 2019, no. 1, Jan. 2019, doi: 10.1155/2019/6429430.

[10] S. Dashti, J. D. Bray, J. Reilly, S. Glaser, A. Bayen, and E. Mari, "Evaluating the Reliability of Phones as Seismic Monitoring Instruments," *Earthquake Spectra*, vol. 30, no. 2, pp. 721–742, May 2014, doi: 10.1193/091711EQS229M.

[11] L. Martinelli, V. Racic, B. A. Dal Lago, and F. Foti, "Testing Walking-Induced Vibration of Floors Using Smartphones Recordings," *Robotics*, vol. 9, no. 2, p. 37, May 2020, doi: 10.3390/robotics9020037.

[12] J. M. Bresolin, M. Kripka, and Z. M. C. Pravia, "Experimental study of human-induced vibrations on glued laminated timber floors," *Structures*, vol. 79, p. 109375, Sep. 2025, doi: 10.1016/j.istruc.2025.109375.

[13] E. Zamperini, "Solai a struttura lignea Dalla conoscenza all'intervento di conservazione e recupero. Parte prima: le tecniche costruttive storiche," *Ingenio (in italian)*, 2016.

[14] E. Pittini, *Architettura tecnica. Corso di elementi costruttivi*. Torino: Giorgio Ed., 1937.

[15] E. Marrullier, *La costruzione degli edifizi*. Torino (in italian): UTET, 1910.

[16] C. Caveglia, *Corso di costruzioni civili e militari. Vol. 3*. Torino (in italian): Scuola d'Applicazione delle Armi d'Artiglieria e Genio, Stamperia dell'unione tipografico-editrice, 1878.

[17] G. A. Breymann and H. LAng, *Allgemeine Bau-konstruktions-lehre mit besonderer Beziehung auf das Hochbauwesen. II. Teil. Konstruktionen in Holz*. Leipzig (in german): Gebhardt, 1885.

[18] J. Weckendorf, T. Toratti, I. Smith, and T. Tannert, "Vibration serviceability performance of timber floors," *European Journal of Wood and Wood Products*, vol. 74, no. 3, pp. 353–367, May 2016, doi: 10.1007/s00107-015-0976-z.

[19] W. P. Council. Woodworks, *U.S. Mass Timber Floor Vibration DESIGN GUIDE*. 2023.

[20] https://www.woodworks.org/learn/mass-timber-clt/, "What is mass timber?"

[21] S. Cuerrier-Auclair, *Design Guide for Timber-Concrete composite floors in Canada*. Pointe-Claire, Quebec: FPInnovation, 2020.

[22] P. G. G. dos Santos, C. E. de J. Martins, J. Skinner, R. Harris, A. M. P. G. Dias, and L. M. C. Godinho, "Modal Frequencies of a Reinforced Timber-Concrete Composite Floor: Testing and Modeling," *Journal of Structural Engineering*, vol. 141, no. 11, Nov. 2015, doi: 10.1061/(ASCE)ST.1943-541X.0001275.

[23] H. Howarth, "Evaluation and assessment of building vibration with respect to human response: a summary of standardised methods," https://www.association-of-noise-consultants.co.uk/wp-content/uploads/2020/11/Evaluation-and-assessement-of-building-vibration-with-respect-to-human-response-Henriette-Howarth.pdf.

[24] K. Jarnerö, A. Brandt, and A. Olsson, "Vibration properties of a timber floor assessed in laboratory and during construction," *Eng Struct*, vol. 82, pp. 44–54, Jan. 2015, doi: 10.1016/j.engstruct.2014.10.019.

[25] V. Racic, A. Pavic, and J. M. W. Brownjohn, "Experimental identification and analytical modelling of human walking forces: Literature review," *J Sound Vib*, vol. 326, no. 1–2, pp. 1–49, Sep. 2009, doi: 10.1016/j.jsv.2009.04.020.

[26] H. Karampour *et al.*, "DESIGN OF LONG-SPAN LIGHTWEIGHT TIMBER FLOORS SUBJECT TO WALKING EXCITATIONS: A CASE STUDY," in *World Conference on Timber Engineering (WCTE 2023)*, As, Norway: World Conference on Timber Engineering (WCTE 2023), 2023, pp. 1873–1879. doi: 10.52202/069179-0247.

[27] A. Aloisio, D. P. Pasca, D. Owolabi, and C. Loss, "Vibration serviceability of hybrid CLT-steel composite floors based on experimental and numerical investigations using random walk models," *Eng Struct*, vol. 304, p. 117600, Apr. 2024, doi: 10.1016/j.engstruct.2024.117600.

[28] L. Kozarić, Đ. Varju, M. Vojnić Purčar, S. Bursać, and A. Čeh, "Experimental investigations and numerical simulations of the vibrational performance of composite timber-lightweight concrete floor structures," *Eng Struct*, vol. 270, p. 114908, Nov. 2022, doi: 10.1016/j.engstruct.2022.114908.

[29] D. Casagrande, I. Giongo, F. Pederzolli, A. Franciosi, and M. Piazza, "Analytical, numerical and experimental assessment of vibration performance in timber floors," *Eng Struct*, vol. 168, pp. 748–758, Aug. 2018, doi: 10.1016/j.engstruct.2018.05.020.

[30] Y. Miyazu and C. Loss, "Evaluation of vibration properties of an 18-story mass timber–concrete hybrid building by on-site vibration tests," *J Civ Struct Health Monit*, vol. 14, no. 4, pp. 909–929, Apr. 2024, doi: 10.1007/s13349-024-00767-z.

[31] A. Kowalska-Koczwara and K. Stypuła, "Influence of crest factor on evaluation of human perception of traffic vibration," *Journal of Measurements in Engineering*, vol. 6, no. 4, pp. 250–255, Dec. 2018, doi: 10.21595/jme.2018.20421.

[32] A. Smith, S. Hicks, and P. Devine, "Design of Floors for Vibration: A New Approach, 2nd ed," *Steel Construction Institute (SCI),Berkshire, UK*, 2009.

[33] N. A. Jacobs, J. Skorecki, and J. Charnley, "Analysis of the vertical component of force in normal and pathological gait," *J Biomech*, vol. 5, no. 1, pp. 11–34, Jan. 1972, doi: 10.1016/0021-9290(72)90016-4.

[34] J. H. Rainer, G. Pernica, and D. E. Allen, "Dynamic loading and response of footbridges," *Canadian Journal of Civil Engineering*, vol. 15, no. 1, pp. 66–71, 1988, doi: 10.1139/l88-007.

[35] T. M. Murray, D. E. Allen, E. E. Ungar, and D. B. Davis, *Steel Design Guide 11 Vibrations of steel-framed structural systems due to human activity. 2nd ed.* Chicago: American Institute of Steel Construction, 2016.

[36] M. R. Willford and P. Young, "A design guide for footfall induced vibration of structures. CCIP-016," *Surrey, UK: Concrete Society.*, 2006.

[37] International Organization for Standardization, "ISO 10137: Bases for design of structures – Serviceability of buildings and walkways against vibrations," *Geneva, Switzerland*, 2007.

[38] EN 1995-1-1:2005, "Eurocode 5: design of timber structures - Part 1-1: General-common rules and rules for buildings, Brussel, Belgium," 2005.

[39] S. Ohlsson, "Ten years of floor vibration research—A review of aspects and some results," in *Symposium/Workshop on Serviceability of Buildings (Movements, Deformations, Vibrations)*, Ottawa, Canada, 1988, pp. 419–434.

[40] J. M. W. Brownjohn and C. J. Middleton, "Procedures for vibration serviceability assessment of high-frequency floors," *Eng Struct*, vol. 30, no. 6, pp. 1548–1559, Jun. 2008, doi: 10.1016/j.engstruct.2007.10.006.

[41] B. R. Ellis, "On the response of long-span floors to walking loads generated by individuals and crowds," *The Structural Engineer*, vol. 78, no. 10, pp. 17–25, 2000.

[42] S. Živanović and A. Pavić, "Probabilistic Modeling of Walking Excitation for Building Floors," *Journal of Performance of Constructed Facilities*, vol. 23, no. 3, pp. 132–143, Jun. 2009, doi: 10.1061/(ASCE)CF.1943-5509.0000005.

[43] J. Brownjohn, V. Racic, and J. Chen, "Universal response spectrum procedure for predicting walking-induced floor vibration," *Mech Syst Signal Process*, vol. 70–71, pp. 741–755, Mar. 2016, doi: 10.1016/j.ymssp.2015.09.010.

[44] A. S. Mohammed, A. Pavic, and V. Racic, "Improved model for human induced vibrations of high-frequency floors," *Eng Struct*, vol. 168, pp. 950–966, Aug. 2018, doi: 10.1016/j.engstruct.2018.04.093.

[45] J. Chen, G. Ding, and S. Živanović, "Stochastic Single Footfall Trace Model for Pedestrian Walking Load," *International Journal of Structural Stability and Dynamics*, vol. 19, no. 03, p. 1950029, Mar. 2019, doi: 10.1142/S0219455419500299.

[46] J. Weckendorf, "Dynamic response of structural timber flooring systems," Ph.D. Thesis, Edinburgh Napier University, Edinburgh, UK, 2009.

[47] M. M. Ebadi, G. Doudak, and I. Smith, "Evaluation of floor vibration caused by human walking in a large glulam beam and deck floor," *Eng Struct*, vol. 196, p. 109349, Oct. 2019, doi: 10.1016/j.engstruct.2019.109349.

[48] A. Polensek, "Structural damping and its effect on human response to floor vibrations," *Forest Research Laboratory, Oregon State University, Corvallis*, 1985.

[49] J. Weckendorf and I. Smith, "Multi-functional interface concept for high-rise hybrid building systems with structural timber," in *World conference on timber engineering, Auckland, New Zealand*, 2012.

[50] L. Hu and S. Gagnon, "Vibration performance of cross-laminated timber floors.," in *Gagnon S, Pirvu C (eds) CLT Handbook*, S. Gagnon and C. Pirvu, Eds., 2011.

[51] S. V Ohlsson and stål-och träbyggnad Chalmers tekniska högskola Institutionen för konstruktionsteknik, "Floor vibrations and human discomfort," Göteborg, Sweden, 1982.

[52] A. Homb, "Low frequency sound and vibrations from impacts on timber floor constructions," 2006.

[53] T. Toratti and A. Talja, "Classification of Human Induced Floor Vibrations," *Building Acoustics*, vol. 13, no. 3, pp. 211–221, Sep. 2006, doi: 10.1260/135101006778605370.

[54] Y. H. Chui, "Vibrational performance of wooden floors in domestic dwellings," Thesis (Ph.D.) - Brighton Polytechnic, 1987.

[55] BS EN 1995-1-1:2004+A1:2008, "UK national annex to Eurocode 5," 2008.

[56] RFS2-CT-2007-00033, "Design of Footbridges Guideline. Human Induced Vibrations of Steel Structures. HIVOSS," *Luxembourg*, 2009.

[57] P. Hamm, A. Richter, and S. Winter, "Floor vibrations–new results," in *11th World Conference on Timber Engineerig (WCTE2010)*, Riva del Garda, Italy, 2010.

[58] F. Solarino, D. V. Oliveira, and L. Giresini, "Wall-to-horizontal diaphragm connections in historical buildings: A state-of-the-art review," *Eng Struct*, vol. 199, p. 109559, Nov. 2019, doi: 10.1016/j.engstruct.2019.109559.

[59] S. Zhang and Y. H. Chui, "Quantifying the effect of end support restraints on vibration serviceability of mass timber floor systems: Testing," *Eng Struct*, vol. 301, p. 117189, Feb. 2024, doi: 10.1016/j.engstruct.2023.117189.

[60] S. Zhang, J. Zhou, J. Niederwestberg, and Y. H. Chui, "Effect of end support restraints on vibration performance of cross laminated timber floors: An analytical approach," *Eng Struct*, vol. 189, pp. 186–194, Jun. 2019, doi: 10.1016/j.engstruct.2019.03.042.

[61] O. A. B. Hassan, "Effect of wooden floorboards on the vibration of timber floor," *Sci Rep*, vol. 14, no. 1, p. 779, Jan. 2024, doi: 10.1038/s41598-023-50015-5.

[62] A. Khokhar, Y. H. Chui, and I. Smith, "Influence of between-joists bridging elements on static and dynamic response of wood joisted floors," *Eng Struct*, vol. 188, pp. 362–368, Jun. 2019, doi: 10.1016/j.engstruct.2019.03.039.

[63] T. Ji and B. Ellis, "Floor vibration induced by dance type loads: Theory," *The Structural Engineer*, vol. 72, pp. 37–44, 1994.

[64] N. Lythgo, C. Wilson, and M. Galea, "Basic gait and symmetry measures for primary school-aged children and young adults whilst walking barefoot and with shoes," *Gait Posture*, vol. 30, no. 4, pp. 502–506, Nov. 2009, doi: 10.1016/j.gaitpost.2009.07.119.

[65] N. Lythgo, C. Wilson, and M. Galea, "Basic gait and symmetry measures for primary school-aged children and young adults. II: Walking at slow, free and fast speed," *Gait Posture*, vol. 33, no. 1, pp. 29–35, Jan. 2011, doi: 10.1016/j.gaitpost.2010.09.017.

[66] H. V. Dang and S. Živanović, "Experimental characterisation of walking locomotion on rigid level surfaces using motion capture system," *Eng Struct*, vol. 91, pp. 141–154, May 2015, doi: 10.1016/j.engstruct.2015.03.003.

[67] S. Živanović, A. Pavic, and V. Racic, "Towards Modelling In-Service Pedestrian Loading of Floor Structures," in *Topics on the Dynamics of Civil Structures, Volume 1*, New York: River Publishers, 2025, pp. 85–94. doi: 10.1007/978-1-4614-2413-0_9.

[68] A. Pachi and T. Ji, "Frequency and velocity of people walking," *The Structural Engineer*, vol. 83, pp. 36–40, 2005.

[69] C. C. Caprani, "Application of the pseudo-excitation method to assessment of walking variability on footbridge vibration," *Comput Struct*, vol. 132, pp. 43–54, Feb. 2014, doi: 10.1016/j.compstruc.2013.11.001.

[70] S. Živanović, A. Pavić, and P. Reynolds, "Probability-based prediction of multi-mode vibration response to walking excitation," *Eng Struct*, vol. 29, no. 6, pp. 942–954, Jun. 2007, doi: 10.1016/j.engstruct.2006.07.004.

[71] G. Piccardo and F. Tubino, "Simplified procedures for vibration serviceability analysis of footbridges subjected to realistic walking loads," *Comput Struct*, vol. 87, no. 13–14, pp. 890–903, Jul. 2009, doi: 10.1016/j.compstruc.2009.04.006.

[72] M. Willford, P. Young, and C. Field, "Predicting footfall-induced vibration: Part 1," *Proceedings of the Institution of Civil Engineers - Structures and Buildings*, vol. 160, no. 2, pp. 65–72, Apr. 2007, doi: 10.1680/stbu.2007.160.2.65.

[73] E. Shahabpoor, A. Pavic, and V. Racic, "Structural vibration serviceability: New design framework featuring human-structure interaction," *Eng Struct*, vol. 136, pp. 295–311, Apr. 2017, doi: 10.1016/j.engstruct.2017.01.030.

[74] Z. Muhammad, P. Reynolds, O. Avci, and M. Hussein, "Review of Pedestrian Load Models for Vibration Serviceability Assessment of Floor Structures," *Vibration*, vol. 2, no. 1, pp. 1–24, Dec. 2018, doi: 10.3390/vibration2010001.

[75] European Commission: Directorate-General for Research and Innovation, *Generalisation of criteria for floor vibrations for industrial, office, residential and public building and gymnastic halls*. Publications Office, 2006.

[76] H. Bachmann *et al.*, *Vibration Problems in Structures*. Basel: Birkhäuser Basel, 1995. doi: 10.1007/978-3-0348-9231-5.

[77] Service d´Etudes Techniques des Routes et Autoroutes, "Footbridges: Assessment of vibrational behaviour of footbridges under pedestrian loading - SETRA," *Paris*, 2006.

[78] J. Fernández Martínez, L. Hermanns, A. Fraile de Lerma, and E. Alarcón Álvarez, "Jumping load models applied on a gymnasium

floor," *Eng Struct*, vol. 125, pp. 26–38, Oct. 2016, doi: 10.1016/j.engstruct.2016.06.051.

[79] J. Sim, A. Blakeborough, M. S. Williams, and G. Parkhouse, "Statistical Model of Crowd Jumping Loads," *Journal of Structural Engineering*, vol. 134, no. 12, pp. 1852–1861, Dec. 2008, doi: 10.1061/(ASCE)0733-9445(2008)134:12(1852).

[80] T. Obata and Y. Miyamori, "Identification of a human walking force model based on dynamic monitoring data from pedestrian bridges," *Comput Struct*, vol. 84, no. 8–9, pp. 541–548, Mar. 2006, doi: 10.1016/j.compstruc.2005.11.003.

[81] V. Racic and J. M. W. Brownjohn, "Stochastic model of near-periodic vertical loads due to humans walking," *Advanced Engineering Informatics*, vol. 25, no. 2, pp. 259–275, Apr. 2011, doi: 10.1016/j.aei.2010.07.004.

[82] E. J. Hudson and P. Reynolds, "Implications of structural design on the effectiveness of active vibration control of floor structures," *Struct Control Health Monit*, vol. 21, no. 5, pp. 685–704, May 2014, doi: 10.1002/stc.1595.

[83] S. Živanović, "Modelling human actions on lightweight structures: experimental and numerical developments," *MATEC Web of Conferences*, vol. 24, p. 01005, Oct. 2015, doi: 10.1051/matecconf/20152401005.

[84] J. M. W. Brownjohn, A. Pavic, and P. Omenzetter, "A spectral density approach for modelling continuous vertical forces on pedestrian structures due to walking," *Canadian Journal of Civil Engineering*, vol. 31, no. 1, pp. 65–77, Jan. 2004, doi: 10.1139/l03-072.

[85] S. C. Kerr, "Human induced loading on staircases," PhD Thesis), Queen Mary University of London, London, 1998.

[86] International Organization for Standardization, " ISO 2631-1:1997 - Mechanical vibration and shock—Evaluation of human exposure to whole-body vibration—Part 1: General requirements," *Geneva, Switzerland*, 1997.

[87] International Organization for Standardization, "ISO 2631-2:2003 - Mechanical Vibration and Shock – Evaluation of Human

Exposure to Whole-Body Vibration – Part 2: Vibration in Buildings (1 Hz to 80 Hz)," *Geneva, Switzerland*, 2003.

[88] P. 1: P. imposed and other actions AS/NZS 1170.1:2002 - . Structural design actions, "National Standard of Australia and New Zealand," 2002.

[89] A. Caprioli, P. Reynolds, and M. Vanali, "Evaluation of serviceability assessment measures for different stadia structures and different live concert events," in *IMAC XXV*, Orlando, Florida, 2007.

[90] M. Setareh, "Vibration Serviceability of a Building Floor Structure. II: Vibration Evaluation and Assessment," *Journal of Performance of Constructed Facilities*, vol. 24, no. 6, pp. 508–518, Dec. 2010, doi: 10.1061/(ASCE)CF.1943-5509.0000135.

[91] "AS 2670.2 - Evaluation of Human Exposure to Whole-Body Vibration Continuous and Shock-Induced Vibration in Buildings (1 to 80 Hz)," 1990.

[92] BS 6472 - Guide to the Evaluation of Human Exposure to Vibration in Buildings (1Hz to 80 Hz), "British Standards Institution, London, UK," 1992.

[93] T. Tedgold, *Elementary Principles of Carpentry*. Crosby Lockwood and Co, 1820.

[94] F. E. Kidder, *The architects and builders pocket-book*. Washington, D.C: Library of Congress, 1885.

[95] C.S.LL.PP. Ministry Decree 17/01/2018, "Italian National Building Code NTC 2018," Italy, 2018.

[96] M.I.T. Circular n. 7 21/01/2019, "Instructions for the application of the "Update of the Technical standards for construction referred to in the Ministerial Decree of 17th January 2018.," 2019.

[97] National Research Council, "CNR-DT 206/2018 Istruzioni per la Progettazione, l'Esecuzione ed il Controllo delle Strutture di Legno," 2018.

[98] A. Aloisio *et al.*, "Vibration issues in timber structures: A state-of-the-art review," *Journal of Building Engineering*, vol. 76, p. 107098, Oct. 2023, doi: 10.1016/j.jobe.2023.107098.

[99] Deutsches Institut für Normung, "DIN 1052:2008-12 - Design of timber structures - General rules and rules for buildings," 2008.

[100] BS 6472-1 - Guide to Evaluation of Human Exposure to Vibration in Buildings. Vibration Sources other than Blasting, "British Standards Institution," 2008.

[101] ISO/TR 21136; Timber Structures—Vibration Performance Criteria for Timber Floors, "International Standards Organisation, Geneva, Switzerland," 2017.

[102] Canadian Standards Association, "CSA O86," 2014.

[103] M. Sciomenta, P. Gualtieri, L. Spera, F. Contu, and M. Fragiacomo, "Timber-timber composite (TTC) joints made of short-supply chain beech: Push-out tests of inclined screw connectors," *Mater Struct*, vol. 57, no. 7, p. 171, Sep. 2024, doi: 10.1617/s11527-024-02443-6.

[104] M. Sciomenta *et al.*, "Comparison between homogeneous beech and hybrid beech- silver fir glulam beams made with short supply chain timber," *Draft - under review*, 2025.

[105] CEN European Committee for Standardization, "EN 408:2010+A1:201 - 2012: Timber structures - Structural timber and glued laminated timber - Determination of some physical and mechanical properties," *Brussel*, 2012.

[106] CEN European Committee for Standardization, "EN 338:2016—structural timber—strength classes, struct timber—strength classes ," *Brussel*, 2003.

[107] EN 12512:2006, "Timber structures. Test methods. Cyclic testing of joints made with mechanical fasteners," 2006.

[108] British Standards Institute, "EN 26891:1991-timber structures—joints made with mechanical fasteners—general principles for the determination of strength and deformation characteristics," 2001.

[109] M. A. Nugent and H. Esmonde, "Android Application to Assess Smartphone Accelerometers and Bluetooth for Real-Time Control," *International Journal of Advanced Computer Science and Applications*, vol. 6, no. 3, 2015, doi: 10.14569/IJACSA.2015.060302.

[110] Z. Ma, Y. Qiao, B. Lee, and E. Fallon, "Experimental Evaluation of Mobile Phone Sensors," in *24th IET Irish Signals and Systems Conference*, Letterskenny, Ireland, 2013.

[111] C. Bedon, S. Noè, M. Fasan, and C. Amadio, "Role of In-Field Experimental Diagnostic Analysis for the Derivation of Residual Capacity Indexes in Existing Pedestrian Glass Systems," *Buildings*, vol. 13, no. 3, p. 754, Mar. 2023, doi: 10.3390/buildings13030754.

[112] CSI, *Computer and Structures inc., SAP User Manual.* 2017.

[113] A. Mazelli and C. Bedon, "Sensitivity of human-induced vibrations and comfort analysis to partially rigid STS joints in timber-to-timber composite floors," *Measurement (Lond)*, vol. 228, 2024, doi: 10.1016/j.measurement.2024.114396.

II-A APPENDIX A

In this Appendix, the results of the laboratory test are reported. In the following Table 52, maximum acceleration, RMS acceleration, maximum rolling RMS accelerations and VDV are shown for each test and for each walking segment N_{seq}. The subscript "S" represents smartphone recordings; an "A" stands for force-balance accelerometer.

Table 52 – Complete results of the laboratory test in terms of maximum, rms, rolling rms acceleration and VDV (smartphone: S; accelerometer: A).

ID	N_{seq}	$a_{S,max}$	$a_{S,rms}$	$a_{S,Rrms}$	VDV_S	$a_{A,max}$	$a_{A,rms}$	$a_{A,Rrms}$	VDV_A
-	-	m/s^2	m/s^2	m/s^2	$m/s^{1.75}$	m/s^2	m/s^2	m/s^2	$m/s^{1.75}$
1	1	0.3294	0.0670	0.1824	0.1522	0.4454	0.0848	0.2282	0.1834
1	2	0.3913	0.0683	0.1531	0.1479	0.4901	0.0867	0.1915	0.1820
1	3	0.1980	0.0571	0.0936	0.0997	0.2994	0.0736	0.1240	0.1256
1	4	0.2559	0.0514	0.1265	0.1103	0.3179	0.0658	0.1585	0.1376
1	5	0.1598	0.0385	0.0634	0.0654	0.2233	0.0495	0.0820	0.0817
1	6	0.1471	0.0359	0.0524	0.0588	0.1961	0.0449	0.0658	0.0707
1	7	0.2472	0.0590	0.1246	0.1237	0.3328	0.0746	0.1583	0.1545
1	8	0.1516	0.0405	0.0749	0.0708	0.2152	0.0530	0.1019	0.0903
1	9	0.2476	0.0474	0.0867	0.0785	0.3735	0.0636	0.1120	0.0987
1	10	0.2383	0.0403	0.0856	0.0790	0.2757	0.0514	0.1102	0.1001
1	11	0.1657	0.0468	0.0741	0.0791	0.2152	0.0610	0.0988	0.1005
1	12	0.2363	0.0451	0.1006	0.0871	0.2983	0.0586	0.1317	0.1103
1	13	0.1863	0.0529	0.0859	0.0851	0.2408	0.0686	0.1065	0.1076
1	14	0.1784	0.0193	0.0902	0.0767	0.3691	0.0290	0.1502	0.0956
2	1	0.5116	0.1003	0.2018	0.2270	0.7522	0.1282	0.2536	0.2860

ID	N_{seq}	$a_{S,max}$	$a_{S,rms}$	$a_{S,Rrms}$	VDV_S	$a_{A,max}$	$a_{A,rms}$	$a_{A,Rrms}$	VDV_A
-	-	m/s^2	m/s^2	m/s^2	$m/s^{1.75}$	m/s^2	m/s^2	m/s^2	$m/s^{1.75}$
2	2	0.6517	0.1080	0.2760	0.2737	0.8786	0.1344	0.3345	0.3336
2	3	0.6798	0.1714	0.3258	0.3543	0.9002	0.2220	0.4483	0.4642
2	4	0.6066	0.1099	0.2729	0.2647	0.7889	0.1396	0.3387	0.3345
2	5	0.6262	0.1315	0.2359	0.2988	0.7155	0.1670	0.2933	0.3759
2	6	0.5636	0.1034	0.2936	0.2686	0.6815	0.1294	0.3574	0.3232
2	7	0.7535	0.1555	0.3598	0.3950	0.8959	0.1989	0.4504	0.4934
2	8	0.6986	0.1279	0.2484	0.2603	0.9193	0.1636	0.3320	0.3423
2	9	0.2836	0.0276	0.1350	0.1227	0.3564	0.0321	0.1756	0.1561
3	1	0.5876	0.1091	0.3126	0.2725	0.7643	0.1374	0.3894	0.3358
3	2	0.5221	0.1323	0.2282	0.2638	0.5924	0.1650	0.2814	0.3207
3	3	0.3636	0.0954	0.1802	0.1819	0.4781	0.1223	0.2242	0.2245
3	4	0.6244	0.1493	0.3046	0.2682	0.7060	0.1806	0.3608	0.3232
3	5	0.3955	0.1098	0.1936	0.1818	0.5097	0.1366	0.2322	0.2185
3	6	0.5673	0.1282	0.2427	0.2682	0.7785	0.1645	0.3222	0.3423
3	7	0.5708	0.1605	0.2916	0.3186	0.7390	0.2006	0.3640	0.3949
3	8	0.6256	0.1305	0.2907	0.2761	0.7115	0.1625	0.3588	0.3352
3	9	0.4999	0.1267	0.2324	0.2478	0.6506	0.1578	0.2941	0.2998
3	10	0.4331	0.1057	0.1940	0.2052	0.5844	0.1335	0.2422	0.2530
3	11	0.3513	0.1084	0.1574	0.1793	0.5243	0.1379	0.2001	0.2233
3	12	0.4568	0.0625	0.2197	0.2237	0.6761	0.0796	0.2788	0.2756
4	1	0.8136	0.2048	0.3471	0.3562	0.9911	0.2529	0.4359	0.4390
4	2	0.7783	0.1703	0.3406	0.3450	0.9612	0.2140	0.4204	0.4318
4	3	0.9607	0.1881	0.4386	0.4283	1.3171	0.2354	0.5431	0.5333
4	4	0.7861	0.0538	0.3396	0.3354	1.0426	0.0667	0.4372	0.4127
5	1	0.1258	0.0262	0.0540	0.0489	0.1639	0.0328	0.0717	0.0578
5	2	0.4406	0.0304	0.1982	0.1729	0.6305	0.0384	0.2553	0.2176
5	3	2.1309	0.0824	0.6979	0.0086	3.4671	0.1123	0.9665	0.0041
5	4	4.0589	0.3192	1.7150	1.5587	6.2645	0.2848	1.4760	1.3248
5	5	2.9323	0.2809	0.9827	0.9245	4.7852	0.3770	1.3259	1.2553
5	6	0.3334	0.0302	0.1224	0.0096	0.4507	0.0411	0.1801	0.0069
5	7	3.7949	0.1485	1.1797	0.0154	6.9858	0.2076	1.6758	0.0170
6	1	0.7440	0.1413	0.3295	0.1340	0.9081	0.1800	0.4144	0.1604
6	2	0.6597	0.1321	0.3514	0.2458	1.0207	0.1703	0.4354	0.3052
6	3	0.5994	0.1526	0.2872	0.2910	0.8352	0.1913	0.3551	0.3601
6	4	0.5710	0.0881	0.2644	0.2640	0.7486	0.1131	0.3295	0.3316
7	1	0.3218	0.0507	0.1659	0.0238	0.4766	0.0663	0.2015	0.0306
7	2	0.1236	0.0277	0.0530	0.0621	0.1605	0.0354	0.0652	0.0736
7	3	0.2106	0.0413	0.0850	0.0926	0.2545	0.0520	0.1046	0.1101
7	4	0.3030	0.0479	0.0984	0.1030	0.3737	0.0628	0.1307	0.1301
7	5	0.2829	0.0638	0.1214	0.1375	0.3548	0.0827	0.1540	0.1716
7	6	0.1994	0.0440	0.0758	0.0867	0.2659	0.0579	0.0980	0.1072
7	7	0.2677	0.0567	0.1225	0.1111	0.3735	0.0704	0.1504	0.1309
7	8	0.1353	0.0295	0.0599	0.0541	0.1965	0.0388	0.0780	0.0664

ID	N_{seq}	$a_{S,max}$	$a_{S,rms}$	$a_{S,Rrms}$	VDV_S	$a_{A,max}$	$a_{A,rms}$	$a_{A,Rrms}$	VDV_A
-	-	m/s^2	m/s^2	m/s^2	$m/s^{1.75}$	m/s^2	m/s^2	m/s^2	$m/s^{1.75}$
7	9	0.2050	0.0321	0.0717	0.0664	0.2314	0.0413	0.0931	0.0860
7	10	0.2785	0.0492	0.1286	0.1243	0.3928	0.0639	0.1594	0.1526
7	11	0.2251	0.0377	0.0988	0.1045	0.2942	0.0475	0.1273	0.1258
8	1	0.4033	0.0720	0.1729	0.0746	0.5756	0.0922	0.2182	0.0859
8	2	0.2692	0.0417	0.1014	0.1113	0.3378	0.0537	0.1263	0.1374
8	3	0.3572	0.0682	0.1699	0.1811	0.5793	0.0883	0.2203	0.2256
8	4	0.3303	0.0590	0.1661	0.1529	0.4137	0.0755	0.2059	0.1903
8	5	0.5425	0.0819	0.2432	0.2286	0.7423	0.1075	0.3214	0.2872
8	6	0.3964	0.0756	0.1833	0.1937	0.4799	0.0960	0.2293	0.2360
8	7	0.4411	0.0680	0.1812	0.1859	0.6301	0.0886	0.2301	0.2274
8	8	0.3282	0.0332	0.1320	0.1187	0.5065	0.0421	0.1688	0.1485
9	1	0.4485	0.0861	0.1746	0.1878	0.6420	0.1194	0.2134	0.2338
9	2	0.3057	0.0689	0.1321	0.1334	0.4378	0.0877	0.1981	0.1649
9	3	0.4368	0.1062	0.1874	0.1969	1.0014	0.1362	0.2418	0.2543
9	4	0.3814	0.0937	0.1786	0.1880	0.5634	0.1210	0.2336	0.2362
9	5	0.4409	0.0920	0.1782	0.1884	0.6133	0.1203	0.2266	0.2285
9	6	0.2422	0.0604	0.0986	0.1223	0.3321	0.0820	0.1319	0.1511
9	7	0.3494	0.0947	0.1507	0.1686	0.4643	0.1190	0.1955	0.1994
9	8	0.4004	0.0770	0.1681	0.1727	0.4622	0.0961	0.2081	0.2071
9	9	0.5344	0.1236	0.2566	0.2587	0.7518	0.1634	0.3181	0.3205
9	10	0.3699	0.0771	0.1722	0.1711	0.4934	0.0987	0.2147	0.2115
9	11	0.3047	0.0791	0.1287	0.1478	0.4270	0.1054	0.1613	0.1849
9	12	0.3929	0.0966	0.1781	0.1833	0.4777	0.1241	0.2254	0.2275
9	13	0.3889	0.1050	0.1853	0.2017	0.5947	0.1369	0.2286	0.2461
9	14	0.4453	0.0603	0.2256	0.2225	0.6409	0.0767	0.2919	0.2828
10	1	0.5720	0.1309	0.2671	0.2504	0.8594	0.1775	0.3409	0.3033
10	2	0.5602	0.0866	0.2382	0.2669	0.6415	0.0619	0.3048	0.1940
11	1	3.8009	0.2187	1.2434	0.0218	4.5438	0.2666	1.5103	0.0272
11	2	6.7004	0.3725	1.5876	1.6683	9.6319	0.5034	2.1467	2.0455
11	3	5.2344	0.4378	1.6296	1.5946	7.6466	0.5608	2.1034	1.9429
11	4	3.2712	0.2676	1.2210	1.1437	4.1547	0.3436	1.5771	1.3909
12	1	0.6862	0.1066	0.2578	0.1681	0.9024	0.1391	0.3324	0.1866
12	2	0.5850	0.0995	0.2199	0.2278	0.7054	0.1246	0.2761	0.2713
12	3	0.3960	0.0654	0.1355	0.1412	0.4961	0.0837	0.1595	0.1737
12	4	0.7062	0.1120	0.2625	0.2820	1.1188	0.1543	0.3663	0.3454
12	5	0.5983	0.1046	0.2098	0.2536	0.8307	0.1367	0.2655	0.3182
12	6	0.5016	0.0956	0.2206	0.2121	0.6924	0.1225	0.2727	0.2591
12	7	0.2934	0.0743	0.1410	0.1421	0.4462	0.1026	0.2053	0.1835
12	8	0.1747	0.0152	0.0665	0.0652	0.3151	0.0191	0.0853	0.0864
13	1	0.2778	0.0539	0.1251	0.1354	0.3912	0.0681	0.1664	0.1700
13	2	0.3867	0.0839	0.1679	0.1864	0.4788	0.1045	0.2008	0.2234
13	3	0.5145	0.0961	0.2257	0.2205	0.6412	0.1208	0.2779	0.2704
13	4	0.5116	0.0729	0.1746	0.1699	0.5717	0.0890	0.2016	0.2028

ID	N_{seq}	$a_{S,max}$	$a_{S,rms}$	$a_{S,Rrms}$	VDV_S	$a_{A,max}$	$a_{A,rms}$	$a_{A,Rrms}$	VDV_A
-	-	m/s^2	m/s^2	m/s^2	$m/s^{1.75}$	m/s^2	m/s^2	m/s^2	$m/s^{1.75}$
13	5	0.3779	0.0867	0.1805	0.1848	0.4943	0.1055	0.2203	0.2263
13	6	0.6318	0.0981	0.2231	0.2037	0.8846	0.1247	0.2876	0.2586
13	7	0.5648	0.1224	0.2495	0.2522	0.6370	0.1515	0.3037	0.3102
13	8	0.3966	0.0659	0.1168	0.1527	0.4834	0.0806	0.1450	0.1760
13	9	0.6032	0.0666	0.1763	0.1503	0.7661	0.0803	0.2214	0.1748
14	1	0.6094	0.0768	0.3231	0.0128	0.8712	0.0943	0.3927	0.0148
14	2	0.7274	0.1221	0.2939	0.2974	0.8914	0.1595	0.3826	0.3644
14	3	0.8229	0.1189	0.3054	0.3157	1.3427	0.1741	0.4431	0.4101
14	4	0.8075	0.1260	0.3362	0.3467	1.1230	0.1594	0.4261	0.4357
14	5	0.6533	0.0941	0.3241	0.2994	0.8555	0.1181	0.4071	0.3671
14	6	0.7823	0.1295	0.3555	0.3663	0.9856	0.1602	0.4434	0.4509
14	7	0.7341	0.1138	0.2937	0.2960	0.9407	0.1477	0.3794	0.3636
14	8	0.7610	0.1052	0.2991	0.2989	0.9542	0.1306	0.3739	0.3670
14	9	0.7147	0.1012	0.2720	0.2757	0.7185	0.1252	0.3314	0.3308
14	10	0.6598	0.0816	0.2572	0.2772	0.8385	0.0997	0.3179	0.3361
15	1	0.6654	0.1269	0.2753	0.3072	1.1199	0.1630	0.3748	0.3839
15	2	0.6727	0.1456	0.2891	0.2923	0.9070	0.1847	0.3785	0.3623
15	3	0.6407	0.1276	0.2583	0.2664	0.7071	0.1615	0.3200	0.3295
15	4	0.4154	0.0717	0.1603	0.1597	0.5351	0.0923	0.1980	0.1928
15	5	0.4152	0.0706	0.1714	0.1549	0.4993	0.0883	0.2055	0.1916
15	6	0.2901	0.0696	0.1149	0.1311	0.3389	0.0894	0.1420	0.1611
15	7	0.2558	0.0589	0.1147	0.1175	0.4003	0.0754	0.1493	0.1487
15	8	0.4016	0.0890	0.1638	0.1695	0.4948	0.1144	0.2128	0.2118
15	9	0.3458	0.0639	0.1680	0.1480	0.4965	0.0804	0.2066	0.1829
15	10	0.2921	0.0407	0.1307	0.1375	0.4792	0.0547	0.1693	0.1728
16	1	0.6034	0.1226	0.2878	0.2902	0.7394	0.1545	0.3648	0.3615
16	2	0.8203	0.1383	0.3163	0.2922	0.9800	0.1746	0.3873	0.3620
16	3	0.4569	0.1270	0.2138	0.2190	0.5793	0.1610	0.2635	0.2788
16	4	0.7418	0.1255	0.2950	0.2722	0.8340	0.1616	0.3601	0.3292
16	5	0.7103	0.1259	0.3087	0.3224	0.8491	0.1591	0.3777	0.3933
17	1	2.1974	0.1256	0.6473	0.0120	2.0411	0.1555	0.8003	0.0114
17	2	2.3379	0.3115	0.9648	0.8267	3.6593	0.3900	1.2044	1.0504
17	3	1.7764	0.2156	0.8004	0.6890	2.4804	0.2696	1.0145	0.8663
17	4	1.7243	0.1931	0.7383	0.6428	2.3114	0.2403	0.9208	0.8079
17	5	1.7467	0.1162	0.5851	0.4922	2.0714	0.1572	0.8042	0.6880
17	6	2.5798	0.2204	1.0283	0.9055	3.8180	0.2894	1.3567	1.2091
17	7	1.4313	0.1855	0.5399	0.4754	1.8386	0.2438	0.7223	0.6143
17	8	1.4941	0.1020	0.7004	0.5717	2.3028	0.1309	0.9110	0.7723
18	1	0.6569	0.0922	0.2528	0.2554	0.7779	0.1164	0.3222	0.3111
18	2	0.6613	0.0859	0.1938	0.2227	0.7033	0.1094	0.2436	0.2712
18	3	0.5569	0.1005	0.2297	0.2140	0.6385	0.1294	0.2868	0.2629
18	4	0.4970	0.0786	0.1744	0.1974	0.8509	0.1030	0.2335	0.2344
18	5	0.7709	0.1327	0.3345	0.3099	0.8813	0.1633	0.4062	0.3688

ID	N_{seq}	$a_{S,max}$	$a_{S,rms}$	$a_{S,Rrms}$	VDV_S	$a_{A,max}$	$a_{A,rms}$	$a_{A,Rrms}$	VDV_A
-	-	m/s^2	m/s^2	m/s^2	$m/s^{1.75}$	m/s^2	m/s^2	m/s^2	$m/s^{1.75}$
18	6	0.6064	0.1019	0.2357	0.2440	0.8150	0.1294	0.2813	0.2965
18	7	0.4404	0.0869	0.1755	0.1920	0.5092	0.1092	0.2127	0.2305
18	8	0.4473	0.0481	0.1337	0.1544	0.5083	0.0617	0.1647	0.1841
19	1	0.4667	0.0542	0.1725	0.0098	0.6591	0.0688	0.2189	0.0082
19	2	0.3163	0.0462	0.0924	0.1247	0.3764	0.0573	0.1213	0.1457
19	3	0.6793	0.0892	0.2259	0.2373	0.7921	0.1113	0.2865	0.2851
19	4	0.4013	0.0588	0.1247	0.1406	0.5264	0.0749	0.1707	0.1723
19	5	0.4455	0.0726	0.1456	0.1648	0.5189	0.0895	0.1808	0.1960
19	6	0.2641	0.0479	0.0926	0.1001	0.3599	0.0617	0.1107	0.1288
19	7	0.3488	0.0624	0.1219	0.1285	0.4125	0.0804	0.1521	0.1686
19	8	0.3802	0.0528	0.1655	0.0969	0.5250	0.0672	0.1972	0.1163
20	1	0.5418	0.0652	0.2181	0.0098	0.7150	0.0824	0.2606	0.0074
20	2	0.3933	0.0522	0.1260	0.1519	0.6165	0.0653	0.1577	0.1794
20	3	0.5754	0.0873	0.1994	0.2371	0.6803	0.1105	0.2445	0.2895
20	4	0.3606	0.0493	0.1257	0.1410	0.5147	0.0624	0.1632	0.1705
20	5	0.4704	0.0769	0.1939	0.2049	0.5956	0.0984	0.2368	0.2558
20	6	0.2689	0.0416	0.0907	0.1075	0.3205	0.0521	0.1058	0.1256
20	7	0.5160	0.0725	0.2013	0.1954	0.6267	0.0929	0.2542	0.2440
20	8	0.2694	0.0377	0.1031	0.1011	0.3990	0.0492	0.1361	0.1298
21	1	0.4915	0.0631	0.1869	0.1302	0.5650	0.0831	0.2289	0.2311
21	2	0.3992	0.0542	0.1285	0.1528	0.5313	0.0846	0.1787	0.1960
21	3	0.4608	0.0804	0.1750	0.1751	0.5268	0.0911	0.2169	0.2051
21	4	0.4243	0.0745	0.1714	0.1303	0.5987	0.0962	0.2160	0.1960
21	5	0.3874	0.0734	0.1587	0.1584	0.5067	0.1039	0.2183	0.2180
21	6	0.5464	0.0940	0.2066	0.2032	0.8681	0.1223	0.2792	0.2534
21	7	0.3015	0.0527	0.1034	0.1195	0.3530	0.0666	0.1618	0.1202
21	8	0.4428	0.0875	0.2025	0.1899	0.5785	0.1177	0.2544	0.2309
21	9	0.4276	0.0412	0.1240	0.1328	0.5944	0.0487	0.1668	0.1685
22	1	0.5496	0.0942	0.1898	0.2372	0.7621	0.1183	0.2655	0.2876
22	2	0.5015	0.0947	0.2061	0.2082	0.6579	0.1232	0.2684	0.2450
22	3	0.3956	0.0721	0.1378	0.1486	0.5907	0.0938	0.1825	0.1913
22	4	0.4984	0.1216	0.2047	0.2324	0.6660	0.1530	0.2536	0.2792
22	5	0.5271	0.0958	0.1726	0.2233	0.6225	0.1210	0.2224	0.2553
22	6	0.5861	0.1125	0.1938	0.2019	1.1476	0.1592	0.3121	0.2688
22	7	0.3510	0.0680	0.1260	0.1385	0.3632	0.0845	0.1484	0.1614
22	8	0.5510	0.1052	0.2294	0.2224	0.7347	0.1353	0.2783	0.2741
22	9	0.4335	0.0372	0.1273	0.1517	0.5989	0.0482	0.1616	0.1906
23	1	1.6792	0.1517	0.6334	0.5542	1.9266	0.1844	0.7743	0.6735
23	2	1.9352	0.1927	0.7120	0.4612	2.4296	0.2323	0.8683	0.5831
23	3	1.4168	0.1297	0.4810	0.4716	1.7196	0.1525	0.5730	0.5394
23	4	1.2331	0.1263	0.3776	0.3658	1.0493	0.1423	0.4463	0.3859
23	5	3.1021	0.1843	0.9941	0.9950	4.4320	0.2216	1.1905	1.1765
24	1	0.5330	0.0741	0.2375	0.2243	0.7785	0.1001	0.3156	0.2904

ID	N_{seq}	$a_{S,max}$	$a_{S,rms}$	$a_{S,Rrms}$	VDV_S	$a_{A,max}$	$a_{A,rms}$	$a_{A,Rrms}$	VDV_A
-	-	m/s^2	m/s^2	m/s^2	$m/s^{1.75}$	m/s^2	m/s^2	m/s^2	$m/s^{1.75}$
24	2	0.2260	0.0561	0.0999	0.1096	0.4648	0.0759	0.1192	0.1384
24	3	0.4212	0.0712	0.1866	0.1772	0.6065	0.0940	0.2365	0.2189
24	4	0.3569	0.0613	0.1228	0.1275	0.6957	0.0845	0.1921	0.1652
24	5	0.3089	0.0600	0.1323	0.1329	0.4514	0.0808	0.1792	0.1669
24	6	0.2594	0.0542	0.0897	0.1089	0.3231	0.0672	0.1179	0.1344
24	7	0.2858	0.0487	0.1106	0.1046	0.7391	0.0709	0.1372	0.1352
24	8	0.3837	0.0640	0.1413	0.1482	0.4709	0.0835	0.1668	0.1794
24	9	0.4014	0.0495	0.1477	0.0807	0.4932	0.0670	0.1876	0.1030
25	1	0.1289	0.0212	0.0514	0.0391	0.2141	0.0298	0.0809	0.0492
25	2	0.3480	0.0637	0.1557	0.1065	0.5012	0.0835	0.2089	0.1401
25	3	0.3323	0.0717	0.1438	0.1359	0.5024	0.0926	0.1882	0.1712
25	4	0.3705	0.0763	0.1726	0.1594	0.6980	0.1017	0.2237	0.2118
25	5	0.3728	0.0871	0.1785	0.1782	0.5060	0.1111	0.2169	0.2163
25	6	0.3671	0.0833	0.1453	0.1463	0.4229	0.1081	0.1845	0.1769
25	7	0.4885	0.0706	0.1913	0.1891	0.6398	0.0916	0.2433	0.2262
26	1	0.2998	0.0160	0.0494	0.0074	0.0148	0.0047	0.0063	0.0062
26	2	0.1476	0.0251	0.0468	0.0526	0.2097	0.0277	0.0859	0.0687
26	3	0.1866	0.0358	0.0832	0.0676	0.2581	0.0467	0.1025	0.0884
26	4	0.4292	0.0745	0.1656	0.1821	0.5947	0.0976	0.2056	0.2227
26	5	0.3636	0.0607	0.1091	0.1261	0.4436	0.0786	0.1375	0.1532
26	6	0.6592	0.1102	0.3304	0.2169	0.9405	0.1435	0.4082	0.2699
27	1	0.1393	0.0184	0.0531	0.0597	0.2316	0.0242	0.0820	0.0791
27	2	0.2979	0.0333	0.0876	0.0345	0.3765	0.0409	0.1160	0.0323
27	3	0.1746	0.0343	0.0756	0.0644	0.2894	0.0459	0.1062	0.0932
27	4	0.2109	0.0342	0.0751	0.0661	0.2957	0.0397	0.1031	0.0910
27	5	0.1746	0.0327	0.0638	0.0634	0.1919	0.0414	0.0716	0.0765
27	6	0.2222	0.0376	0.0838	0.0868	0.3059	0.0485	0.1082	0.1093
28	1	0.2308	0.0224	0.0932	0.0299	0.2635	0.0264	0.1084	0.0446
28	2	0.1959	0.0350	0.0752	0.0728	0.2669	0.0494	0.1055	0.1070
28	3	0.2675	0.0345	0.1058	0.0942	0.2421	0.0348	0.0983	0.0956
28	4	0.2899	0.0622	0.1068	0.1252	0.4119	0.0758	0.1529	0.1619
28	5	0.2861	0.0498	0.1355	0.1141	0.3283	0.0647	0.1502	0.1427
28	6	0.3234	0.0552	0.1271	0.1313	0.3529	0.0596	0.1394	0.1441
28	7	0.2139	0.0377	0.0770	0.0876	0.2396	0.0446	0.1048	0.1017
28	8	0.2775	0.0462	0.0953	0.0997	0.3446	0.0588	0.1263	0.1323
28	9	0.2343	0.0357	0.0851	0.0877	0.2986	0.0458	0.1000	0.1041
29	1	0.1274	0.0208	0.0526	0.0443	0.1858	0.0243	0.0495	0.0506
29	2	0.1565	0.0207	0.0590	0.0498	0.1445	0.0224	0.0602	0.0531
29	3	0.3667	0.0359	0.0964	0.0986	0.3797	0.0428	0.1066	0.1136
29	4	0.3222	0.0348	0.0627	0.0695	0.3791	0.0448	0.0945	0.0785
29	5	0.1999	0.0463	0.0863	0.0885	0.2475	0.0605	0.1074	0.1040
29	6	0.2039	0.0472	0.0808	0.0904	0.2628	0.0574	0.1103	0.1123
29	7	0.2325	0.0422	0.0887	0.0823	0.2376	0.0524	0.1129	0.1032

ID	N_{seq}	$a_{S,max}$	$a_{S,rms}$	$a_{S,Rrms}$	VDV_S	$a_{A,max}$	$a_{A,rms}$	$a_{A,Rrms}$	VDV_A
-	-	m/s^2	m/s^2	m/s^2	$m/s^{1.75}$	m/s^2	m/s^2	m/s^2	$m/s^{1.75}$
29	8	0.1633	0.0324	0.0588	0.0664	0.2729	0.0442	0.0736	0.0815
29	9	0.1817	0.0347	0.0567	0.0724	0.1862	0.0425	0.0773	0.0844
29	10	0.2575	0.0452	0.0795	0.0883	0.3357	0.0543	0.1286	0.1125
29	11	0.1566	0.0380	0.0608	0.0735	0.2397	0.0471	0.0746	0.0898
29	12	0.2207	0.0405	0.0774	0.0799	0.2636	0.0525	0.1086	0.1083
30	1	0.0988	0.0164	0.0363	0.0296	0.1333	0.0194	0.0428	0.0408
30	2	0.2266	0.0356	0.0816	0.0856	0.2637	0.0439	0.0933	0.1101
30	3	0.3390	0.0689	0.1216	0.1265	0.3881	0.0880	0.1530	0.1570
30	4	0.5733	0.0918	0.2317	0.1806	0.6937	0.1082	0.2553	0.2190
30	5	0.2824	0.0717	0.1404	0.1288	0.3643	0.0818	0.1400	0.1465
30	6	0.3615	0.0837	0.1473	0.1391	0.5178	0.1010	0.1750	0.1705
30	7	0.2814	0.0625	0.1077	0.1145	0.4829	0.0784	0.1609	0.1482
30	8	0.3892	0.0885	0.1473	0.1520	0.5680	0.1106	0.1934	0.2063
31	1	3.9434	0.1719	1.0642	0.0097	5.6515	0.2826	1.7905	0.0120
31	2	2.5936	0.2437	0.8049	0.6661	4.3748	0.4354	1.4722	1.2690
31	3	2.8495	0.2229	0.7833	0.6570	4.3810	0.4211	1.5138	1.2369
31	4	2.6333	0.2761	0.9087	0.7814	4.5266	0.4811	1.6190	1.3946
31	5	3.2499	0.2638	0.9504	0.7914	5.3307	0.4802	1.7655	1.4957
32	1	0.2346	0.0260	0.0790	0.0741	0.2378	0.0280	0.0803	0.0785
32	2	0.2895	0.0486	0.0957	0.1039	0.4555	0.0761	0.1600	0.1747
32	3	0.3509	0.0707	0.1396	0.1466	0.4446	0.0899	0.1858	0.1831
32	4	0.7347	0.0730	0.1437	0.1585	0.9185	0.1022	0.2445	0.2088
32	5	0.3518	0.0856	0.1506	0.1669	0.3944	0.1052	0.1635	0.1932
32	6	0.4348	0.0971	0.2063	0.1978	0.6215	0.1323	0.2454	0.2558
32	7	0.4833	0.0977	0.1813	0.1968	0.6313	0.1270	0.2522	0.2586
32	8	0.4447	0.0940	0.2005	0.1947	0.5003	0.1169	0.2157	0.2285
32	9	0.3685	0.0723	0.1323	0.1464	0.4322	0.0875	0.1630	0.1780
33	1	0.4901	0.0686	0.1954	0.1407	0.5852	0.0735	0.2060	0.1457
33	2	0.3079	0.0725	0.1214	0.1484	0.3241	0.0805	0.1381	0.1580
33	3	0.3614	0.0780	0.1366	0.1603	0.3735	0.0853	0.1499	0.1728
33	4	0.3106	0.0679	0.1274	0.1481	0.3285	0.0763	0.1417	0.1604
33	5	0.4227	0.0726	0.1520	0.1586	0.4281	0.0817	0.1738	0.1786
33	6	0.4776	0.0760	0.1699	0.1466	0.4032	0.0821	0.1853	0.1579
33	7	0.3399	0.0635	0.1088	0.1448	0.3597	0.0702	0.1286	0.1574
33	8	0.3815	0.0769	0.1631	0.1505	0.3546	0.0850	0.1798	0.1663
33	9	0.3010	0.0366	0.1207	0.1330	0.3680	0.0412	0.1405	0.1515

II-B | APPENDIX B

In this Appendix, the results of the case study tests are reported. In the following Tables 53 - 58, maximum acceleration, RMS acceleration, maximum Rolling RMS acceleration and VDV values are shown, considering both smartphone (S) and force-balance accelerometer (A).

B.1 Case study 1 – Meraviglia 1st floor

Table 53 – Complete results of the walking tests of the first case study in terms of maximum, rms, rolling rms acceleration and VDV (smartphone: S; accelerometer: A).

Test	Seq	$a_{max,A}$	$a_{max,S}$	$a_{rms,A}$	$a_{rms,S}$	$a_{Rrms,A}$	$a_{Rrms,S}$	VDV_A	VDV_S
		m/s^2	m/s^2	m/s^2	m/s^2	m/s^2	m/s^2	$m/s^{1.75}$	$m/s^{1.75}$
1	1	0.1224	0.1062	0.0142	0.0129	0.0450	0.0404	0.0548	0.0489
1	2	0.0572	0.0510	0.0094	0.0096	0.0204	0.0181	0.0265	0.0240
1	3	0.0575	0.0428	0.0103	0.0090	0.0199	0.0178	0.0274	0.0250
1	4	0.0841	0.0650	0.0115	0.0123	0.0284	0.0251	0.0376	0.0332
1	5	0.0645	0.0537	0.0096	0.0093	0.0216	0.0183	0.0290	0.0261
1	6	0.0614	0.0631	0.0093	0.0097	0.0217	0.0210	0.0278	0.0264
1	7	0.0591	0.0433	0.0080	0.0081	0.0189	0.0185	0.0257	0.0235
1	8	0.1744	0.1392	0.0186	0.0180	0.0571	0.0491	0.0682	0.0591
1	9	0.0558	0.0586	0.0077	0.0080	0.0203	0.0195	0.0262	0.0240
1	10	0.0831	0.0596	0.0083	0.0097	0.0196	0.0172	0.0286	0.0249

Test	Seq	$a_{max,A}$ m/s^2	$a_{max,S}$ m/s^2	$a_{rms,A}$ m/s^2	$a_{rms,S}$ m/s^2	$a_{Rrms,A}$ m/s^2	$a_{Rrms,S}$ m/s^2	VDV_A $m/s^{1.75}$	VDV_S $m/s^{1.75}$
1	11	0.0448	0.0385	0.0060	0.0066	0.0142	0.0127	0.0178	0.0158
1	12	0.0837	0.0660	0.0083	0.0090	0.0192	0.0181	0.0263	0.0240
2	1	0.0915	0.0900	0.0144	0.0136	0.0287	0.0252	0.0427	0.0387
2	2	0.0938	0.0826	0.0191	0.0181	0.0323	0.0297	0.0502	0.0430
2	3	0.0843	0.0719	0.0163	0.0144	0.0311	0.0289	0.0430	0.0378
2	4	0.0797	0.0681	0.0127	0.0117	0.0257	0.0221	0.0382	0.0334
2	5	0.1050	0.0929	0.0159	0.0150	0.0359	0.0348	0.0479	0.0443
2	6	0.1180	0.1077	0.0188	0.0170	0.0410	0.0391	0.0544	0.0488
2	7	0.1254	0.1073	0.0153	0.0143	0.0402	0.0360	0.0517	0.0448
2	8	0.0833	0.0769	0.0148	0.0124	0.0278	0.0240	0.0407	0.0354
2	9	0.1033	0.0841	0.0151	0.0148	0.0369	0.0291	0.0495	0.0410
2	10	0.1090	0.0901	0.0173	0.0144	0.0337	0.0292	0.0478	0.0413
2	11	0.1267	0.1071	0.0160	0.0156	0.0437	0.0375	0.0552	0.0473
2	12	0.0925	0.0747	0.0146	0.0125	0.0289	0.0252	0.0407	0.0352
2	13	0.0930	0.0796	0.0148	0.0135	0.0296	0.0245	0.0411	0.0346
2	14	0.1089	0.0896	0.0176	0.0147	0.0375	0.0331	0.0537	0.0452
2	15	0.0790	0.0767	0.0125	0.0130	0.0282	0.0259	0.0392	0.0347
2	16	0.0943	0.0884	0.0119	0.0113	0.0343	0.0286	0.0426	0.0352
2	17	0.0919	0.0855	0.0156	0.0140	0.0336	0.0311	0.0440	0.0406
2	18	0.1218	0.1181	0.0202	0.0189	0.0438	0.0380	0.0617	0.0544
2	19	0.1104	0.0969	0.0153	0.0150	0.0377	0.0327	0.0520	0.0446
2	20	0.0878	0.0747	0.0157	0.0147	0.0302	0.0281	0.0443	0.0397
2	21	0.1004	0.0865	0.0156	0.0155	0.0341	0.0281	0.0450	0.0386
2	22	0.0950	0.0767	0.0146	0.0125	0.0273	0.0234	0.0405	0.0347
2	23	0.0985	0.0790	0.0162	0.0150	0.0340	0.0312	0.0476	0.0413
2	24	0.0850	0.0772	0.0172	0.0156	0.0311	0.0272	0.0467	0.0401
2	25	0.0791	0.0680	0.0126	0.0118	0.0272	0.0234	0.0376	0.0327
2	26	0.0785	0.0687	0.0126	0.0127	0.0272	0.0249	0.0384	0.0344
2	27	0.0642	0.0638	0.0133	0.0125	0.0234	0.0208	0.0359	0.0312
2	28	0.1123	0.0808	0.0151	0.0130	0.0365	0.0310	0.0471	0.0400
2	29	0.1086	0.0849	0.0138	0.0121	0.0338	0.0287	0.0427	0.0358
2	30	0.0930	0.0795	0.0129	0.0123	0.0317	0.0269	0.0414	0.0350
2	31	0.0691	0.0678	0.0108	0.0104	0.0252	0.0226	0.0324	0.0281
2	32	0.0759	0.0674	0.0121	0.0111	0.0284	0.0247	0.0362	0.0315
2	33	0.0575	0.0531	0.0097	0.0098	0.0215	0.0209	0.0287	0.0277
2	34	0.0548	0.0531	0.0094	0.0088	0.0222	0.0193	0.0281	0.0253
2	35	0.1246	0.1096	0.0137	0.0137	0.0420	0.0373	0.0522	0.0466
2	36	0.0527	0.0551	0.0108	0.0104	0.0205	0.0193	0.0287	0.0259
3	1	0.0771	0.0625	0.0123	0.0116	0.0215	0.0188	0.0306	0.0273
3	2	0.0721	0.0651	0.0110	0.0106	0.0288	0.0271	0.0380	0.0347
3	3	0.0551	0.0494	0.0111	0.0106	0.0188	0.0177	0.0300	0.0274
3	4	0.0502	0.0503	0.0108	0.0101	0.0188	0.0162	0.0292	0.0251

Test	Seq	$a_{max,A}$ m/s²	$a_{max,S}$ m/s²	$a_{rms,A}$ m/s²	$a_{rms,S}$ m/s²	$a_{Rrms,A}$ m/s²	$a_{Rrms,S}$ m/s²	VDV_A m/s$^{1.75}$	VDV_S m/s$^{1.75}$
3	5	0.0631	0.0503	0.0087	0.0086	0.0179	0.0161	0.0267	0.0222
3	6	0.0903	0.0711	0.0115	0.0105	0.0235	0.0222	0.0360	0.0272
3	7	0.0827	0.0629	0.0095	0.0092	0.0208	0.0177	0.0291	0.0252
3	8	0.0545	0.0519	0.0100	0.0096	0.0203	0.0176	0.0265	0.0239
3	9	0.0487	0.0403	0.0082	0.0089	0.0150	0.0147	0.0202	0.0188
3	10	0.0545	0.0463	0.0096	0.0094	0.0206	0.0175	0.0269	0.0262
3	11	0.0571	0.0472	0.0112	0.0103	0.0190	0.0157	0.0299	0.0251
3	12	0.0508	0.0515	0.0107	0.0106	0.0188	0.0170	0.0275	0.0251
3	13	0.0698	0.0694	0.0109	0.0100	0.0240	0.0196	0.0346	0.0290
3	14	0.1072	0.0748	0.0114	0.0104	0.0244	0.0205	0.0326	0.0262
3	15	0.0582	0.0532	0.0123	0.0109	0.0229	0.0187	0.0308	0.0259
3	16	0.0673	0.0641	0.0118	0.0113	0.0253	0.0230	0.0357	0.0324
3	17	0.0561	0.0532	0.0092	0.0096	0.0212	0.0186	0.0257	0.0234
3	18	0.0598	0.0445	0.0103	0.0098	0.0183	0.0153	0.0260	0.0212
3	19	0.0902	0.0589	0.0112	0.0105	0.0220	0.0193	0.0316	0.0263
3	20	0.0590	0.0576	0.0128	0.0116	0.0228	0.0202	0.0308	0.0271
3	21	0.0875	0.0782	0.0147	0.0128	0.0300	0.0255	0.0414	0.0349
3	22	0.0582	0.0400	0.0085	0.0089	0.0170	0.0158	0.0217	0.0199
3	23	0.0552	0.0488	0.0104	0.0099	0.0178	0.0178	0.0270	0.0239
3	24	0.0768	0.0532	0.0100	0.0096	0.0246	0.0204	0.0292	0.0246
3	25	0.1595	0.1348	0.0193	0.0167	0.0478	0.0398	0.0616	0.0516
3	26	0.0619	0.0650	0.0090	0.0088	0.0199	0.0184	0.0241	0.0214
3	27	0.0636	0.0526	0.0110	0.0104	0.0242	0.0213	0.0290	0.0261
3	28	0.0814	0.0687	0.0082	0.0087	0.0221	0.0203	0.0258	0.0239
3	29	0.0677	0.0741	0.0127	0.0124	0.0251	0.0243	0.0315	0.0299
3	30	0.0898	0.0679	0.0117	0.0113	0.0255	0.0222	0.0302	0.0260
3	31	0.0781	0.0567	0.0105	0.0101	0.0231	0.0203	0.0292	0.0253
3	32	0.0626	0.0563	0.0100	0.0097	0.0186	0.0171	0.0269	0.0248
3	33	0.0676	0.0556	0.0123	0.0114	0.0254	0.0208	0.0321	0.0265
3	34	0.0798	0.0654	0.0114	0.0113	0.0197	0.0185	0.0278	0.0257
3	35	0.1108	0.0888	0.0156	0.0139	0.0388	0.0315	0.0498	0.0402
3	36	0.1434	0.1341	0.0143	0.0129	0.0487	0.0406	0.0601	0.0500
3	37	0.0725	0.0566	0.0135	0.0122	0.0254	0.0223	0.0330	0.0274
3	38	0.0727	0.0601	0.0106	0.0100	0.0222	0.0192	0.0296	0.0264
3	39	0.0891	0.0526	0.0098	0.0093	0.0209	0.0172	0.0428	0.0254
3	40	0.0615	0.0483	0.0081	0.0077	0.0214	0.0167	0.0262	0.0204
4	1	0.0970	0.0800	0.0140	0.0123	0.0263	0.0234	0.0377	0.0316
4	2	0.0782	0.0700	0.0157	0.0143	0.0280	0.0257	0.0412	0.0368
4	3	0.0878	0.0732	0.0120	0.0111	0.0218	0.0192	0.0314	0.0269
4	4	0.0661	0.0499	0.0129	0.0119	0.0221	0.0187	0.0314	0.0271
4	5	0.1077	0.0997	0.0210	0.0187	0.0394	0.0345	0.0564	0.0490
4	6	0.0654	0.0553	0.0128	0.0117	0.0241	0.0193	0.0299	0.0254
4	7	0.0786	0.0756	0.0138	0.0128	0.0288	0.0243	0.0373	0.0322

Test	Seq	$a_{max,A}$	$a_{max,S}$	$a_{rms,A}$	$a_{rms,S}$	$a_{Rrms,A}$	$a_{Rrms,S}$	VDV_A	VDV_S
		m/s^2	m/s^2	m/s^2	m/s^2	m/s^2	m/s^2	$m/s^{1.75}$	$m/s^{1.75}$
4	8	0.0559	0.0492	0.0122	0.0119	0.0204	0.0194	0.0266	0.0245
4	9	0.0903	0.0781	0.0158	0.0143	0.0307	0.0275	0.0473	0.0419
4	10	0.1272	0.1187	0.0232	0.0208	0.0425	0.0381	0.0560	0.0510
4	11	0.0747	0.0632	0.0137	0.0123	0.0243	0.0211	0.0314	0.0265
4	12	0.0846	0.0691	0.0148	0.0133	0.0264	0.0217	0.0375	0.0318
4	13	0.1096	0.0949	0.0157	0.0143	0.0357	0.0316	0.0452	0.0386
4	14	0.1063	0.0987	0.0150	0.0138	0.0350	0.0294	0.0474	0.0408
4	15	0.1010	0.0914	0.0161	0.0147	0.0397	0.0354	0.0500	0.0451
4	16	0.0915	0.0656	0.0143	0.0129	0.0287	0.0234	0.0398	0.0340
4	17	0.0867	0.0726	0.0126	0.0117	0.0263	0.0242	0.0309	0.0275
4	18	0.0781	0.0654	0.0131	0.0124	0.0233	0.0200	0.0365	0.0328
4	19	0.0834	0.0693	0.0148	0.0137	0.0325	0.0281	0.0442	0.0387
4	20	0.0775	0.0670	0.0157	0.0149	0.0239	0.0231	0.0351	0.0317
4	21	0.0473	0.0447	0.0107	0.0105	0.0178	0.0182	0.0266	0.0250
4	22	0.0708	0.0589	0.0169	0.0151	0.0248	0.0210	0.0377	0.0322
4	23	0.0576	0.0496	0.0118	0.0113	0.0202	0.0177	0.0275	0.0246
4	24	0.0690	0.0608	0.0145	0.0129	0.0262	0.0223	0.0431	0.0369
4	25	0.1217	0.1082	0.0181	0.0163	0.0410	0.0374	0.0549	0.0486
4	26	0.0869	0.0670	0.0174	0.0162	0.0304	0.0275	0.0429	0.0378
4	27	0.1144	0.0928	0.0191	0.0164	0.0333	0.0284	0.0488	0.0410
4	28	0.1046	0.0798	0.0221	0.0194	0.0361	0.0293	0.0503	0.0426
4	29	0.1087	0.0970	0.0192	0.0178	0.0386	0.0352	0.0512	0.0457
4	30	0.0826	0.0719	0.0186	0.0176	0.0285	0.0268	0.0418	0.0384
4	31	0.1006	0.0781	0.0176	0.0155	0.0327	0.0278	0.0420	0.0359
4	32	0.0864	0.0854	0.0220	0.0202	0.0316	0.0282	0.0481	0.0427
6	1	0.1035	0.0786	0.0166	0.0149	0.0392	0.0331	0.0506	0.0425
6	2	0.1071	0.0859	0.0162	0.0146	0.0369	0.0315	0.0501	0.0416
6	3	0.0806	0.0713	0.0126	0.0122	0.0288	0.0250	0.0387	0.0341
6	4	0.1379	0.1131	0.0186	0.0165	0.0472	0.0396	0.0608	0.0514
6	5	0.1122	0.1013	0.0174	0.0157	0.0407	0.0337	0.0520	0.0449
6	6	0.1127	0.0997	0.0176	0.0151	0.0417	0.0341	0.0544	0.0445
6	7	0.1088	0.0909	0.0183	0.0166	0.0359	0.0313	0.0533	0.0468
6	8	0.1311	0.1182	0.0187	0.0173	0.0467	0.0422	0.0595	0.0540
6	9	0.1022	0.0856	0.0163	0.0147	0.0331	0.0272	0.0484	0.0411
6	10	0.1278	0.1130	0.0196	0.0175	0.0445	0.0406	0.0628	0.0550
6	11	0.1166	0.0986	0.0182	0.0165	0.0387	0.0344	0.0557	0.0486
6	12	0.1417	0.1174	0.0207	0.0181	0.0500	0.0451	0.0648	0.0557
6	13	0.1503	0.1180	0.0211	0.0188	0.0511	0.0444	0.0674	0.0581
6	14	0.1312	0.1125	0.0194	0.0170	0.0388	0.0328	0.0578	0.0486
6	15	0.1756	0.1576	0.0237	0.0210	0.0611	0.0549	0.0778	0.0679
6	16	0.1577	0.1394	0.0231	0.0203	0.0487	0.0452	0.0711	0.0607
6	17	0.1322	0.1072	0.0237	0.0204	0.0463	0.0384	0.0638	0.0528
6	18	0.1170	0.1087	0.0223	0.0196	0.0451	0.0384	0.0603	0.0533

Test	Seq	$a_{max,A}$	$a_{max,S}$	$a_{rms,A}$	$a_{rms,S}$	$a_{Rrms,A}$	$a_{Rrms,S}$	VDV_A	VDV_S
		m/s^2	m/s^2	m/s^2	m/s^2	m/s^2	m/s^2	$m/s^{1.75}$	$m/s^{1.75}$
8	1	0.1317	0.1073	0.0212	0.0188	0.0432	0.0379	0.0566	0.0487
8	2	0.1176	0.1133	0.0207	0.0190	0.0423	0.0379	0.0613	0.0550
8	3	0.1656	0.1357	0.0220	0.0191	0.0545	0.0450	0.0696	0.0575
8	4	0.1157	0.0979	0.0190	0.0168	0.0398	0.0346	0.0561	0.0477
8	5	0.1445	0.1259	0.0197	0.0173	0.0497	0.0402	0.0645	0.0548
8	6	0.1007	0.0926	0.0195	0.0176	0.0342	0.0303	0.0541	0.0473
8	7	0.1547	0.1259	0.0203	0.0180	0.0523	0.0440	0.0662	0.0565
8	8	0.1226	0.1053	0.0222	0.0188	0.0455	0.0389	0.0615	0.0503
8	9	0.0996	0.0898	0.0155	0.0143	0.0351	0.0304	0.0474	0.0421
8	10	0.1207	0.1065	0.0193	0.0173	0.0435	0.0392	0.0580	0.0507
8	11	0.1093	0.0966	0.0199	0.0177	0.0407	0.0341	0.0562	0.0492
8	12	0.1612	0.1426	0.0258	0.0216	0.0512	0.0425	0.0744	0.0598
8	13	0.0985	0.0808	0.0166	0.0150	0.0343	0.0293	0.0480	0.0410
8	14	0.1605	0.1357	0.0252	0.0215	0.0500	0.0435	0.0706	0.0596
8	15	0.0841	0.0771	0.0173	0.0154	0.0345	0.0306	0.0458	0.0401
8	16	0.1737	0.1708	0.0251	0.0224	0.0654	0.0596	0.0827	0.0737
8	17	0.0930	0.0828	0.0176	0.0157	0.0325	0.0294	0.0495	0.0423
8	18	0.1421	0.1240	0.0208	0.0190	0.0473	0.0418	0.0678	0.0599
8	19	0.1011	0.0885	0.0194	0.0175	0.0400	0.0355	0.0574	0.0504
8	20	0.1042	0.0955	0.0185	0.0164	0.0356	0.0317	0.0503	0.0438
8	21	0.1617	0.1240	0.0228	0.0196	0.0533	0.0439	0.0686	0.0558
8	22	0.1327	0.1191	0.0236	0.0207	0.0485	0.0400	0.0691	0.0589
8	23	0.1423	0.1240	0.0254	0.0223	0.0514	0.0435	0.0697	0.0599
8	24	0.1220	0.0996	0.0173	0.0158	0.0386	0.0353	0.0556	0.0493

Table 54 – Complete results of the heel-drop tests of the first case study in terms of maximum, rms, rolling rms acceleration and VDV (smartphone: S; accelerometer: A).

Test	Seq	$a_{max,A}$	$a_{max,S}$	$a_{rms,A}$	$a_{rms,S}$	$a_{Rrms,A}$	$a_{Rrms,S}$	VDV_A	VDV_S
		m/s^2	m/s^2	m/s^2	m/s^2	m/s^2	m/s^2	$m/s^{1.75}$	$m/s^{1.75}$
5	1	0.9012	0.8020	0.1270	0.1114	0.2837	0.2521	0.3583	0.3128
5	2	0.8055	0.7131	0.1187	0.0986	0.2370	0.1965	0.3082	0.2583
5	3	1.1751	1.0285	0.1776	0.1543	0.3551	0.3092	0.4539	0.3971
5	4	0.7937	0.6491	0.1182	0.0968	0.2358	0.1923	0.3034	0.2441
5	5	1.0218	0.8759	0.1537	0.1372	0.3071	0.2759	0.3925	0.3519
5	6	1.2149	1.0662	0.1429	0.1150	0.3779	0.3059	0.4765	0.3824
5	7	0.6375	0.5141	0.0859	0.0715	0.1915	0.1588	0.2393	0.1978
5	8	0.6208	0.5041	0.0998	0.0821	0.1836	0.1493	0.2290	0.1886
5	9	0.5417	0.4229	0.0876	0.0736	0.1562	0.1306	0.1945	0.1635
5	10	0.5563	0.4390	0.0959	0.0808	0.2048	0.1720	0.0795	0.0581

Test	Seq	$a_{max,A}$	$a_{max,S}$	$a_{rms,A}$	$a_{rms,S}$	$a_{Rrms,A}$	$a_{Rrms,S}$	VDV_A	VDV_S
		m/s^2	m/s^2	m/s^2	m/s^2	m/s^2	m/s^2	$m/s^{1.75}$	$m/s^{1.75}$
5	11	0.5699	0.4502	0.0897	0.0761	0.1734	0.1449	0.1993	0.1675
5	12	0.7902	0.6686	0.1566	0.1311	0.2788	0.2323	0.2994	0.2497
5	13	0.6954	0.5549	0.1012	0.0789	0.2020	0.1559	0.2368	0.1949
5	14	1.0097	0.8895	0.1728	0.1376	0.3455	0.2752	0.4189	0.3300
5	15	0.9064	0.8244	0.1645	0.1368	0.3286	0.2698	0.3875	0.3369
5	16	1.0237	0.9308	0.1703	0.1417	0.3403	0.2841	0.4142	0.3520
5	17	1.0378	0.8692	0.1460	0.1261	0.3262	0.2812	0.4042	0.3532

B.2 Case study 2 – Meraviglia 2nd floor

Table 55 – Complete results of the walking tests of the second case study in terms of maximum, rms, rolling rms acceleration and VDV (smartphone: S; accelerometer: A).

Test	Seq	$a_{max,A}$	$a_{max,S}$	$a_{rms,A}$	$a_{rms,S}$	$a_{Rrms,A}$	$a_{Rrms,S}$	VDV_A	VDV_S
		m/s^2	m/s^2	m/s^2	m/s^2	m/s^2	m/s^2	$m/s^{1.75}$	$m/s^{1.75}$
2	1	0.2511	0.2359	0.0594	0.0563	0.1172	0.1146	0.1440	0.1384
2	2	0.3117	0.2834	0.0680	0.0639	0.1262	0.1213	0.1717	0.1621
2	3	0.3197	0.3107	0.0659	0.0645	0.1396	0.1376	0.1679	0.1655
2	4	0.2894	0.2610	0.0653	0.0632	0.1074	0.1056	0.1520	0.1426
2	5	0.2983	0.2854	0.0713	0.0676	0.1394	0.1319	0.1687	0.1555
2	6	0.2662	0.2374	0.0585	0.0546	0.1161	0.1057	0.1470	0.1357
2	7	0.3817	0.3427	0.0823	0.0762	0.1652	0.1545	0.1964	0.1742
2	8	0.3079	0.2860	0.0713	0.0685	0.1224	0.1186	0.1590	0.1523
2	9	0.3923	0.3757	0.0780	0.0726	0.1635	0.1496	0.1928	0.1775
2	10	0.2803	0.2783	0.0629	0.0601	0.1219	0.1097	0.1543	0.1448
2	11	0.1935	0.1848	0.0415	0.0401	0.0877	0.0875	0.1031	0.1007
2	12	0.2749	0.2708	0.0570	0.0528	0.1138	0.1052	0.1526	0.1434
2	13	0.2513	0.2186	0.0539	0.0488	0.1109	0.1014	0.1292	0.1111
2	14	0.3142	0.2913	0.0637	0.0612	0.1246	0.1194	0.1600	0.1535
2	15	0.2699	0.2498	0.0541	0.0518	0.1228	0.1158	0.1423	0.1357
2	16	0.2533	0.2234	0.0575	0.0551	0.0927	0.0859	0.1317	0.1236
2	17	0.2868	0.2610	0.0556	0.0512	0.1196	0.1080	0.1473	0.1312
2	18	0.4562	0.3740	0.0673	0.0630	0.1678	0.1542	0.1983	0.1796
2	19	0.2404	0.2227	0.0528	0.0479	0.0975	0.0901	0.1291	0.1140
2	20	0.2468	0.2734	0.0521	0.0511	0.1056	0.1044	0.1330	0.1294
2	21	0.2785	0.2708	0.0491	0.0461	0.1162	0.1115	0.1371	0.1286
2	22	0.2500	0.2296	0.0471	0.0450	0.0972	0.0898	0.1239	0.1173
2	23	0.2884	0.2708	0.0562	0.0534	0.1170	0.1162	0.1513	0.1458
2	24	0.2458	0.2348	0.0523	0.0496	0.1026	0.0994	0.1332	0.1265
2	25	0.3396	0.3107	0.0608	0.0567	0.1286	0.1229	0.1668	0.1557

Test	Seq	$a_{max,A}$	$a_{max,S}$	$a_{rms,A}$	$a_{rms,S}$	$a_{Rrms,A}$	$a_{Rrms,S}$	VDV_A	VDV_S
		m/s^2	m/s^2	m/s^2	m/s^2	m/s^2	m/s^2	$m/s^{1.75}$	$m/s^{1.75}$
2	26	0.2596	0.2345	0.0515	0.0504	0.0980	0.0992	0.1293	0.1266
2	27	0.1889	0.3796	0.0383	0.0406	0.0791	0.0955	0.1058	0.1235
2	28	0.2457	0.2374	0.0574	0.0528	0.0999	0.0934	0.1367	0.1217
2	29	0.3052	0.3084	0.0523	0.0526	0.1247	0.1305	0.1465	0.1460
2	30	0.2079	0.2123	0.0438	0.0430	0.0844	0.0817	0.1175	0.1135
2	31	0.2976	0.2868	0.0479	0.0450	0.1090	0.0981	0.1434	0.1308
2	32	0.2779	0.2617	0.0585	0.0566	0.1198	0.1154	0.1505	0.1424
2	33	0.2636	0.2620	0.0481	0.0458	0.1068	0.1030	0.1308	0.1250
2	34	0.3439	0.2924	0.0515	0.0491	0.1199	0.1143	0.1431	0.1401
2	35	0.2519	0.2531	0.0475	0.0440	0.0937	0.0876	0.1190	0.1103
2	36	0.2813	0.2319	0.0415	0.0398	0.0889	0.0861	0.1161	0.1102
2	37	0.2606	0.2458	0.0501	0.0469	0.1024	0.1007	0.1290	0.1242
2	38	0.3138	0.2716	0.0652	0.0605	0.1265	0.1138	0.1617	0.1458
2	39	0.3241	0.2867	0.0617	0.0571	0.1309	0.1242	0.1578	0.1486
2	40	0.2058	0.1880	0.0524	0.0487	0.0841	0.0789	0.1173	0.1085
2	41	0.3352	0.3100	0.0589	0.0566	0.1354	0.1279	0.1569	0.1500
2	42	0.3358	0.3257	0.0570	0.0520	0.1360	0.1276	0.1657	0.1530
2	43	0.3195	0.2717	0.0570	0.0525	0.1294	0.1223	0.1527	0.1403
2	44	0.2730	0.2372	0.0558	0.0542	0.0994	0.0966	0.1374	0.1320
2	45	0.3400	0.3159	0.0673	0.0612	0.1399	0.1307	0.1807	0.1594
2	46	0.2638	0.2414	0.0496	0.0481	0.0983	0.0965	0.1443	0.1376
3	1	0.2031	0.1906	0.0408	0.0389	0.0859	0.0812	0.1115	0.1059
3	2	0.2169	0.1803	0.0424	0.0387	0.0902	0.0758	0.1087	0.0958
3	3	0.2647	0.2199	0.0460	0.0428	0.1042	0.0942	0.1178	0.1117
3	4	0.1688	0.1431	0.0359	0.0337	0.0715	0.0668	0.0869	0.0827
3	5	0.2299	0.2046	0.0480	0.0451	0.0880	0.0795	0.1128	0.1070
3	6	0.3130	0.2454	0.0503	0.0466	0.1003	0.0871	0.1235	0.1141
3	7	0.2855	0.2650	0.0523	0.0465	0.1023	0.0958	0.1275	0.1148
3	8	0.3131	0.2119	0.0491	0.0414	0.1179	0.0932	0.1308	0.1012
3	9	0.3128	0.2143	0.0480	0.0422	0.0954	0.0818	0.1217	0.1073
3	10	0.2434	0.2336	0.0419	0.0408	0.0963	0.0962	0.1152	0.1131
3	11	0.3330	0.2630	0.0576	0.0544	0.1120	0.1078	0.1409	0.1322
3	12	0.2452	0.2234	0.0451	0.0423	0.0956	0.0872	0.1130	0.1035
3	13	0.3281	0.2297	0.0494	0.0423	0.1125	0.0980	0.1339	0.1153
3	14	0.2762	0.2248	0.0518	0.0488	0.0972	0.0953	0.1227	0.1172
3	15	0.3209	0.2336	0.0576	0.0523	0.1180	0.1112	0.1410	0.1302
3	16	0.2998	0.2699	0.0551	0.0524	0.1082	0.1026	0.1312	0.1262
3	17	0.3297	0.2653	0.0522	0.0459	0.1016	0.0857	0.1228	0.1090
3	18	0.2628	0.2092	0.0446	0.0392	0.0994	0.0816	0.1225	0.1033
3	19	0.2938	0.2374	0.0452	0.0425	0.1162	0.1112	0.1282	0.1223
3	20	0.3170	0.2484	0.0494	0.0453	0.1244	0.1136	0.1328	0.1197
3	21	0.3211	0.2302	0.0478	0.0436	0.1120	0.1049	0.1268	0.1179
3	22	0.3310	0.2643	0.0438	0.0416	0.1044	0.0977	0.1245	0.1165

Test	Seq	$a_{max,A}$	$a_{max,S}$	$a_{rms,A}$	$a_{rms,S}$	$a_{Rrms,A}$	$a_{Rrms,S}$	VDV_A	VDV_S
		m/s^2	m/s^2	m/s^2	m/s^2	m/s^2	m/s^2	$m/s^{1.75}$	$m/s^{1.75}$
3	23	0.2754	0.2222	0.0476	0.0464	0.0987	0.0963	0.1203	0.1180
3	24	0.2628	0.2235	0.0501	0.0453	0.0971	0.0835	0.1237	0.1105
3	25	0.2870	0.2617	0.0530	0.0484	0.1188	0.1116	0.1385	0.1318
3	26	0.3483	0.3277	0.0527	0.0480	0.1170	0.1106	0.1421	0.1340
3	27	0.3562	0.2748	0.0513	0.0437	0.1292	0.1123	0.1441	0.1289
3	28	0.2089	0.1738	0.0318	0.0303	0.0765	0.0709	0.0893	0.0839
3	29	0.2214	0.1881	0.0470	0.0417	0.0906	0.0808	0.1175	0.1047
3	30	0.2448	0.2218	0.0427	0.0376	0.0874	0.0787	0.1114	0.0988
3	31	0.3048	0.2282	0.0516	0.0471	0.1025	0.0954	0.1240	0.1181
3	32	0.1715	0.1534	0.0369	0.0337	0.0779	0.0732	0.0945	0.0866
3	33	0.3163	0.2583	0.0453	0.0418	0.0889	0.0866	0.1165	0.1102
3	34	0.2864	0.2522	0.0392	0.0371	0.0990	0.0950	0.1162	0.1126
3	35	0.3878	0.2914	0.0513	0.0475	0.1080	0.1018	0.1302	0.1262
3	36	0.2344	0.2203	0.0426	0.0410	0.0939	0.0937	0.1127	0.1103
3	37	0.2438	0.2064	0.0476	0.0441	0.0862	0.0797	0.1159	0.1067
3	38	0.2661	0.2233	0.0378	0.0358	0.0998	0.0949	0.1134	0.1107
3	39	0.2988	0.2550	0.0505	0.0473	0.0960	0.0952	0.1252	0.1201
3	40	0.2217	0.1851	0.0374	0.0358	0.0825	0.0770	0.0961	0.0902
3	41	0.3264	0.2625	0.0452	0.0416	0.1197	0.1137	0.1368	0.1302
3	42	0.1760	0.1696	0.0368	0.0347	0.0685	0.0642	0.0869	0.0819
3	43	0.2338	0.2047	0.0450	0.0425	0.0959	0.0913	0.1148	0.1083
3	44	0.1902	0.1792	0.0386	0.0342	0.0825	0.0712	0.1054	0.0922
3	45	0.2647	0.2083	0.0377	0.0340	0.0916	0.0812	0.1041	0.0939
3	46	0.2662	0.2218	0.0445	0.0409	0.0988	0.0918	0.1159	0.1054
3	47	0.2687	0.2228	0.0492	0.0442	0.1124	0.1020	0.1264	0.1127
3	48	0.2689	0.2464	0.0394	0.0369	0.0933	0.0867	0.1162	0.1086
3	49	0.2140	0.1660	0.0448	0.0375	0.0851	0.0674	0.1032	0.0830
3	50	0.2582	0.2193	0.0479	0.0441	0.1058	0.0944	0.1252	0.1125
3	51	0.3639	0.2336	0.0462	0.0440	0.1244	0.1190	0.1367	0.1306
3	52	0.2903	0.2548	0.0497	0.0453	0.1237	0.1118	0.1377	0.1253
4	1	0.3645	0.3105	0.0616	0.0564	0.1294	0.1212	0.1421	0.1304
4	2	0.3541	0.3071	0.0871	0.0818	0.1626	0.1499	0.1853	0.1721
4	3	0.3707	0.2710	0.0607	0.0551	0.1411	0.1295	0.1508	0.1382
4	4	0.3674	0.3072	0.0717	0.0673	0.1420	0.1352	0.1613	0.1518
4	5	0.2387	0.2222	0.0606	0.0573	0.1029	0.1010	0.1321	0.1225
4	6	0.4907	0.4122	0.0836	0.0761	0.2084	0.1929	0.2300	0.2110
4	7	0.3304	0.2938	0.0686	0.0633	0.1427	0.1318	0.1618	0.1484
4	8	0.4585	0.3662	0.0824	0.0748	0.1824	0.1698	0.2008	0.1837
4	9	0.3030	0.2823	0.0583	0.0569	0.1270	0.1257	0.1375	0.1399
4	10	0.4407	0.3905	0.0812	0.0761	0.1750	0.1688	0.1951	0.1807
4	11	0.2900	0.2314	0.0674	0.0600	0.1215	0.1081	0.1498	0.1275
4	12	0.3225	0.2880	0.0628	0.0585	0.1196	0.1180	0.1488	0.1427
4	13	0.3054	0.2510	0.0633	0.0559	0.1315	0.1130	0.1531	0.1298

Test	Seq	$a_{max,A}$	$a_{max,S}$	$a_{rms,A}$	$a_{rms,S}$	$a_{Rrms,A}$	$a_{Rrms,S}$	VDV_A	VDV_S
		m/s^2	m/s^2	m/s^2	m/s^2	m/s^2	m/s^2	$m/s^{1.75}$	$m/s^{1.75}$
4	14	0.3261	0.2499	0.0656	0.0609	0.1246	0.1161	0.1520	0.1398
4	15	0.2913	0.2418	0.0466	0.0438	0.1161	0.1150	0.1290	0.1222
4	16	0.4071	0.2901	0.0644	0.0617	0.1394	0.1343	0.1563	0.1483
4	17	0.2174	0.1857	0.0548	0.0491	0.0881	0.0809	0.1211	0.1093
4	18	0.2721	0.2591	0.0614	0.0575	0.1235	0.1200	0.1435	0.1389
4	19	0.3079	0.2620	0.0585	0.0522	0.1445	0.1281	0.1549	0.1356
4	20	0.3506	0.2897	0.0487	0.0465	0.1266	0.1203	0.1450	0.1392
4	21	0.2651	0.2520	0.0593	0.0570	0.1102	0.1083	0.1352	0.1312
4	22	0.2402	0.1997	0.0495	0.0440	0.0897	0.0835	0.1145	0.1042
4	23	0.2836	0.2199	0.0453	0.0402	0.0983	0.0795	0.1147	0.0978
4	24	0.2505	0.2104	0.0536	0.0462	0.0986	0.0892	0.1277	0.1093
4	25	0.2449	0.2065	0.0429	0.0419	0.0880	0.0865	0.1068	0.1031
4	26	0.3329	0.2789	0.0585	0.0538	0.1266	0.1153	0.1481	0.1324
4	27	0.2877	0.2526	0.0443	0.0407	0.1140	0.1031	0.1312	0.1197
4	28	0.3256	0.2887	0.0711	0.0657	0.1286	0.1261	0.1504	0.1461
4	29	0.2896	0.2655	0.0552	0.0520	0.1166	0.1101	0.1376	0.1309
4	30	0.3895	0.3416	0.0714	0.0660	0.1639	0.1532	0.1841	0.1721
4	31	0.3363	0.2836	0.0544	0.0517	0.1211	0.1150	0.1369	0.1286
4	32	0.3301	0.2542	0.0603	0.0551	0.1076	0.0963	0.1277	0.1144
4	33	0.2737	0.2374	0.0552	0.0511	0.1042	0.0977	0.1326	0.1226
4	34	0.2547	0.2426	0.0595	0.0557	0.1165	0.1134	0.1407	0.1316
4	35	0.1703	0.1251	0.0359	0.0325	0.0588	0.0558	0.0833	0.0754
4	36	0.2959	0.2561	0.0614	0.0570	0.1366	0.1273	0.1544	0.1428
4	37	0.2797	0.2642	0.0535	0.0498	0.1134	0.1085	0.1288	0.1248
4	38	0.2907	0.2094	0.0523	0.0483	0.1054	0.0943	0.1307	0.1197
4	39	0.2329	0.2191	0.0550	0.0508	0.1000	0.0871	0.1290	0.1179
4	40	0.3761	0.3029	0.0658	0.0588	0.1478	0.1295	0.1677	0.1495
4	41	0.2888	0.2487	0.0511	0.0473	0.1105	0.0981	0.1259	0.1184
4	42	0.3397	0.2674	0.0694	0.0606	0.1393	0.1137	0.1645	0.1397
4	43	0.2205	0.1857	0.0473	0.0459	0.0919	0.0877	0.1099	0.1052
4	44	0.3386	0.3320	0.0607	0.0595	0.1459	0.1438	0.1655	0.1676
4	45	0.2849	0.2804	0.0507	0.0474	0.1136	0.1061	0.1275	0.1227
4	46	0.3749	0.3201	0.0672	0.0649	0.1469	0.1399	0.1693	0.1640
4	47	0.3156	0.2981	0.0543	0.0512	0.1035	0.0954	0.1325	0.1260
4	48	0.4263	0.3235	0.0659	0.0645	0.1439	0.1388	0.1652	0.1620
4	49	0.2425	0.1958	0.0486	0.0447	0.0796	0.0692	0.1046	0.0947
4	50	0.3951	0.3104	0.0861	0.0803	0.1573	0.1418	0.1931	0.1823
4	51	0.2452	0.2291	0.0432	0.0406	0.1002	0.0917	0.1228	0.1163
6	1	0.2463	1.5853	0.0384	0.0766	0.0856	0.2044	0.0956	0.2254
6	2	0.2023	0.1448	0.0268	0.0244	0.0503	0.0446	0.0625	0.0587
6	3	0.3131	0.2927	0.0462	0.0444	0.1120	0.1074	0.1409	0.1361
6	4	0.2271	0.2035	0.0412	0.0381	0.0642	0.0604	0.0941	0.0881
6	5	0.2772	0.2280	0.0500	0.0451	0.0940	0.0793	0.1167	0.1021

Test	Seq	$a_{max,A}$	$a_{max,S}$	$a_{rms,A}$	$a_{rms,S}$	$a_{Rrms,A}$	$a_{Rrms,S}$	VDV_A	VDV_S
		m/s^2	m/s^2	m/s^2	m/s^2	m/s^2	m/s^2	$m/s^{1.75}$	$m/s^{1.75}$
6	6	0.3334	0.2951	0.0486	0.0435	0.1195	0.1055	0.1366	0.1210
6	7	0.2242	0.2340	0.0473	0.0445	0.0692	0.0709	0.1086	0.0971
6	8	0.3172	0.2721	0.0460	0.0433	0.0911	0.0894	0.1172	0.1133
6	9	0.2763	0.2394	0.0587	0.0545	0.1125	0.1065	0.1498	0.1378
6	10	0.3676	0.3020	0.0559	0.0507	0.1097	0.0947	0.1404	0.1251
6	11	0.2448	0.2198	0.0470	0.0418	0.0898	0.0850	0.1145	0.1059
6	12	0.3277	0.2963	0.0503	0.0460	0.1122	0.1021	0.1375	0.1280
6	13	0.2488	0.2083	0.0429	0.0378	0.0780	0.0710	0.1066	0.0951
6	14	0.4813	0.3198	0.0522	0.0474	0.1295	0.1203	0.1530	0.1447
6	15	0.3339	0.2889	0.0491	0.0441	0.1173	0.1092	0.1440	0.1325
6	16	0.3939	0.2958	0.0506	0.0456	0.1113	0.1013	0.1370	0.1248
6	17	0.2611	0.2171	0.0443	0.0394	0.0833	0.0744	0.1140	0.1015
6	18	0.3864	0.2391	0.0470	0.0419	0.0917	0.0770	0.1185	0.1082
6	19	0.3239	0.2962	0.0529	0.0480	0.1004	0.0935	0.1347	0.1232
6	20	0.3933	0.3004	0.0541	0.0484	0.1072	0.0921	0.1313	0.1191
6	21	0.2572	0.2161	0.0456	0.0416	0.0966	0.0867	0.1252	0.1149
6	22	0.3485	0.2908	0.0552	0.0494	0.1131	0.1036	0.1479	0.1341
6	23	0.2769	0.3226	0.0497	0.0465	0.1018	0.0982	0.1166	0.1168
6	24	0.3503	0.3158	0.0486	0.0446	0.0880	0.0827	0.1164	0.1097
7	1	0.4619	0.4136	0.0551	0.0456	0.1152	0.0918	0.1338	0.1157
7	2	0.3552	0.2507	0.0589	0.0524	0.1234	0.1065	0.1401	0.1270
7	3	0.5406	0.3126	0.0593	0.0510	0.1231	0.1016	0.1356	0.1222
7	4	0.3412	0.3175	0.0613	0.0556	0.1408	0.1276	0.1593	0.1482
7	5	0.5828	0.4441	0.0554	0.0477	0.1370	0.1173	0.1501	0.1368
7	6	0.3236	0.2868	0.0505	0.0436	0.1225	0.1020	0.1347	0.1156
7	7	0.6782	0.4351	0.0775	0.0666	0.1773	0.1474	0.1973	0.1709
7	8	0.2956	0.2724	0.0543	0.0487	0.1175	0.1064	0.1331	0.1207
7	9	0.3331	0.2794	0.0597	0.0551	0.1158	0.1126	0.1439	0.1322
7	10	0.2944	0.2689	0.0414	0.0372	0.0879	0.0815	0.1114	0.1000
7	11	0.2957	0.2248	0.0484	0.0431	0.0802	0.0678	0.1052	0.0966
7	12	0.3957	0.3486	0.0607	0.0543	0.1554	0.1402	0.1726	0.1559
7	13	0.4150	0.3258	0.0526	0.0471	0.1331	0.1196	0.1496	0.1343
7	14	0.1836	0.1694	0.0396	0.0353	0.0839	0.0763	0.0951	0.0874
7	15	0.3002	0.2334	0.0523	0.0465	0.0903	0.0869	0.1225	0.1127
7	16	0.2727	0.2279	0.0408	0.0361	0.0855	0.0763	0.1101	0.0979
7	17	0.4253	0.3380	0.0619	0.0583	0.1247	0.1197	0.1445	0.1403
7	18	0.3350	0.2905	0.0583	0.0534	0.1432	0.1291	0.1652	0.1508
7	19	0.7473	0.4396	0.0731	0.0634	0.1803	0.1511	0.1958	0.1689
7	20	0.3598	0.3184	0.0528	0.0467	0.1394	0.1228	0.1565	0.1382
7	21	0.4157	0.2829	0.0458	0.0383	0.1127	0.0906	0.1298	0.1079
7	22	0.3685	0.3390	0.0557	0.0493	0.1480	0.1318	0.1623	0.1474
7	23	0.7572	0.4847	0.0753	0.0613	0.1903	0.1537	0.2052	0.1677
7	24	0.8705	0.4801	0.0665	0.0569	0.2208	0.1900	0.2414	0.2162

Test	Seq	$a_{max,A}$ m/s²	$a_{max,S}$ m/s²	$a_{rms,A}$ m/s²	$a_{rms,S}$ m/s²	$a_{Rrms,A}$ m/s²	$a_{Rrms,S}$ m/s²	VDV_A m/s$^{1.75}$	VDV_S m/s$^{1.75}$
7	25	0.8705	0.4801	0.0933	0.0787	0.2210	0.1908	0.2348	0.2098
7	26	0.2975	0.2815	0.0591	0.0535	0.1228	0.1142	0.1465	0.1362
7	27	0.4851	0.3669	0.0695	0.0567	0.1581	0.1271	0.1817	0.1424
7	28	0.3173	0.2785	0.0472	0.0425	0.1231	0.1109	0.1385	0.1259
7	29	0.6365	0.3238	0.0603	0.0493	0.1380	0.1171	0.1574	0.1359
7	30	0.3208	0.2523	0.0449	0.0394	0.0834	0.0741	0.1128	0.1008
7	31	0.6409	0.4498	0.0667	0.0588	0.1729	0.1520	0.2017	0.1826

Table 56 – Complete results of the heel-drop tests of the second case study in terms of maximum, rms, rolling rms acceleration and VDV (smartphone: S; accelerometer: A).

Test	Seq	$a_{max,A}$ m/s²	$a_{max,S}$ m/s²	$a_{rms,A}$ m/s²	$a_{rms,S}$ m/s²	$a_{Rrms,A}$ m/s²	$a_{Rrms,S}$ m/s²	VDV_A m/s$^{1.75}$	VDV_S m/s$^{1.75}$
5	1	2.6327	2.2592	0.3139	0.2809	0.6946	0.6267	0.7487	0.6802
5	2	2.9709	1.7688	0.4275	0.3527	0.8487	0.6915	0.9414	0.7641
5	3	3.0346	2.196	0.3731	0.3411	0.8611	0.7754	0.9444	0.8937
5	4	2.6092	1.7976	0.3319	0.3006	0.7789	0.6938	0.8535	0.7729
5	5	2.2862	2.2041	0.3658	0.3465	0.8112	0.7798	0.8966	0.8427
5	6	2.1927	1.6453	0.3254	0.2938	0.7486	0.676	0.824	0.7321
5	7	1.9104	1.5544	0.276	0.2595	0.6698	0.6281	0.7419	0.7085
5	8	2.6071	1.6626	0.3707	0.3211	0.7735	0.6707	0.8439	0.7400
5	9	1.8467	1.6908	0.3189	0.3106	0.7217	0.7023	0.7961	0.7719
5	10	2.4649	1.7298	0.3813	0.3299	0.7584	0.6501	0.8304	0.7216
5	11	3.2741	2.5388	0.3184	0.2597	0.7754	0.6284	0.8526	0.7025

B.3 Case Study 3 – "Historical Palace"

Table 57 – Complete results of the walking tests of the third case study in terms of maximum, rms, rolling rms acceleration and VDV (smartphone: S; accelerometer: A).

Test	Seq	$a_{max,A}$ m/s²	$a_{max,S}$ m/s²	$a_{rms,A}$ m/s²	$a_{rms,S}$ m/s²	$a_{Rrms,A}$ m/s²	$a_{Rrms,S}$ m/s²	VDV_A m/s$^{1.75}$	VDV_S m/s$^{1.75}$
1	1	0.0454	0.0469	0.0084	0.0094	0.0232	0.0224	0.0154	0.0160
1	2	0.0693	0.0611	0.0109	0.0112	0.0266	0.0232	0.0328	0.0310
1	3	0.0420	0.0453	0.0093	0.0098	0.0189	0.0167	0.0237	0.0231
1	4	0.0541	0.0479	0.0108	0.0113	0.0211	0.0197	0.0300	0.0290
1	5	0.0409	0.0430	0.0102	0.0103	0.0194	0.0186	0.0240	0.0224

Test	Seq	$a_{max,A}$ m/s²	$a_{max,S}$ m/s²	$a_{rms,A}$ m/s²	$a_{rms,S}$ m/s²	$a_{Rrms,A}$ m/s²	$a_{Rrms,S}$ m/s²	VDV_A m/s$^{1.75}$	VDV_S m/s$^{1.75}$
1	6	0.0661	0.0642	0.0121	0.0121	0.0281	0.0264	0.0350	0.0329
1	7	0.0502	0.0418	0.0115	0.0115	0.0212	0.0202	0.0307	0.0291
1	8	0.0381	0.0384	0.0097	0.0106	0.0173	0.0192	0.0244	0.0250
1	9	0.0348	0.0346	0.0093	0.0099	0.0149	0.0161	0.0208	0.0210
1	10	0.0406	0.0404	0.0101	0.0103	0.0183	0.0164	0.0244	0.0235
1	11	0.0441	0.0466	0.0112	0.0113	0.0199	0.0194	0.0254	0.0253
1	12	0.0421	0.0420	0.0102	0.0103	0.0166	0.0159	0.0239	0.0224
1	13	0.0575	0.0551	0.0117	0.0117	0.0259	0.0238	0.0319	0.0303
1	14	0.0329	0.0346	0.0092	0.0097	0.0147	0.0152	0.0189	0.0186
1	15	0.0457	0.0410	0.0106	0.0107	0.0188	0.0172	0.0259	0.0243
1	16	0.0390	0.0405	0.0106	0.0109	0.0169	0.0172	0.0275	0.0258
1	17	0.0473	0.0479	0.0101	0.0105	0.0208	0.0207	0.0274	0.0264
1	18	0.0382	0.0361	0.0107	0.0113	0.0159	0.0166	0.0247	0.0238
1	19	0.0524	0.0459	0.0125	0.0123	0.0218	0.0201	0.0339	0.0287
2	1	0.0702	0.0623	0.0154	0.0147	0.0283	0.0255	0.0250	0.0241
2	2	0.0683	0.0641	0.0199	0.0188	0.0312	0.0291	0.0471	0.0432
2	3	0.0768	0.0764	0.0198	0.0189	0.0325	0.0316	0.0481	0.0458
2	4	0.0747	0.0592	0.0177	0.0167	0.0316	0.0295	0.0447	0.0414
2	5	0.0527	0.0474	0.0154	0.0147	0.0233	0.0225	0.0366	0.0328
2	6	0.0776	0.0775	0.0181	0.0174	0.0351	0.0337	0.0451	0.0431
2	7	0.0572	0.0516	0.0164	0.0162	0.0259	0.0257	0.0388	0.0433
2	8	0.0724	0.0693	0.0165	0.0157	0.0328	0.0305	0.0402	0.0377
2	9	0.0659	0.0670	0.0165	0.0159	0.0286	0.0267	0.0393	0.0382
2	10	0.0653	0.0601	0.0173	0.0163	0.0292	0.0235	0.0413	0.0376
2	11	0.0477	0.0503	0.0143	0.0138	0.0225	0.0217	0.0313	0.0300
2	12	0.0566	0.0497	0.0120	0.0119	0.0222	0.0223	0.0295	0.0285
2	13	0.0476	0.0477	0.0139	0.0138	0.0238	0.0224	0.0346	0.0332
2	14	0.0650	0.0523	0.0147	0.0140	0.0305	0.0258	0.0374	0.0342
2	15	0.0689	0.0670	0.0156	0.0148	0.0281	0.0262	0.0388	0.0361
2	16	0.0720	0.0675	0.0167	0.0160	0.0332	0.0317	0.0392	0.0372
2	17	0.0507	0.0503	0.0165	0.0159	0.0235	0.0230	0.0353	0.0339
2	18	0.0637	0.0621	0.0151	0.0147	0.0273	0.0259	0.0340	0.0326
2	19	0.0569	0.0477	0.0133	0.0134	0.0234	0.0214	0.0300	0.0285
2	20	0.0546	0.0607	0.0139	0.0134	0.0250	0.0244	0.0343	0.0363
2	21	0.0561	0.0523	0.0140	0.0137	0.0250	0.0226	0.0343	0.0335
2	22	0.0701	0.0700	0.0163	0.0158	0.0300	0.0285	0.0376	0.0365
2	23	0.0499	0.0477	0.0113	0.0112	0.0222	0.0211	0.0262	0.0253
2	24	0.0480	0.0454	0.0135	0.0136	0.0208	0.0204	0.0295	0.0291
2	25	0.0678	0.0648	0.0161	0.0158	0.0291	0.0269	0.0352	0.0331
2	26	0.0408	0.0449	0.0116	0.0119	0.0166	0.0168	0.0257	0.0257
3	1	0.0554	0.0525	0.0128	0.0125	0.0254	0.0242	0.0211	0.0203
3	2	0.0492	0.0468	0.0127	0.0122	0.0200	0.0190	0.0314	0.0286

Test	Seq	$a_{max,A}$	$a_{max,S}$	$a_{rms,A}$	$a_{rms,S}$	$a_{Rrms,A}$	$a_{Rrms,S}$	VDV_A	VDV_S
		m/s^2	m/s^2	m/s^2	m/s^2	m/s^2	m/s^2	$m/s^{1.75}$	$m/s^{1.75}$
3	3	0.0823	0.0756	0.0177	0.0172	0.0335	0.0335	0.0436	0.0415
3	4	0.0479	0.0427	0.0131	0.0132	0.0211	0.0214	0.0306	0.0296
3	5	0.0714	0.0555	0.0160	0.0160	0.0257	0.0242	0.0387	0.0377
3	6	0.0567	0.0515	0.0127	0.0124	0.0250	0.0227	0.0321	0.0293
3	7	0.0695	0.0643	0.0146	0.0146	0.0267	0.0249	0.0367	0.0350
3	8	0.0609	0.0555	0.0143	0.0142	0.0268	0.0257	0.0362	0.0344
3	9	0.0700	0.0643	0.0168	0.0161	0.0303	0.0274	0.0418	0.0388
3	10	0.0585	0.0564	0.0148	0.0147	0.0258	0.0250	0.0367	0.0354
3	11	0.0502	0.0574	0.0136	0.0140	0.0218	0.0217	0.0333	0.0328
3	12	0.0511	0.0461	0.0137	0.0136	0.0214	0.0214	0.0336	0.0327
3	13	0.0644	0.0557	0.0150	0.0147	0.0274	0.0249	0.0383	0.0364
3	14	0.0528	0.0506	0.0147	0.0147	0.0240	0.0244	0.0365	0.0354
3	15	0.0667	0.0555	0.0162	0.0154	0.0281	0.0263	0.0395	0.0366
3	16	0.0523	0.0509	0.0135	0.0138	0.0244	0.0237	0.0362	0.0355
3	17	0.0595	0.0570	0.0162	0.0156	0.0268	0.0257	0.0383	0.0360
3	18	0.0623	0.0506	0.0155	0.0149	0.0257	0.0230	0.0376	0.0346
3	19	0.0526	0.0517	0.0132	0.0136	0.0231	0.0231	0.0341	0.0339
3	20	0.0648	0.0574	0.0141	0.0140	0.0290	0.0268	0.0378	0.0359
3	21	0.0435	0.0418	0.0102	0.0106	0.0182	0.0163	0.0269	0.0264
3	22	0.0700	0.0613	0.0154	0.0154	0.0293	0.0264	0.0407	0.0396
3	23	0.0558	0.0604	0.0164	0.0159	0.0261	0.0251	0.0414	0.0390
3	24	0.0751	0.0656	0.0165	0.0160	0.0274	0.0257	0.0426	0.0397
3	25	0.0503	0.0604	0.0120	0.0123	0.0230	0.0228	0.0316	0.0306
3	26	0.0501	0.0604	0.0126	0.0128	0.0231	0.0241	0.0323	0.0317
3	27	0.0576	0.0574	0.0135	0.0135	0.0242	0.0237	0.0346	0.0336
3	28	0.0537	0.0548	0.0142	0.0141	0.0234	0.0236	0.0362	0.0351
3	29	0.0519	0.0495	0.0133	0.0135	0.0223	0.0211	0.0324	0.0315
3	30	0.0465	0.0407	0.0115	0.0118	0.0200	0.0211	0.0297	0.0286
3	31	0.0388	0.0455	0.0117	0.0121	0.0186	0.0194	0.0284	0.0280
4	1	0.0972	0.0842	0.0175	0.0168	0.0350	0.0334	0.0428	0.0401
4	2	0.0876	0.0860	0.0213	0.0196	0.0412	0.0357	0.0508	0.0461
4	3	0.1046	0.0971	0.0224	0.0210	0.0399	0.0379	0.0523	0.0492
4	4	0.0665	0.0618	0.0178	0.0165	0.0324	0.0292	0.0382	0.0348
4	5	0.0813	0.0723	0.0176	0.0166	0.0331	0.0295	0.0414	0.0377
4	6	0.0933	0.0853	0.0196	0.0181	0.0434	0.0398	0.0489	0.0429
4	7	0.1183	0.1106	0.0185	0.0175	0.0505	0.0469	0.0573	0.0548
4	8	0.0769	0.0685	0.0173	0.0160	0.0343	0.0302	0.0410	0.0367
4	9	0.0802	0.0734	0.0175	0.0159	0.0353	0.0300	0.0443	0.0387
4	10	0.0879	0.0804	0.0206	0.0191	0.0348	0.0329	0.0439	0.0412
4	11	0.0883	0.0762	0.0197	0.0186	0.0371	0.0335	0.0471	0.0433
4	12	0.0924	0.0855	0.0188	0.0171	0.0377	0.0325	0.0464	0.0406
4	13	0.0774	0.0674	0.0194	0.0179	0.0338	0.0292	0.0421	0.0379
4	14	0.1050	0.0948	0.0217	0.0202	0.0384	0.0333	0.0515	0.0473

Test	Seq	$a_{max,A}$	$a_{max,S}$	$a_{rms,A}$	$a_{rms,S}$	$a_{Rrms,A}$	$a_{Rrms,S}$	VDV_A	VDV_S
		m/s^2	m/s^2	m/s^2	m/s^2	m/s^2	m/s^2	$m/s^{1.75}$	$m/s^{1.75}$
4	15	0.0937	0.0860	0.0202	0.0186	0.0421	0.0373	0.0502	0.0463
4	16	0.0778	0.0719	0.0201	0.0184	0.0325	0.0286	0.0454	0.0412
4	17	0.0789	0.0772	0.0198	0.0182	0.0383	0.0347	0.0485	0.0441
4	18	0.0954	0.0889	0.0237	0.0215	0.0392	0.0356	0.0513	0.0461
4	19	0.1116	0.1056	0.0238	0.0229	0.0501	0.0488	0.0585	0.0559
4	20	0.0794	0.0681	0.0193	0.0180	0.0297	0.0269	0.0424	0.0387
4	21	0.0837	0.0817	0.0174	0.0160	0.0331	0.0302	0.0433	0.0394
4	22	0.0807	0.0611	0.0179	0.0164	0.0299	0.0243	0.0401	0.0356
4	23	0.1055	0.0892	0.0191	0.0179	0.0390	0.0353	0.0453	0.0416
4	24	0.0957	0.0840	0.0234	0.0211	0.0368	0.0318	0.0508	0.0451
4	25	0.0973	0.0909	0.0207	0.0191	0.0438	0.0395	0.0501	0.0460
4	26	0.0793	0.0674	0.0188	0.0175	0.0327	0.0289	0.0452	0.0416
4	27	0.0676	0.0621	0.0144	0.0139	0.0287	0.0258	0.0346	0.0324
4	28	0.1070	0.1008	0.0209	0.0192	0.0385	0.0350	0.0501	0.0452
4	29	0.0926	0.0968	0.0193	0.0179	0.0412	0.0380	0.0501	0.0463
4	30	0.0919	0.0821	0.0174	0.0166	0.0346	0.0305	0.0417	0.0387
4	31	0.0693	0.0591	0.0178	0.0171	0.0321	0.0284	0.0402	0.0369
4	32	0.0887	0.0772	0.0196	0.0177	0.0338	0.0312	0.0448	0.0397
4	33	0.0862	0.0742	0.0215	0.0200	0.0385	0.0351	0.0499	0.0448
6	1	0.0906	0.0825	0.0183	0.0165	0.0365	0.0315	0.0500	0.0444
6	2	0.0796	0.0697	0.0168	0.0155	0.0357	0.0306	0.0416	0.0361
6	3	0.1036	0.0898	0.0197	0.0177	0.0426	0.0364	0.0450	0.0386
6	4	0.0863	0.0727	0.0179	0.0163	0.0367	0.0327	0.0467	0.0414
6	5	0.0875	0.0813	0.0192	0.0173	0.0362	0.0329	0.0500	0.0436
6	6	0.0863	0.0734	0.0162	0.0147	0.0350	0.0298	0.0395	0.0364
6	7	0.0724	0.0685	0.0170	0.0155	0.0302	0.0282	0.0410	0.0379
6	8	0.0869	0.0780	0.0166	0.0152	0.0376	0.0320	0.0352	0.0324
6	9	0.0887	0.0821	0.0166	0.0153	0.0381	0.0332	0.0344	0.0326
6	10	0.0850	0.0729	0.0172	0.0158	0.0376	0.0315	0.0393	0.0340
6	11	0.0914	0.0748	0.0164	0.0152	0.0383	0.0313	0.0390	0.0349
7	1	0.1059	0.0999	0.0210	0.0189	0.0448	0.0378	0.0291	0.0289
7	2	0.1416	0.1228	0.0274	0.0242	0.0557	0.0491	0.0563	0.0491
7	3	0.1420	0.1117	0.0255	0.0230	0.0566	0.0479	0.0486	0.0461
7	4	0.1109	0.0909	0.0226	0.0201	0.0492	0.0420	0.0483	0.0447
7	5	0.0978	0.0852	0.0233	0.0211	0.0415	0.0355	0.0560	0.0507
7	6	0.1491	0.1332	0.0263	0.0235	0.0566	0.0495	0.0787	0.0688
7	7	0.1159	0.0999	0.0247	0.0217	0.0497	0.0413	0.0559	0.0503
7	8	0.1275	0.0913	0.0213	0.0188	0.0422	0.0365	0.0436	0.0386
7	9	0.1173	0.0901	0.0238	0.0212	0.0478	0.0413	0.0512	0.0448
7	10	0.1207	0.1040	0.0221	0.0198	0.0516	0.0452	0.0387	0.0359
7	11	0.1304	0.1117	0.0241	0.0213	0.0498	0.0421	0.0597	0.0513
7	12	0.1041	0.0874	0.0190	0.0171	0.0421	0.0367	0.0391	0.0353
7	13	0.0748	0.0666	0.0193	0.0170	0.0340	0.0297	0.0451	0.0377

Test	Seq	$a_{max,A}$ m/s^2	$a_{max,S}$ m/s^2	$a_{rms,A}$ m/s^2	$a_{rms,S}$ m/s^2	$a_{Rrms,A}$ m/s^2	$a_{Rrms,S}$ m/s^2	VDV_A $m/s^{1.75}$	VDV_S $m/s^{1.75}$
8	1	0.1269	0.1203	0.0227	0.0211	0.0500	0.0434	0.0078	0.0098

Table 58 – Complete results of the heel-drop tests of the third case study in terms of maximum, rms, rolling rms acceleration and VDV (smartphone: S; accelerometer: A).

Test	Seq	$a_{max,A}$ m/s^2	$a_{max,S}$ m/s^2	$a_{rms,A}$ m/s^2	$a_{rms,S}$ m/s^2	$a_{Rrms,A}$ m/s^2	$a_{Rrms,S}$ m/s^2	VDV_A $m/s^{1.75}$	VDV_S $m/s^{1.75}$
5	1	0.4188	0.3889	0.0874	0.0814	0.1717	0.1636	0.1960	0.1836
5	2	0.3047	0.2746	0.0636	0.0568	0.1234	0.1101	0.1425	0.1296
5	3	0.2489	0.2246	0.0504	0.0449	0.0964	0.0856	0.1118	0.1010
5	4	0.3625	0.3374	0.0743	0.0631	0.1447	0.1237	0.1637	0.1439
5	5	0.3020	0.2621	0.0629	0.0530	0.1220	0.1008	0.1363	0.1167
5	6	0.3836	0.3389	0.0536	0.0482	0.1471	0.1314	0.1709	0.1548
5	7	0.2052	0.1847	0.0391	0.0372	0.0808	0.0771	0.0959	0.0913
5	8	0.1733	0.1582	0.0304	0.0296	0.0648	0.0624	0.0694	0.0663
5	9	0.1194	0.1118	0.025	0.0243	0.0469	0.0461	0.0510	0.0491
5	10	0.1830	0.1550	0.0308	0.0294	0.0717	0.0667	0.0752	0.0706
5	11	0.2003	0.1758	0.0341	0.0328	0.0733	0.0713	0.0788	0.0757
5	12	0.1549	0.1301	0.0319	0.0296	0.0662	0.0616	0.0710	0.0646
5	13	0.1668	0.1481	0.0376	0.0345	0.0707	0.0653	0.0716	0.0667
5	14	0.2048	0.1774	0.044	0.0404	0.0823	0.075	0.0853	0.0780
5	15	0.1733	0.1376	0.0394	0.0363	0.0738	0.0676	0.0725	0.0671
5	16	0.2359	0.1811	0.0442	0.0396	0.0821	0.0726	0.0835	0.0739

ACKNOWLEDGEMENTS

I wish to express my deepest gratitude to my supervisor prof. Chiara Bedon and my co-supervisor prof. Antonino Morassi for the opportunity of improving my passion for timber structures and for their guidance. I also extend my appreciation to Dr. Martina Sciomenta for her help and for our interesting scientific discussions.

I heartily thank my family, my mother Loredana, my father Corrado and my brother Gianluca, to have always encouraged me throughout my studies. A deep thank also to my friends Manuela, Mattia, Silvia, Gabriele and Elisa for their constant support on this adventure.

I wish to gratefully thank Pasqualino, Gloria and Angelo for their support during the tests in L'Aquila, and Stefano for all the challenging engineering discussions during these three years. The municipality of L'Aquila is gratefully acknowledged, for providing the opportunity to analyse three interesting case studies. The ReLUIS consortium is acknowledged for supporting the first part of the thesis.

Finally, I want to remember prof. Alessandra Gubana, who always encouraged me to continue studying and improving myself.